Technische Universität München

Fakultät für Chemie

Lehrstuhl für Pharmazeutische Radiochemie

Novel GRPR-targeted antagonists with improved pharmacokinetics for imaging and therapy of GRPR-expressing malignancies

Thomas Günther

Vollständiger Abdruck der von der Fakultät für Chemie der Technischen Universität München zur Erlangung des akademischen Grades eines

Doktors der Naturwissenschaften (Dr. rer. nat.)

genehmigten Dissertation

Vorsitzender: Prof. Dr. Job Boekhoven

Prüfer der Dissertation:

1. Prof. Dr. Hans-Jürgen Wester
2. Prof. Dr. Matthias Eiber

Die Dissertation wurde am 22.06.2020 bei der Technischen Universität München eingereicht und durch die Fakultät für Chemie am 04.02.2021 angenommen.

„Success consists of going
from failure to failure
without loss of enthusiasm.“

– Winston Churchill –

Danksagung

Zu aller erst möchte ich mich bei Prof. Dr. Hans-Jürgen Wester für die vielen Möglichkeiten in den letzten sechs Jahren bedanken. Angefangen bei der Bachelorarbeit über Forschungspraktika und Masterarbeit bis hin zur Doktorarbeit. Ich bedanke mich ebenfalls für mein Bombesin-Thema, von dem ich behaupten kann, dass es mir von Tag eins bis jetzt sehr viel Spaß gemacht hat und es mir nach wie vor sehr viel bedeutet. Des Weiteren bedanke ich mich für die vielen gemeinsamen Diskussionen, die mich sehr gefördert und letztendlich zum Durchbruch bei meinem Forschungsprojekt verholfen haben. Ich bin Ihnen auch sehr dankbar, dass ich bereits an mehreren internationalen Konferenzen teilnehmen durfte, bei denen ich sehr viele Erfahrungen sammeln konnte. Zu guter Letzt schätze ich Ihr Vertrauen und dass Sie mir die Chance gegeben haben, weiter am Lehrstuhl zu bleiben und als Postdoc zu arbeiten. Hierbei freue ich mich auf die weitere, hoffentlich erfolgreiche Zusammenarbeit!

Ein weiterer sehr großer Dank gilt meiner Mentorin, Prof. Dr. Margret Schottelius, die mich mehr oder weniger in den letzten Jahren wissenschaftlich großgezogen hat. Ich werde nie vergessen, wie sich mich damals im Klinikum rechts der Isar als jungen Studenten in Empfang genommen und innerhalb der kurzen Zeit mein Interesse für die Pharmazeutische Radiochemie geweckt haben! Ebenfalls bedanke ich mich für die vielen Denkanstöße und Aufmunterungen während aller Arbeiten, bei denen Sie mich betreut haben.

Ich möchte mich auch bei allen ehemaligen Kollegen für die tolle Zusammenarbeit und die ein oder andere andauernde Freundschaft bedanken. Des Weiteren auch vielen Dank für sämtliche Tipps und Tricks, die ihr mir alle in den letzten Jahren beigebracht habt! Ebenso für alle Sachen, wobei ihr mir geholfen habt, egal ob praktisch oder theoretisch! Leider kann ich das alles gar nicht in der Ausführlichkeit beschreiben, wie ihr es verdient hättet. Deswegen ein besonders großes Dankeschön an Alex, Theresa, Steffi, Tina, Stephi, Andi, Moni, Sven, Frauke, Hannes, Behrooz, Kuba und Frau Kaul.

Des Weiteren ist es mir auch äußerst wichtig, all meinen Kollegen zu danken, die mich und meinen Humor seit sehr vielen Jahren fast täglich ertragen müssen. Ohne euch wäre der Laboralltag nicht so angenehm wie er es für mich ist und zudem hätte ich dann niemanden, den ich aufs Korn nehmen könnte. Aus diesem Grund ein super großes Dankeschön an Alex, Vroni, Daniel, Roswitha, Matthias, Mara, Markus, Basti, Jan-Philip, León, Jana, Tanja, Nicole und Christine. Ihr alle habt mit eurer Art mir gegenüber dazu beigetragen und tragt noch immer dazu bei, dass ich mich sehr wohl am Lehrstuhl fühle und nie die Lust an der Arbeit verloren habe! Ich würde lügen, wenn ihr nicht ein großer Grund dafür seid, dass ich über meine Promotion hinaus hierbleiben wollte. Ich freue mich daher auf hoffentlich noch viele schöne Momente mit euch, auch wenn natürlich in den nächsten Jahren einige gehen werden. Aber diese Zeit werde ich nie vergessen und ihr seid alle ein großer und wichtiger Teil gewesen!

Ein weiterer Dank gilt all meiner studentischen Helferleine, die ich in den Jahren betreuen durfte und denen ich hoffentlich ein bisschen Knowhow weitergeben konnte. Jeder von euch hat einen Teil zu

dieser Dissertation beigetragen und ohne euch hätte ich all dies nicht verwirklichen können! Ich bin mir sicher, dass ich die ein oder andere Person in den kommenden Jahren wieder an der Backe haben werde, aber darauf freue ich mich bereits sehr! Deswegen nochmal ein großer Dank an Basti, Nadine, Sandy, Katharina, Max, Amy, Clara, Simone, Julia und Christopher.

Ein großer Dank gilt auch allen klinischen Kooperationspartnern, die mir bei der klinischen Translation vielversprechender Liganden geholfen haben bzw. noch helfen werden. Deswegen nochmals vielen Dank an Prof. Dr. Wolfgang Weber, Prof. Dr. med. Matthias Eiber und Prof. Dr. med. Constantin Lapa. Ebenso die jeweiligen Teams dahinter, die sämtliche Radiosynthesen und sonstige notwendige Arbeiten verrichtet haben.

Ebenfalls Dankeschön an die Kollegen der Radiochemie, die uns in vielen Strahlenschutz-technischen Aspekten unterstützen und ohne die unsere tägliche Arbeit nicht möglich wäre!

Ein großes Dankeschön auch an all meine Freunde, die mich im Laufe meines Lebens begleitet haben und mir so ein eigentlich sehr einfaches und auch schönes Leben ermöglicht haben.

Ein besonderer Dank gilt natürlich meiner Familie, allen voran meinen Eltern, die mich großgezogen und fast drei Jahrzehnte unterstützt haben – finanziell und beratend. Ich hoffe, dass ich euch einen kleinen Teil davon in irgendeiner Form wieder zurückgeben kann. Danke auch an meine Brüder, Schwägerinnen und Schwager sowie Schwiegereltern für die stets liebevolle Art und dass wir uns so gut verstehen! Ebenfalls vielen Dank für all die süßen Neffen und Nichten, die entweder schon da sind oder noch kommen.

Zu guter Letzt noch ein infinites Dankeschön an die wichtigste Person in meinem Leben. Als ich dich vor über sieben Jahren kennengelernt habe, hätte ich nicht einmal im Traum daran gedacht, dass wir jetzt an diesem Punkt stehen und alles so perfekt laufen würde, wie es eben geschehen ist. Deshalb vielen Dank an meine Frau Elisabeth, dass du mich in all den Jahren so unterstützt hast und mir immer beigestanden bist! Ich bin mir sehr sicher, dass ich all das nicht in dieser Form geschafft hätte, wenn du nicht da gewesen wärst! Ich danke dir für die schönen Momente, die wir bereits gemeinsam erlebt haben und freue mich auf eine gemeinsame Zukunft mit dir und die schönen Momente, die noch kommen werden!

Table of Contents

Abstract

Aim: Due to the insufficient metabolic stability *in vivo* of currently known GRPR-targeted peptides as a consequence of proteolytic cleavage, especially by the neutral endopeptidase (NEP, EC 3.4.24.11), we investigated different structural modifications (cyclization, substitution by unnatural amino acids) to address these issues. Based on the structure of the current gold standard among gastrin-releasing peptide receptor (GRPR-) targeted ligands, RM2 (DOTA-Pip^{5}-phe^{6}-Gln^{7}-Trp^{8}-Ala^{9}-Val^{10}-Gly^{11}-His^{12}-Sta^{13}-Leu^{14}-NH_2), several analogs were designed and examined by state-of-the-art experiments (IC_{50}, log$D_{7.4}$, receptor-mediated internalization, plasma stability, biodistribution and imaging studies in mice). Furthermore, the novel radiohybrid (rh) concept developed by our group and successfully applied to prostate-specific membrane antigen (PSMA) inhibitors, was to be transferred to bombesin (BBN)-based compounds. Therefore, a silicon-fluoride-acceptor (SiFA) moiety and several *N*-terminal modifications required for the compensation of the bulky and lipophilic SiFA group, were introduced.

Methods: All compounds were synthesized *via* standard Fmoc-based solid-phase peptide synthesis (SPPS). ^{177}Lu-labeling was carried out at 95 °C within 10 min (1.0 M sodium acetate buffer, *pH* = 5.5, 0.1 M sodium ascorbate). GRPR affinity (IC_{50}) and receptor-mediated internalization (37 °C, 1 h) were evaluated on PC-3 cells. Lipophilicity (expressed as *n*-octanol/PBS distribution coefficient; log$D_{7.4}$) and metabolic stability *in vitro* in murine as well as in human plasma (37 °C, 72 ± 2 h) were investigated. Biodistribution studies 24 h post-injection (p.i.) and μSPECT/CT imaging 1, 4, 8, 24 and 28 h p.i. were carried out on PC-3 tumor-bearing CB17-SCID mice.

Results: Synthesis of the RM2 analogs *via* SPPS yielded 4-15% HPLC-purified labeling precursor. ^{177}Lu-labeling proceeded quantitatively. Among the designed ^{177}Lu-labeled RM2 derivatives, particularly those substituted by unnatural amino acids at the metabolically less stable Gln^{7}-Trp^{8} site, revealed promising overall data *in vitro* (IC_{50} [nM], log$D_{7.4}$, receptor-mediated internalization [%], metabolic stability in murine vs. human plasma [%]): RM2 (3.5 ± 0.2, −2.51 ± 0.02, 2.92 ± 0.20, 71.2 ± 3.6, 33.5 ± 2.7), NeoBOMB1 (4.2 ± 0.1, −0.57 ± 0.03, 13.91 ± 0.64, 73.5 ± 3.4, 60.8 ± 1.2), DOTA-[Cit^{7}]MJ9 (11.6 ± 2.1, −3.22 ± 0.15, 1.82 ± 0.16, 72.9 ± 0.8, 38.3 ± 12.4), DOTA-[Hse^{7}]MJ9 (19.7 ± 1.6, −2.25 ± 0.06, 1.40 ± 0.16, 70.8 ± 3.5, 45.4 ± 7.6), DOTA-[Bta^{8}]MJ9 (4.6 ± 0.2, −1.81 ± 0.02, 2.26 ± 0.18, 58.3 ± 6.0, 16.2 ± 3.5), DOTA-[α-Me-Trp^{8}]MJ9 = AMTG (3.0 ± 0.1, −2.28 ± 0.06, 3.03 ± 0.18, 75.0 ± 11.5, 77.6 ± 10.1) and DOTA-GA-[α-Me-Trp^{8}]MJ9 = AMTG2 (4.7 ± 0.2, −2.51 ± 0.11, 5.88 ± 0.33, 80.8 ± 3.8, 64.4 ± 4.7).

In vivo, [^{177}Lu]AMTG exhibited the highest tumor-to-blood ratio 24 h p.i. as well as a favorable overall biodistribution profile. As demonstrated by μSPECT/CT imaging, [^{177}Lu]AMTG revealed a less rapid clearance from the tumor and the pancreas than [^{177}Lu]RM2. Interestingly, both DOTA-[Hse^{7}]MJ9 and DOTA-[Bta^{8}]MJ9, which showed low tumor-to-background ratios 24 h p.i., displayed favorable biodistribution profiles 1 h p.i., as tumor uptake was comparable or even increased to RM2 but clearance from

non-tumor organs was more rapid. Despite several *N*-terminal linker modifications, BBN-SiFA ligands suffered from moderate GRPR affinity and lipophilicity, which resulted in low retention in the tumor 24 h p.i. Moreover, high renal retention (> 100 %ID/g) was observed, most likely as a consequence of the various hydrophilic modifications.

Due to its favorable preclinical data *in vitro* and *in vivo*, AMTG was selected for a proof of concept (PoC) study in a prostate cancer (PCa) patient, which revealed high accumulation of [^{177}Lu]AMTG in several tumor lesions 1 and 4 h p.i.

Conclusion: Based on its improved metabolic stability and very promising overall data, the novel GRPR-targeted antagonist AMTG might have the potential to outperform the current gold standards among GRPR-targeted ligands (RM2, NeoBOMB1) for targeted radiotherapy in men. Both modifications, homoserine (Hse) and *β*-(3-benzothienyl)alanine (Bta), could be useful for the future design of diagnostic compounds, as both revealed superior pharmacokinetics in the early window due to a decreased metabolic stability, which accelerated clearance from non-tumor organs, whereas tumor uptake was not negatively affected. BBN-SiFA ligands require further optimization within the *N*-terminal linker section, as retention in the kidneys was massively increased for these compounds, whereas retention in the tumor was low 24 h p.i.

Kurzzusammenfassung

Zielsetzung: Aufgrund unzureichender metabolischer Stabilität *in vivo* gegenwärtig eingesetzter GRPR-gerichteter Peptide als Konsequenz proteolytischer Spaltung, insbesondere durch die Neutrale Endopeptidase (NEP, EC 3.4.24.11), wurden verschiedene strukturelle Modifikationen (Zyklisierung, Substitution durch unnatürliche Aminosäuren) untersucht, um dieses Problem zu beheben. Basierend auf der Struktur des Goldenen Standards innerhalb der gastrin-releasing peptide receptor (GRPR-) gerichteten Liganden, RM2 (DOTA-Pip^{5}-phe^{6}-Gln^{7}-Trp^{8}-Ala^{9}-Val^{10}-Gly^{11}-His^{12}-Sta^{13}-Leu^{14}-NH_2), wurden mehrere Analoga entworfen und in State-of-the-Art Experimenten (IC_{50}, log$D_{7.4}$, Rezeptor-induzierte Internalisierung, Plasmastabilität, Biodistributions- und Bildgebungsstudien in Mäusen) untersucht. Des Weiteren sollte das neue Radiohybrid (rh) Konzept, welches in unserer Gruppe entwickelt und erfolgreich bei Prostata-spezifischen Membranantigen (PSMA) Inhibitoren angewandt wurde, auf Bombesin (BBN)-basierte Verbindungen übertragen werden. Hierfür wurde eine Silikon-Fluorid-Akzeptor (SiFA) Einheit sowie mehrere *N*-terminale Modifikationen eingeführt, welche zur Kompensation der sperrigen, lipophilen SiFA Gruppe notwendig waren.

Methoden: Alle Verbindungen wurden durch Fmoc-basierte Festphasen-Peptidsynthese (SPPS) hergestellt. ^{177}Lu-Markierungen wurden bei 95 °C in 10 min durchgeführt (1.0 M Natriumacetat-Puffer, pH = *pH* = 5.5, 0.1 M Natriumascorbatlösung). Die GRPR-Affinität (IC_{50}) und die Rezeptor-induzierte Internalisierung (37 °C, 1 h) wurde auf PC-3 Zellen evaluiert. Die Lipophilie (als *n*-Octanol/PBS-Distributionskoeffizient ausgedrückt; log$D_{7.4}$) und die metabolische Stabilität *in vitro* in murinem und humanem Plasma (37 °C, 72 ± 2 h) wurde untersucht. Biodistributionsstudien 24 h p.i. sowie Bildgebung *via* μSPECT/CT 1, 4, 8, 24 und 28 h p.i. wurden in PC-3 Tumor-tragenden CB17-SCID Mäusen untersucht.

Ergebnisse: Die Synthese der RM2-Analoga durch SPPS wurden 4-15% an HPLC-aufgereinigtem Markierungsvorläufer erhalten. Die ^{177}Lu-Markierungen verliefen quantitativ. Innerhalb der synthetisierten ^{177}Lu-markierten RM2-Derivate zeigten vor allem diejenigen vielversprechende *in vitro*-Daten (IC_{50} [nM], log$D_{7.4}$, Rezeptor-induzierte Internalisierung [%], metabolische Stabilität in murinem vs. Humanem Plasma [%]), welche an der unstabilen Gln^{7}-Trp^{8} Stelle durch unnatürliche Aminosäuren substituiert wurden: RM2 (3.5 ± 0.2, −2.51 ± 0.02, 2.92 ± 0.20, 71.2 ± 3.6 vs. 33.5 ± 2.7), NeoBOMB1 (4.2 ± 0.1, −0.57 ± 0.03, 13.91 ± 0.64, 73.5 ± 3.4 vs. 60.8 ± 1.2), DOTA-[Cit^{7}]MJ9 (11.6 ± 2.1, −3.22 ± 0.15, 1.82 ± 0.16, 72.9 ± 0.8 vs. 38.3 ± 12.4), DOTA-[Hse^{7}]MJ9 (19.7 ± 1.6, −2.25 ± 0.06, 1.40 ± 0.16, 70.8 ± 3.5 vs. 45.4 ± 7.6), DOTA-[Bta^{8}]MJ9 (4.6 ± 0.2, −1.81 ± 0.02, 2.26 ± 0.18, 58.3 ± 6.0 vs. 16.2 ± 3.5), DOTA-[α-Me-Trp^{8}]MJ9 = AMTG (3.0 ± 0.1, −2.28 ± 0.06, 3.03 ± 0.18, 75.0 ± 11.5 vs. 77.6 ± 10.1) und DOTA-GA-[α-Me-Trp^{8}]MJ9 = AMTG2 (4.7 ± 0.2, −2.51 ± 0.11, 5.88 ± 0.33, 80.8 ± 3.8 vs. 64.4 ± 4.7).

[^{177}Lu]AMTG zeigte *in vivo* 24 h nach Injektion (p.i.) die höchsten Tumor-zu-Blut- und Tumor-zu-Muskel-Verhältnisse sowie ein vorteilhaftes Biodistributionsprofil. Wie durch Bildgebung mit μSPECT/CT gezeigt, offenbarte [^{177}Lu]AMTG eine langsamere Clearance aus dem Tumor und dem Pankreas als [^{177}Lu]RM2. Interessanterweise zeigten sowohl DOTA-[Hse^{7}]MJ9 als auch DOTA-[Bta^{8}]MJ9 vorteilhafte Biodistributionsprofile 1 h p.i., obwohl beide geringe Tumor-zu-Hintergrund-Verhältnisse 24 h p.i. vorzeigten. Dies war dadurch gegeben, dass die Tumoraufnahme vergleichbar oder sogar verbessert war als bei RM2 und gleichzeitig die Clearance aus Nicht-Tumor-Organen schneller verlief. Trotz mehrerer *N*-terminaler Modifikationen litten BBN-SiFA-Liganden unter der moderaten GRPR-Affinität und Lipophilie, was in einer geringen Tumorretention resultierte. Des Weiteren wurden hohe renale Retentionen (> 100 %ID/g) beobachtet, was höchstwahrscheinlich der Vielzahl an hydrophilen Modifikationen geschuldet ist.

Aufgrund seiner vorteilhaften präklinischen *in vitro*- und *in vivo*-Daten wurde AMTG für eine Proof-of-Concept (PoC) Studie in einem Prostatakrebs (PCa) Patienten ausgewählt, welche eine hohe Akkumulation von [^{177}Lu]AMTG in mehreren Tumorläsionen 1 und 4 h p.i. zeigte.

Schlussfolgerung: Aufgrund seiner verbesserten metabolischen Stabilität und äußerst vielversprechenden Daten, könnte der neue GRPR-gerichtete Antagonist AMTG das Potential haben, die gegenwärtigen Goldenen Standards innerhalb der GRPR-gerichteten Liganden (RM2, NeoBOMB1) bei der Endoradiotherapie zu übertreffen. Beide Modifikationen, Homoserine (Hse) und β-(3-benzothienyl)alanin (Bta) könnten für das Design zukünftiger Verbindungen nützlich sein, da beide eine verbesserte Pharmakokinetik zu früheren Zeitpunkten offenbarten. Dies war einer verringerten metabolischen Stabilität geschuldet, welche zu einer beschleunigten Clearance aus Nicht-Tumor-Organen führte, wohingegen die Tumoraufnahme nicht negativ beeinflusst wurde. Die BBN-SiFA-Liganden benötigen weitere Optimierungen innerhalb des *N*-terminalen Linkers, da die Nierenretention dieser Verbindungen massiv erhöht, die Tumorretention 24 h p.i. aber gering war.

I. Introduction

1. General

As a consequence to poor survival rates at progressed stages of disease, prostate cancer (PCa) and breast cancer (BCa), the most common cancer types in the respective sexes globally, remain difficult tasks to medical treatment[1-3]. As it was shown that treatment success is higher the sooner it is diagnosed and treated, new options for early detection and treatment are desired[1, 4].

PCa is commonly screened by digital rectal examination (DRE) or elevated prostate specific antigen (PSA) values in the blood. However in both cases, biopsy and subsequent histopathological verification are necessary to confirm the medical diagnosis[5]. Whereas increased PSA levels are a potential indicator for early-stage disease, biopsy-detected PCa revealed that high-grade disease is not infrequently found in men showing normal PSA levels[6, 7]. On the contrary, elevated PSA values were also determined in case of non-malignant conditions, such as prostatitis or benign prostatic hyperplasia (BPH)[8, 9].

For diagnosis of BCa, screening methods such as mammography, which reveals reliable findings especially in women above the age of 50, and ultrasonography examination of the breast are the ones most commonly used[10, 11]. However, mammography is reportedly more controversial in younger women (age < 50), most commonly due to over-diagnosis[12-14]. Although mammography is strongly recommended by medical guidelines, additional biopsy is often required in order to prevent false-positive findings[13].

Improved prognosis for different cancer types has been accomplished since introduction of the Gleason score (GS), a value obtained by histological examination of glandular tissue from biopsy samples. An elevated GS generally correlates with advanced disease and poor survival prognosis[15, 16]. Furthermore, the TNM (tumor, node, metastasis) classification was implemented for accurate staging of the disease. Therefore, extent of the main tumor (T), possible infiltration of adjacent lymph nodes (N) as well as probably present metastasis (M) are described[17]. Non-invasive techniques, such as computed tomography (CT), magnetic resonance imaging (MRI) and bone scintigraphy are also used for tumor localization and staging although reliable visualization remains difficult[4, 5].

Over the last decades, application of positron emission tomography (PET) or single-photon emission computed tomography (SPECT), mostly in combination with CT or MRI have gathered growing interest[18]. Both non-invasive techniques are based on radiolabeled molecules, which accumulate fast and almost exclusively at the tumor site[19]. This allows for an improved detection rate compared to conventional imaging methods[20, 21].

Considering PCa, prostate-specific membrane antigen (PSMA) addressing tracers are currently most commonly used for imaging and targeted radiotherapy (TRT) of PCa the[22]. Nevertheless, due to its abundance and overexpression in PCa and BCa, the gastrin-releasing peptide receptor (GRPR) has emerged as a viable alternative[23-26]. GRPR is found to show higher expression levels and density in early

stages of PCa whereas PSMA overexpression is observed to be higher in advanced stages of disease[24, 27, 28]. Furthermore, especially estrogen receptor (ER)-rich BCa (ER expressed in over 80% of all breast cancers) and its metastases show high GRPR expression[29, 30].

For this reason, GRPR-targeted tracers could be a useful tool as an alternative for PCa patients with low or absent PSMA expression. Additionally, the same GRPR-addressing ligands could also be applied for diagnosis and therapy of BCa.

2. The gastrin-releasing peptide receptor (GRPR)

2.1. Composition of bombesin receptors

The mammalian bombesin (BBN) receptor family consists of the neuromedin-B receptor (NMBR, BB_1), the gastrin-releasing peptide receptor (GRPR, BB_2) as well as the bombesin receptor subtype 3 (BRS-3, BB_3). As part of the family of G protein-coupled receptors (GPCR), the three receptors show similarities among each other and also with other GPCRs, for example somatostatin (SST) and cholecystokinin (CCK) receptors[31].

Each of the mentioned receptors contains seven regions of hydrophobic amino acids, which are compatible with the typical seven transmembrane structure of GPCRs (**Fig. 1**, solid boxes)[32]. The human GRPR protein comprises 384 amino acids and shows a homology of about 90% to the murine GRPR protein[32]. Furthermore, human GRPR demonstrates an amino acid overlap of 55% to human NMBR (**Fig. 1**) and an amino acid similarity of 51% to human BRS-3[32, 33].

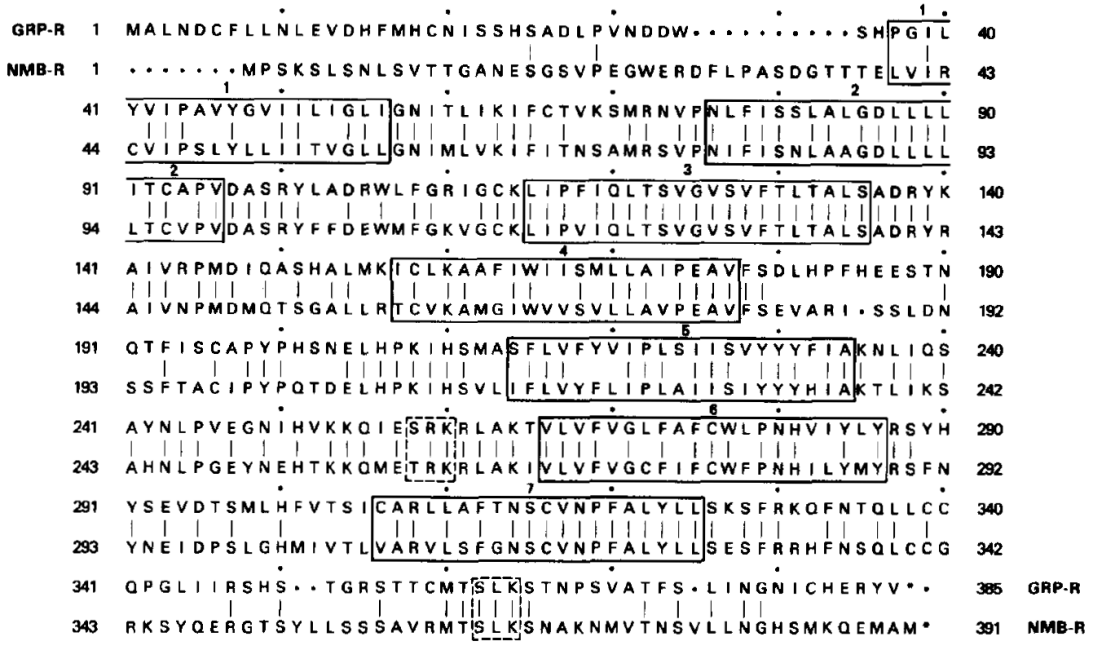

Fig. 1: Amino acid overlap for human GRPR (upper sequence) and NMBR (lower sequence). Vertical lines show amino acid identity between both receptors. Seven regions composed predominantly of hydrophobic amino acids, and which as such are indicators of the typical transmembrane domains of GPCRs, are shown for both receptors (solid boxes)[32].

Each of the three mammalian BBN receptors comprises a conserved DRY (Asp-Arg-Tyr) sequence within the second intracellular loop as well as many serine (S) and threonine (T) residues within the intracellular tail (**Fig. 1**-**2**). The DRY sequence was shown to be essential for binding of the heterotrimeric G protein in most GPCRs. S and T residues enable binding of protein kinase C (PKC), which is responsible *inter alia* for down-regulation of the receptor after its activation[31, 34].

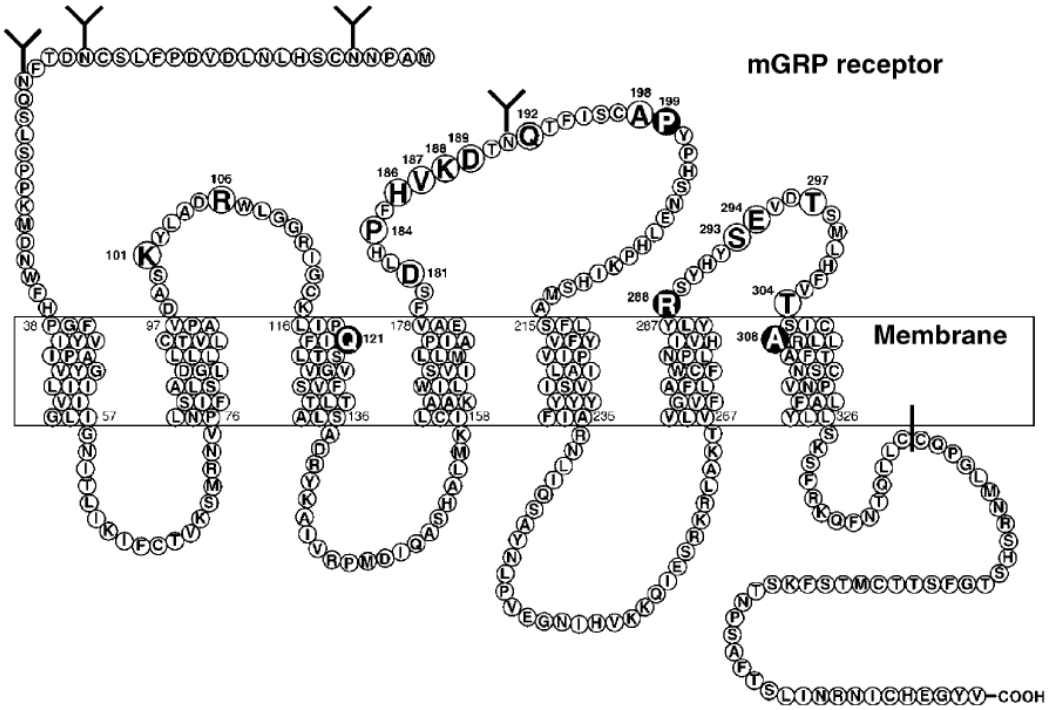

Fig. 2: Amino acid sequence of the murine GRPR (90% identity to human GRPR), displaying the extracellular side above and the intracellular side below. Glycosylation sites are shown by asparagine residues (N) containing a Y symbol. The 14 amino acids within the extracellular side, which are assumed to play important roles for high affinity binding of the gastrin-releasing peptide (GRP), are highlighted by white circles[35].

The molecular mass of human and murine GRPR has been determined to 60 ± 1 kDa and 82 ± 2 kDa, respectively. The noticeably enhanced molecular mass of the murine GRPR, despite its high sequential homology, is attributed to two additional glycosylated asparagine (N) sites[36].

Selectivity studies by *Nakagawa et al.* exhibited several amino acids (**Fig. 2**, white circles) within the extracellular domain (EC) of the murine GRPR that are responsible for high affinity binding of the mammalian endogenous ligand, the gastrin-releasing peptide (GRP)[35]. Additionally, *Nakagawa et al.* estimated a large cavity between the seven transmembrane regions and the extracellular loops for the murine GRPR by molecular modeling, which was associated with the putative binding pocket (**Fig. 3**, orange)[35]. Furthermore, the helical transmembrane domains were expected to be rigid, for which reason amino acid residues within these domains are only able to rotate their side chains for potential interactions with ligands[35]. In contrast, extracellular loops were assumed to be more flexible, allowing their amino acids more possibilities to shift towards feasible interactions[35]. Several amino acids pointing inwards within a distance of less than 6 Å to the putative binding pocket were determined to be important for ligand binding (**Fig. 3**, yellow and green colored amino acids)[35].

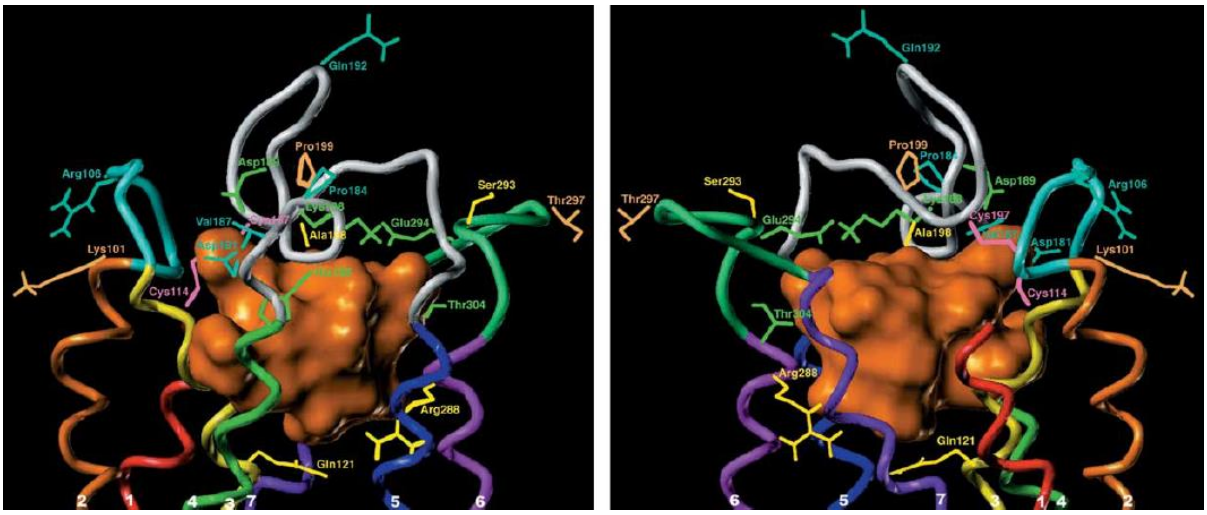

Fig. 3: Molecular modeling of the murine GRPR from both sides of view, revealing seven rigid helical transmembrane domains and the more flexible extracellular loops (cyan, white, dark green). The large putative binding pocket (orange) is located between the seven transmembrane regions and the extracellular loops. Several colored amino acids pointing towards the binding pocket were determined to be important for ligand binding (yellow and green colored amino acids)[35].

Early structure activity relationship (SAR) studies of the natural, amphibian tetradecapeptide bombesin (*H*-pGlu[1]-Gln[2]-Arg[3]-Leu[4]-Gly[5]-Asn[6]-Gln[7]-Trp[8]-Ala[9]-Val[10]-Gly[11]-His[12]-Leu[13]-Met[14]-NH_2) showed that its aromatic amino acids (Trp[8] and His[12]) play a key role in biologic activity for BBN receptors[31]. This was indirectly confirmed *via* computational analysis by *Sharma et al.*, reporting a helical arrangement of the ligand inside GRPR, which is stabilized by π-π stacking through Trp and His[37].

Further SAR studies revealed that the two *C*-terminal amino acids of BBN analogs are not necessary for receptor binding but indeed, for its activation and internalization[31]. Thus, most antagonists are designed by disruption of the *C*-terminal amino acid or introduction of a pseudopeptide bond between the penultimate and the last amino acid at the *C*-terminus[31, 38-42]. This likely leads to enhanced flexibility and rotational freedom of the *C*-terminus within the receptor due to the absence of hydrogen bonding, which then impedes its biological activation[43]. However, as GRPR shows enhanced tolerance towards this grade of flexibility compared to NMBR or BRS-3, there are noticeably more GRPR antagonists available to date[31].

2.2. Occurrence of GRPR

Expression of GRPR mRNA was found in several human tissues, especially in the pancreas and the gastrointestinal (GI) tract[44]. Binding of GRP to GRPR mediates a variety of physiological and pathophysiological processes, such as stimulating contraction of smooth muscle cells in the GI tract and the urogenital system[31, 45]. GRPR-GRP interaction also plays a significant role in secretion and releasing of gastrointestinal hormones and neurotransmitters, for example gastrin, insulin and somatostatin (SST)[45-47].

Moreover, GRPR mRNA expression levels were also discovered in the central nervous system (CNS) and the brain. Studies with GRPR knockout mice, which are not able to express GRPR, revealed issues concerning regulation of circadian rhythm, body temperature, anxiety behavior and satiety[31, 48]. For this reason, a similar role of GRPR in human CNS is presumed but has not yet been confirmed[45]. Binding of GRP to GRPR was also reported to have distinct effects on immune cells[49]. Additionally, GRPR is further supposed to play a key role in early fetal lung branching[50].

In addition to occurring in a variety of healthy tissues, GRPR expression was also observed in a multitude of malignant tissues. It was found *inter alia* in PCa (100% in early stages, ~60% in later stages of disease), BCa (76%), colorectal cancer (24-100%), SCLC (53%), NSCLC (63%), glio-/neuroblastomas (72-85%) and head/neck squamous cell cancers (up to 100%)[25, 30, 31, 51-53]. However, in these studies, the discovery of even small amounts of GRPR mRNA was counted as positive for this statistic, alhough, most of these expression levels are too insignificant for successful targeting by radiopharmaceuticals. For the usually administered pico- or nanomolar ligand concentrations in nuclear medicine, high receptor densities on the respective tumor cells are necessary to obtain appropriate amounts of bound activity.

Using autoradiographic methodology, *Reubi et al.* determined GRPR expression densities in a variety of tumors. Therefore, receptor density values were estimated by disintegrations per minute per milligram tissue (dpm/mg), whereas values beyond 1000 dpm/mg and 5000 dpm/mg were considered as high and very high receptor densities, respectively[25, 26, 54, 55]. However, the authors suggested that a receptor density of > 2000 dpm/mg can be considered as sufficient for radiotherapy[26]. Mean receptor density of GRPR in PCa and BCa was determined as approximately 5000 dpm/mg and 10000 dpm/mg, respectively[25, 26, 54]. In contrast to the high expression density in malignant PCa tissue, its respective receptor density in benign prostatic hyperplasia (BPH) and normal prostate tissue was ascertained to be either absent or very low[54, 56]. Nevertheless, several reports showed that GRPR expression in high densities is present especially in primary PCa (85-100%), which decreases in later, Androgen-independent stages of disease (~50%)[51, 54, 57, 58].

GRPR was also found to be overexpressed in high density in over 70% of primary BCa, especially in estrogen receptor (ER) rich BCa[26, 30, 59]. *Dalm et al.* demonstrated high mRNA levels of somatostatin-2 receptor (SST2R) and GRPR in about 75% of ER-positive tissues, whereas ER-negative tissue exhibited rather high C-X-C chemokine receptor type 4 (CXCR4) expression[29]. Additionally, it was shown that high GRPR expression in primary BCa is retained in 95% of nodal metastases[29, 30]. Not surprisingly, several studies with different ^{68}Ga-labeled GRPR-targeted tracers enabled high-contrast imaging of (ER-positive) BCa[60-62].

Good uptake of GRPR-targeted compounds was also found in normal breast tissue[61, 62]. Interestingly, uptake seemed to correlate with menstrual cycle of pre-menopausal women, as accumulation in the secretory phase was increased. In comparison, post-menopausal women as well as women in the non-secretory phase revealed decreased uptake. The authors suggested an influence of the menstrual cycle on ER expression, which is known to correlate with GRPR expression[62]. Nonetheless, this has to be considered when administering GRPR-addressing radiopharmaceuticals, as this accumulation characteristic could negatively influence the contrast of malignant and healthy breast tissue.

As already mentioned, GRPR expression has also been determined in non-small cell lung cancer (NSCLC), small cell lung cancer (SCLC) and a variety of cancers in the gastrointestinal tract. However, in most cases, expression was associated with minor receptor densities [53, 63, 64].

2.3. Differences to PSMA expression in prostate cancer (PCa)

The prostate-specific membrane antigen (PSMA) is a type II transmembrane glycoprotein, which comprises 750 amino acids and has a molecular weight of ~100 kDa[65]. It is also known as folate hydrolase I, *N*-acetyl-L-aspartyl-L-glutamate peptidase I as well as carboxypeptidase II and requires dimerization for enzymatic activity[66, 67]. In healthy tissue, it is highly expressed in the proximal tubules of the kidney, the salivary glands, the spleen and duodenum[68]. Low expression is also found in the cell membrane of healthy prostate cells[66, 68]. Nonetheless, overexpression in PCa cells is found to be noticeably higher than in normal prostate cells (up to 1000-fold)[68, 69].

PSMA expression correlates with the stage of PCa with highest levels found in later stages, especially in hormone-refractory and metastatic castration-resistant PCa (mCRPC) patients[70, 71]. Radiolabeled PSMA inhibitors typically show fast blood clearance and rapid tumor accumulation, most likely due to the high affinity and low lipophilicity of the small molecules[72-74]. Not surprisingly, ^{18}F- and ^{68}Ga-labeled as well as ^{177}Lu-labeled PSMA-targeted ligands demonstrated intense uptake in PCa lesions and allowed for the detection or therapy of even small metastases[69, 74-79].

However, PSMA expression in Androgen-dependent stages seems to be unfavorable, thus requiring alternatives for improved primary staging[60, 80, 81]. This could open up a niche for other targets, for example GRPR, which demonstrates overexpression more commonly in early, Androgen-dependent stages of PCa (**Fig. 4**)[51, 52, 60].

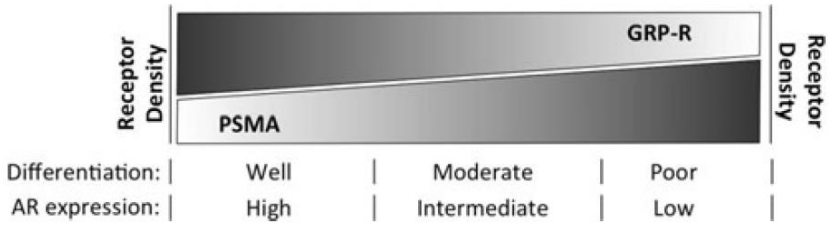

Fig. 4: Simplified model for the differences between GRPR and PSMA in PCa in terms of receptor expression density compared to the grade of histological differentiation and expression of the Androgen receptor (AR)[60].

A meaningful comparison between PSMA- and GRPR-targeted ligands for PCa is difficult because there are few studies that investigate both tracers within the same patients. However in general, PSMA-targeted compounds reveal significantly higher standardized uptake values (SUVs) in tumor lesions compared to GRPR-targeted analogs[20, 72]. On the one hand, a recent study by *Hoberück et al.* revealed no additional benefit for eight PSMA-negative patients using [^{68}Ga]RM2, as no uptake was observed in any of these patients[75]. On the other hand, *Minamimoto et al.* reported a comparative study in seven PCa patients with BCR (GS = 6-9) using both, [^{68}Ga]PSMA-11 and [^{68}Ga]RM2. In this study, no significant differences were observed between these two compounds in most patients in terms of tumor detection, as SUV_{mean} was comparable for both (**Fig. 5**)[82]. Obviously, biodistribution was different, as the GRPR-

targeted compound was only observed in the pancreas and the bladder whereas the PSMA-targeted analog was found in the kidneys, the salivary glands, the liver and the spleen[82].

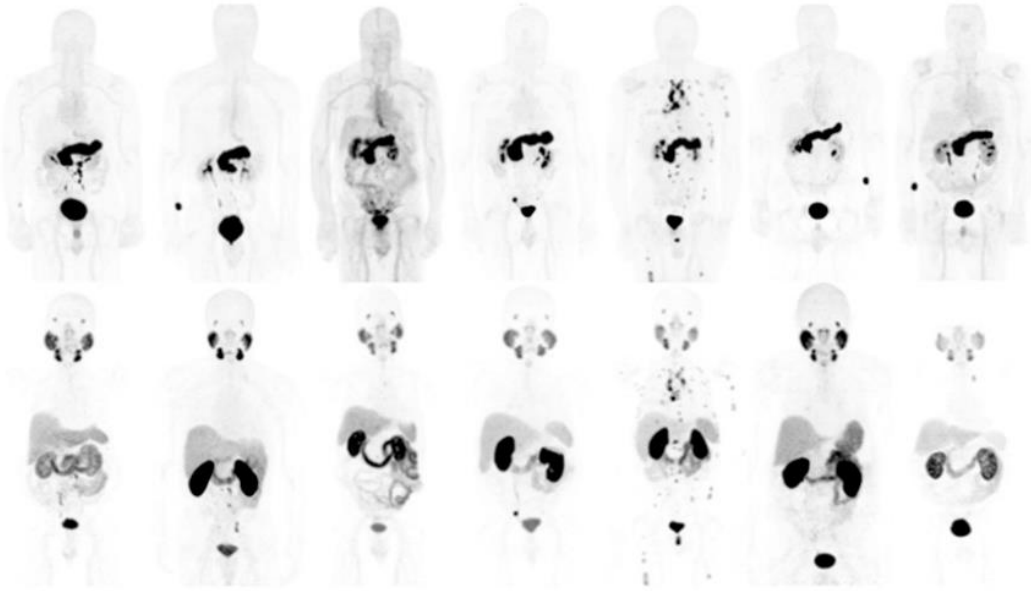

Fig. 5: Whole body scan of seven PCa patients examined with both, [^{68}Ga]RM2 (above) and [^{68}Ga]PSMA-11 (below) revealing different biodistribution but comparable uptake in tumor lesions[82].

Schollhammer et al. reported that [^{111}In]RM2 was able to discriminate between low-risk PCa and intermediate-risk PCa samples *in vitro*, which was not observed for [^{111}In]PSMA-617 in the same samples[83]. This could be beneficial for primary staging of PCa and support a superior role of GRPR-targeted agents for imaging and improved staging. Interestingly, *Baratto et al.* report a patient examined with both, [^{68}Ga]RM2 and [^{68}Ga]PSMA-11, revealing two different primary PCa lesions in the same patient[84]. Therefore, a complementary role of GRPR- and PSMA-targeted ligands in PCa patients is assumed.

Nonetheless, based on the generally lower GRPR expression in advanced stages and the higher expression at early stages of PCa, it would be preferable to address early-stage PCa with BBN-based analogs[20, 58, 75, 83, 85, 86]. However, as shown for some patients so far, there is a possibility of positive GRPR-targeted imaging and therapy in PSMA-negative patients despite an advanced stage character[87]. For this reason, more data is necessary for GRPR-targeted conjugates in order to understand their clinical impact.

3. Design of GRPR-targeted ligands

3.1. Historical development

The tetradecapeptidic hormone BBN was first isolated in 1971 from the skin of the frog *Bombina bombina*, which was adopted eponymously for this class of ligands[88]. The 27 amino acid containing GRP, exhibiting ten equal amino acids to BBN at the *C*-terminus except for position 7 (His^7 instead of Gln^7), was first isolated from porcine stomach (1979) and later also discovered in humans[89]. Both are natural ligands with high affinity for GRPR, for which reason both were used as a lead structure for early radiopharmaceutical purposes.

Therefore, either a chelating agent was attached at the *N*-terminus or radioiodination was performed in order to generate radiolabeled analogs[90]. However, radiolabeled BBN and GRP demonstrated rapid degradation *in vivo*, which was addressed by co-injection of Phosphoramidon (PA), an inhibitor of the neutral endopeptidase (NEP, EC 3.4.24.11) amongst others[91, 92]. This protease is shown to cleave peptidic sequences at the *N*-terminal side of hydrophobic residues and is considered a main issue for BBN-based structures *in vivo*[93-95]. Nonetheless, in order to limit potential side effects in humans, application of tracers without co-administration of enzyme inhibitors is preferred, as a lot of such compounds are found to be toxic to the GI tract or the pancreas[96].

For this reason, BBN/GRP derivatives have to be structurally modified, for example *via* substitution by unnatural amino acids[97, 98]. As GRP derivatives were shown to be highly unstable *in vivo*, ligand development has concentrated on the structure of BBN for further modifications[99]. Therefore, general numbering of GRPR-targeted conjugates is based on the 14 amino acid sequence of the natural BBN (**Fig. 6**).

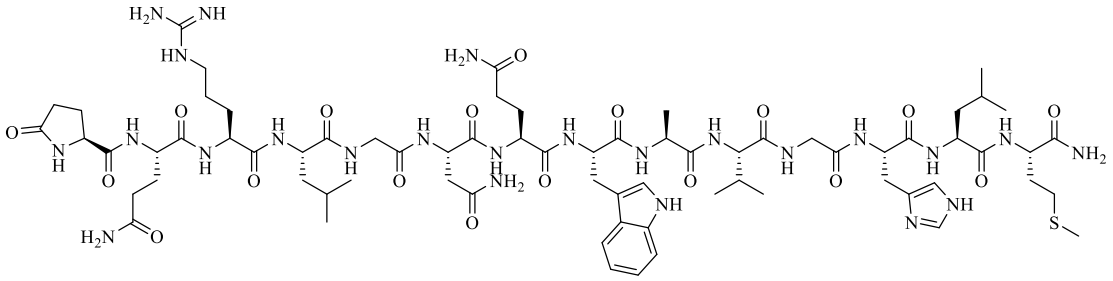

***H*-pGlu^1-Gln^2-Arg^3-Leu^4-Gly^5-Asn^6-Gln^7-Trp^8-Ala^9-Val^{10}-Gly^{11}-His^{12}-Leu^{13}-Met^{14}-NH$_2$**

Fig. 6: Molecular structure of the tetradecapeptide bombesin, which typically forms the basis for numbering of GRPR-targeted analogs.

Truncated BBN conjugates, likewise BBN$_{6\text{-}14}$ analogs, were shown to retain their biological activity. Concurrently, increased metabolic stability *in vivo* was determined after introducing a D-phenylalanine (phe^6) moiety at the *N*-terminal position[43, 100-102]. Substitution of phe^6 by the structurally similar tyr^6 additionally enabled ^{125}I-labeling by means of the Iodo-Gen® method. This yielded the potent GRPR-addressing conjugate [3-[^{125}I]*I*-tyr^6, *β*-Ala^{11}, Phe^{13}, Nle^{14}]BBN$_{6\text{-}14}$, which is also called universal radioligand. Unexpectedly, this derivative also displayed high affinity to each of the other two mammalian

BBN receptors as well as a fourth BBN receptor, which is found in amphibians but not in mammals[25, 102, 103]. By virtue of its poor selectivity towards each BBN receptor, further analogs were required to successfully address only GRPR-expressing tumor sites in animal studies and humans.

Due to the former belief that compounds have to internalize in order to yield prolonged retention in tumors, only agonists were designed initially[90, 97, 104]. This was challenging because modifications within the pharmacophore (Gln^{7}-Trp^{8}-Ala^{9}-Val^{10}-Gly^{11}-His^{12}) as well as its peptide backbone were reported to noticeably decrease GRPR affinity[43, 105-107]. Furthermore, agonists were observed to clear relatively slowly from GRPR-positive non-tumor organs, likewise the pancreas and the GI tract. This resulted in unfavorable tumor-to-background (T/B) ratios in PET and SPECT images[108, 109]. Additionally, GRPR agonists caused severe side effects after intravenous administration, for example nausea, diarrhea and abdominal cramps[58, 110].

Since SST receptor antagonists were shown to exhibit unexpectedly superior characteristics *in vivo* compared to agonists, the focus of GRPR research also shifted towards antagonistic structures [111]. Disruption of the *C*-terminal amino acid or deletion of the carbonyl oxygen between positions 13 and 14 did not cause significant loss of receptor affinity, but resulted in antagonists[43]. Interestingly, GRPR antagonists displayed noticeably improved selectivity towards the other BBN receptors. It was supposed that both NMBR and BRS-3 are not as tolerable towards *C*-terminal modifications as GRPR. This would explain why there are noticeably more antagonistic ligands available for GRPR- than for NMBR-/BRS-3-targeting[31].

Comparison of GRPR-targeted antagonists and agonists within the same tumor model revealed higher uptake and retention in tumors as well as a more rapid clearance from GRPR-positive non-tumor organs[108, 109, 112]. Moreover, antagonists were not observed to cause side effects after intravenous administration[56, 87, 113]. Thus, most GRPR-targeted derivatives nowadays are designed with antagonistic character[39, 41, 114]. However, there are also reports of agonistic BBN analogs, especially concerning potential α-radiation therapy[115-117].

3.2. State of the art in the development of BBN-based ligands

Over the last decade, several GRPR-targeted conjugates have been developed and evaluated preclinically, whereas only a few were investigated in clinical studies[20, 40, 58, 66, 85, 87, 118, 119]. Despite some promising results, there is currently no GRPR-targeted ligand in clinical routine. This is likely due to the limited data available from the small patient cohorts examined so far. Nonetheless, there are some positive examples for successfully administered BBN analogs for imaging (and therapy) of GRPR-targeted tumor lesions, which will be discussed below.

3.2.1. Imaging with GRPR-targeted tracers

3.2.1.1. Currently used isotopes and BBN-based compounds

^{99m}Tc-technetium

In recent years, several ^{99m}Tc-labeled GRPR-addressing conjugates for SPECT imaging were reported, demonstrating some positive findings preclinically and clinically[40, 58, 60, 120, 121]. Due to its favorable properties ($t_{1/2}$ = 6.0 h, E_{max} = 141 keV), its excellent availability from commercially distributed ^{99}Mo/^{99m}Tc generators and ease of synthesis, ^{99m}Tc-technetium is widely used in nuclear medicine[122]. Early ^{99m}Tc-labeled GRPR agonists, which were examined in mice, suffered either from low tumor uptake or high uptake in background organs, such as pancreas, liver and intestine[123-126].

Nonetheless, in a first-in-man study using [^{99m}Tc]Demobesin-4 some tumor lesions could be detected, especially in patients with early-stage PCa[58]. More recently, *Nock et al.* demonstrated enhanced tumor uptake and retention in mice with several mimics of the potent antagonist [^{99m}Tc]Demobesin-1 ([^{99m}Tc]N_4'-diglycolate-[phe^6, Leu-NHEt^{13}]BBN_{6-13}) though, mostly at cost of increased accumulation in the pancreas and the intestine[40].

Kaloudi et al. also reported two GRP-based tracers, [^{99m}Tc]N_4-GRP_{14-27} and [^{99m}Tc]N_4-GRP_{18-27}, which exhibited good tumor uptake 4 h p.i. (8.4 ± 4.2 %ID/g and 7.1 ± 1.3 %ID/g, respectively). However, uptake in pancreas and intestine at the same time was also high (35.2 ± 4.7 %ID/g and 7.6 ± 2.2 %ID/g [N_4-GRP_{14-27}] as well as 35.2 ± 4.7 %ID/g and 7.6 ± 2.2 %ID/g [N_4-GRP_{18-27}], respectively). Co-injection of the enzyme inhibitor PA increased tumor uptake 4 h p.i. noticeably (38.2 ± 4.8 %ID/g and 28.4 ± 8.1 %ID/g, respectively) although pancreas accumulation rose to about 100 %ID/g for both analogs[121]. For this reason, there is still a lot of room for improvement concerning ^{99m}Tc-labeled BBN derivatives.

^{111}In-indium

Besides ^{99m}Tc-labeling, other GRPR-targeted compounds for SPECT imaging are mostly labeled with ^{111}In-indium[39, 114, 127-130]. Because of its long half-life ($t_{1/2}$ = 67.2 h), ^{111}In-indium is often used for dosimetric studies as a surrogate for therapeutic isotopes with similar coordination chemistry, such as ^{177}Lu-lutetium and ^{90}Y-yttrium[131].

A few years ago, *Mansi et al.* reported a novel antagonist, [^{111}In]RM2, which revealed superior pharmacokinetic properties in mice, especially at later time points due to its rapid clearance from GRPR-positive non-tumor organs (pancreas, intestine)[39]. This derivative is currently considered as the gold standard of BBN-based peptides and is the most clinically evaluated derivative of the GRPR-targeted ligands. However, most studies used different isotopes (^{68}Ga-gallium or ^{177}Lu-lutetium)[85, 87, 132].

In contrary, ^{111}In-labeled GRP-based analogs (agonists) suffered from high pancreatic and intestinal uptake and retention as well as low tumor uptake[127]. A comparative study using different chelators for ^{111}In-labeling of a GRPR antagonist (RM26) by *Mitran et al.* revealed low tumor and background uptake for all tested compounds[128]. Another antagonist, [^{111}In]SB3, exhibited good tumor and low pancreatic uptake 1 h p.i., resulting in favorable T/B ratios[94]. Later time points additionally increased these ratios, as the activity in the pancreas was cleared more rapidly compared to the activity in the tumor[94]. SB3 had already been used for a clinical study with ^{68}Ga-gallium, visualizing about 50% of all tumor lesions despite the advanced stage of the patients' PCa[60].

Lymperis et al. examined a potential benefit of substituting glycine by D-alanine within the SB3 structure yielding [^{111}In]SB4. Most likely due to a threefold decreased affinity, [^{111}In]SB4 revealed lower tumor uptake compared to [^{111}In]SB3. However, biodistribution with co-injection of PA showed noticeably less benefit compared to [^{111}In]SB3, indicating a stabilization effect by this substitution[129]. Another report by the same group showed immense tumor uptake and retention of a novel antagonist, [^{111}In]SB9, which indeed suffered from massive pancreatic uptake and retention[114].

As mentioned above, ^{111}In-indium is mostly used as a surrogate in preclinical studies, for which reason no clinical studies have been published in recent years using this isotope.

^{64}Cu-copper

Only a few BBN derivatives using ^{64}Cu-copper ($t_{1/2}$ = 12.7 h, E_{max} = 655 keV [18%]) have been published over the last years[122, 133-135]. Availability of ^{64}Cu-copper is limited as it requires cyclotron production. However, its long half-life enables distribution even from distant production sites[122].

Gourni et al. observed favorable biodistribution in mice with a ^{64}Cu-labeled RM2 analog (NOTA and NODAGA instead of DOTA)[135]. Another study utilizing the structurally similar RM26 revealed poor to moderate tumor uptake and poor retention. Moreover, background organs such as pancreas and liver showed high and moderate uptake, respectively[134]. *Wieser et al.* reported a first-in-man study in four patients suffering from primary PCa using a ^{64}Cu-labeled GRPR antagonist. This conjugate revealed high tumor uptake in three and moderate tumor uptake in one patient[66]. Based on the small number of published data in recent years, impact of ^{64}Cu-copper for GRPR-targeted conjugates can be currently considered as modest.

^{68}Ga-gallium

Its favorable availability (^{68}Ge/^{68}Ga generator) compensates for the relatively short half-life ($t_{1/2}$ = 68.1 min) of the PET isotope ^{68}Ga-gallium. Despite its relatively high positron emission energy (E_{mean} = 890 keV), ^{68}Ga-gallium was used most frequently over the last decade for PET imaging in nuclear medicine[122]. This is due to its short half-life, which also limited absorbed dose to healthy tissue of patients. For this reason, several preclinical and clinical reports utilizing ^{68}Ga-labeled BBN-based tracers have been published over the last years[20, 59, 62, 75, 82, 85, 87, 132, 135-137].

One recent clinical study in PCa patients revealed that there is potential for GRPR-targeted imaging and subsequent TRT in PCa patients with BCR who do not demonstrate sufficient PSMA expression[87]. Additionally, it was shown that ^{68}Ga-labeled BBN-based tracers exhibited favorable performance, especially in rather early-stage patients[20, 60, 83, 85]. Similar results were observed for imaging of BCa[59-62]. The agent frequently used for clinical studies was the potent GRPR antagonist RM2 or analogs thereof, which showed high potential for further studies. Nevertheless, other ^{68}Ga-labeled derivatives, such as NeoBOMB1, SB3 or derivatives thereof, also displayed promising preclinical and clinical data[60, 62, 130, 137-139]. Not surprisingly, [^{68}Ga]RM2 as well as [^{68}Ga]NeoBOMB1 are currently enrolled in several phase I and II studies[140-145].

In conclusion, ^{68}Ga-labeled GRPR-targeted tracers currently have a distinct clinical impact and further studies with this isotope are expected in the coming years.

^{18}F-fluorine

In addition to ^{68}Ga-gallium, the PET isotope ^{18}F-fluorine has gathered growing interest in recent years. As a consequence of its unique physical properties ($t_{1/2}$ = 109.7 min, E_{max} = 635 keV), it allows the generation of superior images with enhanced resolution compared to other PET isotopes[23, 99]. However, as cyclotron production is required, overall availability of this isotope is limited due to its relatively short half-life. Furthermore, by virtue of its high electronegativity, rigorous reaction conditions are required to attach [^{18}F]fluoride to a carbon atom of a (in most cases) prosthetic group[146, 147]. Therefore, high precursor amounts and time-consuming purification steps are necessary, resulting in low radiochemical yields (RCYs) and molar activities[148]. For this reason, other labeling strategies were developed, exploiting the higher affinity of fluoride to boron, aluminum or silicon compared to carbon atoms[23, 146, 149, 150].

In general, only a few studies about ^{18}F-labeled GRPR-targeted analogs have been reported in recent years[56, 99, 148, 150-154]. *Dijkgraaf et al.* described a ^{18}F-labeled GRPR agonist, which was generated *via* chelation of aluminum fluoride (AlF) by NOTA in about 45 min (single-step), yielding RCYs of 50-90% [decay corrected (d.c.)] and molar activities (A_M) of about 10 GBq/µmol[99]. Nonetheless, tumor uptake was low 1 h p.i., whereas pancreatic uptake was high[99]. Applying the same labeling technique, *Varasteh et al.* obtained a ^{18}F-labeled RM26 analog (antagonist) within 1 h, resulting in RCYs of 60-65% [d.c.] and molar activities of about 55 GBq/µmol[152]. Biodistribution studies in mice exhibited good

tumor uptake 3 h p.i., but the tracer also suffered from increased uptake in the GI tract[152]. Similar labeling results were reported by *Carlucci et al.* for an agonistic BBN derivative (50-60% RCY [d.c.], 1 h synthesis time, A_M > 30 GBq/µmol). However, biodistribution did not demonstrate significant tumor uptake[153]. *Chatalic et al.* also described a [^{18}F]AlF-labeled GRPR antagonist, obtained in a one-step synthesis within 20 min and without further purification, which resulted in yields of about 88% [n.d.c.] and an A_M of 35 GBq/µmol[150]. Biodistribution data showed moderate tumor uptake 1 h p.i. as well as low overall background accumulation[150].

Another approach was implemented by *Pourghiasian et al.*, using isotopic exchange reaction with an ammoniomethyltrifluoroborate ($AmBF_3$) moiety within an antagonistic tracer (^{18}F-$AmBF_3$-MJ9)[23]. This enabled one-step synthesis within 25 min and rapid purification by cartridge, yielding RCYs of 23 ± 5% [n.d.c.] and molar activities of 100 ± 32 GBq/µmol[23]. However, tumor uptake 1 h p.i. was low whereas intestinal and pancreatic uptake was slightly increased[23]. A first-in-man study by *Sah et al.*, investigating a potent ^{18}F-labeled GRPR antagonist (3-cyano-4-trimethylammonium-benzoyl moiety for nucleophilic substitution), yielded a RCY of approximately 15% [d.c.] and a molar activity of about 170 GBq/µmol. PET imaging in ten patients (five with preliminary PCa, five with BCR) revealed positive findings in three patients with preliminary PCa and in two PCa patients with BCR[56, 151].

Another reported technique using a silicon fluoride acceptor (SiFA) moiety for rapid isotopic exchange was also applied for BBN-based compounds[148]. This resulted in unfavorable images due to the typical enhanced lipophilic character of the SiFA group[148]. Nevertheless, facile one-step labeling with short overall synthesis time (purification by cartridge) is suggested, resulting in high molar activities of up to 680 GBq/µmol[155]. Adaption of this technique and further optimization by our group yielded superior [^{18}F]SiFA-PSMA inhibitors within 15 min and RCYs of 50 ± 10% [d.c.], which resulted in high molar activities of about 60 GBq/µmol[156]. Lipophilicity issues were compensated by introduction of a novel radiohybrid strategy, which enabled superior PET images with PSMA inhibitors. Thus, this strategy will be discussed in the following chapter.

3.2.1.2. SiFA methodology and radiohybrid concept

In order to obtain high RCYs and molar activities, ^{18}F-labeling should proceed rapidly. Furthermore, time-consuming purification steps, such as RP-HPLC, should be avoided due to the relatively fast decay of the isotope[146]. A smart approach for ^{18}F-labeling for subsequent *in vivo* studies was already reported in 1985 by *Rosenthal et al.*, using the affinity of silicon to fluorine for facilitated labeling[157]. However, rapid hydrolysis in aqueous medium was observed. This was most likely due to the lack of stabilizing moieties for the silicon-fluorine (Si-F) bond, which led to a release of free [^{18}F]fluoride[157].

In 2006, *Schirrmacher et al.* described enhanced stability of the Si-F bond towards hydrolysis. In order to shield the Si-F bond from water molecules, sterically demanding substituents (phenyl moiety and two *tert*-butyl moieties) were attached to the silicon atom[149]. Indeed, studies performed in mice with a [^{18}F]SiFA-containing SST2R agonist did not demonstrate accumulation in bone, confirming the enhanced hydrolytic stability of the Si-^{18}F bond. However, as a consequence of the enhanced lipophilicity associated with the bulky SiFA group, uptake in liver and GI tract was massively increased[158]. This was addressed by a variety of hydrophilic modifications, such as carbohydrates and aspartate moieties, resulting in good pharmacokinetics in mice for a SiFA-bearing SST2R-targeted compound[158].

This newly achieved stability of the Si-F bond towards hydrolysis allowed for further optimization of the labeling procedure. Employing the *Munich method* for drying of [^{18}F]fluoride instead of azeotropic drying, the labeling procedure was significantly accelerated and further simplified[159-161]. Using this methodology, *Niedermoser et al.* reported the achievement of high RCYs (50 ± 6%, n = 20) and radiochemical purities (RCP) of at least 98% within 20-25 min for labeling of an SST derivative[158]. Due to the small amounts of precursor used (25 nmol), high molar activities of 44-63 GBq/µmol were determined[158]. Moreover, due to mild labeling conditions and the chemical identity of precursor and labeled product, purification was rapidly achieved by cartridge.

On the one hand, this methodology is based on the affinity between silicon and fluorine. On the other hand, it is based on vacant low energy d-orbitals of the tetravalent silicon atom, which enables formation of hypervalent intermediate states[162]. The activation energy of the isotopic exchange reaction is also reported to be relatively low. Furthermore, the Arrhenius pre-exponential factor is increased compared to the nucleophilic substitution reaction at a carbon atom. Thus, an equilibrium for substitution of [^{19}F]fluoride by [^{18}F]fluoride at the silicon atom is rapidly reached[163].

The Arrhenius pre-exponential factor indicates the frequency of collisions between reactant molecules. This was demonstrated to be noticeably in favor for the SiFA group ($A_{SiFA} = 7.6 \times 10^{13}\ M^{-1}s^{-1}$) compared to a commonly used prosthetic group, ethyleneglycol-di-*p*-tosylate ($A_{Tosylate} = 2.9 \times 10^{9}\ M^{-1}s^{-1}$)[163]. Moreover, as an excess amount of precursor that carries ^{19}F-fluorine is used, the probability of a reversible reaction of free [^{19}F]fluoride (subsequent to the substitution by [^{18}F]fluoride) is negligible. For this reason, the isotopic exchange reaction can be considered as irreversible under these circumstances[163]. The

rapid incorporation of [^{18}F]fluoride is apparent, which explains the aforementioned good results of this labeling procedure.

Despite the promising observations so far, limitations remain. This is also reflected by the small number of preclinical and lack of clinical studies published in recent years applying the SiFA methodology[156, 162]. The major issue remains the high steric demand as well as the lipophilicity of the SiFA unit. By virtue of this drastic gain of lipophilicity, several hydrophilic modifications are typically required in order to obtain suitable SiFA-containing conjugates[158, 159, 163-165].

This major drawback was converted into an advantage by developing a novel concept of radiohybrid (rh) compounds. The lipophilic character of this group was therefore addressed *inter alia* by hydrophilic chelators, such as DOTA and DOTA-GA. Such rh ligands contain a SiFA moiety and a chelating unit allowing for chemically identical derivatives (X), irrespective of the hot and cold isotopes used ([^{19}F][^{68}Ga/^{111}In/^{177}Lu]X is chemically indistinguishable from [^{18}F][^{nat}Ga/^{nat}In/^{nat}Lu]X)[166]. A conventional theranostic pair, such as [^{68}Ga/^{177}Lu]X, is not chemically equal because of the different coordination chemistry of gallium and lutetium, for example.

However, a suitable position for the bulky SiFA unit as well as the variety of modifications within the sequence also has to be determined. As previously mentioned, this concept has already been successfully implemented within our group for PSMA-targeted ligands[166]. For this reason, it is suggested that this concept could also lead to improved imaging properties for other targets, for example GRPR.

3.2.2. Targeted radiotherapy (TRT) with GRPR-targeted compounds

Kirby et al. reported a relapse rate of 10-20% of PCa patients within five years of follow-up, leading to mCRPC[167]. Despite some research progress in recent years, prognosis for mCRPC patients remains rather poor[4]. Due to insufficient conventional therapy options, especially for late-stage disease, novel enhanced treatment options are desired. In the field of nuclear medicine, receptor-targeted radiotherapy is currently applied for late-stage PCa. Particularly PSMA-targeted compounds that are labeled with either an α- or a β^--emitting nuclide, accumulate preferably at the tumor site and deliver significant amounts of cytotoxic radiation dose[168].

Over the last years, a few ^{177}Lu-labeled PSMA-addressing ligands were reported to successfully treat PCa tumor lesions by TRT, for example PSMA-617 and PSMA I&T[74, 169-171]. In a German multicenter study reported by *Rahbar et al.*, receptor-mediated TRT with ^{177}Lu-labeled PSMA-targeted conjugates were determined to be a more appropriate choice for mCRPC patients compared to other third-line therapies, due to their high efficiency[172].

However, as mentioned above, there are reports of mCRPC patients who did not show sufficient PSMA expression despite a late-stage character of the respective tumors or metastases[81, 87]. For those cases, powerful alternatives for TRT are necessary, which opens the door for other targets, such as GRPR. Moreover, GRPR expression in high density lymph node metastases derived from GRPR-positive primary breast tumors was observed in about 95%, making GRPR an attractive target for TRT[30].

Both, GRPR agonists and antagonists have been and are currently used for addressing PCa and BCa though, only for diagnostic purposes[20, 40, 66, 82, 85, 99, 113, 121, 132]. GRPR agonists showed some painful side effects after administration and displayed worse pharmacokinetics due to a slower washout from non-tumor tissues. Thus, development of GRPR antagonists for TRT increased in recent years[39, 86, 97, 173]. However, only one study in humans using a GRPR antagonist for TRT in PCa patients has been reported so far.

The GRPR antagonist most often used, RM2, showed favorable pharmacokinetics as high tumor accumulation, fast clearance from non-tumor tissue and good retention in the tumor. Particularly at later time points, this conjugate demonstrated high contrast in mice as well as in humans[20, 39, 61, 82]. For this reason, [^{177}Lu]RM2 was utilized in a first-in-human dosimetry study and TRT in four PCa patients (GS = 8-10), who were not eligible for PSMA-targeted therapy.

Administration of [^{177}Lu]RM2 (4.5 ± 0.9 GBq) was reported to be safe, as no side effects were observed in these patients. Two of four patients received a second cycle[87]. Tracer uptake in non-tumor organs was only observed in the pancreas and the bladder, whereas several tumor lesions displayed significant accumulation (**Fig. 7**)[87]. Mean absorbed dose in the pancreas was high (1.08 ± 0.44 Gy/GBq), whereas other organs revealed lower absorbed doses (0.35 ± 0.14 Gy/GBq [kidneys], 0.05 ± 0.02 Gy/GBq

[liver], 0.10 ± 0.06 Gy/GBq [spleen], 0.016 ± 0.009 Gy/GBq [red bone marrow]). The mean dose for tumor lesions was calculated to be 6.20 ± 3.00 Gy/GBq.

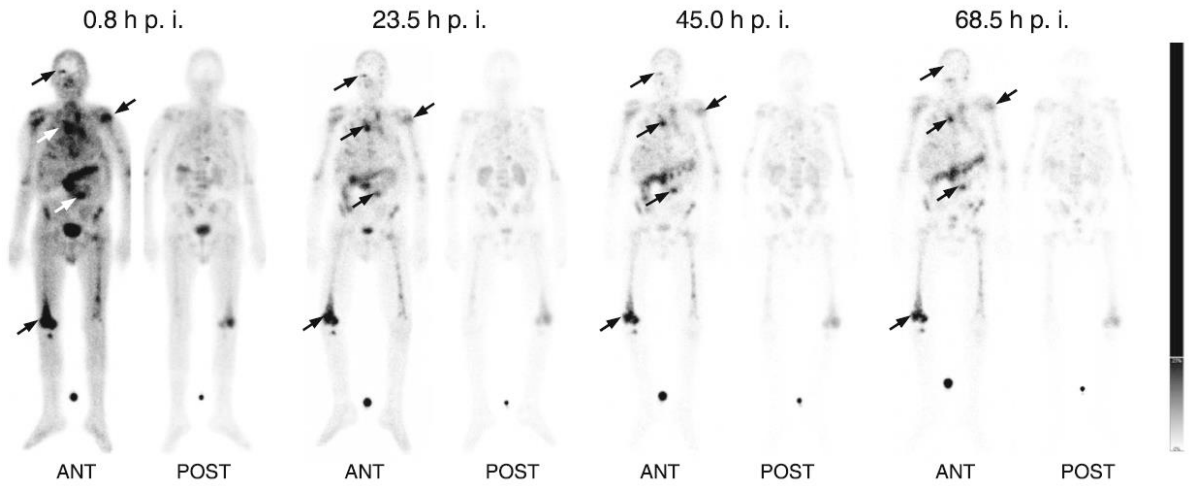

Fig. 7: Whole-body SPECT images showing uptake and retention of [^{177}Lu]RM2 at different time points in a mCRPC patient. High accumulation is found in the pancreas, which was cleared within the first 24 h. Tumor retention was still present 68.5 h p.i., suggesting sufficient radiation duration in tumor lesions[87].

Despite promising results of RM2 in the TRT and dosimetric study mentioned, there is still a lot of room for improvement, as BBN-based peptides still suffer from metabolic instability *in vivo*[39, 132]. Another recently published derivative, NeoBOMB1, showed enhanced stability *in vitro* and *in vivo* in preclinical studies[130, 137, 139]. Furthermore, PET imaging with [^{68}Ga]NeoBOMB1 visualized several tumor lesions in mCRPC patients, indicating a potential role for therapeutic purposes, too[130]. However, dosimetric calculations for [^{177}Lu]NeoBOMB1 in humans exhibited unfavorable absorbed doses for red bone marrow (~0.11 Gy/GBq), GI tract (~0.15-0.17 Gy/GBq) and osteogenic cells (~0.45 Gy/GBq) due to the enhanced lipophilicity of this compound[138, 174]. In contrast to the high hydrophilic PSMA inhibitors, BBN-based compounds generally show higher lipophilicities (log$D_{7.4}$ of > −3, ^{177}Lu-RM2: −2.51 ± 0.02), which is sufficient but could be optimized to further improve clearance kinetics[138, 153, 175, 176].

Further dosimetric or therapeutic studies with ^{177}Lu-labeled GRPR-targeted analogs have not been reported yet. Translation of promising diagnostic candidates, such as SB3 or SB9 for TRT will be difficult because of the high pancreatic uptake and retention determined in preclinical studies[60, 94, 114].

3.2.3. Instability issues of GRPR-targeted ligands

Considering BBN-based compounds, there are several reports about metabolic instability *in vivo*, most likely limiting further accumulation in malignant tissues[39, 94, 138, 139]. Problems occurring from the metabolic degradation of linear BBN structures are suggested to be caused by the neutral endopeptidase (NEP, EC 3.4.24.11), which is known to cleave linear peptides at the *N*-terminal side of hydrophobic amino acids[93, 95].

Linder et al. evaluated the metabolic stability of the GRPR agonist [^{177}Lu]AMBA (DOTA-4-aminobenzoyl-Gln^{7}-Trp^{8}-Ala^{9}-Val^{10}-Gly^{11}-His^{12}-Leu^{13}-Met^{14}-NH_2) in murine and human plasma *in vitro*, revealing several cleavage sites within its sequence. The major unstable sites were determined to be His^{12}-Leu^{13} in both plasmas as well as Met^{14}-OH in murine and Trp^{8}-Ala^{9} in human plasma. Furthermore, enzymatic cleavage between Gln^{7}-Trp^{8} seemed to be accelerated after first cleavage (Trp^{8}-Ala^{9}) had occurred. Moreover, this study did not demonstrate any affinity for the determined metabolites, suggesting a necessity for an intact pharmacophore for appropriate receptor binding[177].

As described earlier, development of GRPR antagonists resulted in several advantages, such as more rapid clearance from the pancreas and increased tumor uptake. Furthermore, enhanced metabolic stability was also observed, most likely due to some key substitutions within the sequence. Substitution of Met^{14} by Leu^{14} led to enhanced stability towards aminopeptidase 3.4.11.1. Introduction of a statine moiety (Sta^{13}) instead of the easily oxidizable Met^{13} yielded enhanced stability towards NEP at the *C*-terminus[178].

Nevertheless, a first-in-man study revealed only 19% of the administered activity of the antagonist [^{68}Ga]RM2 (DOTA-Pip^{5}-phe^{6}-Gln^{7}-Trp^{8}-Ala^{9}-Val^{10}-Gly^{11}-His^{12}-Sta^{13}-Leu^{14}-NH_2) to be still intact 65 min p.i.[132]. RM2 was reported to be cleaved in humans between DOTA and Pip^{5} (major cleavage site), Ala^{9} and Val^{10} as well as at the side chain of Gln^{7} (hydrolysis)[85]. Particularly the major cleavage site, however, could not be confirmed by *Popp et al.* in a stability study in mice[179].

Structural modifications within the pharmacophore (Gln^{7}-Trp^{8}-Ala^{9}-Val^{10}-Gly^{11}-His^{12}) were considered as time-consuming and assumed to negatively influence the peptide's pharmacokinetics[94, 180]. For this reason, metabolic instability has often been addressed indirectly by co-injection of PA, an inhibitor of NEP[94, 129]. Despite the stability issues within the pharmacophore, many groups focused their work preferably on modifying BBN-based analogs at the *C*- and/or *N*-terminus[39, 41, 42, 94, 138]. Thus, studies to metabolically stabilize the pharmacophore by introduction of unnatural amino acids at dedicated positions are rare. Amongst others, substitution of Gly^{11} by *N*-Me-Gly^{11} or ala^{11} was reported, wherein both modifications revealed slightly positive effects on metabolic stability[129, 178, 181].

Taking into account the small amount of intact tracer mentioned (19% 65 min p.i. for [^{68}Ga]RM2), a virtually stabilized [^{177}Lu]RM2 would have likely resulted in enhanced tumor accumulation and retention in the aforementioned TRT study by *Kurth et al.* (**Fig. 7**)[87]. However, increased metabolic stability of the linear structure towards enzymes *in vivo* could also lead to augmented uptake and retention in the pancreas, which was indirectly shown in mice by co-injection of PA[94, 114, 116]. This has to be considered for potential GRPR-targeted TRT in future examinations.

4. Objectives

Due to the high incidence and difficult treatment at later stages of disease, novel options for earlier detection and treatment of both PCa and BCa are warranted, which could be achieved by molecular imaging as well as TRT applied in nuclear medicine. For diagnosis and TRT of PCa, PSMA inhibitors are currently applied the most. However, particularly in earlier disease stages (Androgen-dependent), PSMA expression seemed to be limited, whereas high GRPR expression was observed in earlier (Androgen-dependent) stages of PCa. For this reason, PSMA and GRPR could play complementary roles in PCa. In case of BCa, over 80% of all tumors showed high ER expression. As a high correlation of ER and GRPR expression was found in BCa, targeting of GRPR could be a powerful tool for diagnosis. Moreover, as 95% of nodal metastases displayed high GRPR expression density when primary BCa also showed high density expression, TRT using GRPR-addressing ligands could be of clinical value.

Currently used GRPR-addressing ligands suffer from enzymatic degradation *in vivo*, which particularly impedes an enhanced therapeutic impact. A first-in-man study using the gold standard among GRPR-targeted ligands, [^{68}Ga]RM2, revealed that only 19% of the administered activity located in blood was still intact. Enzymatic degradation is mainly caused by NEP, which is reported to cleave BBN-based conjugates particularly at the dipeptidic Gln^{7}-Trp^{8} site.

Therefore, the major objective of this thesis is the development of novel GRPR antagonists with increased metabolic stability compared to RM2. The less stable sites within the pharmacophore are therefore to be substituted by unnatural amino acids, especially the Gln^{7}-Trp^{8} site. We hypothesize that unnatural amino acids located at these unstable sites impede enzymatic recognition and thus cleavage of linear BBN-based compounds. Furthermore, overall lipophilicity should be improved *via* substitution of different positions by more hydrophilic amino acids, as it has been shown that more lipophilic structures are generally more prone to enzymatic degradation in the liver than hydrophilic conjugates. Besides stabilization of linear peptides, cyclization approaches (disulfide bridge formation, *Click* chemistry) already applied for other receptors of the GPCR family (SST2R, CXCR4) are also considered as a potential strategy to improve metabolic stability. Each modified RM2 analog will first be evaluated in IC_{50} studies, as high GRPR affinity is a prerequisite for successful molecular imaging or TRT. Promising RM2 derivatives will be further investigated by state-of-the-art *in vitro* (log$D_{7.4}$, receptor-mediated internalization, plasma stability studies) and *in vivo* (biodistribution and imaging studies) experiments with the aim of a clinical translation of a novel GRPR antagonist with distinctly improved metabolic stability and thus enhanced pharmacokinetics.

A second objective of this thesis is the transfer of a novel radiohybrid (rh) concept to BBN-based compounds. This concept was developed within our group for PSMA-targeted analogs and exhibited outstanding results in terms of imaging quality (^{18}F-fluorine PET), preparation time and synthetic yields. While typical ^{18}F-labeling approaches suffer from long synthesis time or poor conversion rates, the SiFA methodology provides high RCYs within short synthesis times as well as easy handling throughout the

whole process. However, the bulky and lipophilic SiFA group requires several hydrophilic modifications to maintain sufficient pharmacokinetics. Therefore, the effect of the SiFA introduction as well as *N*-terminal linker modifications on GRPR affinity and lipophilicity will be studied. Promising BBN-SiFA compounds will be further investigated in biodistribution studies to discover potential positive or negative effects of these modifications on pharmacokinetics *in vivo*.

II. Materials and Methods

1. General information

The Fmoc-(9-fluorenylmethoxycarbonyl-) and all other protected amino acid analogs were purchased from *Bachem Inc.* (Bubendorf, Switzerland), *Sigma-Aldrich GmbH* (Munich, Germany) or *Iris Biotech GmbH* (Marktredwitz, Germany). The *H*-Rink amide ChemMatrix® resin (35-100 mesh particle size, 0.4-0.6 mmol/g loading) was purchased from *Sigma-Aldrich GmbH* (Munich, Germany). *CheMatech* (Dijon, France) delivered the chelators DOTA(^{t}Bu)$_3$ as well as DOTA-GA(^{t}Bu)$_4$. Peptide syringes were obtained from *VWR International GmbH* (Bruchsal, Germany).

All necessary solvents and other organic reagents were purchased from either, *Alfa Aesar* (Karlsruhe, Germany), *Sigma-Aldrich GmbH* (Munich, Germany) or *VWR International GmbH* (Bruchsal, Germany). Solid-phase synthesis of the peptides was carried out by manual operation using a Scilogex MX-RL-E Analog Rotisserie Tube Rotator (*Scilogex*, Rocky Hill, CT, USA). H_2O was used after purification by a Barnstead MicroPure system (*Thermo Fisher Scientific Inc.*, Waltham, MA, USA).

Analytical and preparative reversed-phase high performance liquid chromatography (RP-HPLC) were performed using Shimadzu gradient systems (*Shimadzu Deutschland GmbH*, Neufahrn, Germany), each equipped with a SPD-20A UV/Vis detector (220 nm, 254 nm). Different gradients of MeCN (0.1% TFA) in H_2O (0.1% TFA) were used as eluents for all RP-HPLC operations.

For analytical measurements, a Nucleosil 100 C18 (125 × 4.6 mm, 5 µm particle size) column (*CS Chromatographie Service GmbH*, Langerwehe, Germany) was used at a flow rate of 1 mL/min. Both specific gradients and the corresponding retention times t_R as well as the capacity factor *K*' are cited in the text. Preparative RP-HPLC purification was done with a Multospher 100 RP 18 (250 × 10 mm, 5 µm particle size) column (*CS Chromatographie GmbH*, Langerwehe, Germany) at a constant flow rate of 5 mL/min. Analytical and preparative radio RP-HPLC was performed using a Nucleosil 100 C18 (5 µm, 125 × 4.0 mm) column (*CS Chromatographie GmbH*, Langerwehe, Germany). Electrospray ionization-mass spectra for characterization of the substances were acquired on an expression^L CMS mass spectrometer (*Advion Ltd.*, Harlow, UK).

For radiolabeling, [^{177}Lu]LuCl$_3$ (Molar Activity (A_M) > 3000 GBq/mg, 740 MBq/mL, 0.04 M HCl, *ITG GmbH*, Garching, Germany) was used. Radioactivity was detected through connection of the outlet of the UV-photometer to an AceMate 925-Scint NaI(Tl) well-type scintillation counter from *EG&G Ortec* (Oak Ridge, TN, USA). Radioactive probes were measured by a WIZARD$^{2®}$ 2480 Automatic γ-Counter (*Perkin Elmer*, Waltham, MA, USA) and determination of IC_{50} values was carried out using GraphPad Prism 6 (*GraphPad Software Inc.*, San Diego, CA, USA). For radio TLC, a Scan-RAM™ Scanner with Laura™ software (*LabLogic Systems Ltd.*, Broomhill, Sheffield, United Kingdom) was used.

NMR spectra were recorded on a Bruker (*Billerica*, United States) AVHD-300 or AVHD-400 spectrometers at 300 K. Lyophilization was accomplished using an Alpha 1-2 LDplus lyophilizer (*Martin Christ Gefriertrocknungsanlagen GmbH*, Osterode am Harz, Deutschland) combined with a RZ-2 vacuum pump (*Vacuubrand GmbH & Co KG*, Olching, Germany).

For *in vitro* and *in vivo* studies, the used nutrition mixture Dulbecco's modified eagle's medium/Ham's F-12 (DMEM/F-12, *v*/*v* = 1/1, with stable glutamine), fetal bovine serum (FBS Superior), phosphate buffered saline (PBS Dulbecco, without Ca^{2+}/Mg^{2+}), trypsin/EDTA (0.05%/0.02% in PBS without Ca^{2+}/Mg^{2+}) solution as well as Hank's balanced salt solution (HBSS, with 0.35 g/L $NaHCO_3$ and Ca^{2+}/Mg^{2+}) were obtained from *Biochrom GmbH* (Berlin, Germany). Solving of purified products was applied using Tracepur® H_2O (*Merck KGaA*, Darmstadt, Germany). Bovine serum albumin (BSA) was purchased from *Biowest* (Nuaillé, France).

Cells were cultured in CELLSTAR® cell culture flasks and seeded in 24-well plates (*Greiner Bio-One GmbH*, Kremsmünster, Austria) after being counted with a Neubauer hemocytometer (*Paul Marienfeld*, Lauda-Königshofen, Germany) using Trypan Blue (0.4% in 0.81% NaCl and 0.06% potassium phosphate) solution (*Sigma-Aldrich GmbH*, Munich, Germany). Cells were handled inside a MSC Advantage laminar flow cabinet and maintained in a Heracell 150i incubator (*Thermo Fisher Scientific Inc.*, Waltham, MA, USA) at 37 °C in a humidified 5% CO_2 atmosphere.

2. Execution protocols

2.1. General procedures of solid-phase peptide synthesis (SPPS)

On-resin peptide formation (GP1)

The respective side-chain protected Fmoc-AA-OH (1.5 eq.) is dissolved in NMP and pre-activated by adding TBTU (1.5 eq.), HOAt (1.5 eq.) and DIPEA (4.5 eq.). After activation for 10 min, the solution is added to resin-bound free amine peptide and shaken for 1.5 h at rt. Subsequently, the resin is washed with NMP (6 × 20 mL/g resin) and after Fmoc deprotection (GP2), the next amino acid is coupled analogously.

On-resin Fmoc deprotection (GP2)

The resin-bound Fmoc-peptide is treated with 20% piperidine in NMP (*v*/*v*) for 5 min and subsequently for 15 min. Afterwards, the resin is washed with NMP (6 × 20 mL/g resin).

On-resin Dde deprotection (GP3)

Dde deprotection is performed by adding a solution of imidazole (75 eq.), hydroxylamine hydrochloride (100 eq.) in NMP (7 mL) and DCM (3 mL) for 3 h at rt. After completed deprotection, the resin is washed with NMP (6 × 20 mL/g resin).

Conjugation of a chelator (GP4)

The protected chelator DOTA(^{t}Bu)$_3$ or DOTA-GA(^{t}Bu)$_4$ (1.5 eq.) is dissolved in NMP and pre-activated by adding TBTU (1.5 eq.), HOAt (1.5 eq.) and DIPEA (4.5 eq.). After activation for 10 min, the solution is added to resin-bound *N*-terminal deprotected peptide (1.0 eq.) and shaken for 3 h at rt. Subsequently, the resin is washed with NMP (3 × 20 mL/g resin) and DCM (3 × 20 mL/g resin).

Peptide cleavage from the resin with additional deprotection of acid labile protecting groups (GP5)

The fully protected resin-bound peptide is washed with DCM, afterwards dissolved in a mixture of TFA/TIPS/DCM (*v*/*v*/*v*; 95/2.5/2.5) and shaken for 45 min. The solution is filtered off and the resin is treated in the same way for another 45 min. Both filtrates are combined and concentrated under a stream of nitrogen. After dissolving the residue in MeOH and precipitation in diethyl ether, the liquid is decanted and the remaining solid is dried.

Complete deprotection of ^{t}Bu (GP6)

Removal of remaining ^{t}Bu/Boc protecting groups after peptide cleavage from the resin (GP5) is carried out by dissolving the crude DOTA or DOTA-GA coupled product in TFA and stirring for 6 h and 16 h at rt, respectively. After removing TFA under a stream of nitrogen, the crude unprotected product is obtained.

2-CTC resin loading (GP7)

Loading of the 2-chlorotrityl chloride (2-CTC) resin (*Bachem Inc.*, Bubendorf, Switzerland) with a Fmoc-protected amino acid (AA) is carried out by shaking a solution of the 2-CTC resin (1.5-1.9 mmol/g) and Fmoc-AA-OH (1.5 eq.) in DMF with DIPEA (1.5 eq.) in a 20 mL peptide syringe at rt for 15 min. After further addition of DIPEA (3.0 eq.), the syringe is shaken at rt for further 2 h. Remaining 2-chlorotrityl chloride is capped by the addition of methanol (2 mL/g resin) for 15 min. Subsequently, the resin is washed five times with each DMF, MeOH and DCM (2 × 5 mL/g resin) as well as dried *in vacuo*. Final loading *l* of Fmoc-AA-OH coupled resin is determined by the following equation:

$$l\ \left[\frac{\mathrm{mmol}}{\mathrm{g}}\right] = \frac{(\mathrm{m_2}-\mathrm{m_1})\times 1000}{(\mathrm{M_W}-\mathrm{M_{HCl}})\,\mathrm{m_2}}$$

m_2 = mass of loaded resin [g]

m_1 = mass of unloaded resin [g]

M_W = molecular weight of AA [g/mol]

M_{HCl} = molecular weight of HCl [g/mol]

Disulfide bridge formation (GP8)

Cyclization *via* disulfide bond formation is obtained applying a procedure published by our group[182]. Therefore, a peptide containing two sulfide side chain residues (cysteine) is resuspended in 50 mL of THF (per 300 mg of peptide). Thereafter, NH_4OAc (5 mM) is added until a clear solution is obtained. Subsequent to adjusting the solution to *pH* = 7 by addition of saturated $NaHCO_3$ solution, 100 µL (per 300 mg of peptide) of H_2O_2 (30%) are added and the mixture is stirred for 30 min at rt. The solvents are evaporated and the cyclized product is purified using preparative RP-HPLC.

On-resin coupling of *p*-nosyl (*p*-Ns) protecting group (GP9)

A solution of *p*-nosyl chloride (5.0 eq.) and 2,4,6-collidine (10.0 eq.) in NMP is added to the resin located in a peptide syringe, shaken for 30 min at rt and then washed with NMP (6 × 20 mL/g resin).

On-resin *N*-alkylation under *Mitsunobu* conditions (GP10)

A solution of triphenylphosphine (0.3 M in dry THF, 5.0 eq.) and the respective alkyl alcohol (10.0 eq.) is added to the resin located in a peptide syringe and the mixture is shaken for 1 min at rt. After adding DIAD (5.0 eq.), the resulting suspension is shaken for 30-60 min and then, the resin is filtered. The procedure is repeated twice and thereafter, the resin is washed with NMP (6 × 20 mL/g resin).

On-resin peptide formation at secondary amines (GP11)

The resin is suspended in dry THF, transferred to a flask containing a septum and heated to 60 °C under stirring. In another flask, *bis*(trichloromethyl) carbonate (2.0 eq.) and Fmoc-AA-OH (5.0 eq.) are dissolved in dry THF and cooled on ice. After adding 2,4,6-collidine (14.0 eq.), the resulting suspension is transferred to the flask containing the resin and stirred at 60 °C for 2 h. The reaction is terminated by cooling to rt and addition of MeOH. Subsequently, the resin is filtered and washed with MeOH (2 × 20 mL/g resin) and NMP (6 × 20 mL/g resin). The procedure is repeated once for enhanced conversion rates.

On-resin azidation of alkyl bromides (GP12)

After washing of the resin with DMF, a solution of sodium azide (5.0 eq.) in DMF is added to the resin located in a peptide syringe, shaken for 16 h at rt and then washed with DMF (3 × 20 mL/g resin) as well as NMP (3 × 20 mL/g resin).

On-resin deprotection of the *p*-nosyl protecting group (GP13)

A solution of *β*-mercaptoethanol (10.0 eq.) and DBU (5.0 eq.) in NMP is added to the resin located in a peptide syringe, shaken for 15 min at rt (twice) and then washed with NMP (6 × 20 mL/g resin).

Cyclization *via Click* chemistry (GP14)

The respective cleaved (from resin) and purified (by RP-HPLC) backbone modified peptides (1.0 eq.) are dissolved in 1 mL Tracepur® H_2O/^{t}BuOH (*v*/*v* = 1/1). After successive addition of sodium ascorbate solution (6.7 eq. in 250 µL Tracepur® H_2O) and $CuSO_4$ solution (4.4 eq. in 250 µL Tracepur® H_2O) the mixture is stirred extensively for 16 h at rt. Thereafter, the brownish suspension is centrifuged, the supernatant decanted and purified by preparative RP-HPLC.

2.2. Synthesis and characterization of the SiFA building block

Synthesis of the silicon fluoride acceptor (SiFA) building block was performed according to a previously published procedure which was slightly modified by our group[183]. All water- and oxygen-sensitive reactions were executed in dried reaction vessels under an argon atmosphere using a vacuum gas manifold.

((4-Bromobenzyl)oxy)(*tert*-butyl)dimethylsilane (3)

To a stirred solution of 4-bromobenzylalcohol (1.0 eq., (**1**)) in anhydrous DMF, imidazole (1.2 eq.) and TBDMS-Cl (1.2 eq., (**2**)) were added and the resulting mixture was stirred at rt for 16 h. The mixture was poured into ice-cold H_2O and extracted five times with Et_2O. The combined organic fractions were washed with saturated $NaHCO_3$ as well as brine, then dried, filtered and concentrated *in vacuo* to give the crude product which was further purified by flash column chromatography (silica, 5% EtOAc in petrol, *v*/*v*) to give ((4-bromobenzyl)oxy)(*ter*t-butyl)dimethylsilane (**3**) as a colorless oil (95%).

RP-HPLC (50→100% MeCN in 15 min): t_R = 15.0 min, *K*‘ = 8.38.

^{1}H-NMR (400 MHz, $CDCl_3$, 300 K): δ [ppm] = 0.10 (6*H*, s, $SiMe_2$*t*Bu), 0.95 (9*H*, s, $SiMe_2$*t*Bu), 4.69 (2*H*, s, CH_2OSi), 7.21 (2*H*, d), 7.46 (2*H*, d).

Di-*tert*-butyl(4-((*tert*-butyldimethylsilyloxy)methyl)phenyl)fluorosilane (5)

At –78 °C under stirring, a solution of ^{t}BuLi (1.7 mol/L in pentane, 2.4 eq.) was added to a solution of ((4-bromobenzyl)oxy)(*tert*-butyl)dimethylsilane ((**3**), 1.0 eq.) in dry THF. After the reaction mixture was stirred at –78 °C for 30 min, the resulting suspension was added dropwise over a period of 30 min to a cooled (–78 °C) solution of di-*tert*-butyldifluorosilane ((**4**), 1.2 eq., *Fluorochem Ltd.*, UK) in dry THF. The reaction mixture was allowed to warm up to rt over a period of 12 h and was then quenched with brine. The organic layer was separated and the aqueous layer was extracted with Et_2O (3 × 100 mL). The combined organic layers were dried over $MgSO_4$ and filtered. The filtrate was concentrated *in vacuo* to afford di-*tert*-butyl(4-((*tert*-butyldimethylsilyloxy)methyl)phenyl)fluorosilane (**5**) as a yellowish oil (95%) which was used for subsequent reactions without further purification.

RP-HPLC (50→100% MeCN in 15 min): t_R = 19.0 min, *K*‘ = 10.88.

4-(Di-*tert*-butylfluorosilanyl)benzyl alcohol (6)

A catalytic amount of concentrated aqueous HCl was added to a suspension of di-*tert*-butyl(4-((*tert*-butyldimethylsilyloxy)methyl)phenyl)fluorosilane ((**5**), 1.0 eq.) in methanol which was stirred for 18 h at rt. The solvent was removed under reduced pressure, the residue then redissolved in Et_2O and the solution was washed with saturated $NaHCO_3$. The aqueous layer was extracted with Et_2O (3 × 100 mL) and the combined organic layers were dried over $MgSO_4$ as well as filtered. The filtrate was concentrated *in vacuo* to yield 4-(di-*tert*-butylfluorosilanyl)benzyl alcohol (**6**) as a yellowish oil (98%) which solidified. The product was used without further purification.

RP-HPLC (50→100% MeCN in 15 min): t_R = 8.2 min, *K*‘ = 4.13.

4-(Di-*tert*-butylfluorosilyl)benzaldehyde (7)

A solution of 4-(di-*tert*-butylfluorosilanyl)benzyl alcohol ((**6**), 1.0 eq.) in dry DCM was added dropwise to a stirred ice-cooled suspension of pyridinium chlorochromate (2.5 eq.) in dry DCM. After the reaction mixture was stirred at 0 °C for 30 min and for additional 2.5 h at rt, anhydrous Et_2O was added and the supernatant was decanted from the black gum-like material. The insoluble material was washed thoroughly with Et_2O and the combined organic phases were passed through a short pad of silica gel (10 cm per gram of crude product) for filtration. The solvents were removed *in vacuo* to yield 4-(di-*tert*-butylfluorosilyl)benzaldehyde (**7**) as a yellowish oil (96%).

RP-HPLC (50→100% MeCN in 15 min): t_R = 10.5 min, *K*‘ = 5.56.

4-(Di-*tert*-butylfluorosilyl)benzoic acid (8)

$KMnO_4$ (1 M in H_2O, 6.0 eq.) was added to a mixture of 4-(di-*tert*-butylfluorosilyl)benzaldehyde ((**7**), 1.0 eq.) in *tert*-butanol, DCM, and $NaH_2PO_4 \cdot H_2O$ buffer (1.25 M in H_2O) at *pH* = 4.0-4.5 (*v*/*v*/*v* = 10/1/7). After the mixture was stirred for 25 min, it was cooled to 5 °C and excess $KMnO_4$ (1.0 eq.) was added. Then, the reaction was quenched by addition of saturated Na_2SO_3. Formed MnO_2 was dissolved by addition of HCl (2 M in H_2O). The resulting solution was extracted with Et_2O three times. The combined organic layers were washed with saturated $NaHCO_3$ solution, dried over $MgSO_4$, filtered, and concentrated *in vacuo*. The obtained solid was purified by recrystallization from Et_2O/n-hexane (*v*/*v* = 1/3), yielding 4-(di-*tert*-butylfluorosilyl)benzoic acid (**8**) as a colorless solid (60%).

RP-HPLC (50→100% MeCN in 15 min): t_R = 8.5 min, *K*‘ = 4.31.

Calculated monoisotopic mass ($C_{15}H_{23}FO_2Si$): 282.4; found: m/z = 281.1 $[M-H]^-$, 235.1 $[M-COOH]^-$.

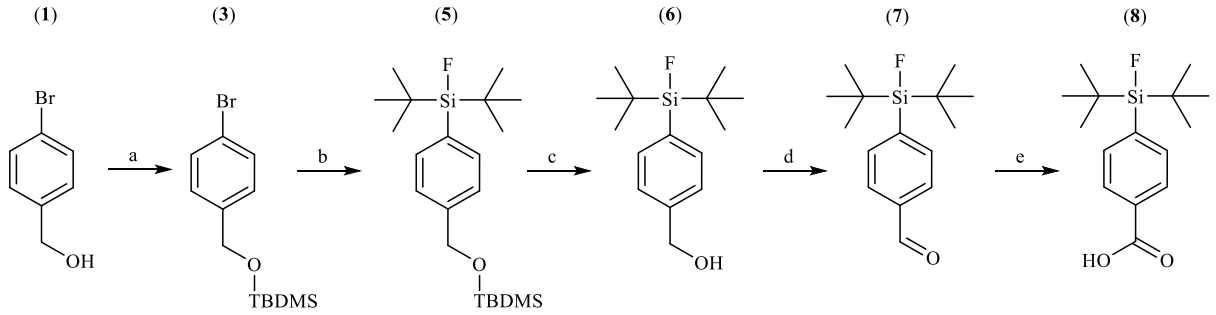

Scheme 1: Synthesis of 4-(di-*tert*-butylfluorosilyl)benzoic acid (**8**): a) TBDMS-Cl (**2**), imidazole (DMF, rt, 16 h); b) ^{t}BuLi, di-*tert*-butyldifluorosilane (**4**) (THF, -78 °C→rt, 12 h); c) HCl (MeOH, rt, 18 h); d) pyridinium chlorochromate (DCM, 0 °C, 30 min and rt, 2.5 h); e) $KMnO_4$ (DCM, *tert*-butanol, NaH_2PO_4 buffer, 5 °C).

2.3. Synthesis and characterization of the glu-urea-glu (eue) motif

The hydrophilic non-PSMA-binding ^{t}Bu-protected glu-urea-glu motif ((tBuO)eue(OtBu)$_2$, (**14**)) was synthesized in analogy to a previously published procedure which was slightly modified[184].

Di-*tert*-butyl-(1*H*-imidazole-1-carbonyl)-D-glutamate (11)

A solution of DCM containing 1-di-*tert*-butyl-D-glutamate·HCl ((**9**), 1.0 eq.) was stirred on ice for 30 min and afterwards treated with TEA (3.5 eq.) and DMAP (0.04 eq.). After additional stirring for 5 min, 1,1'-carbonyldiimidazole (CDI (**10**), 2.0 eq.) dissolved in DCM was slowly added over a period of 30 min. The reaction mixture was further stirred for 16-24 h and allowed to warm up to rt. The reaction was stopped using saturated $NaHCO_3$ and subsequent washing twice each with H_2O and brine. The remaining solvent was removed *in vacuo* yielding di-*tert*-butyl-(1*H*-imidazole-1-carbonyl)-D-glutamate (**11**) as a colorless oil (91%) which was used without further purification.

RP-HPLC (10→90% MeCN in 15 min): t_R = 14.5 min, *K*‘ = 8.06.
Calculated monoisotopic mass ($C_{17}H_{27}N_3O_5$): 353.2; found: m/z = 376.3 $[M+Na]^+$.

5-Benzyl-1-(*tert*-butyl)-(((*R*)-1,5-di-*tert*-butoxy-1,5-dioxopentan-2-yl)carbamoyl)-D-glutamate (13)

A solution of di-*tert*-butyl-(1*H*-imidazole-1-carbonyl)-D-glutamate ((**11**), 1.0 eq.) in 1,2-dichloroethane (DCE) was cooled on ice for 30 min. After addition of TEA (3.0 eq.) and *H*-glu(OBn)-O^{t}Bu·HCl ((**12**), 1.0 eq.), the solution was stirred at 40 °C for 16 h. The remaining solvent was evaporated under reduced pressure and the crude product was purified by silica gel flash-chromatography with an eluent mixture containing EtOAc, n-hexane and TEA (*v*/*v*/*v* = 500/500/0.8). After removal of the solvent, 5-benzyl-1-(*tert*-butyl)-(((*R*)-1,5-di-*tert*-butoxy-1,5-dioxopentan-2-yl)carbamoyl)-D-glutamate (**13**) was obtained as a colorless oil (84%).

RP-HPLC (10→90% MeCN in 20 min): t_R = 17.4 min, *K*‘ = 9.88.
Calculated monoisotopic mass ($C_{30}H_{46}N_2O_9$): 578.3; found: m/z = 411.3 $[M-3^{t}Bu+H]^+$, 467.3 $[M-2^{t}Bu+H]^+$, 523.3 $[M-^{t}Bu+H]^+$, 601.5 $[M+Na]^+$.

D-(^{t}BuO)glutamate-urea-D-glutamate(O^{t}Bu)$_2$ ((^{t}BuO)eue(O^{t}Bu)$_2$) (14)

A mixture of 5-benzyl-1-(*tert*-butyl)-(((*R*)-1,5-di-*tert*-butoxy-1,5-dioxopentan-2-yl)carbamoyl)-D-glutamate ((**13**), 1.0 eq.) dissolved in EtOH and palladium (10% on activated charcoal, 0.1 eq.) was initially purged with hydrogen gas and stirred for 16 h at rt under light hydrogen gas pressure. The crude product was purified through celite and the obtained solvent was evaporated *in vacuo* yielding D-(^{t}BuO)glutamate-urea-D-glutamate(O^{t}Bu)$_2$ ((^{t}BuO)eue(O^{t}Bu)$_2$) (**14**) as a colorless oil (82%) which solidified.

RP-HPLC (10→90% MeCN in 15 min): t_R = 12.0 min, *K*‘ = 6.50.
Calculated monoisotopic mass ($C_{23}H_{49}N_2O_9$): 488.3; found: m/z = 489.5 $[M+H]^+$, 516.4 $[M+Na]^+$.

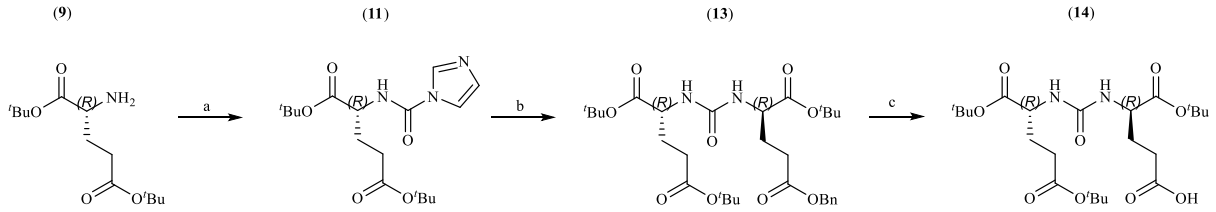

Scheme 2: Synthesis of (^{t}BuO)eue(O^{t}Bu)$_2$ (**14**): a) TEA, DMAP, CDI (**10**) (DCM, 0 °C→rt, 16-24 h); b) *H*-glu(OBn)-O^{t}Bu·HCl (**12**), TEA (DCE, 40 °C, 16 h); c) Pd/C (10%), H_2 (EtOH, rt, 16 h).

2.4. Labeling Experiments

2.4.1. Cold Complexations

^{nat}Ga-gallium complexation: The purified chelator-containing compound (10^{-3} M in Tracepur® H_2O, 1.0 eq.) and [^{nat}Ga]$Ga(NO_3)_3$ • 6 H_2O (10 mM in Tracepur® H_2O, 1.5 eq.) were diluted with Tracepur® H_2O to a final concentration of 10^{-4} M and heated to 70 °C for 30 min. After cooling to rt, the crude product was obtained.

^{nat}Lu-lutetium complexation: The purified chelator-containing ligand (10^{-3} M in Tracepur® H_2O, 1.0 eq.) and [^{nat}Lu]$LuCl_3$ (20 mM in Tracepur® H_2O, 2.5 eq.) were diluted with Tracepur® H_2O to a final concentration of 10^{-4} M and heated to 95 °C for 30 min. After cooling to rt, the crude product was obtained.

2.4.2. Radiolabeling

^{125}I-labeling: The respective reference ligands for IC_{50} studies ([3-[^{125}I]*I*-Tyr^4]BBN, [3-[^{125}I]*I*-tyr^6, *β*-Ala^{11}, Phe^{13}, Nle^{14}]BBN_{6-14}, [3-[^{125}I]*I*-tyr^6]MJ9) were prepared according to a previously published procedure which was slightly modified by our group[35]. Briefly, 0.2 mg of the respective precursors ([Tyr^4]BBN, [tyr^6, *β*-Ala^{11}, Phe^{13}, Nle^{14}]BBN_{6-14}, [tyr^6]MJ9) were dissolved in 20 µL Tracepur® H_2O and 280 µL TRIS buffer (25 mM TRIS HCl, 0.4 M NaCl, *pH* = 7.9). After addition of the solution to a vial containing 150 µg Iodo-Gen® (1,3,4,6-Tetrachloro-3*α*,6*α*-diphenylglycouril, surface-bound, *Merck KGaA*, Darmstadt, Germany), 5.0 µL (16 MBq) [^{125}I]NaI (74 TBq/mmol, 3.1 GBq/mL, 40 mM NaOH, *Hartmann Analytic*, Braunschweig, Germany) were added. The reaction solution was incubated for 15 min at rt and purified by RP-HPLC. Immediately after purification, sodium ascorbate (0.1 M in Tracepur® H_2O, 10 vol-%) was added to prevent radiolysis.

RP-HPLC (15→35% MeCN in 15 min): t_R = 8.3 min, *K'* = 4.53 ([3-[^{125}I]*I*-Tyr^4]BBN).
RP-HPLC (15→35% MeCN in 15 min): t_R = 14.5 min, *K'* = 8.66 ([3-[^{125}I]*I*-tyr^6, *β*-Ala^{11}, Phe^{13}, Nle^{14}]-BBN_{6-14}).
RP-HPLC (20→35% MeCN in 20 min): t_R = 18.9 min, *K'* = 10.46 ([3-[^{125}I]*I*-tyr^6]MJ9).

[3-[^{125}I]I-Tyr^4]BBN

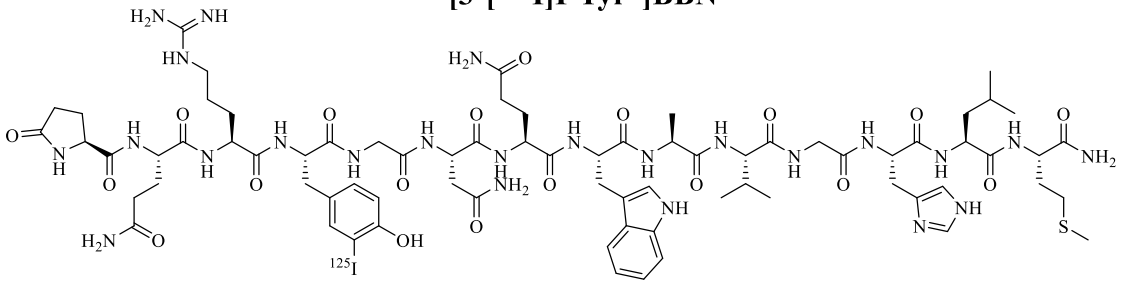

[3-[^{125}I]I-tyr^{6}, beta-Ala^{11}, Phe^{13}, Nle^{14}]BBN$_{6-14}$

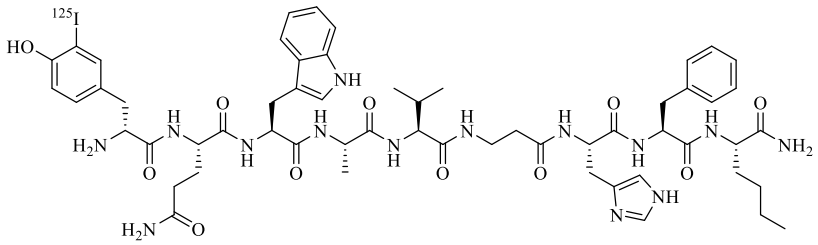

[3-[^{125}I]I-tyr^{6}]MJ9

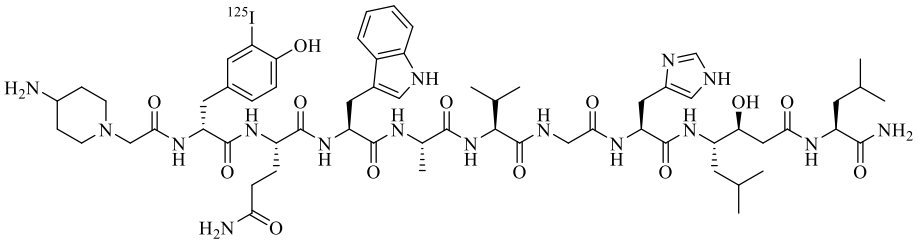

^{177}Lu-labeling (preclinical): ^{177}Lu-labeling was done using a procedure developed within the group. Therefore, a solution of the purified chelator-containing ligand (10^{-3} M in Tracepur® H_2O, 1 µL), NaOAc buffer (1 M, *pH* = 5.50, 10 µL) and approximately 10-30 MBq [^{177}Lu]$LuCl_3$ (0.04 M in HCl) were diluted with HCl (0.04 M) to a total volume of 90 µL and heated to 95 °C for 10 min. Immediately after labeling, sodium ascorbate (0.1 M, 10 µL) was added to prevent radiolysis. Incorporation of the ^{177}Lu-lutetium was determined by radio TLC (ITLC-SG chromatography paper, mobile phase: 0.1 M trisodium citrate). Radiochemical purity of the labeled compound was determined by radio RP-HPLC.

^{177}Lu-labeling (clinical): For patient studies, test synthesis was executed applying an established protocol at the *Klinikum rechts der Isar* (TU Munich, Germany). Therefore, 20 µg of the purified AMTG (AcOH salt) were dissolved in Tracepur® H_2O containing 10 vol-% of a NaOAc buffer (1 M in Tracepur® H_2O, *pH* = 5.50) and then, the mixture was labeled with 1 GBq [^{177}Lu]$LuCl_3$ (0.04 M in HCl) by heating to 95 °C for 15 min. Immediately after labeling, 10 vol-% of a sodium ascorbate solution (0.1 M in Tracepur® H_2O) was added to prevent radiolysis. Radiochemical purity of the labeled ligand was determined by radio RP-HPLC. After confirmation of a quantitative labeling, the solution containing [^{177}Lu]AMTG was filtered *via* a sterile filter and diluted with NaCl solution (0.9% in PBS, *v*/*v*) to the desired volume.

2.5. *In vitro* experiments

2.5.1. Determination of receptor affinity (IC_{50})

Cells were harvested 24 ± 2 h before the experiment and seeded in 24-well plates (1.5×10^5 cells in 1 mL/well). After removal of the culture medium, the cells were washed once with 500 µL of HBSS (Hank's balanced salt solution, *Biochrom GmbH*, Berlin, Germany, with addition of 1% bovine serum albumin (BSA, *v*/*v*)) and left in 200 µL HBSS (1% BSA, *v*/*v*) for 9 min at rt for equilibration. Next, 25 µL per well of solutions, containing either HBSS (1% BSA, *v*/*v*) as control or the respective compound in increasing concentration (10^{-10} M – 10^{-4} M in HBSS (1% BSA, *v*/*v*)), were added with subsequent addition of 25 µL of the respective competing radiolabeled reference ([3-[^{125}I]*I*-Tyr^4]BBN, [3-[^{125}I]*I*-tyr^6, *β*-Ala^{11}, Phe^{13}, Nle^{14}]BBN$_{6-14}$, [3-[^{125}I]*I*-tyr^6]MJ9) (2.0 nM) in HBSS (1% BSA, *v*/*v*).

All experiments were performed in triplicate for each concentration. After 2 h incubation at rt, the experiment was terminated by removal of the medium and consecutive rinsing with 300 µL of HBSS (1% BSA, *v*/*v*). The media of both steps were combined in one fraction and represent the amount of free radiolabeled reference. Afterwards, the cells were lysed with 300 µL of 1 M NaOH for at least 15 min and united with the 300 µL NaOH of the following washing step. Quantification of bound and free radiolabeled reference was accomplished in a *γ*-counter. IC_{50} determination for each conjugate was repeated twice.

2.5.2. *n*-Octanol-PBS distribution coefficient ($\log D_{7.4}$)

Approximately 1 MBq of the labeled tracer was dissolved in 1 mL of a 1:1 mixture (*v*/*v*) of phosphate buffered saline (PBS, *pH* = 7.4) and *n*-octanol in an Eppendorf tube (1.5 mL). After vigorous mixing of the suspension for 3 min at rt, the vial was centrifuged at 9000 rpm for 5 min (Biofuge 15, *Heraeus Sepatech*, Osterode, Germany) and 200 µL aliquots of both layers were measured in a *γ*-counter. The experiment was repeated at least five times.

2.5.3. Receptor-mediated internalization studies

For internalization studies, PC-3 cells were harvested 24 ± 2 h before the experiment and seeded in poly-L-lysine coated 24-well plates (1.5×10^5 cells/well, 1 mL, *Greiner Bio-One*, Kremsmünster, Austria). Subsequent to the removal of the culture medium, the cells were washed once with 500 µL DMEM/F-12 (5% BSA, *v*/*v*) and left to equilibrate at 37 °C for at least 15 min in 200 µL DMEM/F-12 (5% BSA, *v*/*v*). Each well was treated with either 25 µL of DMEM/F-12 (5% BSA, *v*/*v*) or 25 µL [^{nat}Lu]RM2 (10^{-3} M) for blockade. Next, 25 µL of the ^{125}I/^{177}Lu-labeled BBN analog (10 nM) was added and the cells were incubated at 37 °C for 60 min.

The experiment was terminated by placing the 24-well plate on ice for 1 min and consecutive removal of the medium. Each well was rinsed with 300 µL ice-cold PBS and the fractions from these first two steps were combined, representing the amount of free radiolabeled reference. Removal of surface bound activity was accomplished by incubation of the cells with 300 µL of ice-cold Acid Wash solution

(0.02 M NaOAc, *pH* = 5.0) for 10 min at rt and rinsed again with 300 µL of ice-cold PBS. The internalized activity was determined by incubation of the cells in 300 µL NaOH (1 M) and the combination with the fraction of a subsequent washing step with 300 µL NaOH (1 M).

Each experiment (control and blockade) was performed sixfold. Free, surface bound and internalized activity was quantified in a γ-counter. Data was corrected for non-specific internalization.

2.5.4. Plasma studies

In vitro stability was determined applying a procedure published by *Linder et al.* which was slightly modified by our group[177]. Therefore, the ^{177}Lu-labeled ligands were accomplished as described above and immediately after labeling, 200 µL of human plasma (100 µL of murine plasma) were added and the mixture (final volume of 300 µL and 200 µL, respectively) was incubated at 37 °C for 72 ± 2 h. Proteins were precipitated by treatment with 150 µL of ice-cold EtOH and 450 µL of ice-cold MeCN (in case of murine plasma: 100 µL EtOH and 300 µL MeCN), followed by centrifugation for 20 min at 13000 rpm. The supernatants were decanted and these samples were analyzed using radio RP-HPLC.

2.6. *In vivo* experiments

2.6.1. General

All animal experiments were conducted in accordance with general animal welfare regulations in Germany (German animal protection act, as amended on 18.05.2018, Art. 141 G v. 29.3.2017 I 626, approval no. 55.2-1-54-2532-71-13) and the institutional guidelines for the care and use of animals. To establish tumor xenografts, PC-3 cells (5.0×10^6 cells per 200 µL) were suspended in a 1:1 mixture (*v*/*v*) of Dulbecco modified Eagle medium / Nutrition Mixture F-12 with Glutamax-I (1:1) and Cultrex® Basement Membrane Matrix Type 3 (*Trevigen*, Gaithersburg, MD, USA) and inoculated subcutaneously onto the right shoulder of 6–10 weeks old CB17-SCID mice (*Charles River*, Sulzfeld, Germany). Mice were used for experiments when tumors had grown to a diameter of 5–8 mm (2-3 weeks after inoculation).

2.6.2. Biodistribution

Approximately 1–5 MBq (100 pmol) of the ^{177}Lu-labeled GRPR antagonists were injected into the tail vein of PC-3 tumor-bearing female CB17-SCID mice and sacrificed after 1 h and 24 h post injection (n = 4). Selected organs were removed, weighted and measured in a γ-counter. For competition studies, 3.62 mg/kg (40 nmol) of [^{nat}Lu]RM2 (10^{-3} M in PBS) was co-administered.

2.6.3. *µ*SPECT/CT imaging

Imaging studies were performed at a MILabs VECTor^4 small-animal SPECT/PET/OI/CT (MILabs, Utrecht, the Netherlands). Data were reconstructed using the MILabs-Rec software (version 10.02) and a pixel-based Similarity-Regulated Ordered Subsets Expectation Maximization (SROSEM) algorithm with a window-based scatter correction (20% below and 20% above the photopeak, respectively). Further data analysis was accomplished using the PMOD4.0 software (PMOD TECHNOLOGIES LLC, Zurich, Switzerland) at defined settings (voxel size CT: 80 µm, voxel size SPECT: 0.8 mm, 1.6 mm (FWHM) Gaussian blurring post processing filter, with calibration factor in kBq/mL and decay correction and no attenuation correction).

For *µ*SPECT studies mice were anesthetized with isoflurane and injected with 2–4 MBq (100 pmol) of the ^{177}Lu-labeled tracer into the tail vein. Static images were recorded 1, 4, 8, 24 and 28 h p.i. with an acquisition time of 45-60 min using the HE-GP-RM collimator and a step-wise multi-planar bed movement. For competition studies, 3.62 mg/kg (40 nmol) of [^{nat}Lu]RM2 (10^{-3} M in PBS) was co-administered.

2.7. Human Application

Clinical evaluation in the patient was conducted under compassionate use in compliance with the German Medicinal Products Act, AMG §13 2b, and in accordance with the responsible regulatory body (Government of Oberbayern). A proof of concept (PoC) study was performed at the *Klinikum rechts der Isar* (TU Munich, Germany).

Human application of [^{177}Lu]AMTG

In a PoC study, one patient suffering from mCRPC PSMA-avid lesions on a pretherapeutic PET scan ([^{18}F][^{nat}Ga]rhPSMA-7.3) received 1.11 GBq of [^{177}Lu]AMTG. The uptake of the tracer was imaged by scintigraphy 1 h and 4 h p.i. Each scan was obtained at a speed of 12 cm/min on a dual-headed SYMBIA T6 (Siemens Medical Solutions, Erlangen, Germany) equipped with 9.5 mm NaI(Tl) crystals and medium-energy low-penetration collimators. A 20% and a 12% energy window were placed around the 208 keV and 113 keV peak of ^{177}Lu-lutetium, respectively.

3. Characterization of GRPR-targeted ligands

3.1. Agonistic derivatives

All mentioned agonists were synthesized by standard Fmoc-based SPPS (**GP1**, **GP2**, **GP5**) using a *H*-Rink amide ChemMatrix® resin (35-100 mesh particle size, 0.4-0.6 mmol/g loading). [Tyr^4]BBN and BBN were purchased from Sigma-Aldrich GmbH (Munich, Germany).

Bombesin (BBN)

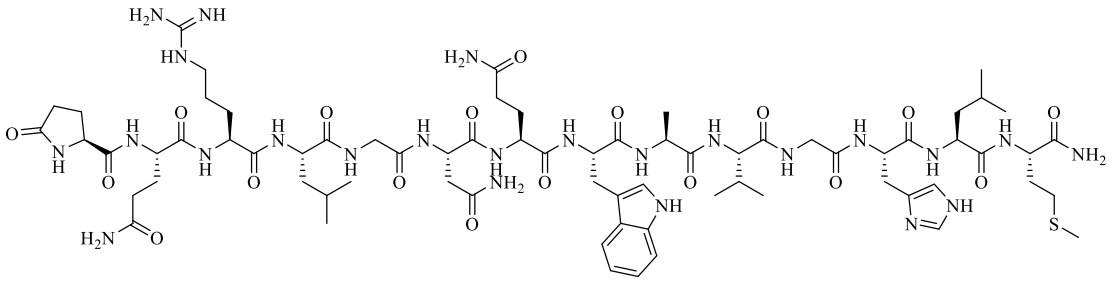

***H*-pGlu^1-Gln^2-Arg^3-Leu^4-Gly^5-Asn^6-Gln^7-Trp^8-Ala^9-Val^{10}-Gly^{11}-His^{12}-Leu^{13}-Met^{14}-NH$_2$**

RP-HPLC (10→90% MeCN in 15 min): t_R = 6.7 min, *K*‘ = 3.19.

Calculated monoisotopic mass ($C_{71}H_{110}N_{24}O_{18}S$): 1618.8, found: m/z = 810.2 $[M+2H]^{2+}$, 1619.2 $[M+H]^+$.

[Tyr^4]BBN

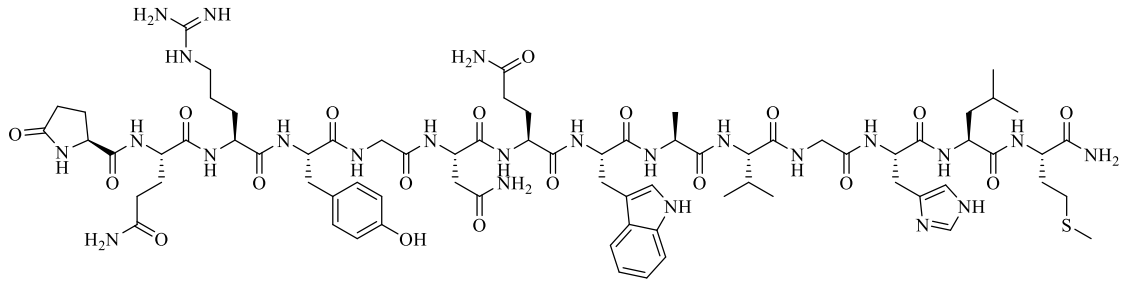

RP-HPLC (10→90% MeCN in 15 min): t_R = 6.6 min, *K*‘ = 3.13.

Calculated monoisotopic mass ($C_{74}H_{108}N_{24}O_{19}S$): 1668.8, found: m/z = 835.1 $[M+2H]^{2+}$, 1669.1 $[M+H]^+$.

[phe^{6}, *β*-Ala^{11}, Phe^{13}, Nle^{14}]BBN$_{6-14}$ (universal ligand, UL)

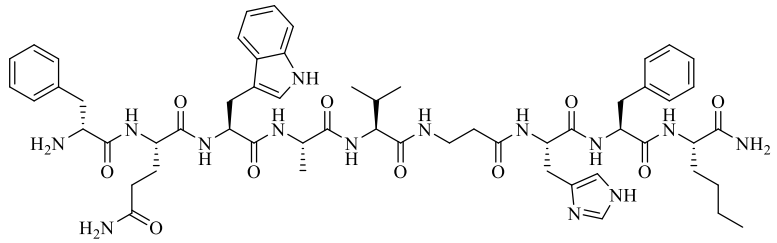

RP-HPLC (10→90% MeCN in 15 min): t_R = 9.7 min, *K*‘ = 5.07.

Calculated monoisotopic mass ($C_{57}H_{76}N_{14}O_{10}$): 1116.6, found: m/z = 559.5 $[M+2H]^{2+}$, 1117.2 $[M+H]^{+}$.

[tyr^{6}, *β*-Ala^{11}, Phe^{13}, Nle^{14}]BBN$_{6-14}$ (labeling precursor of agonistic radiolabeled reference)

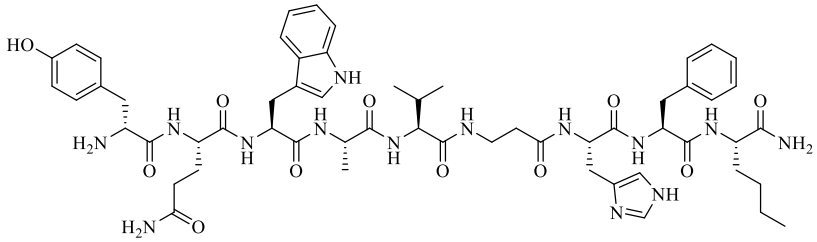

RP-HPLC (10→90% MeCN in 15 min): t_R = 9.1 min, *K*‘ = 4.67.

Calculated monoisotopic mass ($C_{57}H_{76}N_{14}O_{11}$): 1132.6, found: m/z = 567.0 $[M+2H]^{2+}$, 1132.9 $[M+H]^{+}$.

[3-*I*-tyr^{6}, *β*-Ala^{11}, Phe^{13}, Nle^{14}]BBN$_{6-14}$ (cold standard of agonistic radiolabeled reference)

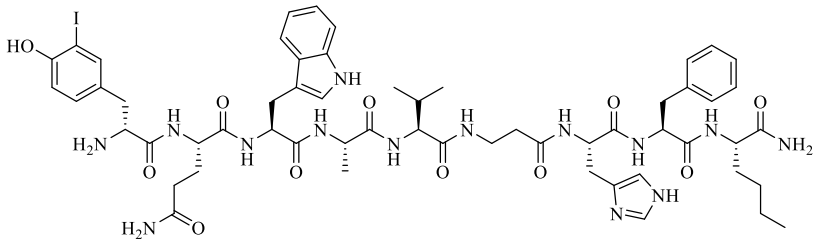

RP-HPLC (10→90% MeCN in 15 min): t_R = 9.5 min, *K*‘ = 4.94.

Calculated monoisotopic mass ($C_{57}H_{75}IN_{14}O_{11}$): 1258.5, found: m/z = 630.2 $[M+2H]^{2+}$, 1259.5 $[M+H]^{+}$.

3.2. MJ9 derivatives

All mentioned compounds based on the core structure of MJ9 were synthesized by standard Fmoc-based SPPS (**GP1**, **GP2**, **GP5**) using a *H*-Rink amide ChemMatrix® resin (35-100 mesh particle size, 0.4-0.6 mmol/g loading). As the structure of MJ9[135] was similar to RM2[39], but contains no chelator, all listed derivatives below were also synthesized without a chelator yielding a free amine at the respective *N*-terminus.

MJ9 (*H*-Pip-phe-Gln-Trp-Ala-Val-Gly-His-Sta-Leu-NH_2)

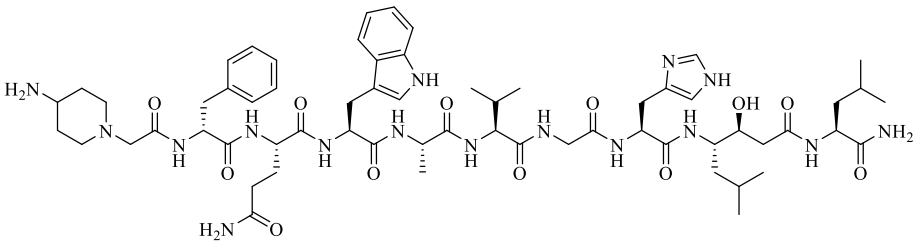

***H*-Pip^{5}-phe^{6}-Gln^{7}-Trp^{8}-Ala^{9}-Val^{10}-Gly^{11}-His^{12}-Sta^{13}-Leu^{14}-NH_2**

RP-HPLC (10→90% MeCN in 15 min): t_R = 9.0 min, *K*‘ = 4.63.

Calculated monoisotopic mass ($C_{62}H_{92}N_{16}O_{12}$): 1252.7, found: m/z = 627.5 $[M+2H]^{2+}$, 1253.4 $[M+H]^{+}$.

[tyr^{6}]MJ9 (labeling precursor of antagonistic radiolabeled reference [3-[^{125}I]*I*-tyr^{6}]MJ9)

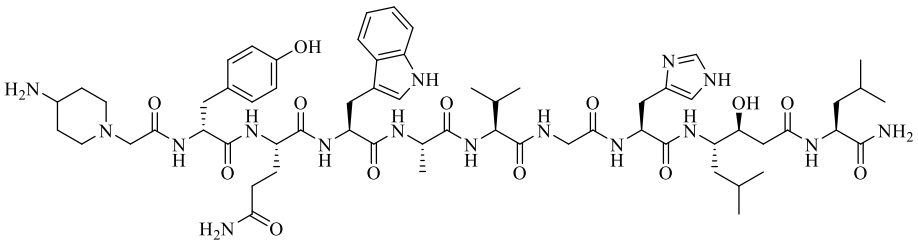

RP-HPLC (10→90% MeCN in 15 min): t_R = 8.9 min, *K*‘ = 4.56.

Calculated monoisotopic mass ($C_{62}H_{92}N_{16}O_{13}$): 1268.7, found: m/z = 635.0 $[M+2H]^{2+}$, 1269.8 $[M+H]^{+}$.

[3-*I*-tyr^{6}]MJ9 (cold standard of antagonistic radiolabeled reference)

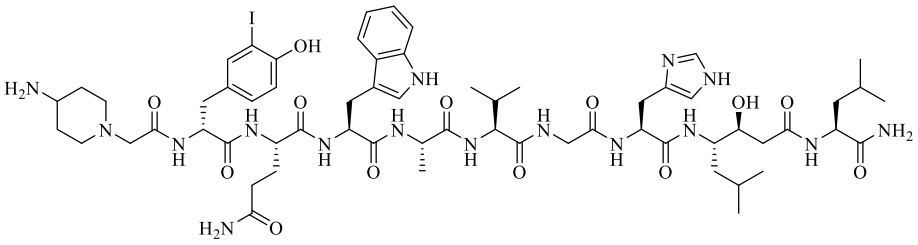

RP-HPLC (10→90% MeCN in 15 min): t_R = 10.1 min, *K*‘ = 5.31.

Calculated monoisotopic mass ($C_{62}H_{91}IN_{16}O_{13}$): 1394.6, found: m/z = 698.4 $[M+2H]^{2+}$, 1395.7 $[M+H]^{+}$.

3.2.1. Ala-Scan derivatives

All mentioned Ala-Scan conjugates based on the core structure of MJ9 were synthesized by standard Fmoc-based SPPS (**GP1**, **GP2**, **GP5**) using a *H*-Rink amide ChemMatrix® resin (35-100 mesh particle size, 0.4-0.6 mmol/g loading). Similar to MJ9, all listed derivatives below were also synthesized without a chelator yielding a free amine at the respective *N*-terminus. Structure of the respective compounds was equal to MJ9 except for the Ala substitutions in the respective positions.

MJ9

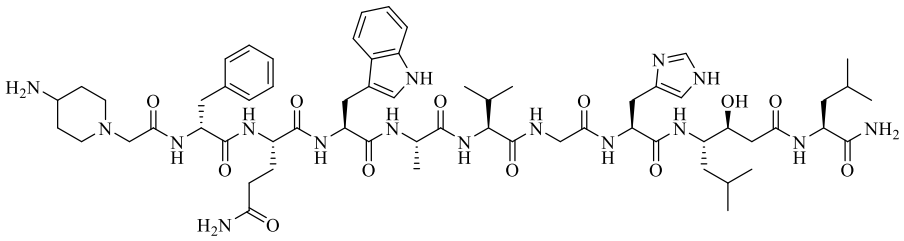

***H*-Pip^{5}-phe^{6}-Gln^{7}-Trp^{8}-Ala^{9}-Val^{10}-Gly^{11}-His^{12}-Sta^{13}-Leu^{14}-NH$_2$**

[Ala^{5}]MJ9

RP-HPLC (10→90% MeCN in 15 min): t_R = 10.7 min, *K*‘ = 5.69.

Calculated monoisotopic mass ($C_{58}H_{85}N_{15}O_{12}$): 1183.7, found: m/z = 592.7 $[M+2H]^{2+}$, 1184.4 $[M+H]^{+}$.

[Ala^{6}]MJ9

RP-HPLC (10→90% MeCN in 15 min): t_R = 9.7 min, *K*‘ = 5.06.

Calculated monoisotopic mass ($C_{56}H_{88}N_{16}O_{12}$): 1176.7, found: m/z = 589.5 $[M+2H]^{2+}$, 1177.7 $[M+H]^{+}$.

[Ala^{7}]MJ9

RP-HPLC (10→90% MeCN in 15 min): t_R = 9.7 min, *K*‘ = 5.06.

Calculated monoisotopic mass ($C_{60}H_{89}N_{15}O_{11}$): 1195.7, found: m/z = 598.9 $[M+2H]^{2+}$, 1196.4 $[M+H]^{+}$.

[Ala^{8}]MJ9

RP-HPLC (10→90% MeCN in 15 min): t_R = 8.7 min, *K*‘ = 4.44.

Calculated monoisotopic mass ($C_{54}H_{87}N_{15}O_{12}$): 1137.7, found: m/z = 569.9 $[M+2H]^{2+}$, 1138.4 $[M+H]^{+}$.

[Ala^{10}]MJ9

RP-HPLC (10→90% MeCN in 15 min): t_R = 10.3 min, *K*‘ = 5.44.

Calculated monoisotopic mass ($C_{60}H_{88}N_{16}O_{12}$): 1224.7, found: m/z = 613.0 $[M+2H]^{2+}$, 1224.6 $[M+H]^{+}$.

[Ala^{11}]MJ9

RP-HPLC (10→90% MeCN in 15 min): t_R = 10.5 min, *K*‘ = 5.56.

Calculated monoisotopic mass ($C_{63}H_{94}N_{16}O_{12}$): 1266.7, found: m/z = 634.3 $[M+2H]^{2+}$, 1267.0 $[M+H]^{+}$.

[Ala^{12}]MJ9

RP-HPLC (10→90% MeCN in 15 min): t_R = 9.9 min, *K*‘ = 5.19.

Calculated monoisotopic mass ($C_{59}H_{90}N_{14}O_{12}$): 1186.7, found: m/z = 594.2 $[M+2H]^{2+}$, 1186.9 $[M+H]^{+}$.

[Ala^{13}]MJ9

RP-HPLC (10→90% MeCN in 15 min): t_R = 9.4 min, *K*‘ = 4.88.

Calculated monoisotopic mass ($C_{57}H_{82}N_{16}O^{11}$): 1166.6, found: m/z = 584.2 $[M+2H]^{2+}$, 1166.9 $[M+H]^{+}$.

[Ala^{14}]MJ9

RP-HPLC (10→90% MeCN in 15 min): t_R = 9.0 min, *K*‘ = 4.63.

Calculated monoisotopic mass ($C_{59}H_{86}N_{16}O_{12}$): 1210.7, found: m/z = 606.2 $[M+2H]^{2+}$, 1211.7 $[M+H]^{+}$.

3.2.2. Backbone *N*-methylated derivatives

All mentioned backbone *N*-methylated analogs based on the core structure of MJ9 were synthesized by standard Fmoc-based SPPS (**GP1**, **GP2**, **GP5**) using a *H*-Rink amide ChemMatrix® resin (35-100 mesh particle size, 0.4-0.6 mmol/g loading). Similar to MJ9, all listed conjugates below were also synthesized without a chelator yielding a free amine at the respective *N*-terminus. Structure of the respective derivatives was equal to MJ9 except for the backbone *N*-methylated substitutions in the respective positions.

H-Pip^{5}-phe^{6}-Gln^{7}-Trp^{8}-Ala^{9}-Val^{10}-Gly^{11}-His^{12}-Sta^{13}-Leu^{14}-NH_2

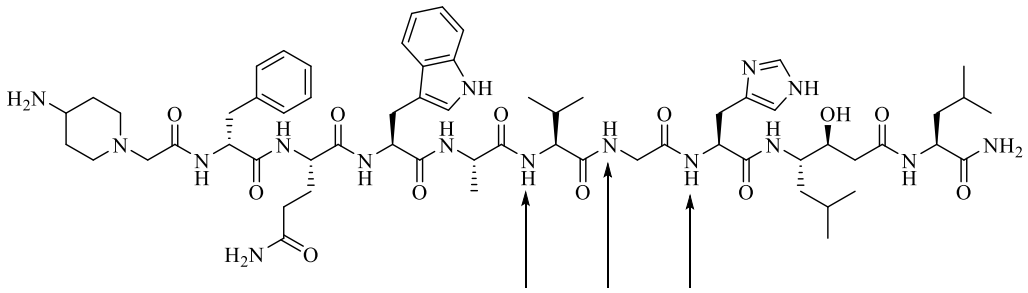

On-resin substitution by corresponding *N*-methyl amino acids

[*N*-Me-Val^{10}]MJ9

RP-HPLC (10→90% MeCN in 15 min): t_R = 9.5 min, *K*‘ = 4.94.

Calculated monoisotopic mass ($C_{63}H_{94}N_{16}O_{12}$): 1266.7, found: m/z = 634.4 $[M+2H]^{2+}$, 1267.2 $[M+H]^{+}$.

[*N*-Me-Gly^{11}]MJ9

RP-HPLC (10→90% MeCN in 15 min): t_R = 9.3 min, *K*‘ = 4.81.

Calculated monoisotopic mass ($C_{63}H_{94}N_{16}O_{12}$): 1266.7, found: m/z = 634.1 $[M+2H]^{2+}$, 1267.4 $[M+H]^{+}$.

[*N*-Me-His^{12}]MJ9

RP-HPLC (10→90% MeCN in 15 min): t_R = 9.4 min, *K*‘ = 4.88.

Calculated monoisotopic mass ($C_{63}H_{94}N_{16}O_{12}$): 1266.7, found: m/z = 634.8 $[M+2H]^{2+}$, 1267.3 $[M+H]^{+}$.

[*N*-Me-Val^{10}, *N*-Me-Gly^{11}]MJ9

RP-HPLC (10→90% MeCN in 15 min): t_R = 9.6 min, *K*‘ = 5.00.

Calculated monoisotopic mass ($C_{64}H_{96}N_{16}O_{12}$): 1280.7, found: m/z = 641.6 $[M+2H]^{2+}$, 1281.6 $[M+H]^{+}$.

[*N*-Me-Val^{10}, *N*-Me-His^{12}]MJ9

RP-HPLC (10→90% MeCN in 15 min): t_R = 10.1 min, *K*‘ = 5.31.

Calculated monoisotopic mass ($C_{64}H_{96}N_{16}O_{12}$): 1280.7, found: m/z = 641.5 $[M+2H]^{2+}$, 1281.0 $[M+H]^{+}$.

[*N*-Me-Gly^{11}, *N*-Me-His^{12}]MJ9

RP-HPLC (10→90% MeCN in 15 min): t_R = 9.8 min, *K*‘ = 5.13.

Calculated monoisotopic mass ($C_{64}H_{96}N_{16}O_{12}$): 1280.7, found: m/z = 641.8 $[M+2H]^{2+}$, 1281.5 $[M+H]^{+}$.

[*N*-Me-Val^{10}, *N*-Me-Gly^{11}, *N*-Me-His^{12}]MJ9

RP-HPLC (10→90% MeCN in 15 min): t_R = 10.3 min, *K*‘ = 5.44.

Calculated monoisotopic mass ($C_{65}H_{98}N_{16}O_{12}$): 1294.8, found: m/z = 648.6 $[M+2H]^{2+}$, 1295.9 $[M+H]^{+}$.

3.2.3. Monosubstituted MJ9 derivatives

All mentioned monosubstituted conjugates based on the core structure of MJ9 were synthesized by standard Fmoc-based SPPS (**GP1**, **GP2**, **GP5**) using a *H*-Rink amide ChemMatrix® resin (35-100 mesh particle size, 0.4-0.6 mmol/g loading). Similar to MJ9, all listed analogs below were also synthesized without a chelator yielding a free amine at the respective *N*-terminus. Structure of the respective derivatives was equal to MJ9 except for the substitutions in the respective positions.

[Txa^{5}]MJ9

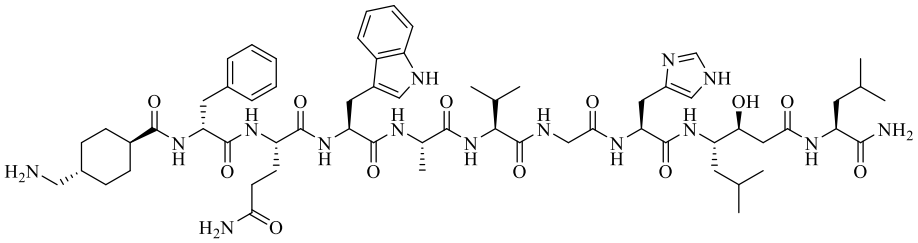

RP-HPLC (10→90% MeCN in 15 min): t_R = 7.6 min, *K*‘ = 3.75.

Calculated monoisotopic mass ($C_{63}H_{93}N_{15}O_{12}$): 1251.7, found: m/z = 626.7 $[M+2H]^{2+}$, 1252.0 $[M+H]^{+}$.

[tyr^{6}]MJ9

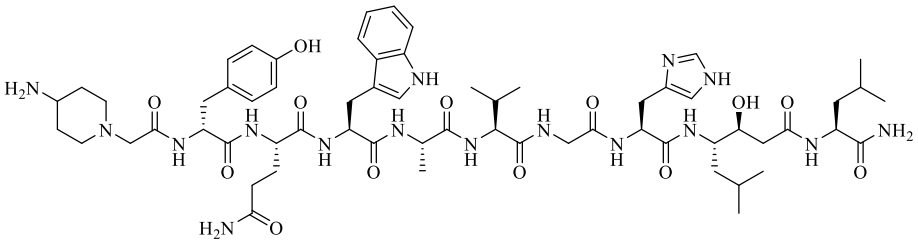

RP-HPLC (10→90% MeCN in 15 min): t_R = 6.7 min, *K*‘ = 3.19.

Calculated monoisotopic mass ($C_{62}H_{92}N_{16}O_{13}$): 1268.7, found: m/z = 635.0 $[M+2H]^{2+}$, 1269.3 $[M+H]^{+}$.

[nal^{6}]MJ9

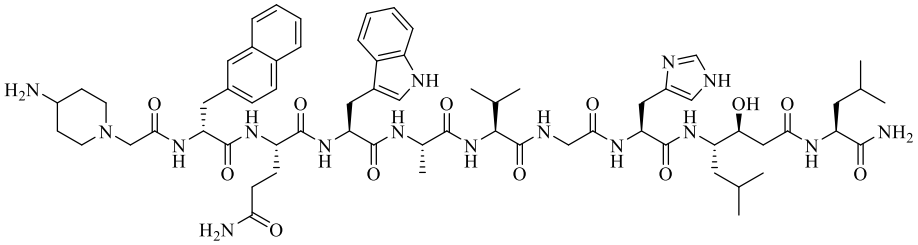

RP-HPLC (10→90% MeCN in 15 min): t_R = 7.0 min, *K*‘ = 3.38.

Calculated monoisotopic mass ($C_{66}H_{94}N_{16}O_{12}$): 1302.7, found: m/z = 652.7 $[M+2H]^{2+}$, 1303.1 $[M+H]^{+}$.

[(4-NH_2)Phe^6]MJ9

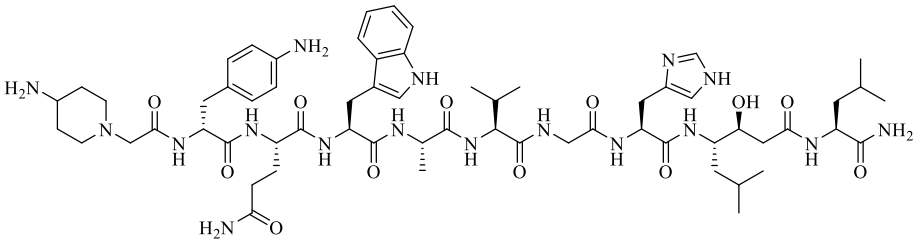

RP-HPLC (10→90% MeCN in 15 min): t_R = 6.5 min, *K*‘ = 3.06.

Calculated monoisotopic mass ($C_{62}H_{93}N_{17}O_{12}$): 1267.7, found: m/z = 634.5 $[M+2H]^{2+}$, 1268.4 $[M+H]^+$.

[Arg^6]MJ9

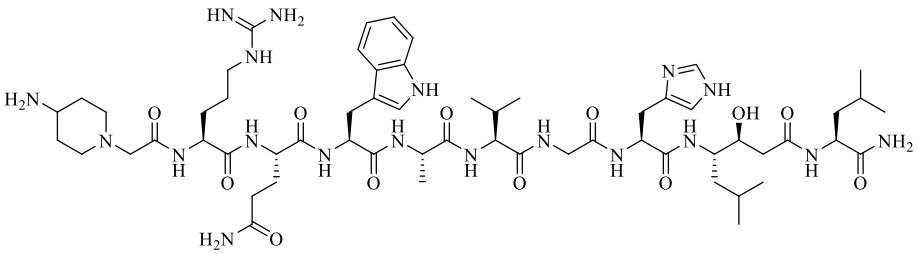

RP-HPLC (10→90% MeCN in 15 min): t_R = 6.2 min, *K*‘ = 2.88.

Calculated monoisotopic mass ($C_{59}H_{95}N_{19}O_{12}$): 1261.7, found: m/z = 631.6 $[M+2H]^{2+}$, 1262.0 $[M+H]^+$.

[arg^6]MJ9

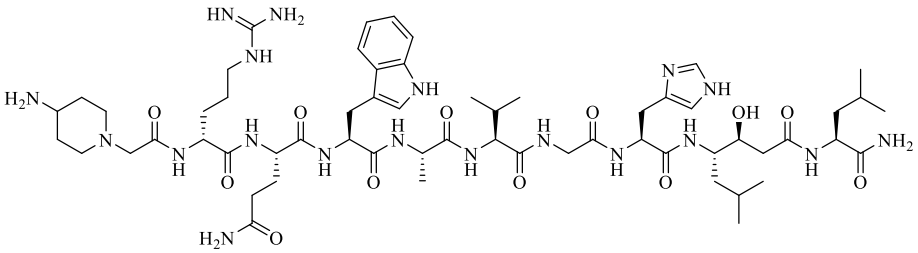

RP-HPLC (10→90% MeCN in 15 min): t_R = 6.2 min, *K*‘ = 2.88.

Calculated monoisotopic mass ($C_{59}H_{95}N_{19}O_{12}$): 1261.7, found: m/z = 631.7 $[M+2H]^{2+}$, 1262.3 $[M+H]^+$.

[Cit^6]MJ9

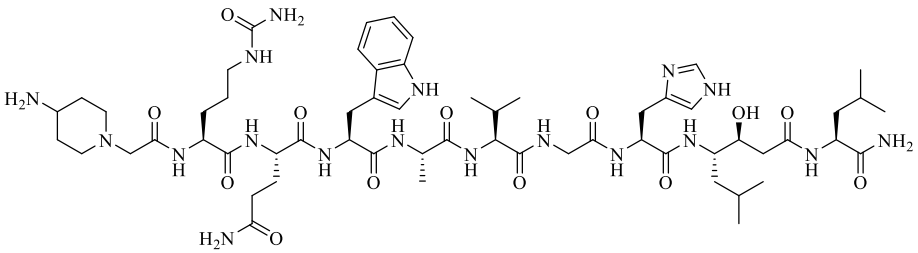

RP-HPLC (10→90% MeCN in 15 min): t_R = 6.4 min, *K*‘ = 3.00.

Calculated monoisotopic mass ($C_{59}H_{94}N_{18}O_{13}$): 1262.7, found: m/z = 632.2 $[M+2H]^{2+}$, 1262.9 $[M+H]^+$.

[cit^{6}]MJ9

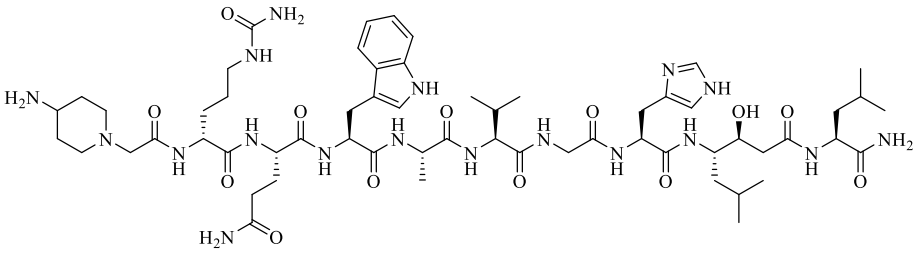

RP-HPLC (10→90% MeCN in 15 min): t_R = 6.4 min, *K*‘ = 3.00.

Calculated monoisotopic mass ($C_{59}H_{94}N_{18}O_{13}$): 1262.7, found: m/z = 632.5 $[M+2H]^{2+}$, 1263.1 $[M+H]^{+}$.

[Hse^{7}]MJ9

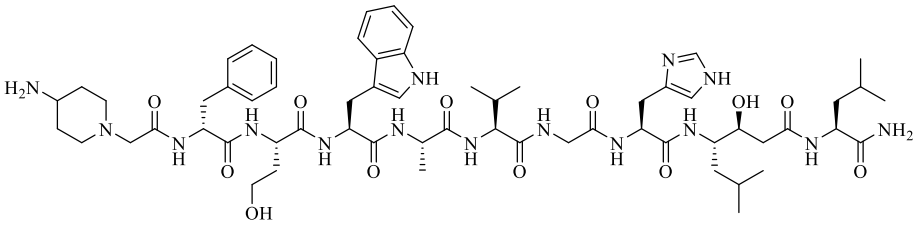

RP-HPLC (10→90% MeCN in 15 min): t_R = 6.9 min, *K*‘ = 3.31.

Calculated monoisotopic mass ($C_{61}H_{91}N_{15}O_{12}$): 1225.7, found: m/z = 614.0 $[M+2H]^{2+}$, 1226.8 $[M+H]^{+}$.

[(4-NH$_2$)Phe^{7}]MJ9

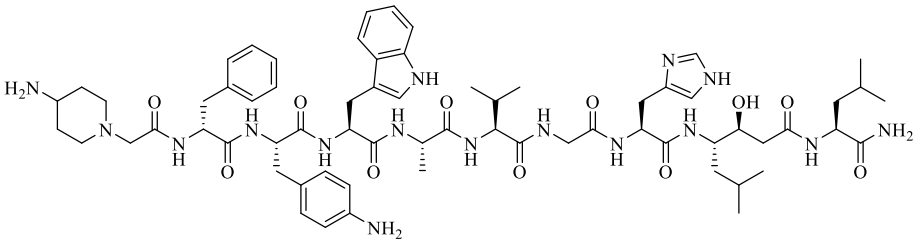

RP-HPLC (10→90% MeCN in 15 min): t_R = 6.5 min, *K*‘ = 3.06.

Calculated monoisotopic mass ($C_{66}H_{94}N_{16}O_{11}$): 1286.7, found: m/z = 644.5 $[M+2H]^{2+}$, 1287.4 $[M+H]^{+}$.

[Orn^{7}]MJ9

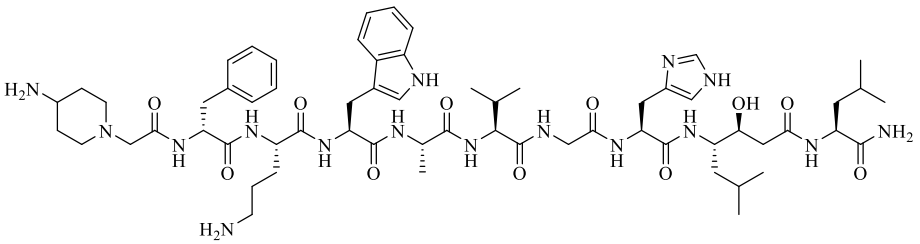

RP-HPLC (10→90% MeCN in 15 min): t_R = 6.5 min, *K*‘ = 3.06.

Calculated monoisotopic mass ($C_{62}H_{94}N_{16}O_{11}$): 1238.7, found: m/z = 620.4 $[M+2H]^{2+}$, 1240.0 $[M+H]^{+}$.

[Bta[8]]MJ9

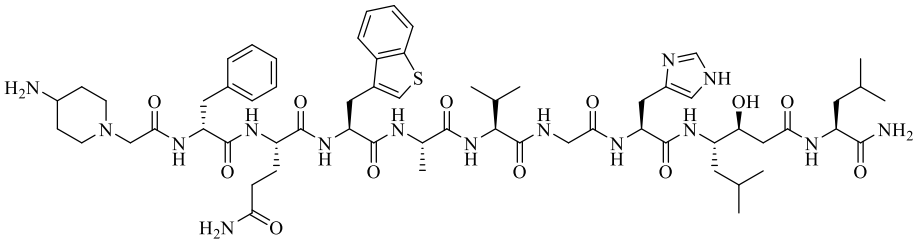

RP-HPLC (10→90% MeCN in 15 min): t_R = 10.3 min, *K*‘ = 5.44.

Calculated monoisotopic mass ($C_{62}H_{91}N_{15}O_{12}S$): 1269.7, found: m/z = 635.9 $[M+2H]^{2+}$, 1271.1 $[M+H]^{+}$.

[3-Me-Tyr[8]]MJ9

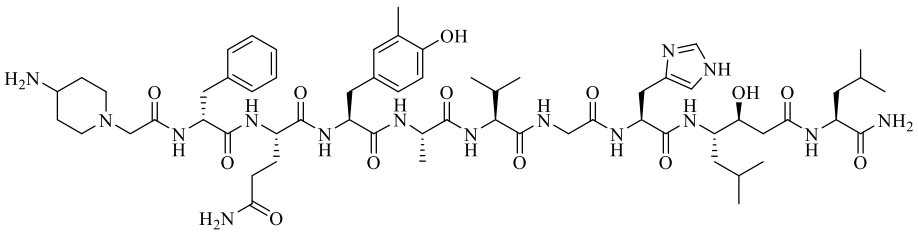

RP-HPLC (10→90% MeCN in 15 min): t_R = 9.4 min, *K*‘ = 4.88.

Calculated monoisotopic mass ($C_{61}H_{93}N_{15}O_{13}$): 1243.7, found: m/z = 623.0 $[M+2H]^{2+}$, 1244.6 $[M+H]^{+}$.

[Dap[9]]MJ9

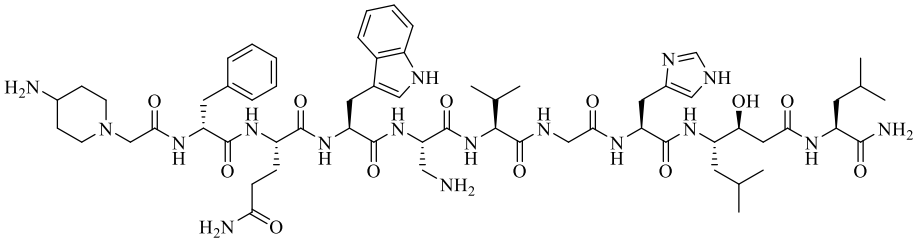

RP-HPLC (10→90% MeCN in 15 min): t_R = 6.7 min, *K*‘ = 3.19.

Calculated monoisotopic mass ($C_{62}H_{93}N_{17}O_{12}$): 1267.7, found: m/z = 635.2 $[M+2H]^{2+}$, 1269.1 $[M+H]^{+}$.

[Ser[9]]MJ9

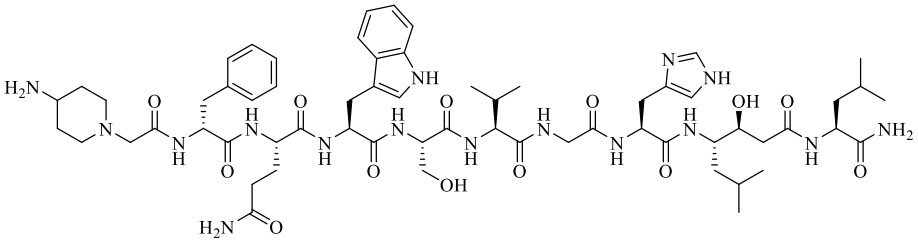

RP-HPLC (10→90% MeCN in 15 min): t_R = 6.8 min, *K*‘ = 3.25.

Calculated monoisotopic mass ($C_{62}H_{92}N_{16}O_{13}$): 1268.7, found: m/z = 635.4 $[M+2H]^{2+}$, 1269.2 $[M+H]^{+}$.

[ala^{9}]MJ9

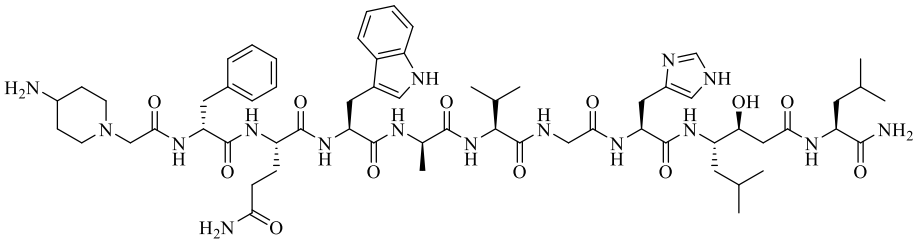

RP-HPLC (10→90% MeCN in 15 min): t_R = 9.0 min, *K*‘ = 4.63.

Calculated monoisotopic mass ($C_{62}H_{92}N_{16}O_{12}$): 1252.7, found: m/z = 627.6 $[M+2H]^{2+}$, 1253.2 $[M+H]^{+}$.

[ser^{9}]MJ9

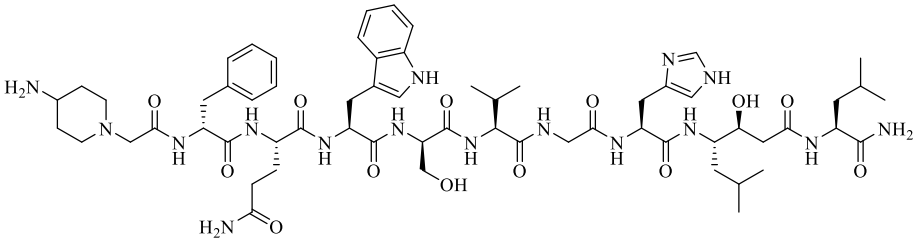

RP-HPLC (10→90% MeCN in 15 min): t_R = 6.8 min, *K*‘ = 3.25.

Calculated monoisotopic mass ($C_{62}H_{92}N_{16}O_{13}$): 1268.7, found: m/z = 635.5 $[M+2H]^{2+}$, 1269.0 $[M+H]^{+}$.

[Hse^{9}]MJ9

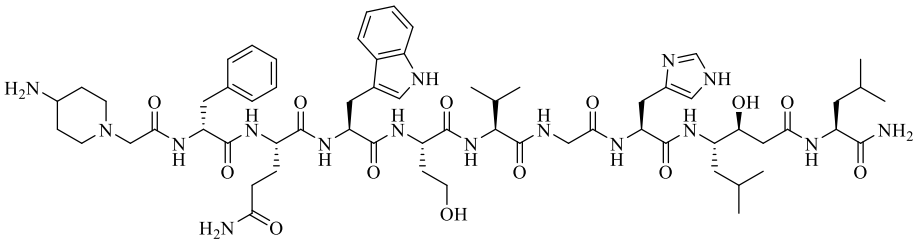

RP-HPLC (10→90% MeCN in 15 min): t_R = 6.8 min, *K*‘ = 3.25.

Calculated monoisotopic mass ($C_{63}H_{94}N_{16}O_{13}$): 1282.7, found: m/z = 642.4 $[M+2H]^{2+}$, 1283.2 $[M+H]^{+}$.

[Chg^{10}]MJ9

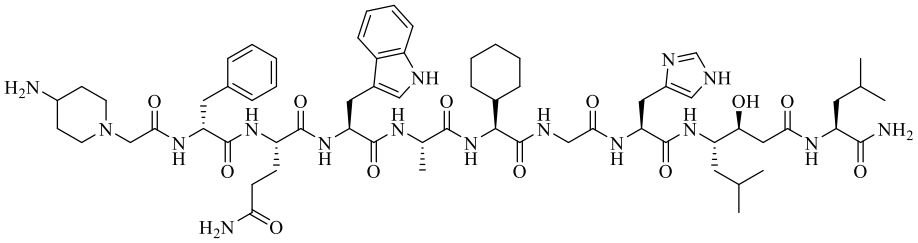

RP-HPLC (10→90% MeCN in 15 min): t_R = 10.7 min, *K*‘ = 5.69.

Calculated monoisotopic mass ($C_{65}H_{96}N_{16}O_{12}$): 1292.7, found: m/z = 647.6 $[M+2H]^{2+}$, 1293.9 $[M+H]^{+}$.

[Cpg^{10}]MJ9

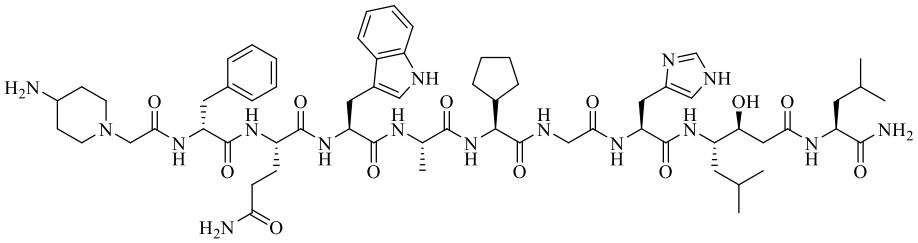

RP-HPLC (10→90% MeCN in 15 min): t_R = 7.2 min, *K*‘ = 3.50.

Calculated monoisotopic mass ($C_{64}H_{94}N_{16}O_{12}$): 1278.7, found: m/z = 640.4 $[M+2H]^{2+}$, 1279.3 $[M+H]^{+}$.

[Sta^{10}]MJ9

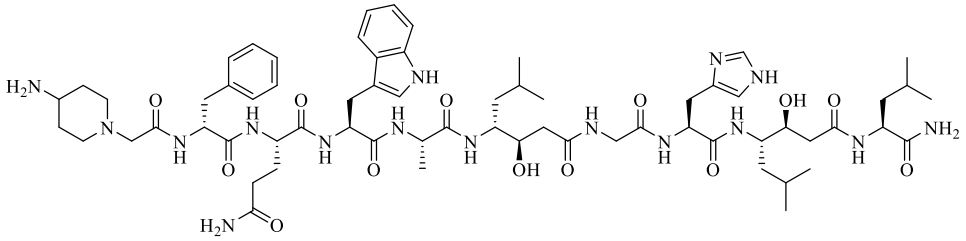

RP-HPLC (10→90% MeCN in 15 min): t_R = 10.1 min, *K*‘ = 5.31.

Calculated monoisotopic mass ($C_{65}H_{98}N_{16}O_{13}$): 1310.8, found: m/z = 656.7 $[M+2H]^{2+}$, 1311.5 $[M+H]^{+}$.

[Asn^{10}]MJ9

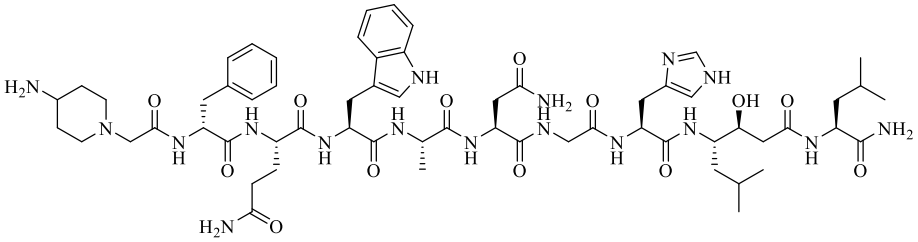

RP-HPLC (10→90% MeCN in 15 min): t_R = 5.4 min, *K*‘ = 2.38.

Calculated monoisotopic mass ($C_{61}H_{89}N_{17}O_{13}$): 1267.7, found: m/z = 635.0 $[M+2H]^{2+}$, 1268.7 $[M+H]^{+}$.

[ala^{11}]MJ9

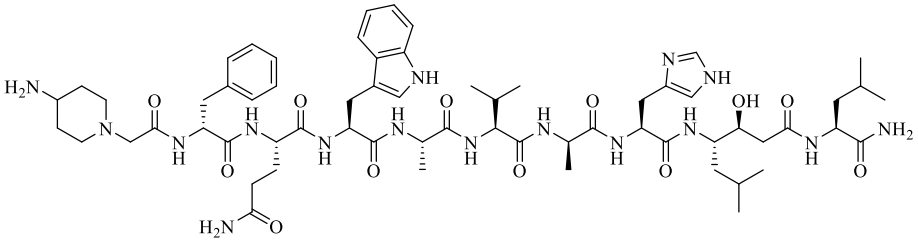

RP-HPLC (10→90% MeCN in 15 min): t_R = 10.5 min, *K*‘ = 5.56.

Calculated monoisotopic mass ($C_{63}H_{94}N_{16}O_{12}$): 1266.7, found: m/z = 634.5 $[M+2H]^{2+}$, 1267.4 $[M+H]^{+}$.

[Orn^{12}]MJ9

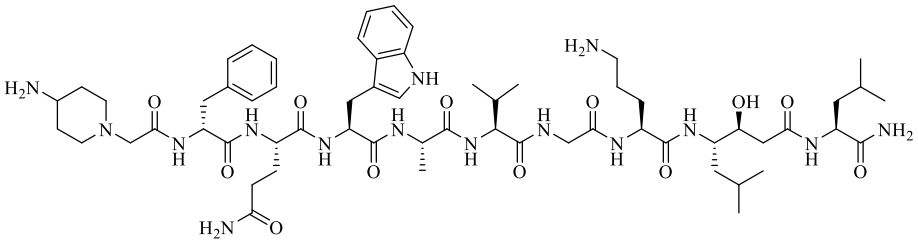

RP-HPLC (10→90% MeCN in 15 min): t_R = 6.5 min, *K*‘ = 3.06.

Calculated monoisotopic mass ($C_{61}H_{95}N_{15}O_{12}$): 1229.2, found: m/z = 615.2 $[M+2H]^{2+}$, 1230.1 $[M+H]^{+}$.

[Tza^{12}]MJ9

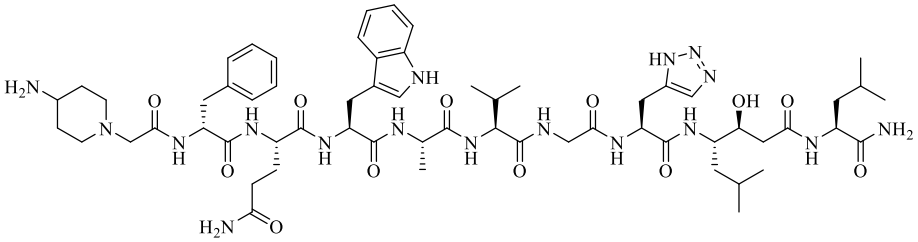

RP-HPLC (10→90% MeCN in 15 min): t_R = 6.4 min, *K*‘ = 3.00.

Calculated monoisotopic mass ($C_{61}H_{91}N_{17}O_{12}$): 1253.7, found: m/z = 628.1 $[M+2H]^{2+}$, 1255.3 $[M+H]^{+}$.

[(4-NH$_2$)Phe^{12}]MJ9

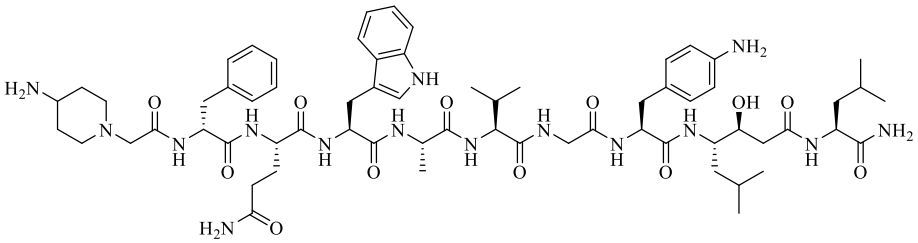

RP-HPLC (10→90% MeCN in 15 min): t_R = 6.9 min, *K*‘ = 3.31.

Calculated monoisotopic mass ($C_{65}H_{95}N_{15}O_{12}$): 1277.7, found: m/z = 640.0 $[M+2H]^{2+}$, 1278.4 $[M+H]^{+}$.

[Orn^{14}]MJ9

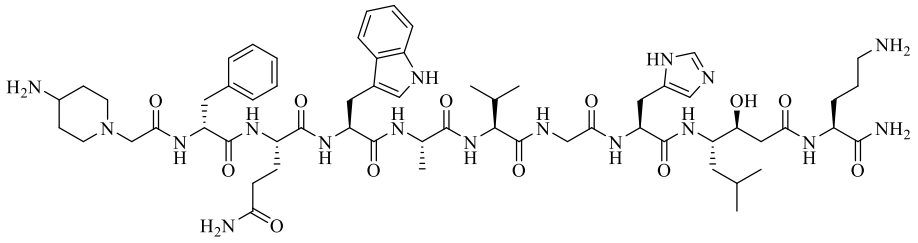

RP-HPLC (10→90% MeCN in 15 min): t_R = 6.0 min, *K*‘ = 2.75.

Calculated monoisotopic mass ($C_{61}H_{91}N_{17}O_{12}$): 1253.7, found: m/z = 627.0 $[M+2H]^{2+}$, 1254.4 $[M+H]^{+}$.

[Ser^{14}]MJ9

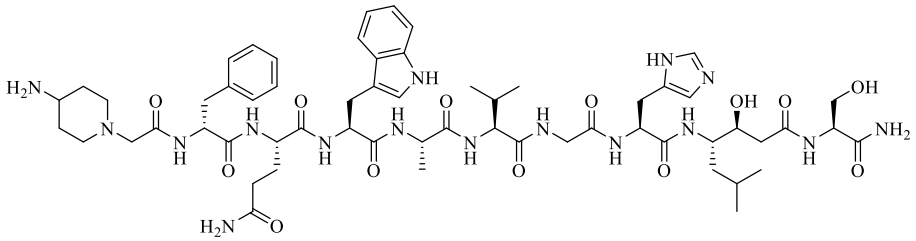

RP-HPLC (10→90% MeCN in 15 min): t_R = 6.1 min, *K*‘ = 2.81.

Calculated monoisotopic mass ($C_{59}H_{86}N_{16}O_{13}$): 1226.7, found: m/z = 614.5 $[M+2H]^{2+}$, 1227.3 $[M+H]^{+}$.

[Thr^{14}]MJ9

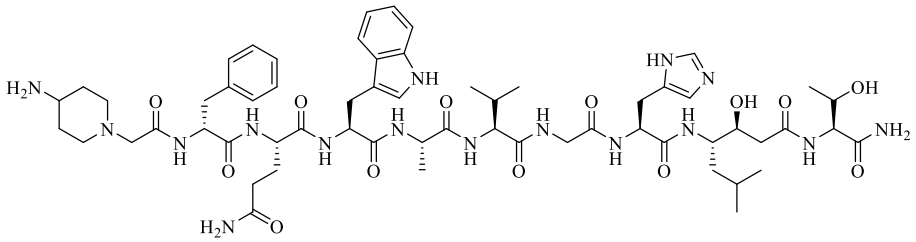

RP-HPLC (10→90% MeCN in 15 min): t_R = 6.1 min, *K*‘ = 2.81.

Calculated monoisotopic mass ($C_{60}H_{88}N_{16}O_{13}$): 1240.7, found: m/z = 621.4 $[M+2H]^{2+}$, 1241.4 $[M+H]^{+}$.

[His^{14}]MJ9

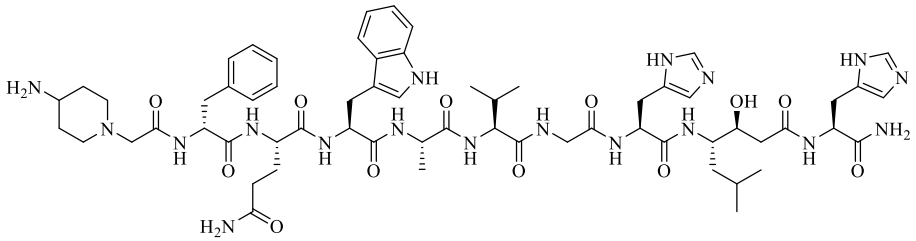

RP-HPLC (10→90% MeCN in 15 min): t_R = 5.9 min, *K*‘ = 2.69.

Calculated monoisotopic mass ($C_{62}H_{88}N_{18}O_{12}$): 1276.7, found: m/z = 639.4 $[M+2H]^{2+}$, 1277.3 $[M+H]^{+}$.

[Hse^{14}]MJ9

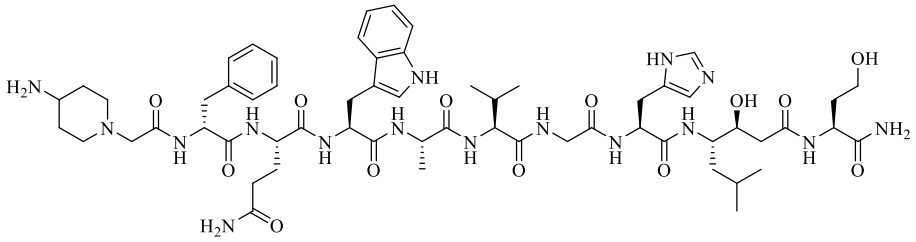

RP-HPLC (10→90% MeCN in 15 min): t_R = 6.0 min, *K*‘ = 2.75.

Calculated monoisotopic mass ($C_{60}H_{88}N_{16}O_{13}$): 1240.7, found: m/z = 621.3 $[M+2H]^{2+}$, 1241.4 $[M+H]^{+}$.

3.2.4. Multisubstituted MJ9 derivatives

All mentioned multisubstituted compounds based on the core structure of MJ9 were synthesized by standard Fmoc-based SPPS (**GP1**, **GP2**, **GP5**) using a *H*-Rink amide ChemMatrix® resin (35-100 mesh particle size, 0.4-0.6 mmol/g loading). Similar to MJ9, all listed conjugates below were also synthesized without a chelator yielding a free amine at the respective *N*-terminus. Structure of the respective analogs was equal to MJ9 except for the multiple substitutions in the respective positions.

[Gly^5, cit^6]MJ9

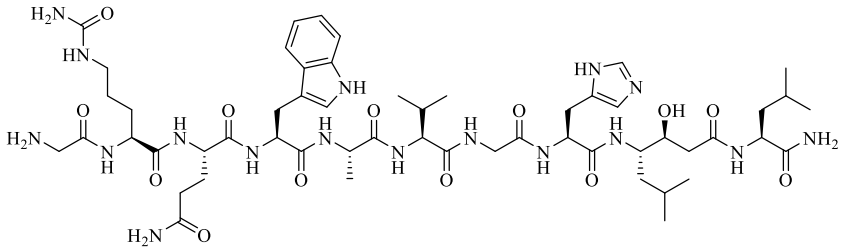

RP-HPLC (10→90% MeCN in 15 min): t_R = 6.4 min, *K*‘ = 3.00.

Calculated monoisotopic mass ($C_{54}H_{85}N_{17}O_{13}$): 1179.7, found: m/z = 590.8 $[M+2H]^{2+}$, 1180.0 $[M+H]^+$.

[Txa^5, arg^6]MJ9

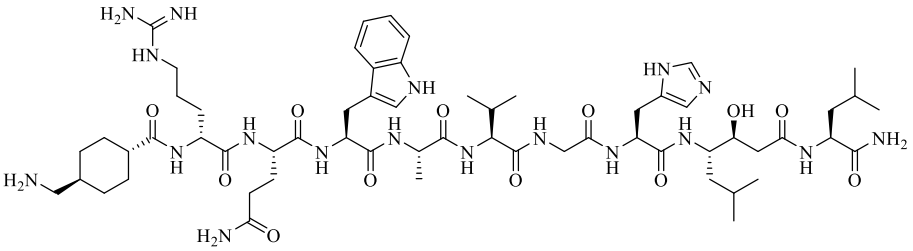

RP-HPLC (10→90% MeCN in 15 min): t_R = 6.3 min, *K*‘ = 2.94.

Calculated monoisotopic mass ($C_{60}H_{96}N_{18}O_{12}$): 1260.8, found: m/z = 631.3 $[M+2H]^{2+}$, 1260.8 $[M+H]^+$.

[Ala^5, Arg^6]MJ9

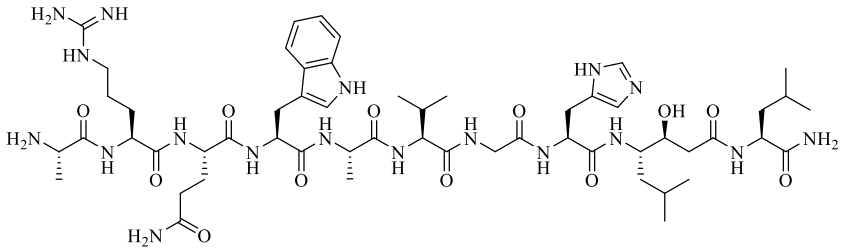

RP-HPLC (10→90% MeCN in 15 min): t_R = 6.4 min, *K*‘ = 3.00.

Calculated monoisotopic mass ($C_{55}H_{88}N_{18}O_{12}$): 1192.7, found: m/z = 597.5 $[M+2H]^{2+}$, 1193.8 $[M+H]^+$.

[ala^5, arg^6]MJ9

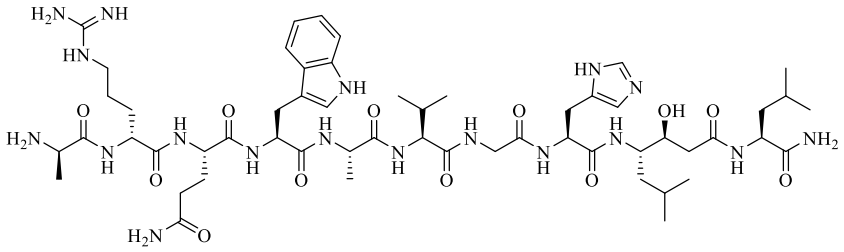

RP-HPLC (10→90% MeCN in 15 min): t_R = 6.4 min, *K*‘ = 3.00.

Calculated monoisotopic mass ($C_{55}H_{88}N_{18}O_{12}$): 1192.7, found: m/z = 597.2 $[M+2H]^{2+}$, 1193.0 $[M+H]^{+}$.

[Gly^5, arg^6]MJ9

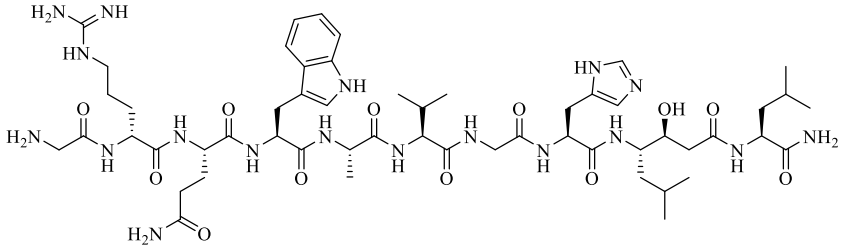

RP-HPLC (10→90% MeCN in 15 min): t_R = 6.2 min, *K*‘ = 2.87.

Calculated monoisotopic mass ($C_{54}H_{86}N_{18}O_{12}$): 1178.7, found: m/z = 590.3 $[M+2H]^{2+}$, 1179.0 $[M+H]^{+}$.

[Ala^5, arg^6]MJ9

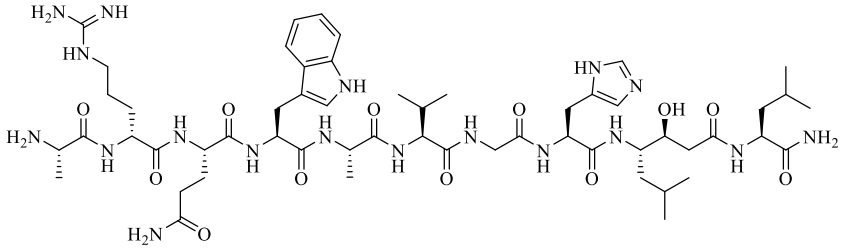

RP-HPLC (10→90% MeCN in 15 min): t_R = 6.3 min, *K*‘ = 2.94.

Calculated monoisotopic mass ($C_{55}H_{88}N_{18}O_{12}$): 1192.7, found: m/z = 597.3 $[M+2H]^{2+}$, 1193.0 $[M+H]^{+}$.

[*des*Pip^5, arg^6]MJ9

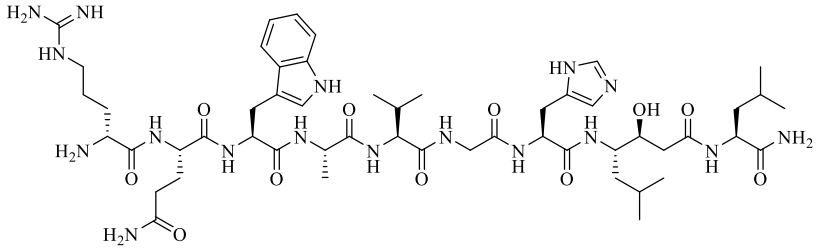

RP-HPLC (10→90% MeCN in 15 min): t_R = 6.4 min, *K*‘ = 3.00.

Calculated monoisotopic mass ($C_{52}H_{83}N_{17}O_{11}$): 1121.7, found: m/z = 561.8 $[M+2H]^{2+}$, 1122.1 $[M+H]^{+}$.

[*des*Pip^{5}, Arg^{6}]MJ9

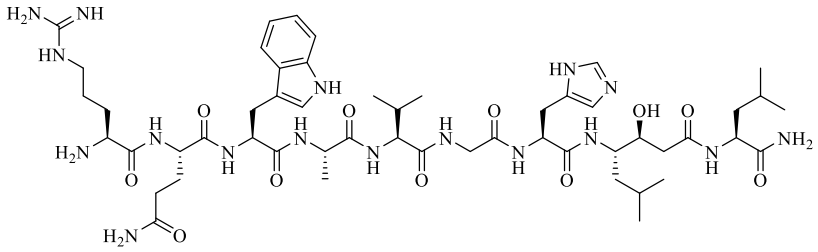

RP-HPLC (10→90% MeCN in 15 min): t_R = 6.3 min, *K*‘ = 2.94.

Calculated monoisotopic mass ($C_{52}H_{83}N_{17}O_{11}$): 1121.7, found: m/z = 561.8 $[M+2H]^{2+}$, 1122.0 $[M+H]^{+}$.

[Arg^{6}, His^{7}]MJ9

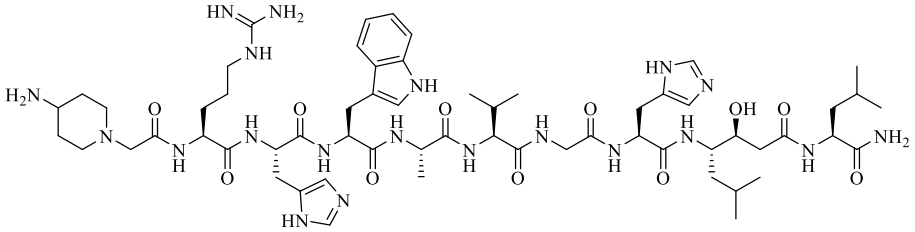

RP-HPLC (10→90% MeCN in 15 min): t_R = 6.0 min, *K*‘ = 2.75.

Calculated monoisotopic mass ($C_{60}H_{94}N_{20}O_{11}$): 1270.7, found: m/z = 636.4 $[M+2H]^{2+}$, 1271.5 $[M+H]^{+}$.

[arg^{6}, His^{7}]MJ9

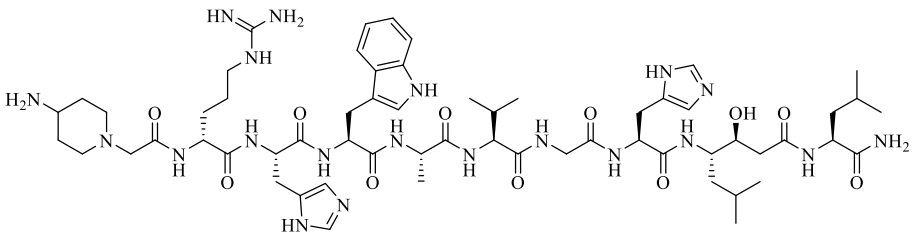

RP-HPLC (10→90% MeCN in 15 min): t_R = 6.0 min, *K*‘ = 2.75.

Calculated monoisotopic mass ($C_{60}H_{94}N_{20}O_{11}$): 1270.7, found: m/z = 636.2 $[M+2H]^{2+}$, 1271.2 $[M+H]^{+}$.

[Bta^{8}, Chg^{10}]MJ9

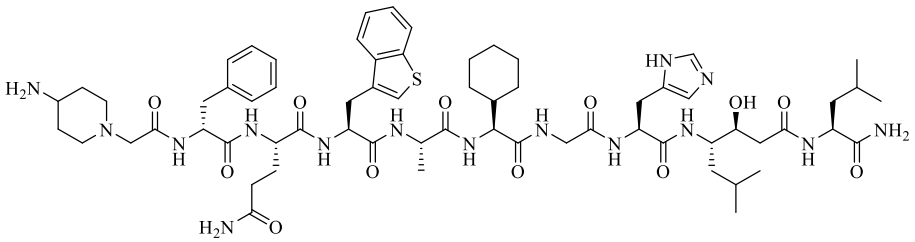

RP-HPLC (10→90% MeCN in 15 min): t_R = 7.8 min, *K*‘ = 3.88.

Calculated monoisotopic mass ($C_{65}H_{95}N_{15}O_{12}S$): 1309.7, found: m/z = 655.8 $[M+2H]^{2+}$, 1310.9 $[M+H]^{+}$.

[Sta^{10}, *des*Gly^{11}]MJ9

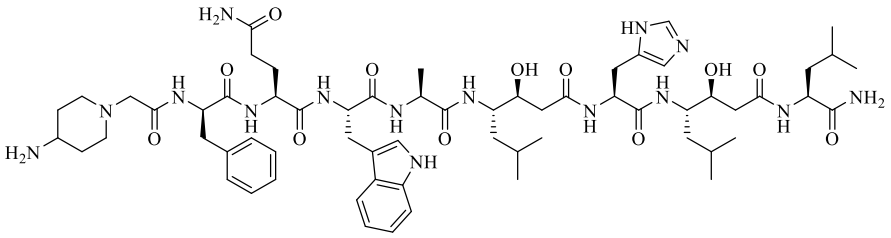

RP-HPLC (10→90% MeCN in 15 min): t_R = 10.4 min, *K*‘ = 5.50.

Calculated monoisotopic mass ($C_{63}H_{95}N_{15}O_{12}$): 1253.7, found: m/z = 627.9 $[M+2H]^{2+}$, 1255.6 $[M+H]^{+}$.

[Valyl-Sta^{10}, *des*Gly^{11}]MJ9

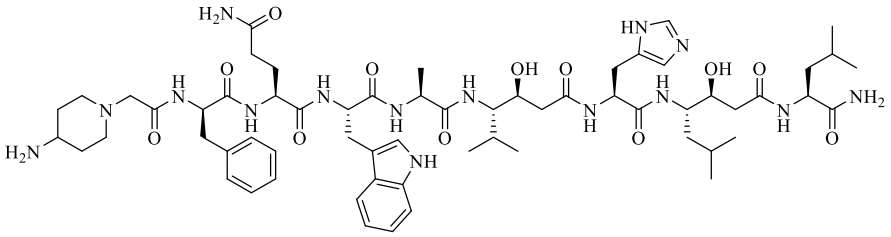

RP-HPLC (10→90% MeCN in 15 min): t_R = 6.4 min, *K*‘ = 3.00.

Calculated monoisotopic mass ($C_{62}H_{93}N_{15}O_{12}$): 1239.7, found: m/z = 620.3 $[M+2H]^{2+}$, 1240.1 $[M+H]^{+}$.

[*γ*-Val^{10}, *des*Gly^{11}]MJ9

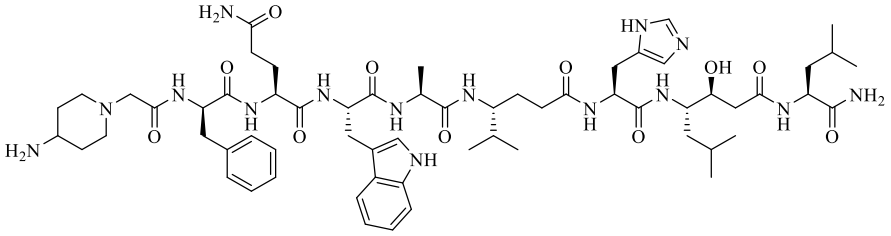

RP-HPLC (10→90% MeCN in 15 min): t_R = 6.6 min, *K*‘ = 3.13.

Calculated monoisotopic mass ($C_{62}H_{93}N_{15}O_{11}$): 1223.7, found: m/z = 613.6 $[M+2H]^{2+}$, 1225.2 $[M+H]^{+}$.

[Txa^{10}, *des*Gly^{11}]MJ9

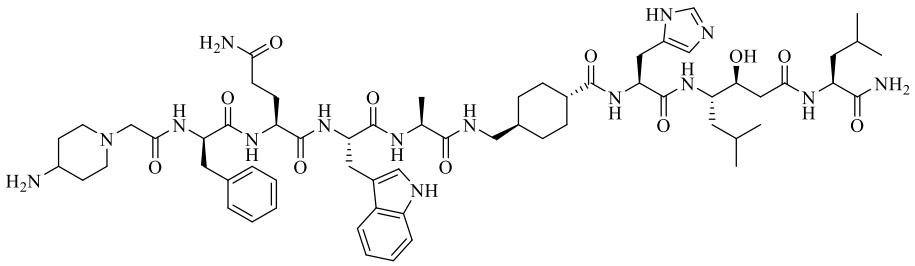

RP-HPLC (10→90% MeCN in 15 min): t_R = 10.6 min, *K*‘ = 5.63.

Calculated monoisotopic mass ($C_{63}H_{93}N_{15}O_{11}$): 1235.7, found: m/z = 619.2 $[M+2H]^{2+}$, 1236.8 $[M+H]^{+}$.

[Gly^{5}, arg^{6}, His^{7}]MJ9

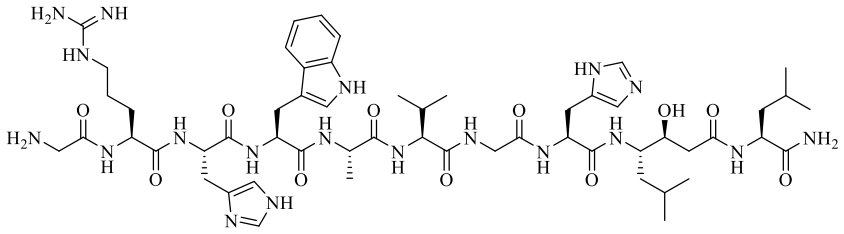

RP-HPLC (10→90% MeCN in 15 min): t_R = 6.2 min, *K*‘ = 2.88.

Calculated monoisotopic mass ($C_{55}H_{85}N_{19}O_{11}$): 1187.7, found: m/z = 594.7 $[M+2H]^{2+}$, 1188.3 $[M+H]^{+}$.

[Txa^{9}, *des*Val^{10}, *des*Gly^{11}]MJ9

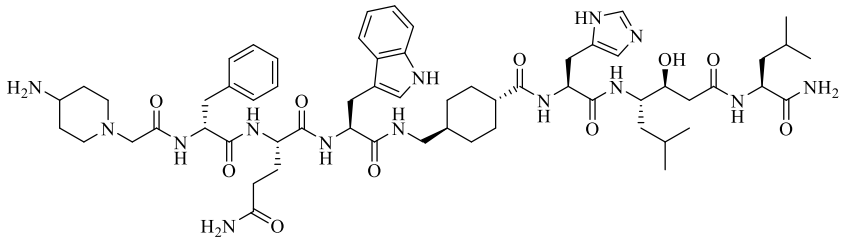

RP-HPLC (10→90% MeCN in 15 min): t_R = 10.2 min, *K*‘ = 5.38.

Calculated monoisotopic mass ($C_{60}H_{88}N_{14}O_{10}$): 1164.7, found: m/z = 583.6 $[M+2H]^{2+}$, 1165.3 $[M+H]^{+}$.

[trp^{8}, ala^{9}, val^{10}, his^{12}]MJ9

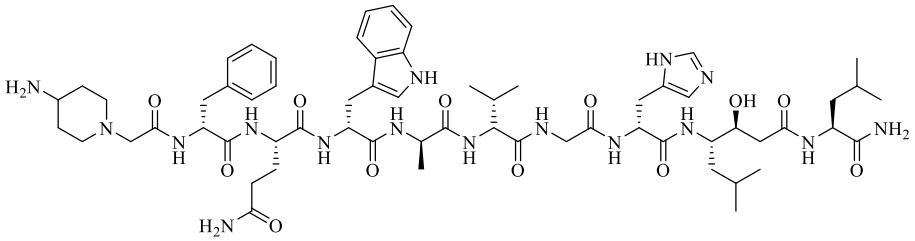

RP-HPLC (10→90% MeCN in 15 min): t_R = 10.8 min, *K*‘ = 5.75.

Calculated monoisotopic mass ($C_{62}H_{92}N_{16}O_{12}$): 1252.7, found: m/z = 627.9 $[M+2H]^{2+}$, 1254.1 $[M+H]^{+}$

3.3. RM2 derivatives

All mentioned compounds based on the core structure of RM2, were synthesized by standard Fmoc-based SPPS (**GP1**, **GP2**, **GP5**) using a *H*-Rink amide ChemMatrix® resin (35-100 mesh particle size, 0.4-0.6 mmol/g loading). After finishing the peptide sequence with slightly modifications within the RM2 sequence, a chelator was coupled at the resin (**GP4**). Thereafter, the peptide was cleaved (**GP5**) and furthermore, remaining acid labile protection groups were deprotected by TFA (**GP6**) and purified by RP-HPLC.

RM2 (DOTA-Pip-phe-Gln-Trp-Ala-Val-Gly-His-Sta-Leu-NH_2)

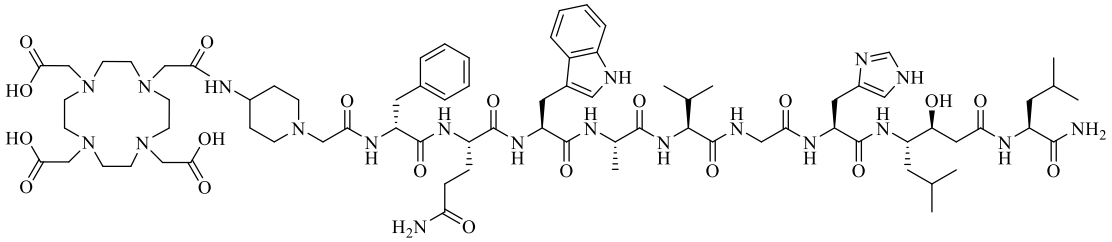

RP-HPLC (10→90% MeCN in 15 min): t_R = 6.8 min, *K*‘ = 3.25.

Calculated monoisotopic mass ($C_{78}H_{118}N_{20}O_{19}$): 1638.9, found: m/z = 820.2 $[M+2H]^{2+}$, 1639.1 $[M+H]^+$.

[^{nat}Ga]RM2: RP-HPLC (10→90% MeCN in 15 min): t_R = 6.7 min, *K*‘ = 3.19.

Calculated monoisotopic mass ($C_{78}H_{115}GaN_{20}O_{19}$): 1704.8, found: m/z = 854.0 $[M+2H]^{2+}$, 1707.3 $[M+H]^+$.

[^{nat}Lu]RM2: RP-HPLC (10→90% MeCN in 15 min): t_R = 6.6 min, *K*‘ = 3.13.

Calculated monoisotopic mass ($C_{78}H_{115}LuN_{20}O_{19}$): 1810.8, found: m/z = 906.2 $[M+2H]^{2+}$, 1811.1 $[M+H]^+$.

3.3.1. Monosubstituted RM2 derivatives

DOTA-[Dap^5]MJ9

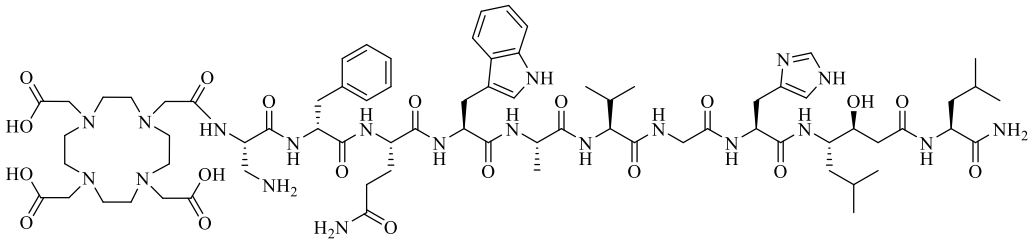

RP-HPLC (10→90% MeCN in 15 min): t_R = 6.7 min, K‘ = 3.19.

Calculated monoisotopic mass ($C_{74}H_{112}N_{20}O_{19}$): 1584.8, found: m/z = 793.0 $[M+2H]^{2+}$, 1584.6 $[M+H]^+$.

DOTA-[Txa^5]MJ9

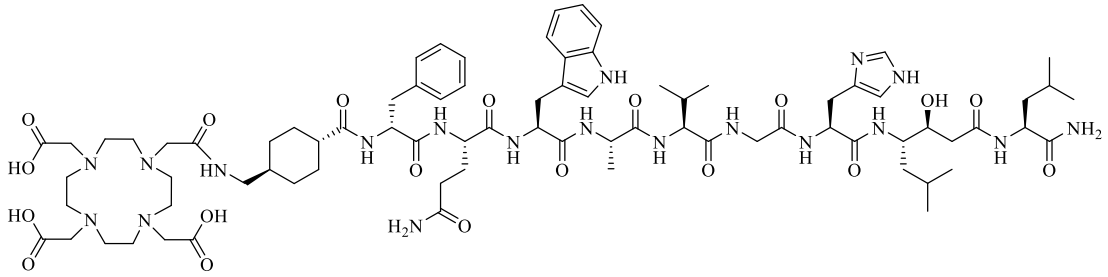

RP-HPLC (10→90% MeCN in 15 min): t_R = 7.4 min, K‘ = 3.63.

Calculated monoisotopic mass ($C_{79}H_{119}N_{19}O_{19}$): 1637.9, found: m/z = 819.5 $[M+2H]^{2+}$, 1637.7 $[M+H]^+$.

DOTA-[Cit^7]MJ9

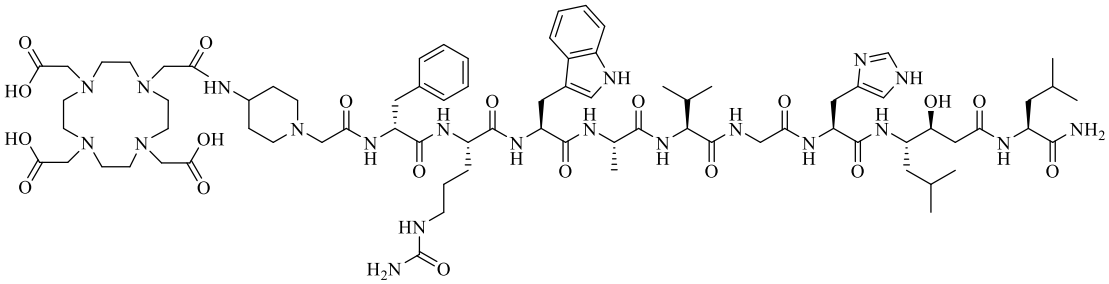

RP-HPLC (10→90% MeCN in 15 min): t_R = 6.7 min, K‘ = 3.19.

Calculated monoisotopic mass ($C_{79}H_{121}N_{21}O_{19}$): 1667.9, found: m/z = 834.9 $[M+2H]^{2+}$, 1669.3 $[M+H]^+$.

[^{nat}Lu]DOTA-[Cit^7]MJ9: RP-HPLC (10→90% MeCN in 15 min): t_R = 6.5 min, K‘ = 3.06.

Calculated monoisotopic mass ($C_{79}H_{118}LuN_{21}O_{19}$): 1839.8, found: m/z = 921.5 $[M+2H]^{2+}$, 1842.4 $[M+H]^+$.

DOTA-[Hse^{7}]MJ9

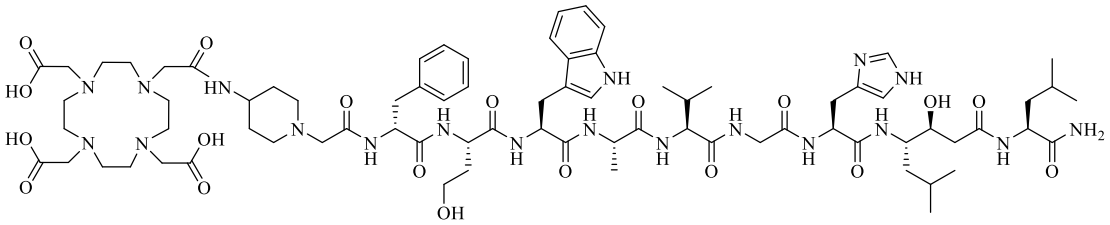

RP-HPLC (10→90% MeCN in 15 min): t_R = 6.9 min, *K*‘ = 3.31.

Calculated monoisotopic mass ($C_{77}H_{117}N_{19}O_{19}$): 1611.9, found: m/z = 807.8 $[M+2H]^{2+}$, 1613.2 $[M+H]^{+}$.

[^{nat}Ga]DOTA-[Hse^{7}]MJ9: RP-HPLC (10→90% MeCN in 15 min): t_R = 6.8 min, *K*‘ = 3.25.

Calculated monoisotopic mass ($C_{77}H_{114}GaN_{19}O_{19}$): 1677.8, found: m/z = 840.2 $[M+2H]^{2+}$, 1679.0 $[M+H]^{+}$.

[^{nat}Lu]DOTA-[Hse^{7}]MJ9: RP-HPLC (10→90% MeCN in 15 min): t_R = 6.8 min, *K*‘ = 3.25.

Calculated monoisotopic mass ($C_{77}H_{114}LuN_{19}O_{19}$): 1783.8, found: m/z = 892.7 $[M+2H]^{2+}$, 1784.5 $[M+H]^{+}$.

DOTA-[Bta^{8}]MJ9

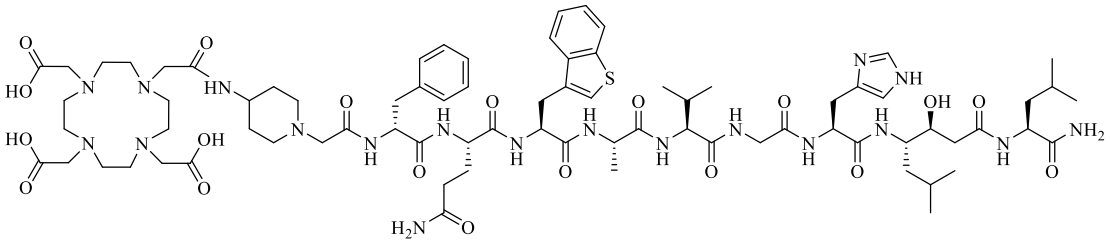

RP-HPLC (10→90% MeCN in 15 min): t_R = 7.1 min, *K*‘ = 3.44.

Calculated monoisotopic mass ($C_{78}H_{117}N_{19}O_{19}S$): 1655.9, found: m/z = 829.2 $[M+2H]^{2+}$, 1657.2 $[M+H]^{+}$.

[^{nat}Ga]DOTA-[Bta^{8}]MJ9: RP-HPLC (10→90% MeCN in 15 min): t_R = 7.0 min, *K*‘ = 3.38.

Calculated monoisotopic mass ($C_{78}H_{114}GaN_{19}O_{19}S$): 1721.8, found: m/z = 862.0 $[M+2H]^{2+}$, 1723.1 $[M+H]^{+}$.

[^{nat}Lu]DOTA-[Bta^{8}]MJ9: RP-HPLC (10→90% MeCN in 15 min): t_R = 7.0 min, *K*‘ = 3.38.

Calculated monoisotopic mass ($C_{78}H_{114}LuN_{19}O_{19}S$): 1827.8, found: m/z = 915.1 $[M+2H]^{2+}$, 1828.9 $[M+H]^{+}$.

AMTG (DOTA-[*α*-Me-Trp^8]MJ9)

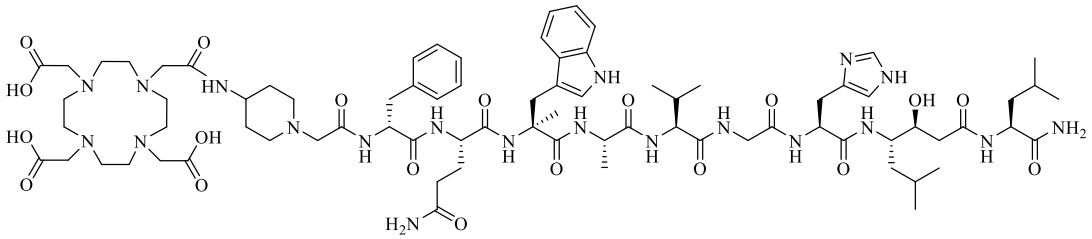

RP-HPLC (10→90% MeCN in 15 min): t_R = 6.9 min, *K*‘ = 3.31.

Calculated monoisotopic mass ($C_{79}H_{120}N_{20}O_{19}$): 1652.9, found: m/z = 826.9 $[M+2H]^{2+}$, 1652.6 $[M+H]^+$.

[^{nat}Ga]AMTG: RP-HPLC (10→90% MeCN in 15 min): t_R = 7.0 min, *K*‘ = 3.38.

Calculated monoisotopic mass ($C_{79}H_{117}GaN_{20}O_{19}$): 1718.8, found: m/z = 860.2 $[M+2H]^{2+}$, 1719.6 $[M+H]^+$.

[^{nat}Lu]AMTG: RP-HPLC (10→90% MeCN in 15 min): t_R = 7.0 min, *K*‘ = 3.38.

Calculated monoisotopic mass ($C_{79}H_{117}LuN_{20}O_{19}$): 1824.8, found: m/z = 913.1 $[M+2H]^{2+}$, 1825.6 $[M+H]^+$.

AMTG2 (DOTA-GA-[*α*-Me-Trp^8]MJ9)

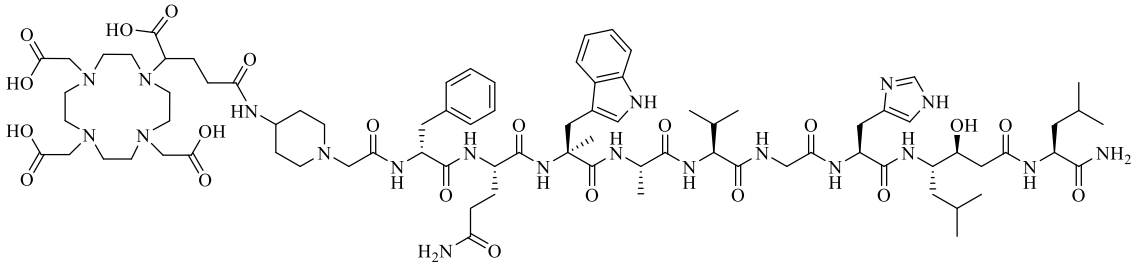

RP-HPLC (10→90% MeCN in 15 min): t_R = 7.0 min, *K*‘ = 3.38.

Calculated monoisotopic mass ($C_{82}H_{124}N_{20}O_{21}$): 1724.9, found: m/z = 863.6 $[M+2H]^{2+}$, 1724.1 $[M+H]^+$.

[^{nat}Ga]AMTG2: RP-HPLC (10→90% MeCN in 15 min): t_R = 6.9 min, *K*‘ = 3.31.

Calculated monoisotopic mass ($C_{82}H_{121}GaN_{20}O_{21}$): 1790.8, found: m/z = 896.3 $[M+2H]^{2+}$, 1792.6 $[M+H]^+$.

[^{nat}Lu]AMTG2: RP-HPLC (10→90% MeCN in 15 min): t_R = 7.0 min, *K*‘ = 3.38.

Calculated monoisotopic mass ($C_{82}H_{121}LuN_{20}O_{21}$): 1896.8, found: m/z = 949.5 $[M+2H]^{2+}$, 1897.6 $[M+H]^+$.

DOTA-[α-Me-trp^{8}]MJ9

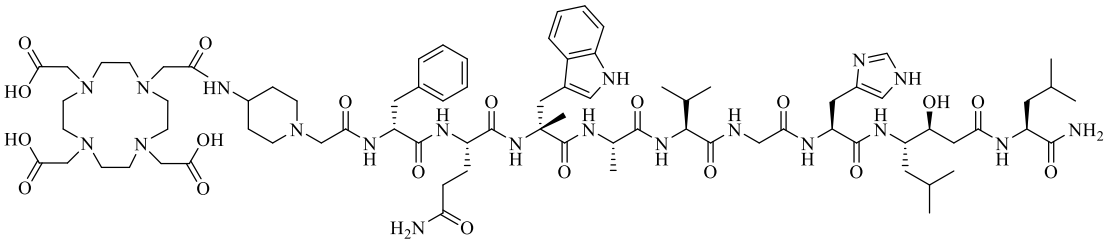

RP-HPLC (10→90% MeCN in 15 min): t_R = 6.9 min, K' = 3.31.

Calculated monoisotopic mass ($C_{79}H_{120}N_{20}O_{19}$): 1652.9, found: m/z = 827.1 $[M+2H]^{2+}$, 1653.5 $[M+H]^{+}$.

[^{nat}Lu]DOTA-[α-Me-trp^{8}]MJ9: RP-HPLC (10→90% MeCN in 15 min): t_R = 7.1 min, K' = 3.44.

Calculated monoisotopic mass ($C_{79}H_{117}LuN_{20}O_{19}$): 1824.8, found: m/z = 913.8 $[M+2H]^{2+}$, 1825.9 $[M+H]^{+}$.

DOTA-[Chg^{10}]MJ9

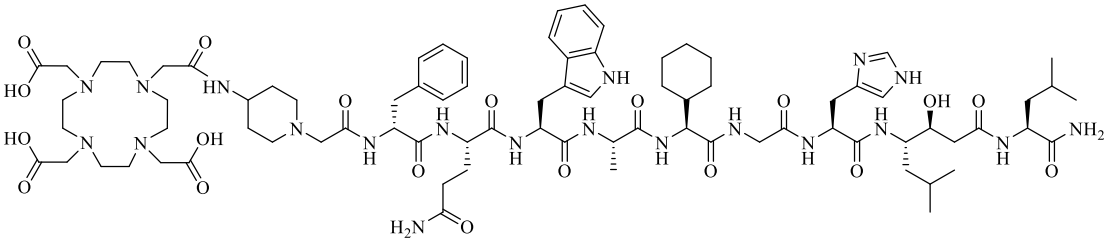

RP-HPLC (10→90% MeCN in 15 min): t_R = 7.2 min, K' = 3.50.

Calculated monoisotopic mass ($C_{81}H_{122}N_{20}O_{19}$): 1678.9, found: m/z = 840.3 $[M+2H]^{2+}$, 1679.6 $[M+H]^{+}$.

DOTA-[Cpg^{10}]MJ9

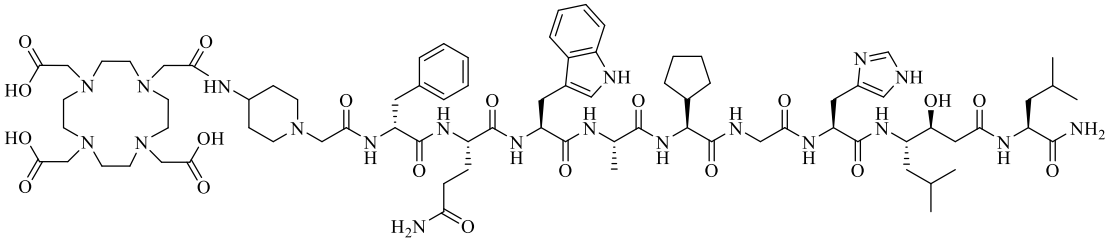

RP-HPLC (10→90% MeCN in 15 min): t_R = 7.0 min, K' = 3.38.

Calculated monoisotopic mass ($C_{80}H_{120}N_{20}O_{19}$): 1664.9, found: m/z = 833.3 $[M+2H]^{2+}$, 1665.4 $[M+H]^{+}$.

3.3.2. Multisubstituted RM2 derivatives

NeoBOMB1 (DOTA-pABzA-DIG-phe-Gln-Trp-Ala-Val-Gly-His-NH-CH[CH_2-$CH(CH_3)_2$]$_2$)

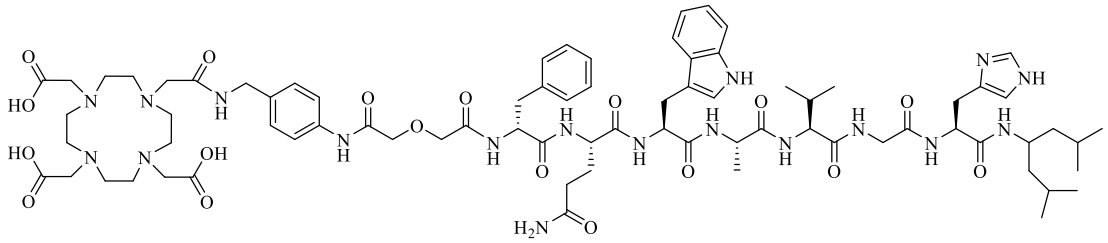

RP-HPLC (10→90% MeCN in 15 min): t_R = 11.8 min, *K*‘ = 6.38.

Calculated monoisotopic mass ($C_{77}H_{110}N_{18}O_{18}$): 1574.8, found: m/z = 788.2 $[M+2H]^{2+}$, 1575.6 $[M+H]^+$.

[^{nat}Lu]NeoBOMB1: RP-HPLC (10→90% MeCN in 15 min): t_R = 9.6 min, *K*‘ = 5.00.

Calculated monoisotopic mass ($C_{77}H_{107}LuN_{18}O_{18}$): 1746.7, found: m/z = 874.5 $[M+2H]^{2+}$, 1747.3 $[M+H]^+$.

DOTA-[*des*Pip^5, arg^6]MJ9

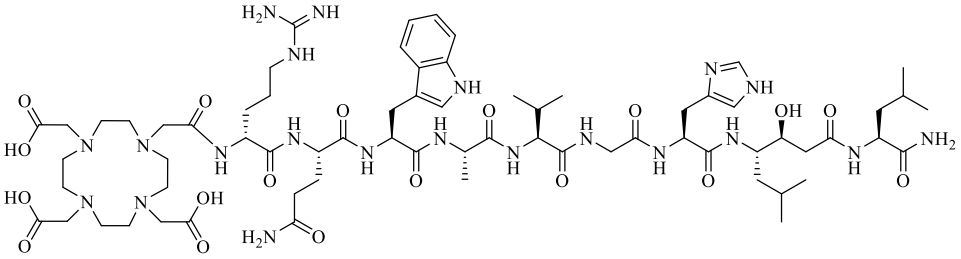

RP-HPLC (10→90% MeCN in 15 min): t_R = 6.2 min, *K*‘ = 2.88.

Calculated monoisotopic mass ($C_{68}H_{109}N_{21}O_{18}$): 1507.8, found: m/z = 754.7 $[M+2H]^{2+}$, 1508.5 $[M+H]^+$.

DOTA-[Hse^7, Bta^8]MJ9

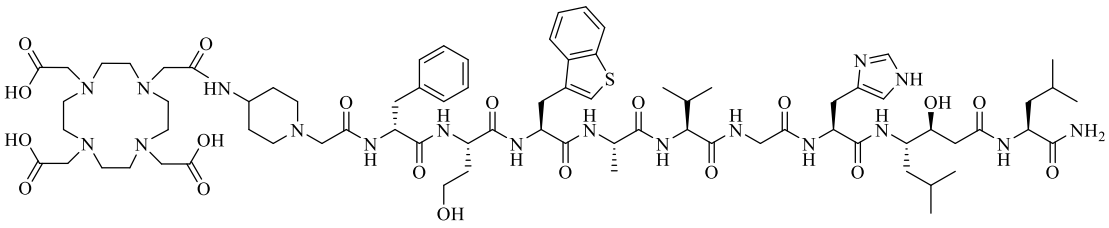

RP-HPLC (10→90% MeCN in 15 min): t_R = 6.0 min, *K*‘ = 2.75.

Calculated monoisotopic mass ($C_{77}H_{116}N_{18}O_{19}S$): 1628.8, found: m/z = 815.6 $[M+2H]^{2+}$, 1629.3 $[M+H]^+$.

[^{nat}Lu]DOTA-[Hse^7, Bta^8]MJ9: RP-HPLC (10→90% MeCN in 15 min): t_R = 6.1 min, *K*‘ = 2.81.

Calculated monoisotopic mass ($C_{77}H_{113}LuN_{18}O_{19}S$): 1800.8, found: m/z = 901.9 $[M+2H]^{2+}$, 1802.7 $[M+H]^+$.

DOTA-[Bta[8], Chg[10]]MJ9

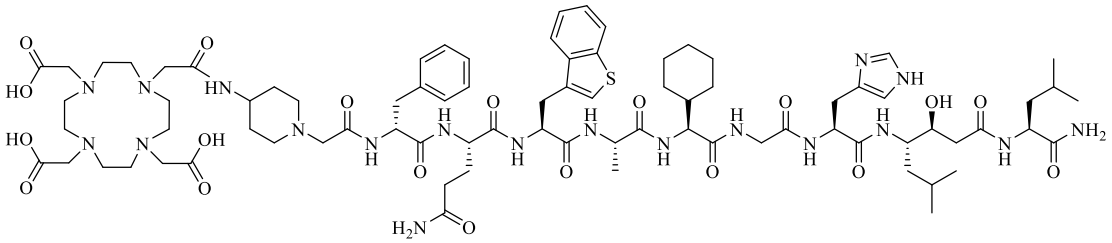

RP-HPLC (10→90% MeCN in 15 min): t_R = 7.6 min, *K*‘ = 3.75.

Calculated monoisotopic mass ($C_{81}H_{121}N_{19}O_{19}S$): 1695.9, found: m/z = 848.8 $[M+2H]^{2+}$, 1696.5 $[M+H]^{+}$.

DOTA-[Bta[8], Cpg[10]]MJ9

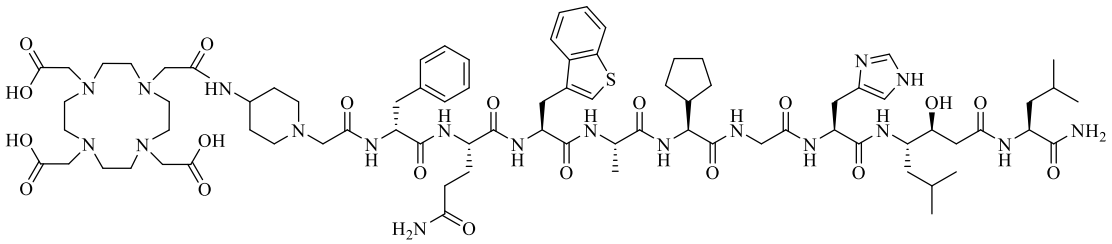

RP-HPLC (10→90% MeCN in 15 min): t_R = 7.3 min, *K*‘ = 3.56.

Calculated monoisotopic mass ($C_{80}H_{119}N_{19}O_{19}S$): 1681.9, found: m/z = 841.9 $[M+2H]^{2+}$, 1682.5 $[M+H]^{+}$.

3.3.4. Linker-extended RM2 derivatives

All mentioned analogs based on the core structure of MJ9 were synthesized by standard Fmoc-based SPPS (**GP1**, **GP2**, **GP5**) using a *H*-Rink amide ChemMatrix® resin (35-100 mesh particle size, 0.4-0.6 mmol/g loading). After finishing the peptide sequence, one or two amino acids were added by SPPS to obtain a linker and thereafter, a chelator was coupled at the resin (**GP4**). Importantly, on-resin coupling of D/L-2,3-diaminopropionic acid was performed by using 2,4,6-collidine (6.0 eq.) instead of DIPEA for its pre-activation. Then, the peptide was cleaved (**GP5**) and furthermore, remaining acid labile protection groups were deprotected by TFA (**GP6**) and purified by RP-HPLC.

DOTA-Dap^4-MJ9

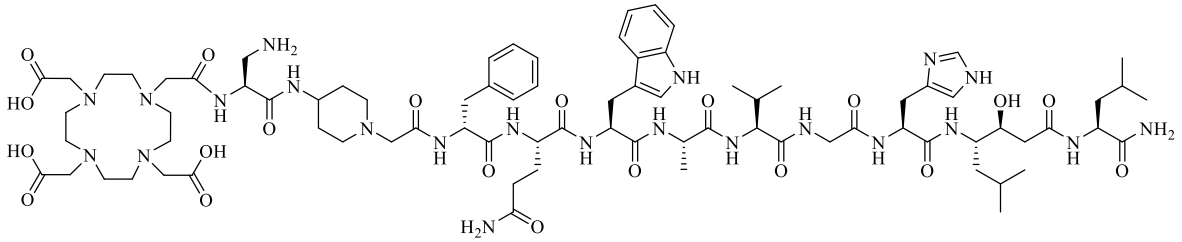

RP-HPLC (10→90% MeCN in 15 min): t_R = 6.6 min, *K*‘ = 3.13.

Calculated monoisotopic mass ($C_{81}H_{124}N_{22}O_{20}$): 1724.9, found: m/z = 864.3 $[M+2H]^{2+}$, 1726.0 $[M+H]^{+}$.

DOTA-Dap^4-[Txa^5]MJ9

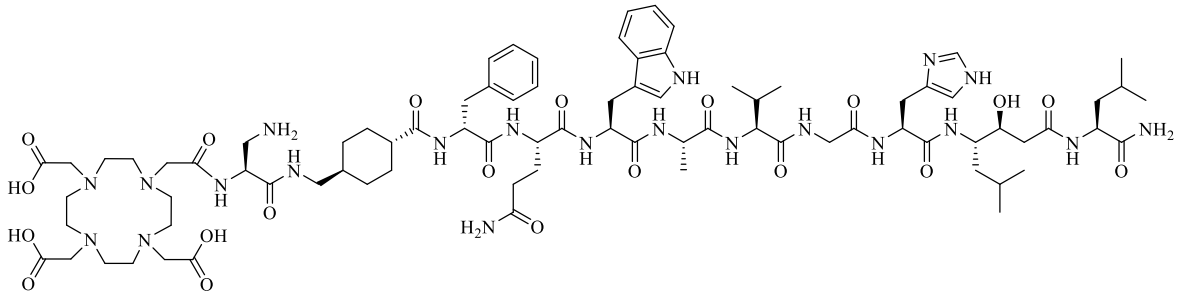

RP-HPLC (10→90% MeCN in 15 min): t_R = 7.2 min, *K*‘ = 3.50.

Calculated monoisotopic mass ($C_{82}H_{125}N_{21}O_{20}$): 1723.9, found: m/z = 863.5 $[M+2H]^{2+}$, 1725.4 $[M+H]^{+}$.

DOTA-Orn^4-MJ9

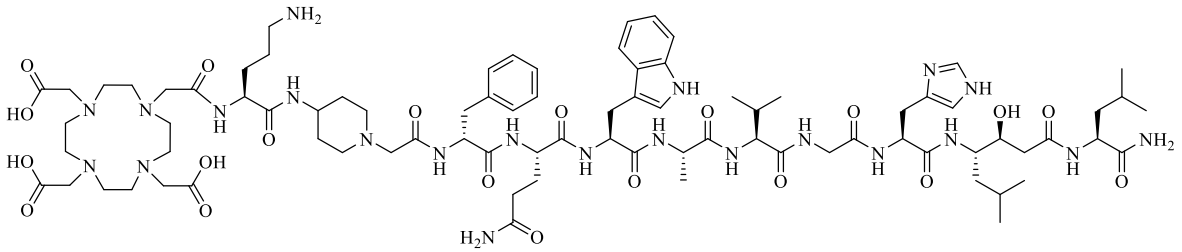

RP-HPLC (10→90% MeCN in 15 min): t_R = 6.5 min, *K*‘ = 3.06.

Calculated monoisotopic mass ($C_{83}H_{128}N_{22}O_{20}$): 1753.0, found: m/z = 878.1 $[M+2H]^{2+}$, 1754.9 $[M+H]^{+}$.

[^{nat}Lu]DOTA-Orn^4-MJ9: RP-HPLC (10→90% MeCN in 15 min): t_R = 6.3 min, *K*‘ = 2.94.

Calculated monoisotopic mass ($C_{83}H_{125}LuN_{22}O_{20}$): 1924.9, found: m/z = 963.9 $[M+2H]^{2+}$, 1926.5 $[M+H]^{+}$.

DOTA-Dap^3-Orn^4-MJ9

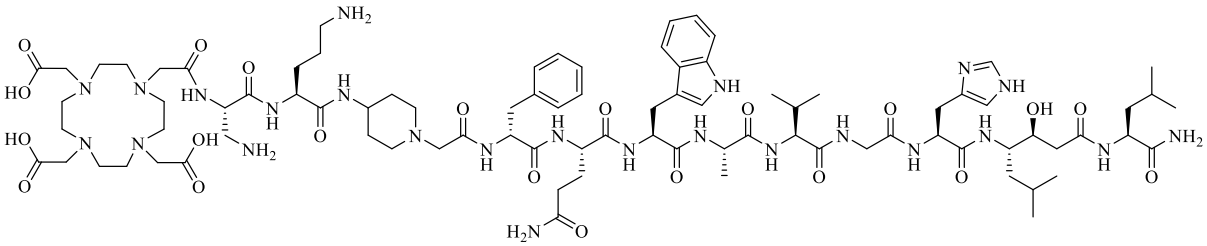

RP-HPLC (10→90% MeCN in 15 min): t_R = 6.5 min, *K*‘ = 3.06.

Calculated monoisotopic mass ($C_{86}H_{134}N_{24}O_{21}$): 1839.0, found: m/z = 921.1 $[M+2H]^{2+}$, 1840.9 $[M+H]^{+}$.

[^{nat}Lu]DOTA-Dap^3-Orn^4-MJ9: RP-HPLC (10→90% MeCN in 15 min): t_R = 6.4 min, *K*‘ = 3.0.

Calculated monoisotopic mass ($C_{86}H_{131}LuN_{24}O_{21}$): 2010.9, found: m/z = 671.7 $[M+3H]^{3+}$, 1007.0 $[M+2H]^{2+}$.

DOTA-Orn^3-Dap^4-MJ9

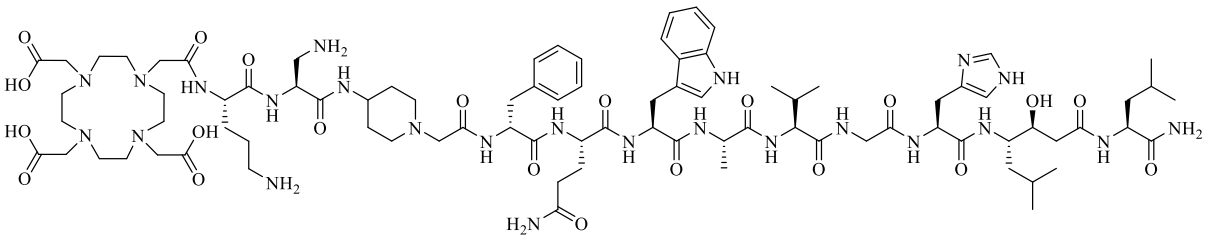

RP-HPLC (10→90% MeCN in 15 min): t_R = 6.5 min, *K*‘ = 3.06.

Calculated monoisotopic mass ($C_{86}H_{134}N_{24}O_{21}$): 1839.0, found: m/z = 921.0 $[M+2H]^{2+}$, 1841.0 $[M+H]^{+}$.

[^{nat}Lu]DOTA-Orn^3-Dap^4-MJ9: RP-HPLC (10→90% MeCN in 15 min): t_R = 6.3 min, *K*‘ = 2.94.

Calculated monoisotopic mass ($C_{86}H_{131}LuN_{24}O_{21}$): 2010.9, found: m/z = 671.8 $[M+3H]^{3+}$, 1007.0 $[M+2H]^{2+}$.

DOTA-orn^3-dap^4-MJ9

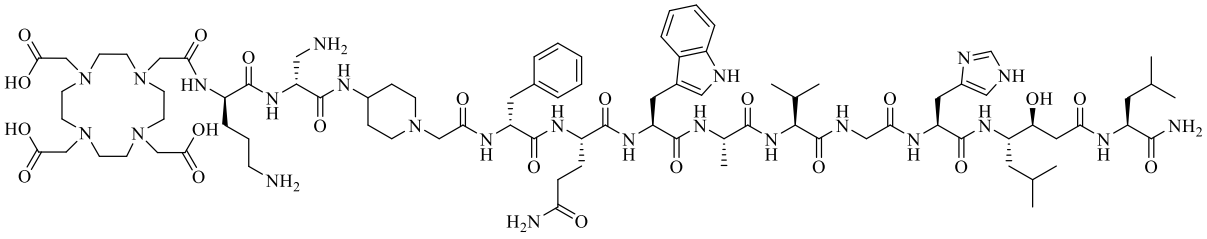

RP-HPLC (10→90% MeCN in 15 min): t_R = 6.5 min, *K*‘ = 3.06.

Calculated monoisotopic mass ($C_{86}H_{134}N_{24}O_{21}$): 1839.0, found: m/z = 920.8 $[M+2H]^{2+}$, 1841.0 $[M+H]^{+}$.

[^{nat}Lu]DOTA-orn^3-dap^4-MJ9: RP-HPLC (10→90% MeCN in 15 min): t_R = 6.4 min, *K*‘ = 3.00.

Calculated monoisotopic mass ($C_{86}H_{131}LuN_{24}O_{21}$): 2010.9, found: m/z = 671.6 $[M+3H]^{3+}$, 1006.7 $[M+2H]^{2+}$.

DOTA-GA-orn^3-dap^4-MJ9

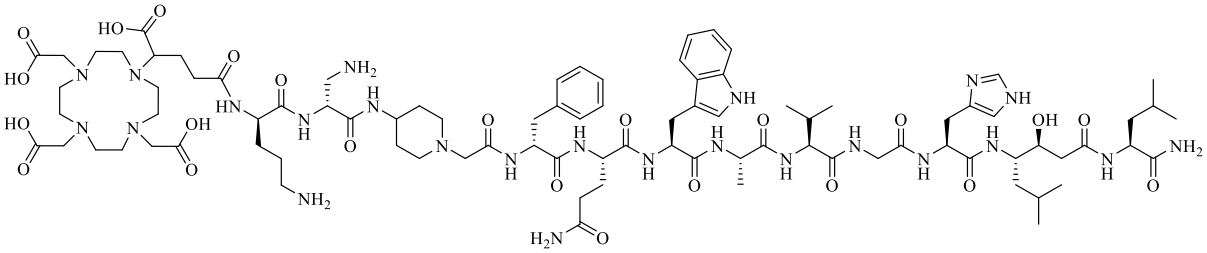

RP-HPLC (10→90% MeCN in 15 min): t_R = 6.5 min, *K*‘ = 3.06.

Calculated monoisotopic mass ($C_{89}H_{138}N_{24}O_{23}$): 1911.0, found: m/z = 638.6 $[M+3H]^{3+}$, 957.2 $[M+2H]^{2+}$.

[^{nat}Lu]DOTA-GA-orn^3-dap^4-MJ9: RP-HPLC (10→90% MeCN in 15 min): t_R = 6.3 min, *K*‘ = 2.94.

Calculated monoisotopic mass ($C_{89}H_{135}LuN_{24}O_{23}$): 2083.0, found: m/z = 695.6 $[M+3H]^{3+}$, 1042.8 $[M+2H]^{2+}$.

DOTA-Pip^3-Pip^4-MJ9

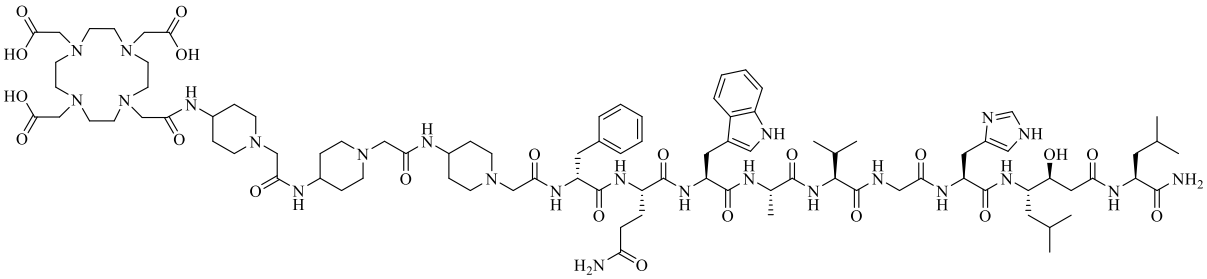

RP-HPLC (10→90% MeCN in 15 min): t_R = 6.5 min, *K*‘ = 3.06.

Calculated monoisotopic mass ($C_{92}H_{142}N_{24}O_{21}$): 1919.9, found: m/z = 961.2 $[M+2H]^{2+}$, 1920.9 $[M+H]^{+}$.

[^{nat}Lu]DOTA-Pip^3-Pip^4-MJ9: RP-HPLC (10→90% MeCN in 15 min): t_R = 6.5 min, *K*‘ = 3.06.

Calculated monoisotopic mass ($C_{92}H_{139}LuN_{24}O_{21}$): 2091.0, found: m/z = 698.3 $[M+3H]^{3+}$, 1046.8 $[M+2H]^{2+}$.

DOTA-dap^3-Pip^4-MJ9

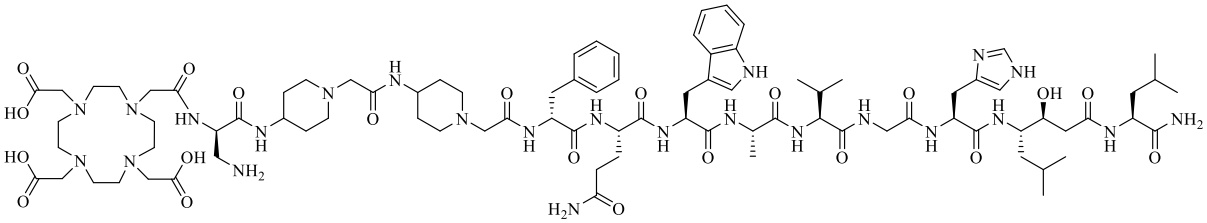

RP-HPLC (10→90% MeCN in 15 min): t_R = 6.7 min, *K*‘ = 3.19.

Calculated monoisotopic mass ($C_{88}H_{136}N_{24}O_{21}$): 1865.0, found: m/z = 623.6 $[M+3H]^{3+}$, 934.4 $[M+2H]^{2+}$.

[^{nat}Lu]DOTA-dap^3-Pip^4-MJ9: RP-HPLC (10→90% MeCN in 15 min): t_R = 6.5 min, *K*‘ = 3.06.

Calculated monoisotopic mass ($C_{88}H_{133}LuN_{24}O_{21}$): 2037.0, found: m/z = 680.9 $[M+3H]^{3+}$, 1020.5 $[M+2H]^{2+}$.

DOTA-ser^3-Pip^4-MJ9

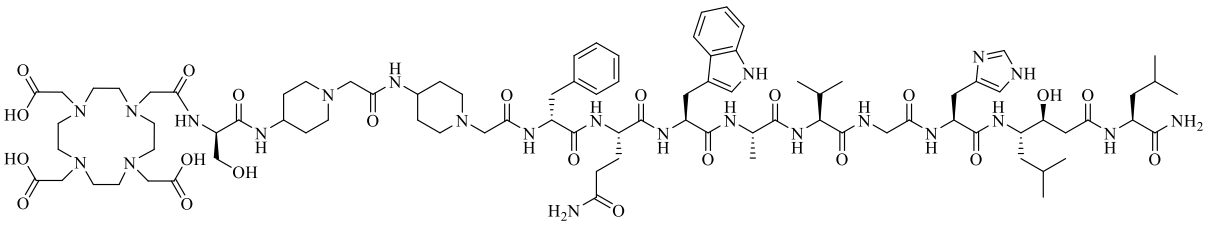

RP-HPLC (10→90% MeCN in 15 min): t_R = 6.6 min, *K*‘ = 3.13.

Calculated monoisotopic mass ($C_{88}H_{135}N_{23}O_{22}$): 1866.0, found: m/z = 623.3 $[M+3H]^{3+}$, 934.2 $[M+2H]^{2+}$.

[^{nat}Lu]DOTA-ser^3-Pip^4-MJ9: RP-HPLC (10→90% MeCN in 15 min): t_R = 6.5 min, *K*‘ = 3.06.

Calculated monoisotopic mass ($C_{88}H_{132}LuN_{23}O_{22}$): 2037.9, found: m/z = 680.1 $[M+3H]^{3+}$, 1019.5 $[M+2H]^{2+}$.

DOTA-orn^3-Pip^4-MJ9

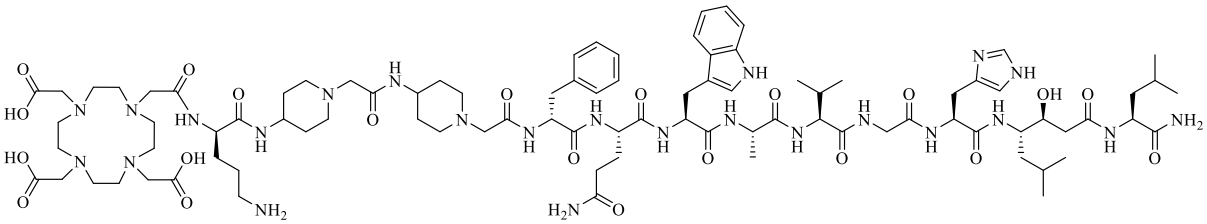

RP-HPLC (10→90% MeCN in 15 min): t_R = 6.6 min, *K*‘ = 3.13.

Calculated monoisotopic mass ($C_{90}H_{140}N_{24}O_{21}$): 1893.1, found: m/z = 632.6 $[M+3H]^{3+}$, 948.2 $[M+2H]^{2+}$.

[^{nat}Lu]DOTA-orn^3-Pip^4-MJ9: RP-HPLC (10→90% MeCN in 15 min): t_R = 6.4 min, *K*‘ = 3.00.

Calculated monoisotopic mass ($C_{90}H_{137}LuN_{24}O_{21}$): 2065.0, found: m/z = 689.7 $[M+3H]^{3+}$, 1034.4 $[M+2H]^{2+}$.

DOTA-asp^3-Pip^4-MJ9

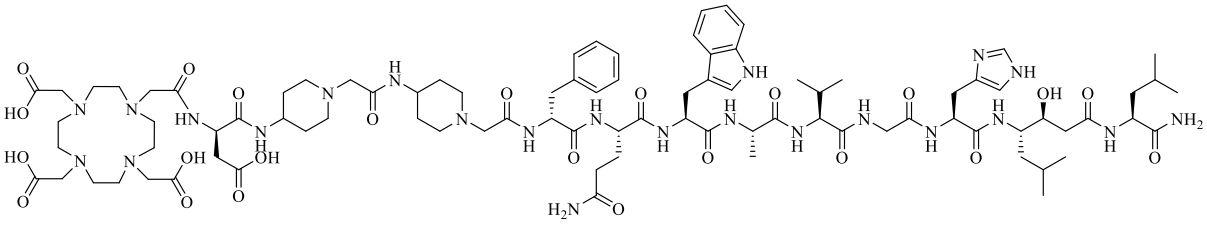

RP-HPLC (10→90% MeCN in 15 min): t_R = 6.8 min, *K*‘ = 3.25.

Calculated monoisotopic mass ($C_{89}H_{135}N_{23}O_{23}$): 1894.0, found: m/z = 632.9 $[M+3H]^{3+}$, 948.5 $[M+2H]^{2+}$.

[^{nat}Lu]DOTA-asp^3-Pip^4-MJ9: RP-HPLC (10→90% MeCN in 15 min): t_R = 6.6 min, *K*‘ = 3.13.

Calculated monoisotopic mass ($C_{89}H_{132}LuN_{23}O_{23}$): 2065.9, found: m/z = 690.4 $[M+3H]^{3+}$.

DOTA-cit^3-Pip^4-MJ9

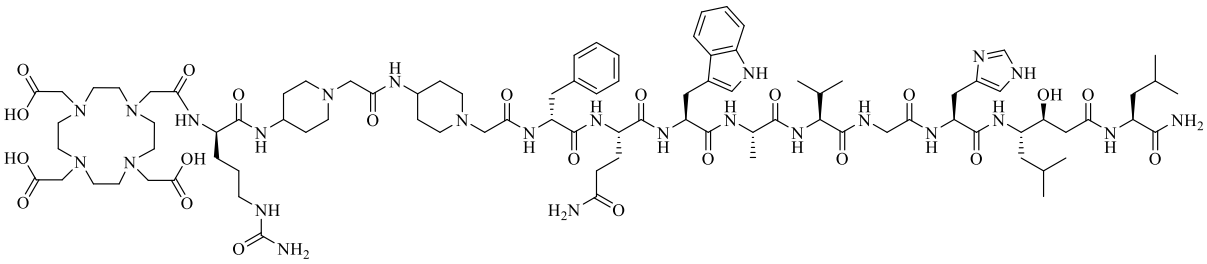

RP-HPLC (10→90% MeCN in 15 min): t_R = 6.7 min, *K*‘ = 3.19.

Calculated monoisotopic mass ($C_{91}H_{141}N_{25}O_{22}$): 1936.1, found: m/z = 647.0 $[M+3H]^{3+}$, 969.3 $[M+2H]^{2+}$.

[^{nat}Lu]DOTA-cit^3-Pip^4-MJ9: RP-HPLC (10→90% MeCN in 15 min): t_R = 6.6 min, *K*‘ = 3.13.

Calculated monoisotopic mass ($C_{91}H_{138}LuN_{25}O_{22}$): 2108.0, found: m/z = 704.3 $[M+3H]^{3+}$.

DOTA-Pip^3-cit^4-MJ9

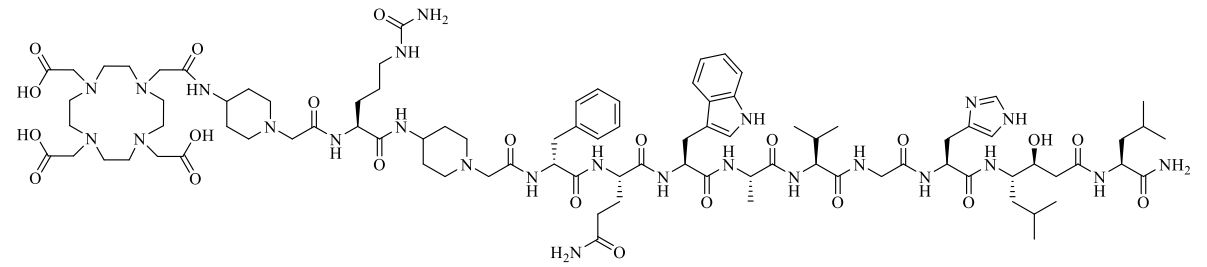

RP-HPLC (10→90% MeCN in 15 min): t_R = 6.8 min, *K*‘ = 3.25.

Calculated monoisotopic mass ($C_{91}H_{141}N_{25}O_{22}$): 1936.1, found: m/z = 646.8 $[M+3H]^{3+}$, 970.6 $[M+2H]^{2+}$.

[^{nat}Lu]DOTA-Pip^3-cit^4-MJ9: RP-HPLC (10→90% MeCN in 15 min): t_R = 6.6 min, *K*‘ = 3.13.

Calculated monoisotopic mass ($C_{91}H_{138}LuN_{25}O_{22}$): 2108.0, found: m/z = 704.3 $[M+3H]^{3+}$, 1056.3 $[M+2H]^{2+}$.

DOTA-Pip^3-ser^4-MJ9

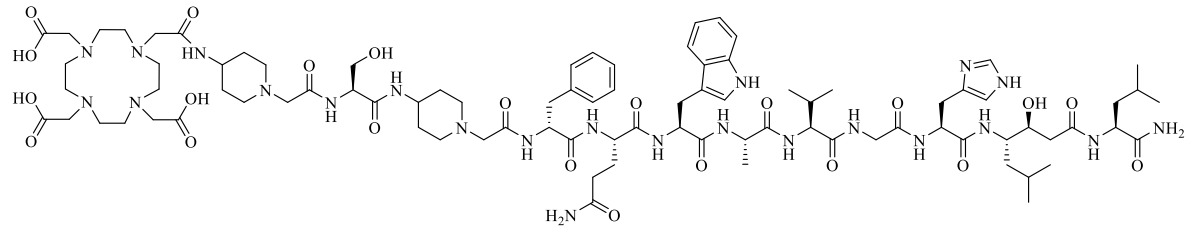

RP-HPLC (10→90% MeCN in 15 min): t_R = 6.6 min, *K*‘ = 3.13.

Calculated monoisotopic mass ($C_{88}H_{135}N_{23}O_{22}$): 1866.0, found: m/z = 623.5 $[M+3H]^{3+}$, 934.6 $[M+2H]^{2+}$.

[^{nat}Lu]DOTA-Pip^3-ser^4-MJ9: RP-HPLC (10→90% MeCN in 15 min): t_R = 6.4 min, *K*‘ = 3.00.

Calculated monoisotopic mass ($C_{88}H_{132}LuN_{23}O_{22}$): 2037.9, found: m/z = 680.4 $[M+3H]^{3+}$, 1019.6 $[M+2H]^{2+}$.

DOTA-Pip^3-asp^4-MJ9

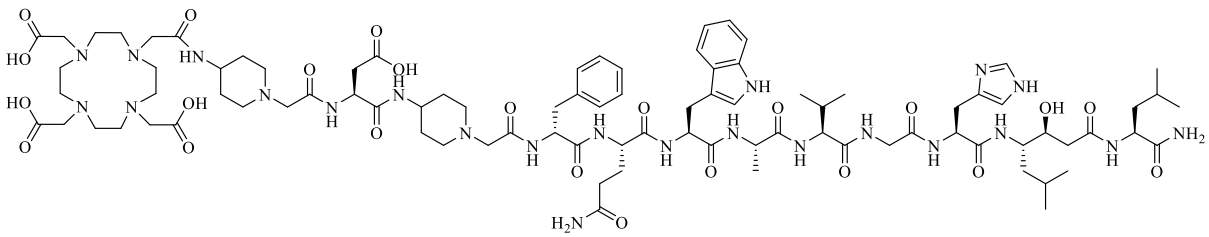

RP-HPLC (10→90% MeCN in 15 min): t_R = 6.8 min, *K*‘ = 3.25.

Calculated monoisotopic mass ($C_{89}H_{135}N_{23}O_{23}$): 1894.0, found: m/z = 632.7 $[M+3H]^{3+}$, 949.1 $[M+2H]^{2+}$.

[^{nat}Lu]DOTA-Pip^3-asp^4-MJ9: RP-HPLC (10→90% MeCN in 15 min): t_R = 6.7 min, *K*‘ = 3.19.

Calculated monoisotopic mass ($C_{89}H_{132}LuN_{23}O_{23}$): 2065.9, found: m/z = 690.2 $[M+3H]^{3+}$.

DOTA-asp^3-asp^4-MJ9

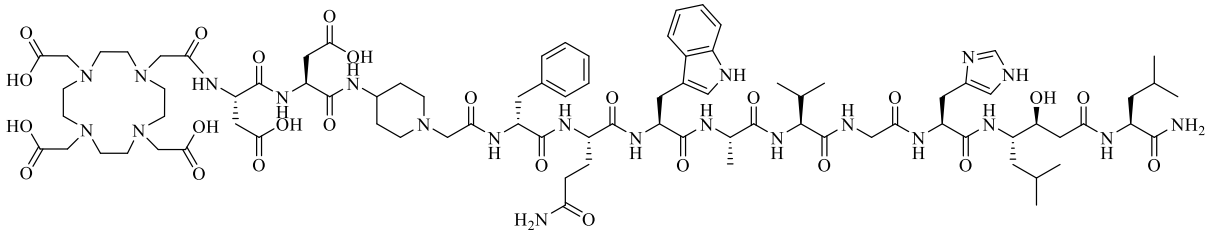

RP-HPLC (10→90% MeCN in 15 min): t_R = 6.9 min, *K*‘ = 3.31.

Calculated monoisotopic mass ($C_{86}H_{128}N_{22}O_{25}$): 1868.9, found: m/z = 624.6 $[M+3H]^{3+}$, 936.3 $[M+2H]^{2+}$.

[^{nat}Lu]DOTA-asp^3-asp^4-MJ9: RP-HPLC (10→90% MeCN in 15 min): t_R = 6.7 min, *K*‘ = 3.19.

Calculated monoisotopic mass ($C_{86}H_{125}LuN_{22}O_{25}$): 2040.9, found: m/z = 681.5 $[M+3H]^{3+}$, 1022.0 $[M+2H]^{2+}$.

3.3.5. BBN-SiFA ligands

3.3.5.1. First generation BBN-SiFA ligands

All mentioned derivatives based on the core structure of MJ9 were synthesized by standard Fmoc-based SPPS (**GP1**, **GP2**, **GP5**) using a *H*-Rink amide ChemMatrix® resin (35-100 mesh particle size, 0.4-0.6 mmol/g loading). On-resin coupling of D/L-2,3-diaminopropionic acid was performed similar to other amino acids (**GP1**), indeed using 2,4,6-collidine (6.0 eq.) instead of DIPEA for its pre-activation. The SiFA group (**II. 2.2**) was coupled *via* the side chain of D/L-2,3-diaminopropionic acid immediately after removal of its Dde protecting group and before its Fmoc deprotection (**GP3**). Chelators were coupled after the end of synthesis of the sequence at the resin (**GP4**). Thereafter, the peptide was cleaved (**GP5**) and furthermore, remaining acid labile protection groups were deprotected by TFA (**GP6**). Thereafter, the peptide was purified by RP-HPLC.

DOTA-GA-[dap(SiFA)^{6}]MJ9

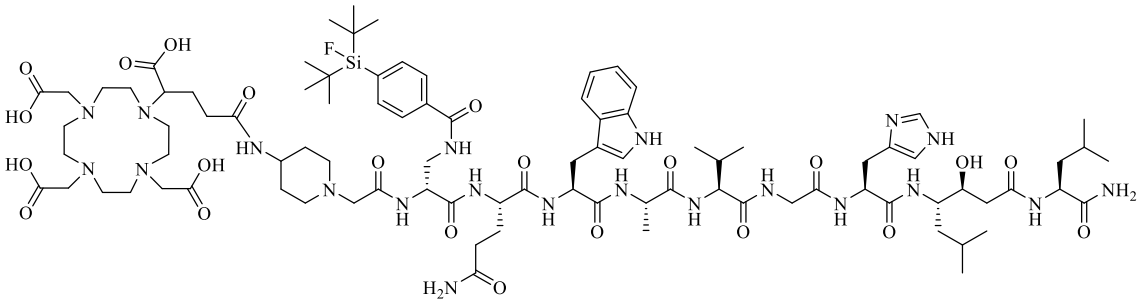

RP-HPLC (10→90% MeCN in 15 min): t_R = 12.4 min, *K*‘ = 6.75.

Calculated monoisotopic mass ($C_{90}H_{140}FN_{21}O_{22}Si$): 1914.0, found: m/z = 638.6 $[M+3H]^{3+}$, 957.5 $[M+2H]^{2+}$.

DOTA-GA-Asp^{4}-[dap(SiFA)^{6}]MJ9

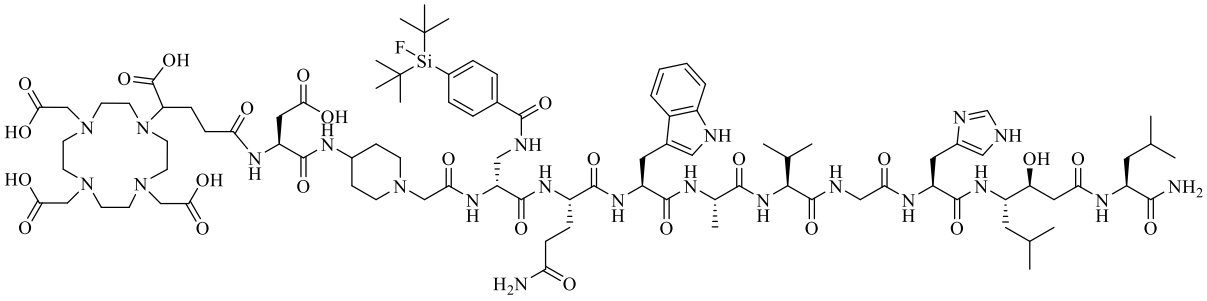

RP-HPLC (10→90% MeCN in 15 min): t_R = 12.4 min, *K*‘ = 6.75.

Calculated monoisotopic mass ($C_{94}H_{145}FN_{22}O_{25}Si$): 2029.1, found: m/z = 677.6 $[M+3H]^{3+}$, 1015.4 $[M+2H]^{2+}$.

DOTA-GA-Asp^3-Asp^4-[dap(SiFA)^6]MJ9

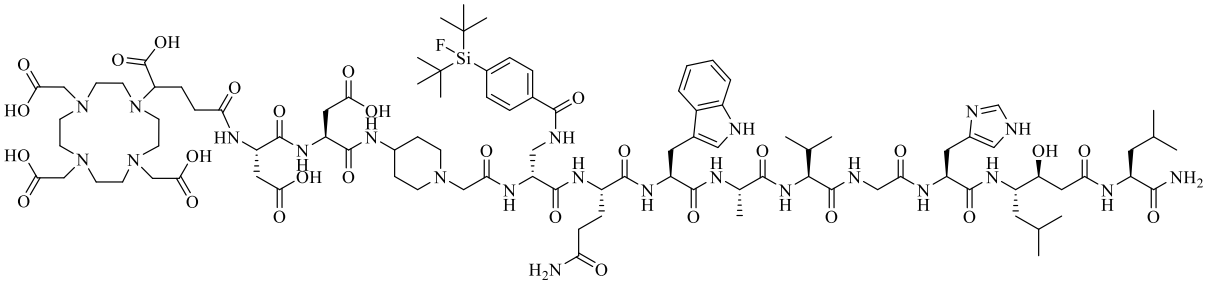

RP-HPLC (10→90% MeCN in 15 min): t_R = 12.1 min, *K*‘ = 6.56.

Calculated monoisotopic mass ($C_{98}H_{150}FN_{23}O_{28}Si$): 2144.1, found: m/z = 715.9 $[M+3H]^{3+}$, 1074.4 $[M+2H]^{2+}$.

DOTA-GA-Ala^4-[dap(SiFA)^6]MJ9

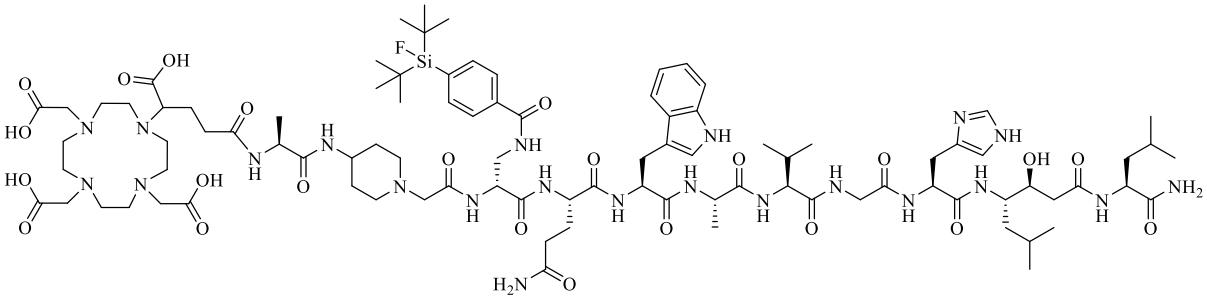

RP-HPLC (10→90% MeCN in 15 min): t_R = 12.2 min, *K*‘ = 6.63.

Calculated monoisotopic mass ($C_{93}H_{145}FN_{22}O_{23}Si$): 1985.1, found: m/z = 662.9 $[M+3H]^{3+}$, 994.0 $[M+2H]^{2+}$.

DOTA-GA-Ala^3-Ala^4-[dap(SiFA)^6]MJ9

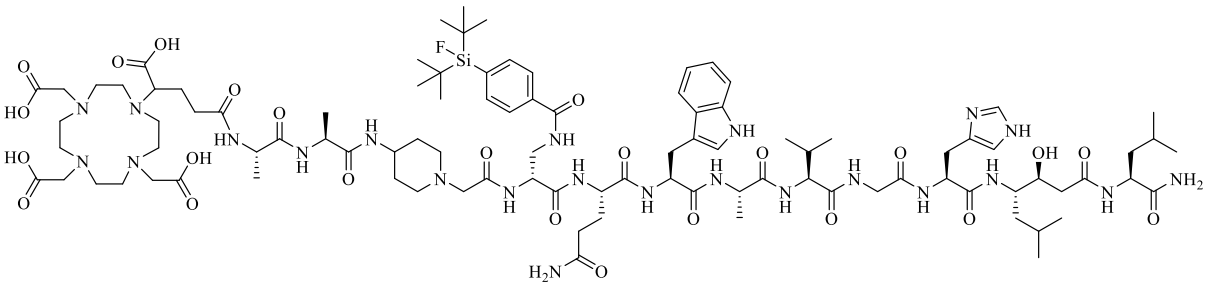

RP-HPLC (10→90% MeCN in 15 min): t_R = 11.7 min, *K*‘ = 6.31.

Calculated monoisotopic mass ($C_{96}H_{150}FN_{23}O_{24}Si$): 2056.1, found: m/z = 686.7 $[M+3H]^{3+}$, 1029.4 $[M+2H]^{2+}$.

[dap(SiFA)^{6}]MJ9

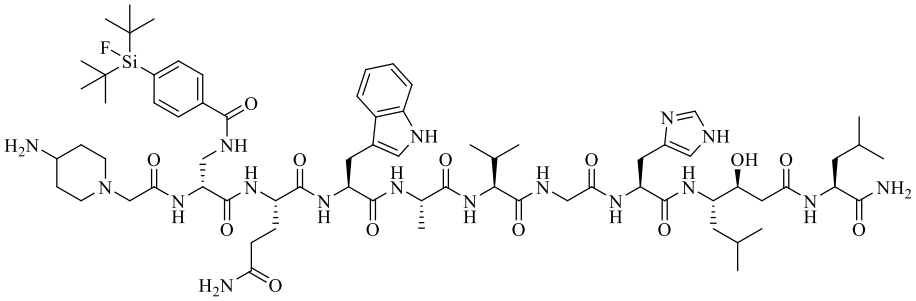

RP-HPLC (10→90% MeCN in 15 min): t_R = 13.9 min, *K*‘ = 7.69.

Calculated monoisotopic mass ($C_{71}H_{110}FN_{17}O_{13}Si$): 1455.8, found: m/z = 728.1 $[M+2H]^{2+}$, 1457.0 $[M+H]^{+}$.

DOTA-GA-[*des*Pip^{5}, dap(SiFA)^{6}]MJ9

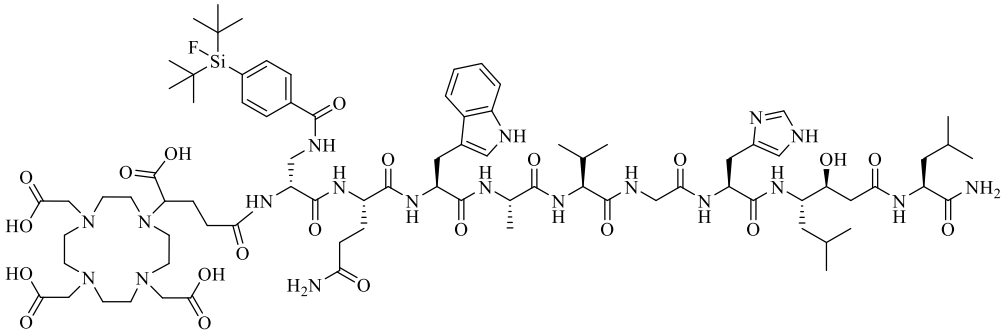

RP-HPLC (10→90% MeCN in 15 min): t_R = 12.5 min, *K*‘ = 6.81.

Calculated monoisotopic mass ($C_{83}H_{128}FN_{19}O_{21}Si$): 1773.9, found: m/z = 888.5 $[M+2H]^{2+}$, 1774.8 $[M+H]^{+}$.

DOTA-GA-[Ala^{5}, dap(SiFA)^{6}]MJ9

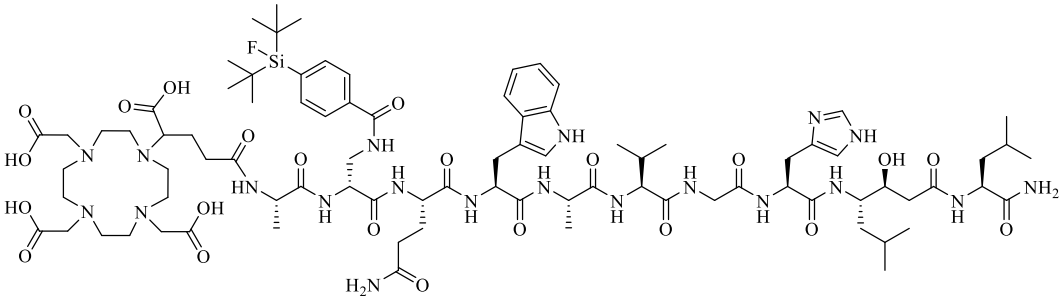

RP-HPLC (10→90% MeCN in 15 min): t_R = 12.4 min, *K*‘ = 6.75.

Calculated monoisotopic mass ($C_{86}H_{133}FN_{20}O_{22}Si$): 1845.0, found: m/z = 616.1 $[M+3H]^{3+}$, 924.0 $[M+2H]^{2+}$.

DOTA-GA-dap(SiFA)^4-MJ9

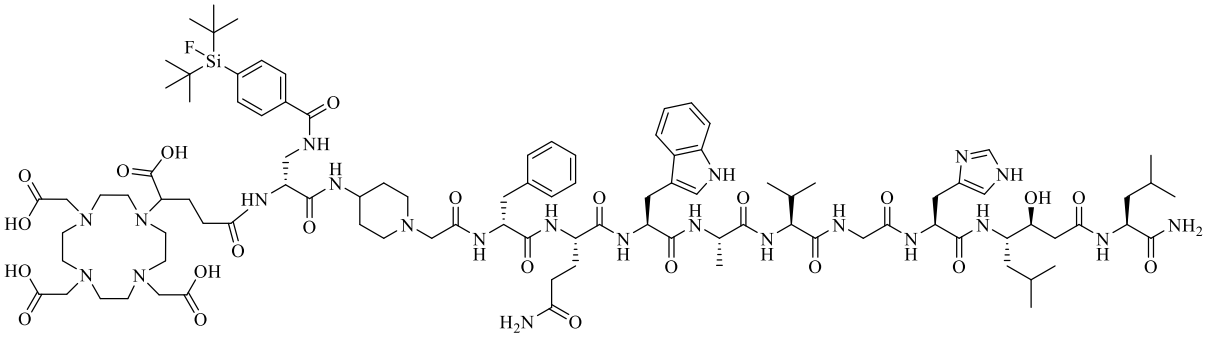

RP-HPLC (10→90% MeCN in 15 min): t_R = 12.3 min, *K*‘ = 6.69.

Calculated monoisotopic mass ($C_{99}H_{149}FN_{22}O_{23}Si$): 2061.1, found: m/z = 688.5 $[M+3H]^{3+}$, 1031.7 $[M+2H]^{2+}$.

3.3.5.2. Second generation BBN-SiFA ligands

All mentioned conjugates based on the core structure of MJ9 were synthesized by standard Fmoc-based SPPS (**GP1**, **GP2**, **GP5**) using a *H*-Rink amide ChemMatrix® resin (35-100 mesh particle size, 0.4-0.6 mmol/g loading). After completion of the peptide sequence, three amino acids were added by SPPS for obtaining a linker. On-resin coupling of L-2,3-diaminopropionic acid was performed similar to other amino acids (**GP1**), indeed using 2,4,6-collidine (6.0 eq.) instead of DIPEA for its pre-activation. The SiFA group (**II. 2.2**) was coupled *via* the side chain of L-2,3-diaminopropionic acid immediately after removing of its Dde protecting group and before its Fmoc deprotection (**GP3**). Chelators were coupled after the end of synthesis of the sequence at the resin (**GP4**). Thereafter, the peptide was cleaved (**GP5**) and furthermore, remaining acid labile protection groups were deprotected by TFA (**GP6**). Thereafter, the peptide was purified by RP-HPLC.

DOTA-GA-dap(SiFA)^{1}-Gln^{2}-Arg^{3}-Leu^{4}-MJ9

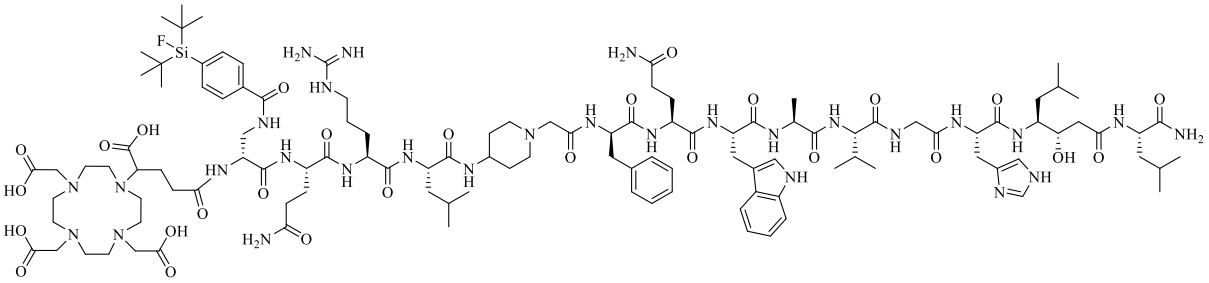

RP-HPLC (10→90% MeCN in 15 min): t_R = 14.8 min, *K*‘ = 8.25.

Calculated monoisotopic mass ($C_{116}H_{180}FN_{29}O_{27}Si$): 2458.3, found: m/z = 821.1 $[M+3H]^{3+}$, 1230.8 $[M+2H]^{2+}$.

[^{nat}Ga]DOTA-GA-dap(SiFA)^{1}-Gln^{2}-Arg^{3}-Leu^{4}-MJ9:

RP-HPLC (10→90% MeCN in 15 min): t_R = 14.7 min, *K*‘ = 8.19.

Calculated monoisotopic mass ($C_{116}H_{177}FGaN_{29}O_{27}Si$): 2524.2, found: m/z = 843.4 $[M+3H]^{3+}$, 1264.6 $[M+2H]^{2+}$.

[^{nat}Lu]DOTA-GA-dap(SiFA)^{1}-Gln^{2}-Arg^{3}-Leu^{4}-MJ9:

RP-HPLC (10→90% MeCN in 15 min): t_R = 14.7 min, *K*‘ = 8.13.

Calculated monoisotopic mass ($C_{116}H_{177}FLuN_{29}O_{27}Si$): 2630.3, found: m/z = 878.4 $[M+3H]^{3+}$, 1317.7 $[M+2H]^{2+}$.

DOTA-GA-dap(SiFA)^1-Asn^2-Arg^3-Asn^4-MJ9

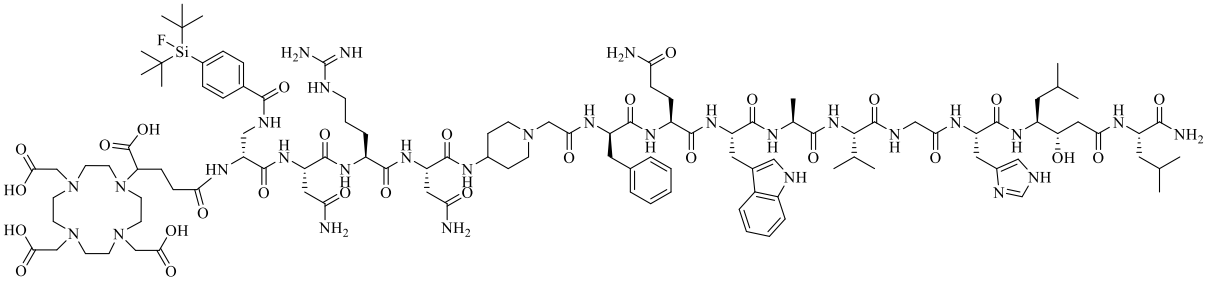

RP-HPLC (10→90% MeCN in 15 min): t_R = 11.4 min, *K*‘ = 6.13.

Calculated monoisotopic mass ($C_{113}H_{173}FN_{30}O_{28}Si$): 2445.3, found: m/z = 816.4 $[M+3H]^{3+}$, 1223.9 $[M+2H]^{2+}$.

[^{nat}Ga]DOTA-GA-dap(SiFA)^1-Asn^2-Arg^3-Asn^4-MJ9:

RP-HPLC (10→90% MeCN in 15 min): t_R = 11.2 min, *K*‘ = 6.00.

Calculated monoisotopic mass ($C_{113}H_{170}FGaN_{30}O_{28}Si$): 2511.2, found: m/z = 839.0 $[M+3H]^{3+}$, 1257.6 $[M+2H]^{2+}$.

[^{nat}Lu]DOTA-GA-dap(SiFA)^1-Asn^2-Arg^3-Asn^4-MJ9:

RP-HPLC (10→90% MeCN in 15 min): t_R = 11.2 min, *K*‘ = 6.00.

Calculated monoisotopic mass ($C_{113}H_{170}FLuN_{30}O_{28}Si$): 2617.2, found: m/z = 873.9 $[M+3H]^{3+}$, 1310.1 $[M+2H]^{2+}$.

DOTA-GA-dap(SiFA)^1-Gln^2-Arg^3-Dap^4-MJ9

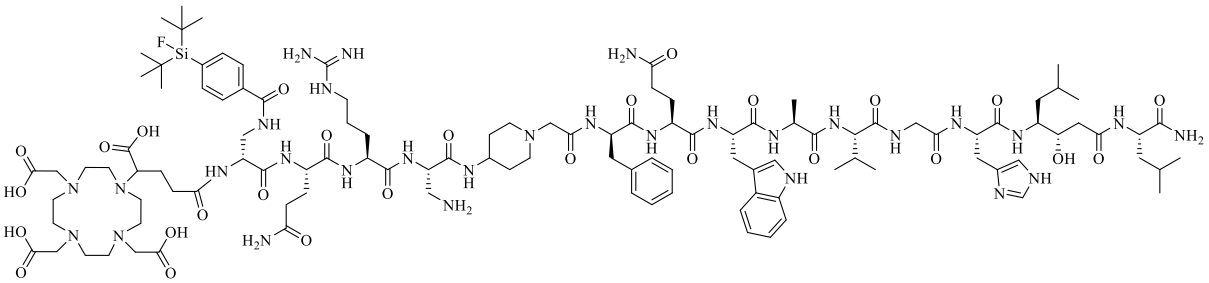

RP-HPLC (10→90% MeCN in 15 min): t_R = 14.4 min, *K*‘ = 8.00.

Calculated monoisotopic mass ($C_{113}H_{175}FN_{30}O_{27}Si$): 2431.3, found: m/z = 811.9 $[M+3H]^{3+}$, 1216.6 $[M+2H]^{2+}$.

[^{nat}Lu]DOTA-GA-dap(SiFA)^1-Gln^2-Arg^3-Dap^4-MJ9:

RP-HPLC (10→90% MeCN in 15 min): t_R = 14.2 min, *K*‘ = 7.88.

Calculated monoisotopic mass ($C_{113}H_{172}FLuN_{30}O_{27}Si$): 2603.2, found: m/z = 869.4 $[M+3H]^{3+}$, 1303.4 $[M+2H]^{2+}$.

DOTA-GA-dap(SiFA)^{1}-Gln^{2}-Dap^{3}-Orn^{4}-MJ9

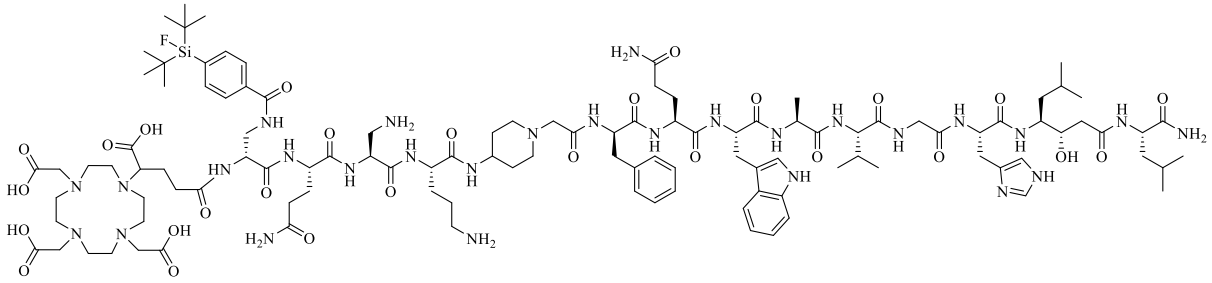

RP-HPLC (10→90% MeCN in 15 min): t_R = 14.0 min, *K*‘ = 7.75.

Calculated monoisotopic mass ($C_{112}H_{173}FN_{28}O_{27}Si$): 2389.3, found: m/z = 797.9 $[M+3H]^{3+}$, 1196.3 $[M+2H]^{2+}$.

[^{nat}Lu]DOTA-GA-dap(SiFA)^{1}-Gln^{2}-Dap^{3}-Orn^{4}-MJ9:

RP-HPLC (10→90% MeCN in 15 min): t_R = 13.9 min, *K*‘ = 7.69.

Calculated monoisotopic mass ($C_{112}H_{170}FLuN_{28}O_{27}Si$): 2561.2, found: m/z = 855.0 $[M+3H]^{3+}$, 1281.9 $[M+2H]^{2+}$.

DOTA-GA-dap(SiFA)^{1}-Gln^{2}-Orn^{3}-Dap^{4}-MJ9

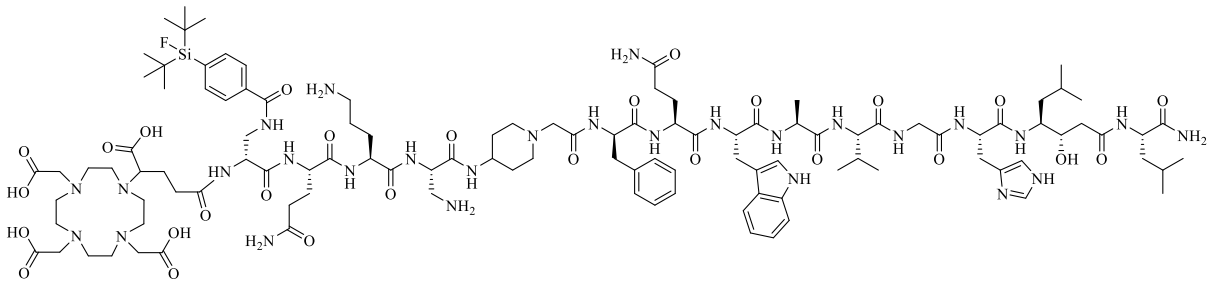

RP-HPLC (10→90% MeCN in 15 min): t_R = 14.0 min, *K*‘ = 7.75.

Calculated monoisotopic mass ($C_{112}H_{173}FN_{28}O_{27}Si$): 2389.3, found: m/z = 797.7 $[M+3H]^{3+}$, 1196.0 $[M+2H]^{2+}$.

[^{nat}Lu]DOTA-GA-dap(SiFA)^{1}-Gln^{2}-Orn^{3}-Dap^{4}-MJ9:

RP-HPLC (10→90% MeCN in 15 min): t_R = 13.9 min, *K*‘ = 7.69.

Calculated monoisotopic mass ($C_{112}H_{170}FLuN_{28}O_{27}Si$): 2561.2, found: m/z = 855.1 $[M+3H]^{3+}$, 1282.1 $[M+2H]^{2+}$.

3.3.5.3. Third generation BBN-SiFA ligands

All mentioned derivatives based on the core structure of MJ9 were synthesized by standard Fmoc-based SPPS (**GP1**, **GP2**, **GP5**) using a *H*-Rink amide ChemMatrix® resin (35-100 mesh particle size, 0.4-0.6 mmol/g loading). After completing the peptide sequence, two or three amino acids were added by SPPS to obtain a linker. On-resin coupling of D/L-2,3-diaminopropionic acid was performed similar to other amino acids (**GP1**), indeed using 2,4,6-collidine (6.0 eq.) instead of DIPEA for its pre-activation. Both, the SiFA group (**II. 2.2**) as well as the chelator (**GP4**) were coupled *via* the side chains of the two successive D-amino acids, each immediately after removing of their respective Dde protecting groups and before their Fmoc deprotection (**GP3**). Finally, the ^{t}Bu-protected eue (glu-urea-glu) motif was coupled to the *N*-terminus. Thereafter, the peptide was cleaved (**GP5**) and furthermore, remaining acid labile protection groups were deprotected by TFA (**GP6**). Thereafter, the peptide was purified by RP-HPLC.

eue-dap(SiFA)^{1}-dap(DOTA-GA)^{2}-orn^{3}-dap^{4}-MJ9

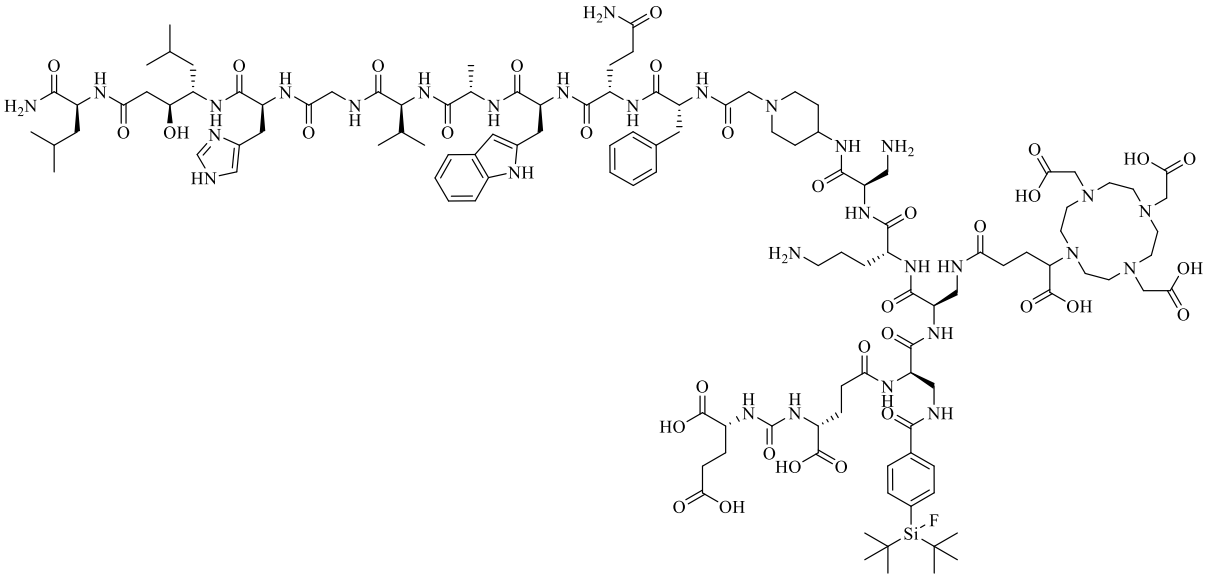

RP-HPLC (10→90% MeCN in 15 min): t_R = 9.2 min, *K*‘ = 4.75.

Calculated monoisotopic mass ($C_{121}H_{185}FN_{30}O_{34}Si$): 2649.3, found: m/z = 885.3 $[M+3H]^{3+}$, 1326.5 $[M+2H]^{2+}$.

eue-dap(SiFA)^{1}-dap([^{nat}Lu]DOTA-GA)^{2}-orn^{3}-dap^{4}-MJ9:

RP-HPLC (10→90% MeCN in 15 min): t_R = 9.0 min, *K*‘ = 4.63.

Calculated monoisotopic mass ($C_{121}H_{182}FLuN_{30}O_{34}Si$): 2821.3, found: m/z = 942.2 $[M+3H]^{3+}$.

eue-dap(SiFA)-dap(DOTA-GA)^{1}-asp^{2}-orn^{3}-dap^{4}-MJ9

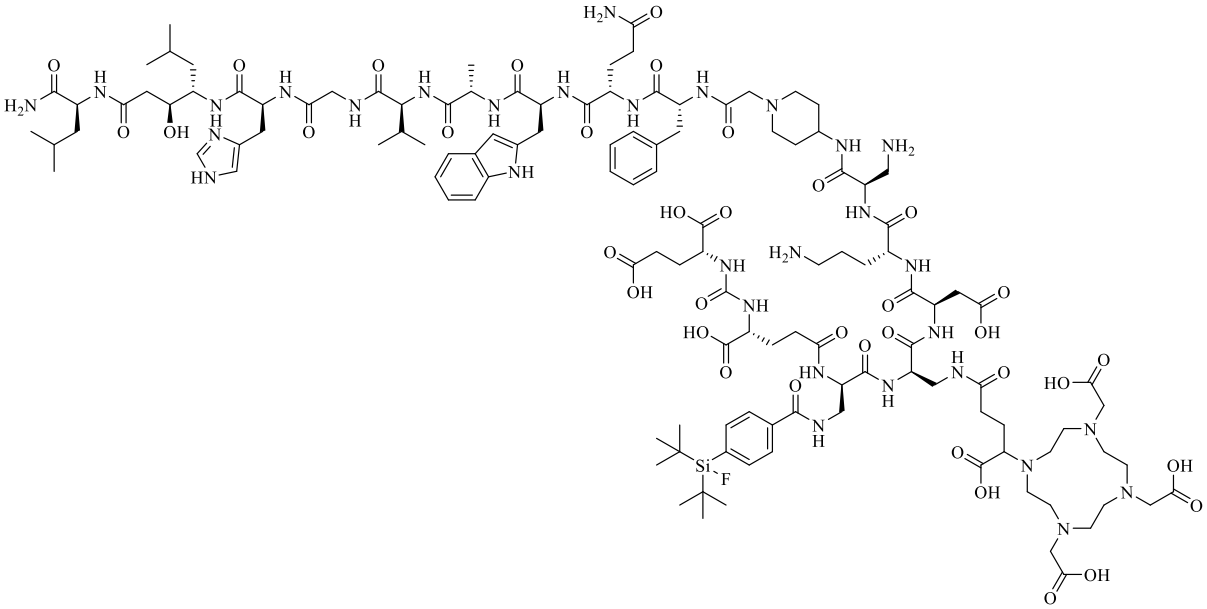

RP-HPLC (10→90% MeCN in 15 min): t_R = 9.2 min, *K*‘ = 4.75.

Calculated monoisotopic mass ($C_{125}H_{190}FN_{31}O_{37}Si$): 2764.4, found: m/z = 692.9 $[M+4H]^{4+}$, 923.4 $[M+3H]^{3+}$.

eue-dap(SiFA)-dap([^{nat}Lu]DOTA-GA)^{1}-asp^{2}-orn^{3}-dap^{4}-MJ9:

RP-HPLC (10→90% MeCN in 15 min): t_R = 9.0 min, *K*‘ = 4.63.

Calculated monoisotopic mass ($C_{125}H_{187}FLuN_{31}O_{37}Si$): 2936.3, found: m/z = 980.9 $[M+3H]^{3+}$.

eue-dap(SiFA)-dap(DOTA-GA)-asp^{1}-asp^{2}-orn^{3}-dap^{4}-MJ9

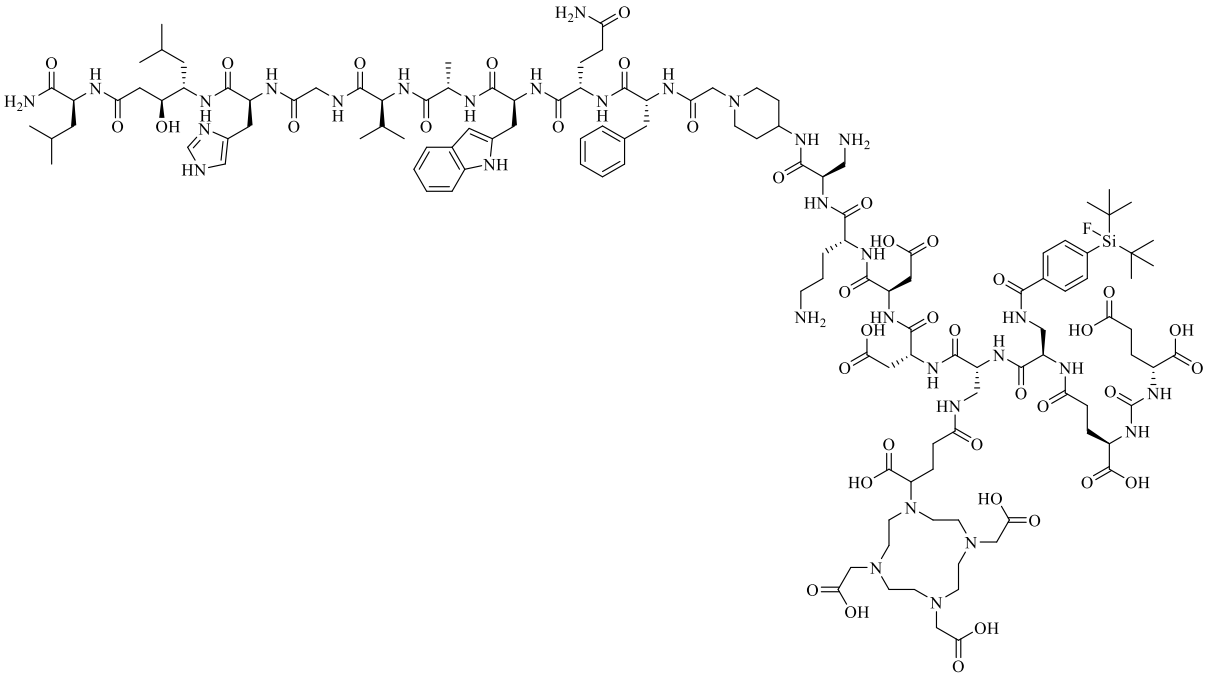

RP-HPLC (10→90% MeCN in 15 min): t_R = 9.2 min, *K*‘ = 4.75.

Calculated monoisotopic mass ($C_{129}H_{195}FN_{32}O_{40}Si$): 2879.4, found: m/z = 721.2 $[M+4H]^{4+}$, 961.7 $[M+3H]^{3+}$.

eue-dap(SiFA)-dap([^{nat}Lu]DOTA-GA)-asp^1-asp^2-orn^3-dap^4-MJ9:

RP-HPLC (10→90% MeCN in 15 min): t_R = 9.0 min, *K*‘ = 4.63.

Calculated monoisotopic mass ($C_{129}H_{192}FLuN_{32}O_{40}Si$): 3051.3, found: m/z = 1019.0 $[M+3H]^{3+}$.

eue-dap(SiFA)-dap(DOTA-GA)^1-orn^2-asp^3-dap^4-MJ9

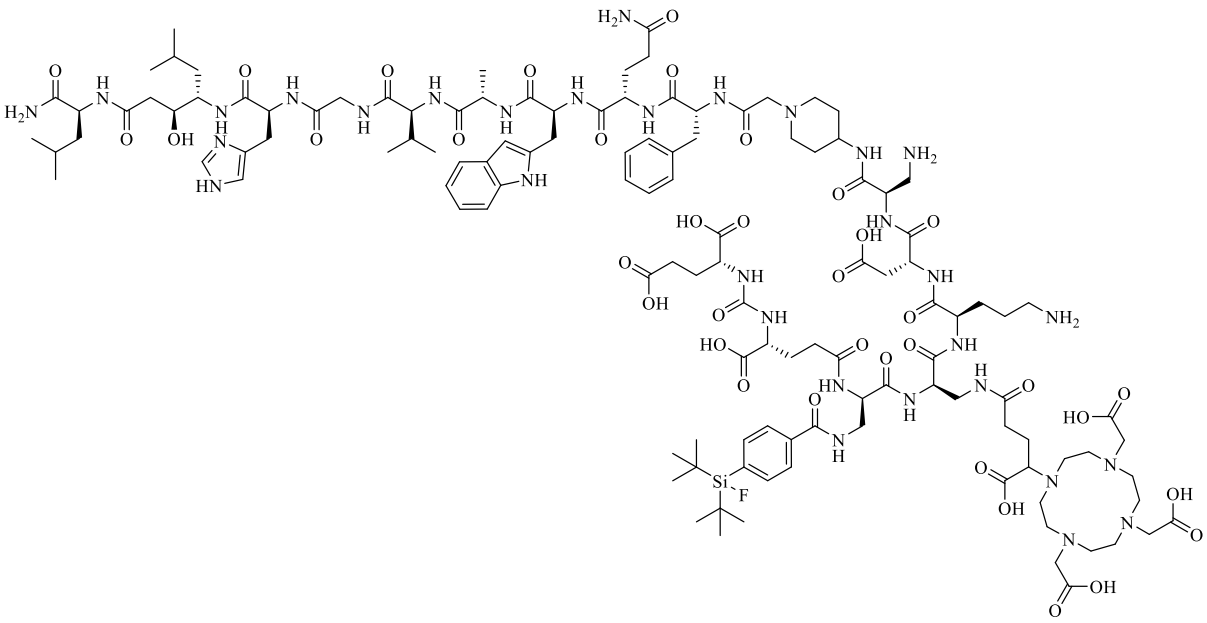

RP-HPLC (10→90% MeCN in 15 min): t_R = 9.2 min, *K*‘ = 4.75.

Calculated monoisotopic mass ($C_{125}H_{190}FN_{31}O_{37}Si$): 2764.4, found: m/z = 692.6 $[M+4H]^{4+}$, 923.3 $[M+3H]^{3+}$.

eue-dap(SiFA)-dap([^{nat}Lu]DOTA-GA)^1-orn^2-asp^3-dap^4-MJ9:

RP-HPLC (10→90% MeCN in 15 min): t_R = 9.0 min, *K*‘ = 4.63.

Calculated monoisotopic mass ($C_{125}H_{187}FLuN_{31}O_{37}Si$): 2936.3, found: m/z = 980.8 $[M+3H]^{3+}$.

eue-dap(SiFA)-dap(DOTA-GA)^{1}-asp^{2}-Pip^{3}-Pip^{4}-MJ9

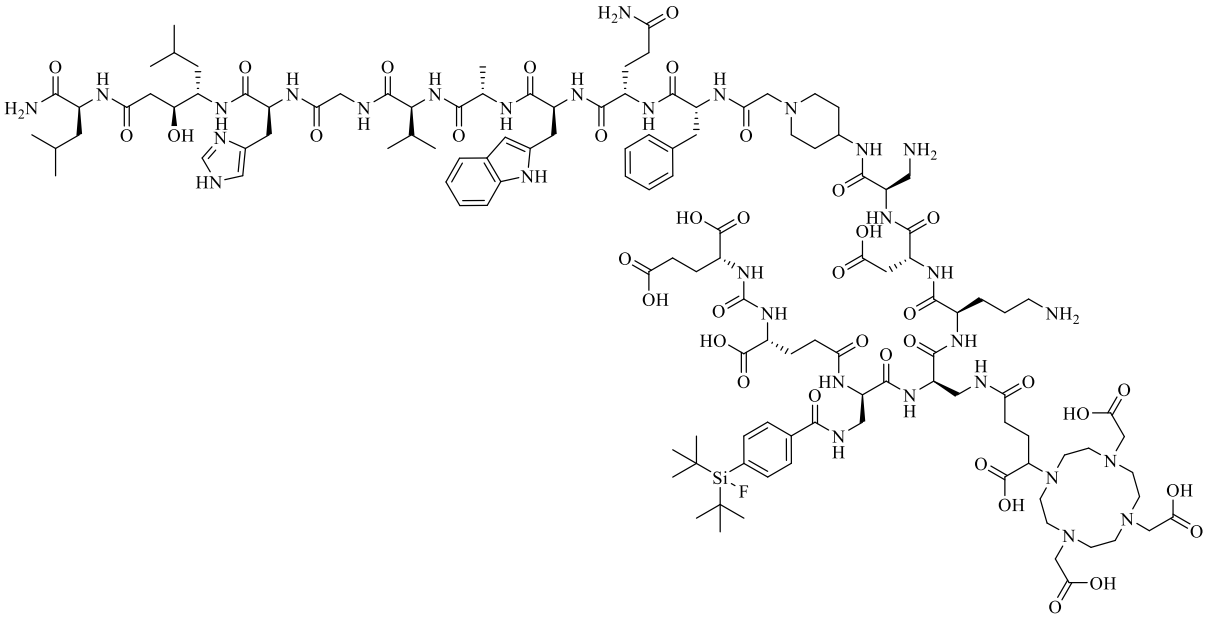

RP-HPLC (10→90% MeCN in 15 min): t_R = 9.3 min, *K*‘ = 4.81.

Calculated monoisotopic mass ($C_{131}H_{198}FN_{31}O_{37}Si$): 2844.4, found: m/z = 711.7 $[M+4H]^{4+}$, 948.6 $[M+3H]^{3+}$.

eue-dap(SiFA)-dap([^{nat}Lu]DOTA-GA)^{1}-asp^{2}-Pip^{3}-Pip^{4}-MJ9:

RP-HPLC (10→90% MeCN in 15 min): t_R = 9.2 min, *K*‘ = 4.75.

Calculated monoisotopic mass ($C_{131}H_{195}FLuN_{31}O_{37}Si$): 3016.4, found: m/z = 1007.1 $[M+3H]^{3+}$.

3.4. Cyclic MJ9 derivatives and linear precursors

Cyclic derivatives were obtained by either disulfide bridge formation when containing cysteine residues within the linear structure or by *Click* chemistry when containing backbone modifications.

3.4.1. Cyclization *via* disulfide bridge formation

All mentioned cyclized analogs based on the core structure of MJ9 were synthesized by standard Fmoc-based SPPS (**GP1**, **GP2**, **GP5**) using a *H*-Rink amide ChemMatrix® resin (35-100 mesh particle size, 0.4-0.6 mmol/g loading) and were cyclized by disulfide bridge formation (**GP8**).

***H*-Gln-Cys-cyclo[Ala-val-Gly-His]-Cys-Leu-NH_2**

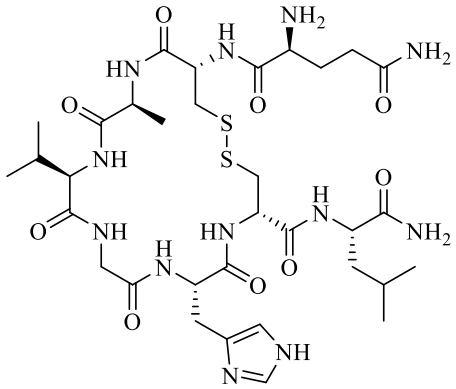

RP-HPLC (10→90% MeCN in 15 min): t_R = 7.6 min, *K*‘ = 3.75 (linear peptide).
RP-HPLC (10→90% MeCN in 15 min): t_R = 7.4 min, *K*‘ = 3.63 (cyclized peptide).
Calculated monoisotopic mass ($C_{33}H_{54}N_{12}O_9S_2$): 826.4, found: m/z = 827.9 $[M+H]^+$.

***H*-phe-Cys-cyclo[Trp-ala-Val-Gly]-Cys-Sta-NH_2**

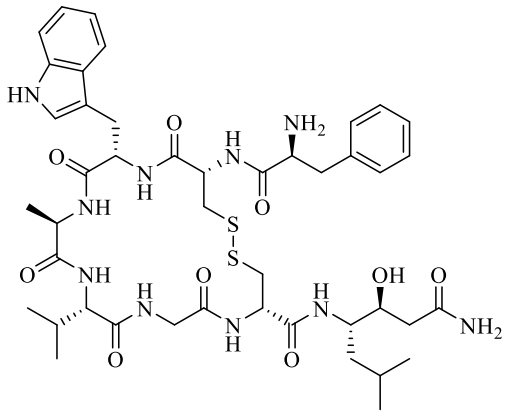

RP-HPLC (10→90% MeCN in 15 min): t_R = 11.1 min, *K*‘ = 5.94 (linear peptide).
RP-HPLC (10→90% MeCN in 15 min): t_R = 11.0 min, *K*‘ = 5.88 (cyclized peptide).
Calculated monoisotopic mass ($C_{44}H_{62}N_{10}O_9S_2$): 938.4, found: m/z = 939.5 $[M+H]^+$.

***H*-Pip-Cys-cyclo[Gln-trp-Ala-Val]-Cys-His-NH_2**

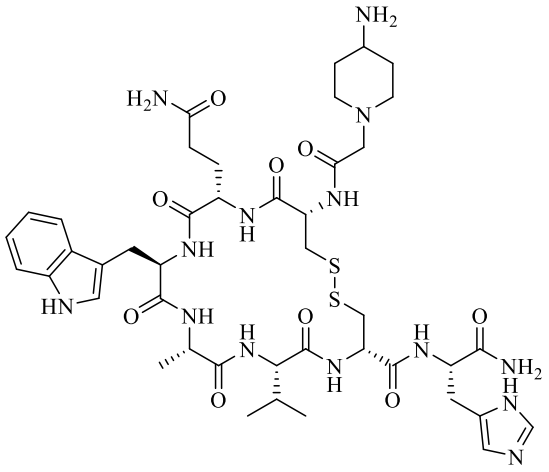

RP-HPLC (10→90% MeCN in 15 min): t_R = 7.8 min, *K*‘ = 3.88 (linear peptide).

RP-HPLC (10→90% MeCN in 15 min): t_R = 7.7 min, *K*‘ = 3.81 (cyclized peptide).

Calculated monoisotopic mass ($C_{43}H_{62}N_{14}O_9S_2$): 982.4, found: m/z = 983.1 $[M+H]^+$.

3.4.2. Cyclization *via Click* chemistry

All mentioned cyclized derivatives based on the core structure of MJ9 were synthesized by standard Fmoc-based SPPS (**GP1**, **GP2**) using a *H*-Rink amide ChemMatrix® resin (35-100 mesh particle size, 0.4-0.6 mmol/g loading). Before propargylation, Fmoc-deprotected *N*-terminus was protected by a *p*-nosyl group (**GP9**) and then propargylated under *Mitsunobu* conditions (**GP10**). After deprotection of the *p*-nosyl group (**GP13**), following coupling required harsher condition to succeed (**GP11**). Thereafter, all couplings were carried out by SPPS (**GP1**, **GP2**) until second alkylation. Therefore, the Fmoc-deprotected *N*-terminus was protected by *p*-nosyl (**GP9**), alkylated with 4-bromobutan-1-ol under *Mitsunobu* conditions (**GP10**) and further azidated (**GP12**). After deprotection of *p*-nosyl (**GP13**), following coupling was accomplished by harsher conditions (**GP11**). After finishing the peptide sequence by SPPS (**GP1**, **GP2**), the linear peptide was cleaved (**GP5**) and purified by RP-HPLC. The peptide was cyclized by *Click* reaction (**GP14**) quantitatively and used without further purification.

***H*-Pip-phe-cyclo[*N*(Gln-Trp-Ala-Val-Gly)]-His-Sta-Leu-NH_2**

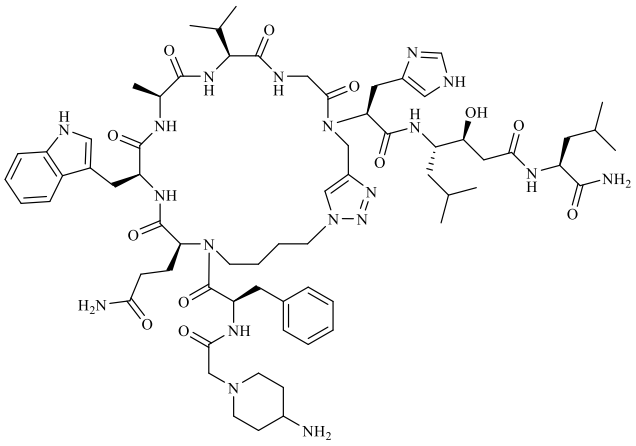

RP-HPLC (30→70% MeCN in 15 min): t_R = 9.5 min, *K*‘ = 4.94 (linear peptide).
RP-HPLC (30→70% MeCN in 15 min): t_R = 7.6 min, *K*‘ = 3.75 (cyclized peptide).
Calculated monoisotopic mass ($C_{69}H_{101}N_{19}O_{12}$): 1387.8, found: m/z = 695.1 $[M+2H]^{2+}$, 1388.8 $[M+H]^{+}$.

***H*-Pip-phe-cyclo[*N*(Gln-Trp-Ala-Val)]-Gly-His-Sta-Leu-NH_2**

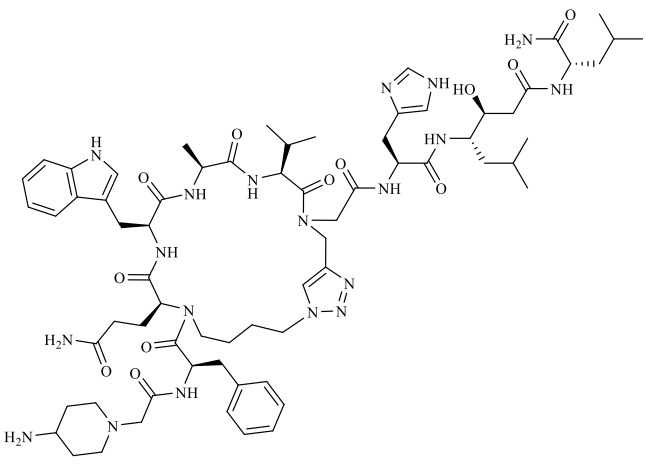

RP-HPLC (30→70% MeCN in 15 min): t_R = 10.1 min, *K*‘ = 5.31 (linear peptide).

RP-HPLC (30→70% MeCN in 15 min): t_R = 8.5 min, *K*‘ = 4.31 (cyclized peptide).

Calculated monoisotopic mass ($C_{69}H_{101}N_{19}O_{12}$): 1387.8, found: m/z = 695.7 $[M+2H]^{2+}$, 1388.9 $[M+H]^{+}$.

***H*-Pip-phe-cyclo[*N*(Gln-Trp-Ala)]-Val-Gly-His-Sta-Leu-NH$_2$**

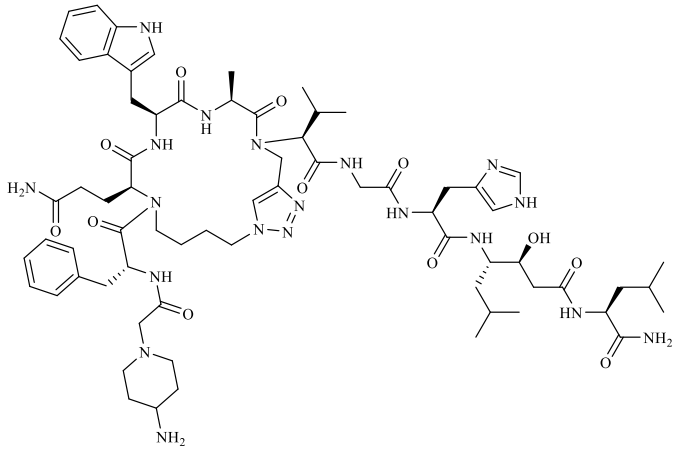

RP-HPLC (30→70% MeCN in 15 min): t_R = 11.6 min, *K*‘ = 6.25 (linear peptide).

RP-HPLC (30→70% MeCN in 15 min): t_R = 10.0 min, *K*‘ = 5.25 (cyclized peptide).

Calculated monoisotopic mass ($C_{69}H_{101}N_{19}O_{12}$): 1387.8, found: m/z = 695.5 $[M+2H]^{2+}$, 1388.2 $[M+H]^{+}$.

***H*-Pip-phe-cyclo[*N*(Gln-Trp)]-Ala-Val-Gly-His-Sta-Leu-NH$_2$**

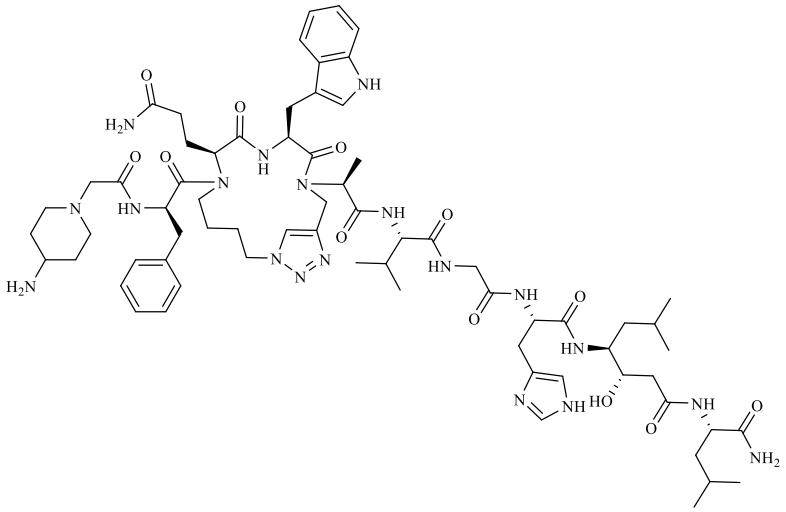

RP-HPLC (30→70% MeCN in 15 min): t_R = 10.4 min, *K*‘ = 5.50 (linear peptide).

RP-HPLC (30→70% MeCN in 15 min): t_R = 8.7 min, *K*‘ = 4.44 (cyclized peptide).

Calculated monoisotopic mass ($C_{69}H_{101}N_{19}O_{12}$): 1387.8, found: m/z = 695.7 $[M+2H]^{2+}$, 1388.6 $[M+H]^{+}$.

***H*-Pip-phe-Gln-cyclo[*N*(Trp-Ala-Val-Gly)]-His-Sta-Leu-NH_2**

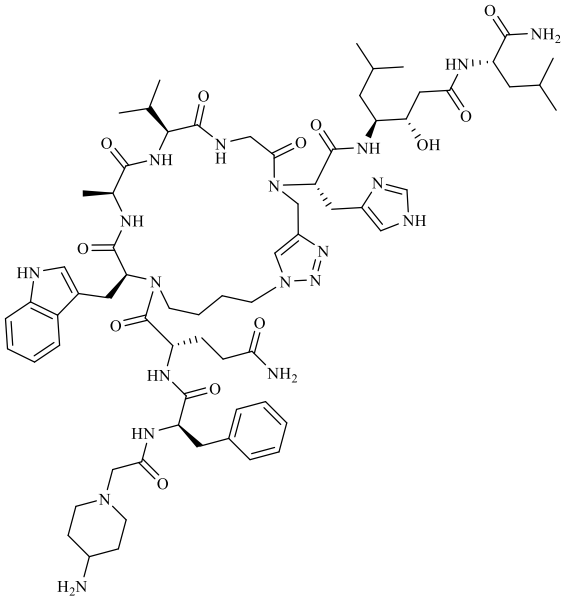

RP-HPLC (30→70% MeCN in 15 min): t_R = 11.3 min, *K*‘ = 6.06 (linear peptide).

RP-HPLC (30→70% MeCN in 15 min): t_R = 9.9 min, *K*‘ = 5.19 (cyclized peptide).

Calculated monoisotopic mass ($C_{69}H_{101}N_{19}O_{12}$): 1387.8, found: m/z = 696.1 $[M+2H]^{2+}$, 1388.4 $[M+H]^{+}$.

***H*-Pip-phe-Gln-cyclo[*N*(Trp-Ala-Val)]-Gly-His-Sta-Leu-NH_2**

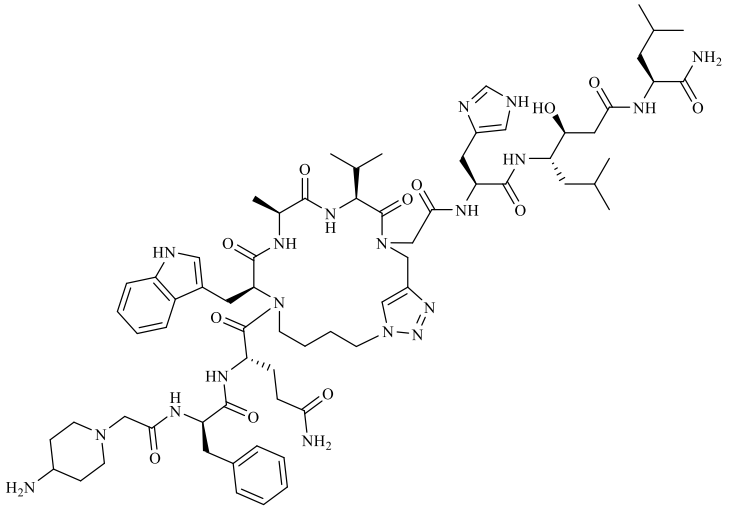

RP-HPLC (30→70% MeCN in 15 min): t_R = 12.0 min, *K*‘ = 6.50 (linear peptide).

RP-HPLC (30→70% MeCN in 15 min): t_R = 10.2 min, *K*‘ = 5.38 (cyclized peptide).

Calculated monoisotopic mass ($C_{69}H_{101}N_{19}O_{12}$): 1387.8, found: m/z = 695.6 $[M+2H]^{2+}$, 1389.0 $[M+H]^{+}$.

***H*-Pip-phe-Gln-cyclo[*N*(Trp-Ala)]-Val-Gly-His-Sta-Leu-NH_2**

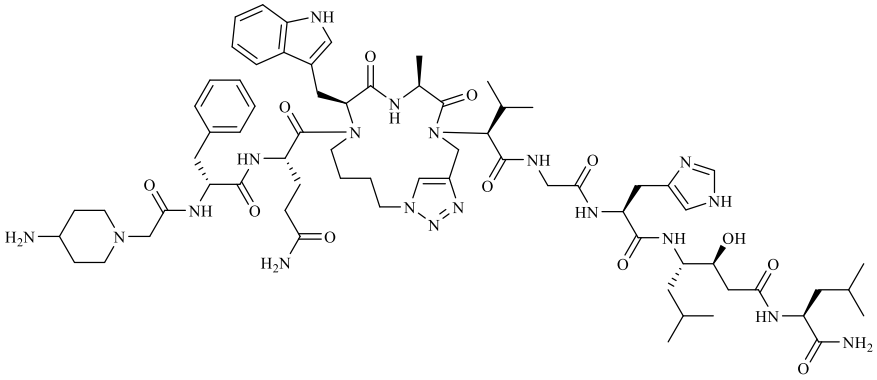

RP-HPLC (30→70% MeCN in 15 min): t_R = 11.9 min, *K*‘ = 6.44 (linear peptide).

RP-HPLC (30→70% MeCN in 15 min): t_R = 9.9 min, *K*‘ = 5.19 (cyclized peptide).

Calculated monoisotopic mass ($C_{69}H_{101}N_{19}O_{12}$): 1387.8, found: m/z = 695.4 $[M+2H]^{2+}$, 1388.6 $[M+H]^{+}$.

III. Results

1. Development of a cell-based assay for GRPR-targeted compounds

1.1. Assay development using agonistic radiolabeled references

Both agonistic precursors ([Tyr^4]BBN and [tyr^6, β-Ala^{11}, Phe^{13}, Nle^{14}]BBN$_{6-14}$) were labeled as described under **II. 2.4.2**. Identity of the respective radiolabeled references was confirmed by quality control (QC) using RP-HPLC with additional co-injection of the respective cold standards (data not shown). ^{125}I-labeling of [Tyr^4]BBN and [tyr^6, β-Ala^{11}, Phe^{13}, Nle^{14}]BBN$_{6-14}$ resulted in RCYs of 0% and 22-32%, respectively. For this reason, [3-[^{125}I]*I*-tyr^6, β-Ala^{11}, Phe^{13}, Nle^{14}]BBN$_{6-14}$ was selected as the reference compound for further competition studies (IC_{50}).

First uptake studies using [3-[^{125}I]*I*-tyr^6, β-Ala^{11}, Phe^{13}, Nle^{14}]BBN$_{6-14}$ as radiolabeled reference were carried out on PC-3 cells according to an established protocol within our group usually applied to LNCaP cells (1.0×10^5 cells/well, pre-incubation at 37 °C for 24 ± 2 h after seeding, incubation of the radiolabeled compound for 1 h on ice on the day of experiment)[184]. After incubation of the GRPR-addressing reference (without addition of competing agents) for 1 h on ice and the following workup, radioactivity uptake was measured *via* a γ-counter. Applying this protocol, the maximum cell uptake of [3-[^{125}I]*I*-tyr^6, β-Ala^{11}, Phe^{13}, Nle^{14}]BBN$_{6-14}$ on PC-3 cells was ≤ 4% (n = 3).

1.2. Improvement of cell uptake by variation of assay conditions

In order to enhance cell uptake of [3-[^{125}I]*I*-tyr^{6}, *β*-Ala^{11}, Phe^{13}, Nle^{14}]BBN$_{6-14}$ on PC-3 cells, different cell numbers, incubation temperatures and times were studied. In a first experiment, the cell number was set to 1.0 × 10^{5} cells/well, whereas the effect of the incubation temperature (ice, rt) and time (0-2.5 h) on the cell uptake of the radiolabeled reference was investigated. Cell uptake at both temperatures did not reach 4% regardless of the incubation time (**Fig. 8**).

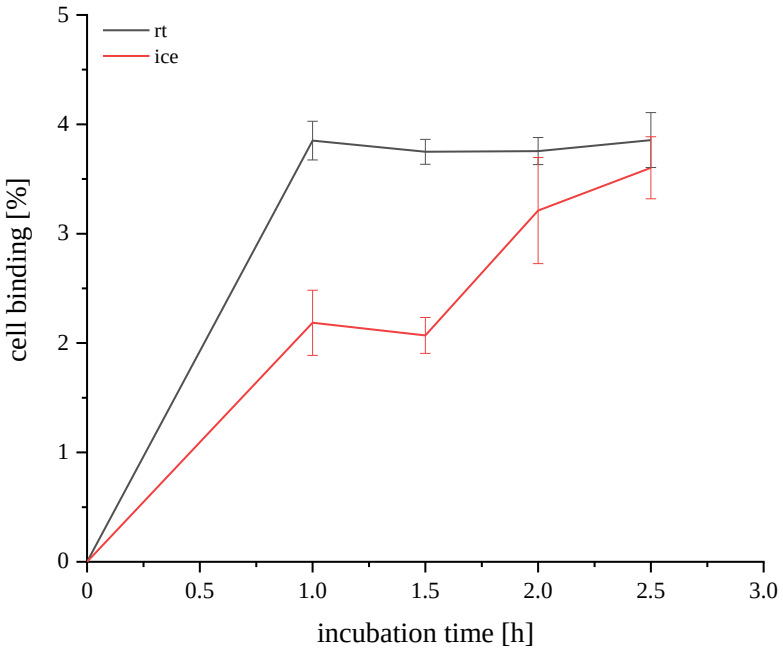

Fig. 8: Cell uptake of [3-[^{125}I]*I*-tyr^{6}, *β*-Ala^{11}, Phe^{13}, Nle^{14}]BBN$_{6-14}$ on GRPR-expressing PC-3 cells (1.0 × 10^{5} cells) in percent, dependent on the incubation time at different temperatures (ice, rt).

However, a cell uptake of about 4% was already reached after incubation for 1.0 h at rt. In contrast, highest cell uptake on ice was observed after incubation for 2.5 h, which was slightly decreased compared to the cell uptake at rt. Moreover, incubation on ice revealed decelerated uptake kinetics over time compared to an incubation at rt.

On the basis of the highest uptake at both temperatures, an incubation time of 2.5 h was set for a second experiment, which included the examination of the cell uptake with increasing cell number. At both temperatures, the radiolabeled reference showed an enhanced uptake with increasing cell number except for a slightly decreased value when incubated on 2.0 × 10^{5} cells on ice (**Fig. 9**).

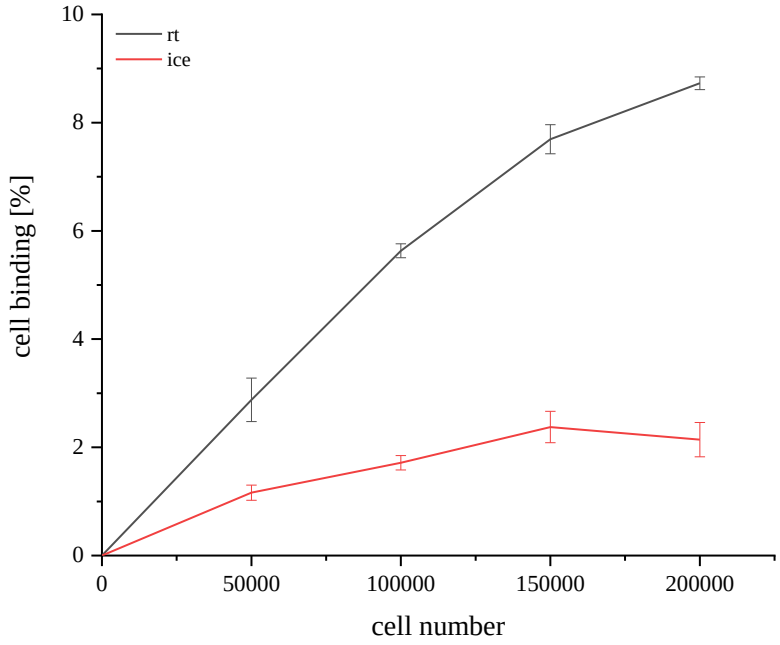

Fig. 9: Cell uptake of [3-[^{125}I]*I*-tyr^{6}, *β*-Ala^{11}, Phe^{13}, Nle^{14}]BBN$_{6-14}$ on PC-3 cells, dependent on the cell number at different temperatures when incubated for 2.5 h.

Interestingly, in this experiment, cell uptake of the radiolabeled reference on 1.0 × 10^5 cells was below 2% when incubated for 2.5 h on ice, which is in contrast to the first experiment (cell uptake ~ 3.5%). However, regardless of the cell number, cell uptake was distinctly higher when incubated at rt compared to the incubation on ice, which is why no cell-based experiments were further executed on ice.

It has to be mentioned that cell uptake of the radiolabeled reference (2.0 × 10^5 cells/well, incubation for 2.5 h at rt) was observed to distinctly decline, dependent on the day of evaluation. When [3-[^{125}I]*I*-tyr^{6}, *β*-Ala^{11}, Phe^{13}, Nle^{14}]BBN$_{6-14}$ was used for cell-based assay studies on the day of synthesis, cell uptakes of ~ 9% were observed. In contrast, cell uptake was ~ 2% under the same conditions when executed one week after synthesis of the radiolabeled reference. QC by radio RP-HPLC revealed an intact tracer amount of < 20% one week after synthesis, despite storage at 4 °C (chromatograms not shown). The observed instability of the radiolabeled reference was attributed to radiolytic degradation over time.

In order to counteract the degradation by radiolysis, ascorbic acid (10 vol-% of a 0.1 M solution in H_2O) was added as a stabilizing agent (radiolytic quencher) immediately after ^{125}I-labeling (by means of the Iodo-Gen® method) and following RP-HPLC purification, according to a reported protocol[185]. By this, ≥ 95% of the radiolabeled reference remained intact when stored at 4 °C for four weeks, which was confirmed by QC *via* radio RP-HPLC (chromatograms not shown).

1.3. First IC_{50} studies and further assay issues

By stabilization of [3-[^{125}I]*I*-tyr^6, *β*-Ala^{11}, Phe^{13}, Nle^{14}]BBN$_{6-14}$ towards radiolysis, cell uptake could be increased up to ~25% (2.0×10^5 cells/well, incubation at rt for 2.5 h). As a comparable cell uptake was achieved when the radiolabeled reference was incubated for 2 h instead of 2.5 h (data not shown), it was decided to execute further cellular assays with 2.0×10^5 cells/well at rt and an incubation time of 2 h.

In order to validate our assay conditions, the binding affinity of several known GRPR agonists (BBN, [Tyr^4]BBN, [phe^6, *β*-Ala^{11}, Phe^{13}, Nle^{14}]BBN$_{6-14}$) was investigated by means of competition studies against the radiolabeled reference (IC_{50}). Furthermore, [3-*I*-tyr^6, *β*-Ala^{11}, Phe^{13}, Nle^{14}]BBN$_{6-14}$ (cold standard), [tyr^6, *β*-Ala^{11}, Phe^{13}, Nle^{14}]BBN$_{6-14}$ (precursor of the radiolabeled reference) and the potent GRPR-targeted antagonist MJ9 were included in this study (**Tab. 1**).

Tab. 1: Binding affinities of the BBN analogs by means of IC_{50} values, determined on PC-3 cells (2.0×10^5 cells/well) and [3-[^{125}I]*I*-tyr^6, *β*-Ala^{11}, Phe^{13}, Nle^{14}]BBN$_{6-14}$ (c = 0.2 nM) as the radiolabeled reference (2 h, rt, HBSS + 1% BSA, *v*/*v*). Data are expressed as mean ± SD (n = 3).

BBN ligand	IC_{50} ± SD [nM] (n = 3)
BBN	35.8 ± 3.9
[tyr^6, *β*-Ala^{11}, Phe^{13}, Nle^{14}]BBN$_{6-14}$	67.4 ± 4.1
[3-*I*-tyr^6, *β*-Ala^{11}, Phe^{13}, Nle^{14}]BBN$_{6-14}$	20.9 ± 1.4
[phe^6, *β*-Ala^{11}, Phe^{13}, Nle^{14}]BBN$_{6-14}$	37.5 ± 5.9
[Tyr^4]BBN	0.42 ± 0.04
MJ9 (1)	0.002 ± 0.000
MJ9 (2)	33.2 ± 1.6

Whereas the native BBN showed an IC_{50} of 35.8 ± 3.9 nM, the IC_{50} value of the truncated BBN derivative [tyr^6, *β*-Ala^{11}, Phe^{13}, Nle^{14}]BBN$_{6-14}$ was twice as high. Interestingly, iodination of this truncated analog led to a more than threefold decreased IC_{50} value. The known BBN-derived universal ligand [phe^6, *β*-Ala^{11}, Phe^{13}, Nle^{14}]BBN$_{6-14}$ revealed a comparable IC_{50} value to the native BBN. Although it differs only in one position compared to the native BBN, [Tyr^4]BBN revealed a picomolar IC_{50} value, whereby it was the most affine agonist within this small study.

Applying these assay conditions, no definite IC_{50} value could be determined for the antagonistic ligand MJ9, as either IC_{50} values comparable to the native BBN or IC_{50} values in the low picomolar range were observed. As other compounds were evaluated on the same respective day as MJ9, cell-derived problems as well as stability issues of the radiolabeled reference could be excluded. However, as each other BBN analog of this small study was an agonist, it was suggested that antagonistic ligands such as MJ9 have to compete against an antagonistic radiolabeled compound under the conditions applied here, because agonists and antagonists generally show different internalization patterns when incubated at rt.

1.4. Assay optimization using a novel antagonistic radiolabeled reference

In order to generate a potent antagonistic radiolabeled reference, the MJ9 derivative [tyr^6]MJ9 (*H*-Pip-tyr-Gln-Trp-Ala-Val-Gly-His-Sta-Leu-NH_2) was radioiodinated by means of the Iodo-Gen® method (**Fig. 10**).

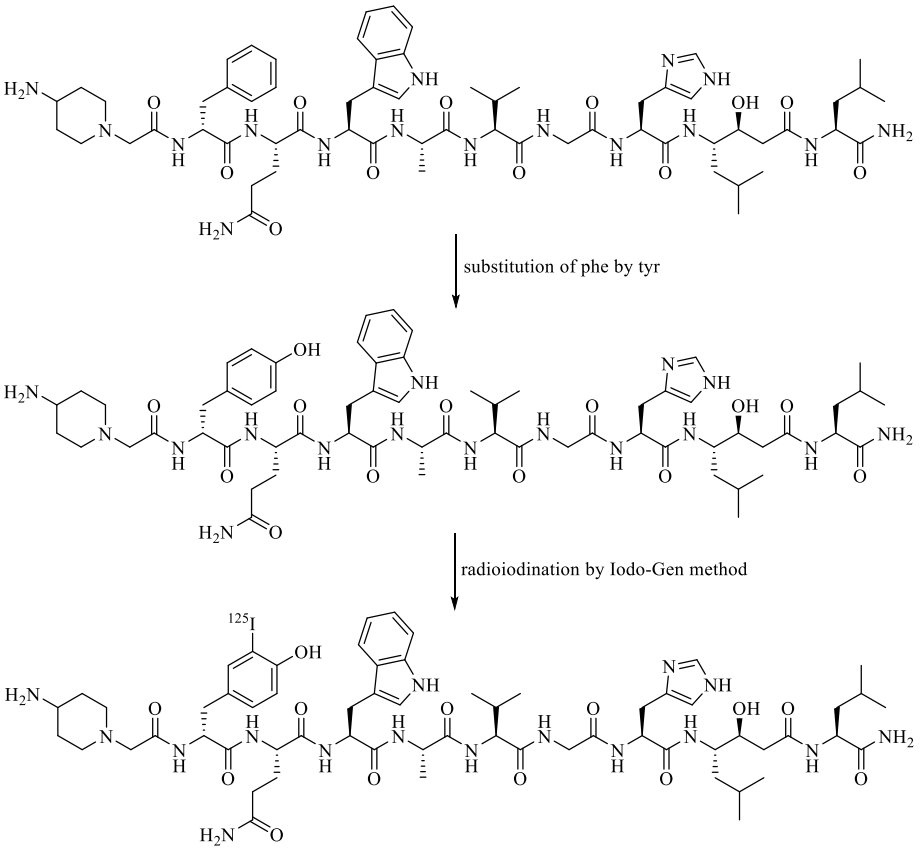

Fig. 10: Chemical structure of the antagonistic precursor (middle) as well as the radiolabeled reference (bottom), both derived from the GRPR-targeted antagonist MJ9 (top).

Synthesis of this novel compound was accomplished by standard Fmoc-based SPPS yielding 16% HPLC-purified precursor. ^{125}I-labeling resulted in RCYs of 33-48% after RP-HPLC purification. Immediately after purification, ascorbic acid (0.1 M in H_2O, 10 vol-%) was added to prevent radiolysis. Characterization of [3-[^{125}I]*I*-tyr^6]MJ9 was accomplished by QC *via* co-injection of the cold standard ([3-*I*-tyr^6]MJ9). Without added quencher solution [3-[^{125}I]*I*-tyr^6]MJ9 was found to be ≥ 95% intact for only three days, whereas it was still ≥ 95% intact after six weeks in a solution containing ascorbic acid.

First uptake studies with the novel antagonistic radiolabeled reference under the above mentioned assay conditions (2.0 × 10^5 cells/well, incubation for 2 h at rt) revealed a total cell binding of about 50% without added competitor. Applying a lower cell number (1.5 × 10^5 cells/well) at the same conditions, cell uptake remained at ~ 50%, for which reason these conditions were defined for all IC_{50} studies of this work. Over the time of this PhD thesis, total cell binding of the respective radiolabeled reference (radiosynthesis of a new batch every six weeks) was in a range of 49-67% (without added competitor) under

these conditions (1.5 × 10^5 cells/well, incubation for 2 h at rt, [3-[^{125}I]*I*-tyr^6]MJ9 as radiolabeled reference).

First competition studies were performed with the potent GRPR antagonist MJ9, [tyr^6]MJ9 (precursor of the radiolabeled reference) as well as [3-*I*-tyr^6]MJ9 (cold standard). Furthermore, [Tyr^4]BBN, which demonstrated the highest affinity among all agonists in the previous study (**Tab. 1**), was examined (**Tab. 2**).

Tab. 2: Binding affinities of the BBN analogs by means of IC_{50} values, determined on PC-3 cells (1.5 × 10^5 cells/well) and [3-[^{125}I]*I*-tyr^6]MJ9 (c = 0.2 nM) as radiolabeled reference (2 h, rt, HBSS + 1% BSA, *v*/*v*). Data are expressed as mean ± SD (*n* = 3). **n* = 5, ***n* = 2

BBN ligand	IC_{50} ± SD [nM] (*n* = 3)
MJ9	0.74 ± 0.09
[tyr^6]MJ9	1.27 ± 0.17
[3-*I*-tyr^6]MJ9	1.33 ± 0.36
[Tyr^4]BBN (1)	0.61 ± 0.05*
[Tyr^4]BBN (2)	35.9 ± 4.3**

All antagonists studied showed IC_{50} values in the high picomolar or low nanomolar range, with MJ9 revealing a higher affinity than its tyr^6- or 3-*I*-tyr^6-substituted derivatives. Similar to MJ9 competing against a radiolabeled agonist, no definite binding affinity could be determined for the agonistic [Tyr^4]BBN competing against a radiolabeled antagonist, as IC_{50} values of 0.61 ± 0.05 nM (*n* = 5) but also IC_{50} values of 42.9 ± 2.3 nM (*n* = 2) were observed under the same conditions. This was also attributed to the different internalization pattern of agonists and antagonists when incubated at rt.

However, as only antagonistic BBN analogs were to be examined in this work, the competition assay developed at rt applying an antagonistic radiolabeled reference was maintained. It has to be stated that over the course of this work, no further issues with indefinite IC_{50} values occurred for the antagonists developed when competing against [3-[^{125}I]*I*-tyr^6]MJ9 within the described assay.

2. *In vitro* studies

In order to metabolically stabilize BBN derivatives and further improve clearance kinetics by decreasing lipophilicity, we aimed to substitute several amino acids within the BBN-based sequence by (hydrophilic) unnatural and natural as well as D-configured amino acids. As mentioned in the introduction, particularly the dipeptidic site Gln^7-Trp^8 is prone to enzymatic degradation by NEP. Substitution at these two positions by unnatural amino acids while maintaining sufficient GRPR affinity were thus considered as particularly beneficial. However, we also addressed further positions within our BBN-based peptides, as instability issues were reported for other sites as well. In order to reduce overall lipophilicity of BBN derivatives, we aimed to substitute amino acids containing lipophilic side chains by more hydrophilic ones. In another approach, we aimed to cyclize linear BBN-based structures to increase metabolic stability, as cyclic compounds such as DOTATATE or CXCR4-targeted ligands were shown to be more stable *in vivo*.

2.1. Linear MJ9 derivatives

In a first set of experiments, the potent GRPR antagonist MJ9 was implied as a reference for structural studies to analyze the effect of the substitutions within its sequence regarding binding affinity (**Fig. 11**).

***H*-Pip^5-phe^6-Gln^7-Trp^8-Ala^9-Val^{10}-Gly^{11}-His^{12}-Sta^{13}-Leu^{14}-NH_2**

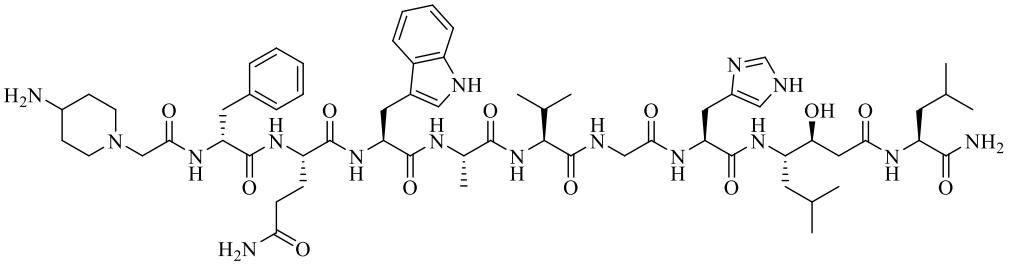

Fig. 11: Chemical structure of the GRPR antagonist MJ9. Numbering of the amino acids is based on the native BBN. Pip = 4-amino-1-carboxymethyl-piperidine

Therefore, we started with an alanine scan to determine the importance of the given amino acids within the MJ9 sequence for high GRPR affinity. Furthermore, a partial *N*-methyl scan was performed to analyze the effect of backbone methylations. Based on these results, both mono- and multisubstituted MJ9 derivatives were evaluated regarding GRPR affinity and assessed considering the suitability of the respective substitution (**Tab. 3**).

Each MJ9 derivative was synthesized by standard Fmoc-based SPPS and subsequently purified by RP-HPLC, resulting in total yields of 9-19%. IC_{50} values were determined as described in chapter **II. 2.5.1**.

Tab. 3: Binding affinities of MJ9 and its derivatives by means of IC_{50} values, determined on PC-3 cells (1.5×10^5 cells/well) and [3-[^{125}I]*I*-tyr^6]MJ9 (c = 0.2 nM) as radiolabeled reference (2 h, rt, HBSS + 1% BSA, *v*/*v*). Data are expressed as mean ± SD (*n* = 3). * Valyl-Sta = (3*S*,4*S*)-4-amino-3-hydroxy-5-methyl-hexanoic acid, ** Tza = *β*-(1,2,3-triazolyl) alanine, R: reference compound

BBN ligand	IC_{50} ± SD [nM] (*n* = 3)	Potential of substitution
MJ9	0.74 ± 0.09	R
Alanine scan derivatives		
[Ala^5]MJ9	1.78 ± 0.28	+
[Ala^6]MJ9	4.12 ± 0.44	+
[Ala^7]MJ9	16.7 ± 1.7	o
[Ala^8]MJ9	153 ± 22	− −
[Ala^{10}]MJ9	27.4 ± 2.7	−
[Ala^{11}]MJ9	2099 ± 226	− − −
[Ala^{12}]MJ9	31.4 ± 9.1	−
[Ala^{13}]MJ9	1439 ± 378	− − −
[Ala^{14}]MJ9	51.5 ± 4.3	−
Partial *N*-methyl scan derivatives		
[*N*-Me-Val^{10}]MJ9	902 ± 7	− − −
[*N*-Me-Gly^{11}]MJ9	3.28 ± 0.49	+
[*N*-Me-His^{12}]MJ9	1463 ± 31	− − −
[*N*-Me-Val^{10}, *N*-Me-Gly^{11}]MJ9	1132 ± 52	− − −
[*N*-Me-Val^{10}, *N*-Me-His^{12}]MJ9	> 10000	− − −
[*N*-Me-Gly^{11}, *N*-Me-His^{12}]MJ9	2099 ± 226	− − −
[*N*-Me-Val^{10}, *N*-Me-Gly^{11}, *N*-Me-His^{12}]MJ9	> 10000	− − −
Monosubstituted MJ9 derivatives		
[Txa^5]MJ9	0.77 ± 0.14	+ +
[tyr^6]MJ9	5.67 ± 0.38	+
[nal^6]MJ9	3.64 ± 0.19	+
[(4-NH$_2$)Phe^6]MJ9	4.96 ± 0.22	+
[Arg^6]MJ9	2.53 ± 0.28	+
[arg^6]MJ9	7.95 ± 0.77	+
[Cit^6]MJ9	6.22 ± 0.56	+
[cit^6]MJ9	13.8 ± 4.5	o
[Hse^7]MJ9	4.61 ± 0.31	+ +
[(4-NH$_2$)Phe^7]MJ9	35.3 ± 0.6	−
[Orn^7]MJ9	1053 ± 37	− − −
[Bta^8]MJ9	2.50 ± 0.53	+ +
[3-Me-Tyr^8]MJ9	50.8 ± 4.7	−

[Dap^{9}]MJ9	86.0 ± 3.5	−
[Ser^{9}]MJ9	3.23 ± 0.13	+
[ala^{9}]MJ9	1743 ± 25	− − −
[ser^{9}]MJ9	1453 ± 82	− − −
[Hse^{9}]MJ9	31.7 ± 2.5	−
[Chg^{10}]MJ9	12.6 ± 1.1	+
[Cpg^{10}]MJ9	1.86 ± 0.19	+ +
[Sta^{10}]MJ9	2647 ± 67	− − −
[Asn^{10}]MJ9	292 ± 10	− −
[ala^{11}]MJ9	36.7 ± 2.1	−
[Orn^{12}]MJ9	3867 ± 325	− − −
[Tza^{12}]MJ9**	104 ± 6	− −
[(4-NH$_2$)Phe^{12}]MJ9	27.8 ± 6.6	−
[Orn^{14}]MJ9	4300 ± 216	− − −
[Ser^{14}]MJ9	8.93 ± 1.26	o
[Thr^{14}]MJ9	6.15 ± 0.90	o
[His^{14}]MJ9	10.3 ± 1.4	−
[Hse^{14}]MJ9	17.2 ± 4.2	−
Multisubstituted MJ9 derivatives		
[Gly^{5}, cit^{6}]MJ9	21.1 ± 3.4	−
[Ala^{5}, Arg^{6}]MJ9	650 ± 27	− −
[Ala^{5}, arg^{6}]MJ9	17.4 ± 0.6	o
[ala^{5}, arg^{6}]MJ9	12.0 ± 1.0	o
[Gly^{5}, arg^{6}]MJ9	6.10 ± 0.74	o
[Txa^{5}, arg^{6}]MJ9	4.16 ± 1.01	+
[*des*Pip^{5}, arg^{6}]MJ9	0.91 ± 0.21	+ +
[*des*Pip^{5}, Arg^{6}]MJ9	36.0 ± 5.9	−
[Arg^{6}, His^{7}]MJ9	5.80 ± 0.29	o
[arg^{6}, His^{7}]MJ9	6.29 ± 0.22	o
[Bta^{8}, Chg^{10}]MJ9	17.7 ± 3.4	o
[Sta^{10}, *des*Gly^{11}]MJ9	163 ± 6	− −
[Valyl-Sta^{10}, *des*Gly^{11}]MJ9*	505 ± 8	− −
[γ-Val^{10}, *des*Gly^{11}]MJ9	> 10000	− − −
[Txa^{10}, *des*Gly^{11}]MJ9	4550 ± 131	− − −
[Gly^{5}, arg^{6}, His^{7}]MJ9	6.43 ± 0.93	o
[Txa^{9}, *des*Val^{10}, *des*Gly^{11}]MJ9	> 10000	− − −
[trp^{8}, ala^{9}, val^{10}, his^{12}]MJ9	> 10000	− − −

Among the alanine scan derivatives of MJ9, each conjugate showed a lower GRPR affinity compared to the parent compound. However, the *N*-terminal located amino acids Pip and phe seemed to be replaceable without a drastic loss of affinity, as both [Ala^5]MJ9 and [Ala^6]MJ9 still displayed IC_{50} values in the low nanomolar range, respectively. In fact, a lot of the substitutions performed at these two *N*-terminal positions maintained good affinity. The replacement of Pip^5 by the structurally similar tranexamic acid (Txa) exhibited comparable IC_{50} values to the unmodified MJ9. Similarly, substitution of phe^6 by other aromatic amino acids (tyr, nal, (4-NH_2)Phe) only slightly decreased GRPR affinity. However, each of the aromatic substitutes revealed a similar IC_{50} value as [Ala^6]MJ9, suggesting that an aromatic residue at this site is not necessary for high binding affinity. We additionally substituted phe^6 by the positively charged D/-L-arginine and the neutral D/-L-citrulline. Interestingly, substitution by a L-enantiomeric arginine showed higher affinity than a substitution by a D-enantiomeric arginine. Moreover, [Arg^6]MJ9 revealed higher affinity than the aromatic substitutes, probably interacting with aromatic residues of the binding pocket through cation-π interactions. Both neutral charged citrulline conformers showed the lowest affinity of all phe^6 substitution derivatives, but still maintained good affinity. Similar to the arginine substitution, the L-enantiomeric citrulline revealed higher affinity than the D-enantiomeric.

In contrast, substitution of the unnatural statin moiety (Sta^{13}→Ala^{13}), which is required for the antagonistic character of statin-based BBN analogs such as MJ9 or RM2 derivatives, led to a micromolar GRPR affinity. As we aimed to focus on statin-based BBN conjugates and wanted to maintain the antagonistic behavior, we did not further substitute the Sta^{13} site in this work. Substitution of Gly^{11} by alanine resulted in a micromolar affinity, which suggests that no side chain residues are tolerated at this site. However, substitution by D-alanine resulted in a moderate affinity pointing that D-conformers are rather tolerated at this position.

Substitution of the key site described for metabolic instability (Gln^7-Trp^8) was rendered by several unnatural amino acids: Gln^7 was replaced by homoserine, (4-NH_2)phenyl alanine and ornithine, while Trp^8 was substituted by 3-Me-Tyr and *β*-(3-benzothienyl)alanine (=Bta). The alanine scan revealed a distinct loss of affinity for the Trp→Ala substitution but only a modest loss of affinity for the Gln→Ala substitution. Interestingly, the positively charged ornithine at position 7 led to a micromolar affinity suggesting that such charges are not tolerated by GRPR. The aromatic (4-NH_2)Phe substitution showed moderate GRPR affinity, whereas the neutral aliphatic amino acid Hse exhibited an only slightly decreased GRPR affinity compared to the parent compound. Whereas substitution of Trp^8 by Ala caused an IC_{50} value in the high nanomolar range, a replacement by aromatic residues led to moderate (3-Me-Tyr) and high GRPR affinity (Bta), suggesting that an aromatic side chain is important at this site.

Substitution of Ala^9 by short positively charged (2,3-diaminopropionic acid = Dap) and neutral (Ser, Hse) amino acids as well as D-enantiomeric (ser, ala) side chains resulted in decreased GRPR affinity compared to MJ9. Whereas substitution by the short neutral amino acid serine maintained an affinity in

the low nanomolar range, the short positively charge Dap showed a high nanomolar IC_{50} value. Positive charges seem to have a negative influence on GRPR affinity at this site, as substitution by the prolonged but neutral charged Hse showed improved IC_{50} values. Interestingly, both D-enantiomeric side chain modifications demonstrated IC_{50} values in the micromolar range.

Replacement of Val^{10} by neutral side chains of different length and spatial demands led to versatile GRPR affinities. The cyclopentyl substitution maintained high GRPR affinity, whereas the cyclohexyl derivative showed slightly increased IC_{50} values. However, both compounds exhibited higher GRPR affinity than the alanine scan derivative, suggesting that more lipophilic or spatially demanding residues are preferred at this site. This was further corroborated, as substitution by the more hydrophilic asparagine led to a low GRPR affinity. As expected, a prolonged peptide backbone by insertion of Sta at this position caused an IC_{50} value in the micromolar range.

His^{12} was substituted by aromatic (β-(1,2,3-triazolyl) alanine = Tza, (4-NH_2)Phe^{12}) or positively charged amino acids (ornithine), as π-π and cation-π interactions with Trp^8 were assumed. Interestingly, substitution by a positively charged Orn yielded poor GRPR affinity. Furthermore, substitution by the enlarged aromatic ring of (4-NH_2)Phe led to a distinctly higher GRPR affinity than substitution by the smaller triazole ring. We thus did not consider further modifications at this site.

Substitution of the *C*-terminal leucine by more hydrophilic amino acids (Orn, Ser, Thr, His, Hse) resulted in noticeably decreased affinities compared to the parent compound. As already observed for the Gln→Orn and His→Orn substitution, the insertion of Orn at position 14 also led to a micromolar affinity, suggesting that BBN derivatives prefer positive charges only at the *N*-terminus. Although the alanine scan ligand only exhibited moderate affinity, which suggests that more lipophilic or spatially demanding side chains such as leucine are favored, substitution by the small serine led to a high affinity. [His^{14}]MJ9 showed an IC_{50} value in the low nanomolar range. Replacement of Leu by Thr, His or Hse revealed only good to moderate GRPR affinity, and thus it was not considered a rational alternative to the lipophilic leucine at the *C*-terminus.

In order to further analyze the impact of modifications within the MJ9 sequence, we performed an *N*-methyl scan within the tripeptidic Val^{10}-Gly^{11}-His^{12} section. All mono- and multisubstituted *N*-methyl compounds were synthesized by standard Fmoc-based SPPS but required a longer coupling time (2.5-3 h instead of 1.5 h for quantitative on-resin coupling to a *N*-methylated amino acid). Among the partial *N*-methyl scan derivatives, only [*N*-Me-Gly^{11}]MJ9 revealed high affinity, whereas each of the other compounds exhibited IC_{50} values in the high nanomolar of micromolar range. Within this tripeptidic section, only the proton of the amidic nitrogen between valine and glycine does not seem to be involved in hydrogen bonding interactions that generally stabilize the arrangement of the peptide within GRPR. For this reason, potential backbone modifications within this part of the peptide could be feasible at that position.

In order to analyze the effect of multiple substitutions within the same peptide on GRPR affinity, we replaced two or more amino acids within the 10 amino acid containing MJ9-based structure. It has to be mentioned that most of these multisubstitutions did not maintain high affinity and are thus not considered as potential building blocks for the improvement of metabolic stability and lipophilicity, respectively. Replacement of *H*-Pip^5 and phe^6 by Ala^5 and Arg^6 led to a poor GRPR affinity. Interestingly, substitution by Ala^5 and arg^6 exhibited a moderate affinity. This was unexpected, as in the monosubstitution analysis, [Arg^6]MJ9 showed a threefold lower IC_{50} value than [arg^6]MJ9. Further multisubstitutions containing arg^6 ([ala^5, arg^6]MJ9, [Gly^5, arg^6]MJ9, [Txa^5, arg^6]MJ9) also revealed good GRPR affinity. Of these three, the most affine compound ([Txa^5, arg^6]MJ9) showed lower IC_{50} values than the monosubstituted [arg^6]MJ9 but still a fivefold higher IC_{50} value than the native MJ9. Noteworthy, the deletion of Pip^5 as well as the insertion of arg^6 led to a comparable IC_{50} value to MJ9, whereas its diastereomer [*des*Pip^5, Arg^6]MJ9 revealed an only moderate affinity. However, if the Pip linker is present in position 5, substitution by Arg leads to superior affinities, which was shown for [Arg^6]MJ9 and [arg^6]MJ9, respectively, and also for [Arg^6, His^7]MJ9 and [arg^6, His^7]MJ9, respectively.

Further multisubstitutions such as [Bta^8, Chg^{10}]MJ9 or [Gly^5, arg^6, His^7]MJ9 revealed moderate to good affinity. However, the use of these substitutions has to be further evaluated by other in vitro experiments, as in case of GRPR affinity, there is no benefit for either conjugate. Stabilization of the MJ9 sequence was also attempted *via* deletion of Gly^{11} and concomitant substitution of Val^{10} by statin analogs (Sta and Valyl-Sta), a prolonged valine derivative (γ-Val) or Txa. However, none of these unnatural amino acids could compensate the loss of the dipeptide Val^{10}-Gly^{11} in terms of GRPR affinity. Partial stereoinversion of the pharmacophore ([trp^8, ala^9, val^{10}, his^{12}]MJ9) caused a drastic loss of affinity, as an IC_{50} value of > 10 µM was determined, suggesting that only minor modifications within the pharmacophoric section are tolerated by GRPR.

2.2. Linear RM2 derivatives

Based on the results of the structural studies of MJ9, the most promising substitutions were further implemented for RM2 analogs. Either DOTA or DOTA-GA was attached as a chelator *N*-terminally. Each mono- or multisubstituted conjugate was compared to the reference compound RM2 and the respective metal complex regarding GRPR affinity (IC_{50}) and lipophilicity ($\log D_{7.4}$). Furthermore, as several groups have shown a positive effect of positive charges at the *N*-terminus on GRPR affinity, we aimed to improve pharmacokinetics of our ligands by addition of positively charged or hydrophilic amino acids. Moreover, due to the success of our PSMA-SiFA ligands, we aimed to transfer the described radiohybrid (rh) methodology to BBN analogs. Therefore, we designed several silicon-fluoride acceptor (SiFA)-comprising compounds with the aim of maintaining high GRPR affinity and also compensating for the high lipophilicity of the SiFA group.

Each RM2 derivative was synthesized by standard Fmoc-based SPPS and was purified by RP-HPLC, resulting in total yields of 4-15%. IC_{50} values were determined as described in chapter **II. 2.5.1**. Lipophilicity was evaluated as *n*-octanol-PBS distribution coefficient at physiological *pH* ($\log D_{7.4}$) as described under **II. 2.5.2**. If not further stated, IC_{50} values were determined with ^{nat}Lu-complexed and $\log D_{7.4}$ values with ^{177}Lu-labeled RM2 analogs (**Tab. 4**).

Tab. 4: Binding affinities of RM2 and its derivatives by means of IC_{50} values, determined on PC-3 cells (1.5×10^5 cells/well) and [3-[^{125}I]*I*-tyr^6]MJ9 (c = 0.2 nM) as radiolabeled reference (2 h, rt, HBSS + 1% BSA, *v*/*v*). Data are expressed as mean ± SD (n = 3). * ^{177}Lu-labeled, R: reference compound

BBN ligand	IC_{50} ± SD [nM] (n = 3)	log$D_{7.4}$ ± SD (n = 6)*	Projected potential of the compound
RM2 (= DOTA-MJ9)	4.45 ± 0.11	/	R
[^{nat}Ga]RM2	1.94 ± 0.16	/	R
[^{nat}Lu]RM2	3.45 ± 0.18	−2.51 ± 0.02	R
Monosubstituted RM2 derivatives			
DOTA-[Dap^5]MJ9	9.40 ± 3.18	−1.99 ± 0.06	o
DOTA-[Txa^5]MJ9	4.43 ± 0.55	−1.85 ± 0.04	+
[^{nat}Lu]DOTA-[Cit^7]MJ9	11.6 ± 2.1	−3.22 ± 0.15	+ +
[^{nat}Ga]DOTA-[Hse^7]MJ9	12.2 ± 0.2	/	+
[^{nat}Lu]DOTA-[Hse^7]MJ9	19.7 ± 1.6	−2.25 ± 0.06	+ +
[^{nat}Ga]DOTA-[Bta^8]MJ9	3.06 ± 0.15	/	+
[^{nat}Lu]DOTA-[Bta^8]MJ9	4.63 ± 0.23	−1.81 ± 0.02	+ +
[^{nat}Ga]DOTA-[α-Me-Trp^8]MJ9 (=AMTG)	3.28 ± 0.33	/	+
[^{nat}Lu]DOTA-[α-Me-Trp^8]MJ9 (=AMTG)	3.04 ± 0.08	−2.28 ± 0.06	+ + +
[^{nat}Ga]DOTA-GA-[α-Me-Trp^8]MJ9 (=AMTG2)	5.82 ± 0.23	/	+
[^{nat}Lu]DOTA-GA-[α-Me-Trp^8]MJ9 (=AMTG2)	4.74 ± 0.23	−2.51 ± 0.11	+ + +
[^{nat}Lu]DOTA-[α-Me-trp^8]MJ9	509 ± 46	n.d.	− −
DOTA-[Chg^{10}]MJ9	67.3 ± 6.6	−1.64 ± 0.10	−
DOTA-[Cpg^{10}]MJ9	36.6 ± 15.9	−1.94 ± 0.04	−
Multisubstituted RM2 derivatives			
[^{nat}Lu]NeoBOMB1	4.22 ± 0.14	−0.57 ± 0.03	R
DOTA-[*des*Pip^5, arg^6]MJ9	12.8 ± 0.9	−3.67 ± 0.08	o
[^{nat}Lu]DOTA-[Hse^7, Bta^8]MJ9	153 ± 20	−1.53 ± 0.05	− −
DOTA-[Bta^8, Chg^{10}]MJ9	95.2 ± 17.4	−1.07 ± 0.05	− −
DOTA-[Bta^8, Cpg^{10}]MJ9	115 ± 21	−1.36 ± 0.03	− −
Linker-extended RM2 derivatives			
DOTA-Dap^4-MJ9	2.94 ± 0.82	−2.56 ± 0.09	+
DOTA-Dap^4-[Txa^5]MJ9	4.61 ± 1.97	−2.42 ± 0.01	o
[^{nat}Lu]DOTA-Orn^4-MJ9	1.73 ± 0.12	−3.64 ± 0.19	+ + +
[^{nat}Lu]DOTA-Dap^3-Orn^4-MJ9	1.06 ± 0.02	−2.52 ± 0.09	+ +
[^{nat}Lu]DOTA-Orn^3-Dap^4-MJ9	0.86 ± 0.06	−2.78 ± 0.08	+ +
[^{nat}Lu]DOTA-orn^3-dap^4-MJ9	0.96 ± 0.03	−3.46 ± 0.14	+ + +
[^{nat}Lu]DOTA-GA-orn^3-dap^4-MJ9	1.65 ± 0.03	−3.72 ± 0.05	+ + +

[^{nat}Lu]DOTA-Pip^3-Pip^4-MJ9	2.14 ± 0.17	−2.62 ± 0.14	+ +
[^{nat}Lu]DOTA-dap^3-Pip^4-MJ9	2.42 ± 0.69	−2.77 ± 0.15	+ +
[^{nat}Lu]DOTA-ser^3-Pip^4-MJ9	2.01 ± 0.43	−2.69 ± 0.09	+ +
[^{nat}Lu]DOTA-orn^3-Pip^4-MJ9	1.20 ± 0.32	−3.07 ± 0.03	+ + +
[^{nat}Lu]DOTA-asp^3-Pip^4-MJ9	2.34 ± 0.36	−3.19 ± 0.08	+ +
[^{nat}Lu]DOTA-cit^3-Pip^4-MJ9	2.12 ± 0.31	−2.97 ± 0.07	+ +
[^{nat}Lu]DOTA-Pip^3-cit^4-MJ9	2.52 ± 0.82	−3.08 ± 0.05	+ +
[^{nat}Lu]DOTA-Pip^3-ser^4-MJ9	4.15 ± 0.28	−3.09 ± 0.08	+
[^{nat}Lu]DOTA-Pip^3-asp^4-MJ9	3.63 ± 0.83	−3.60 ± 0.08	+ +
[^{nat}Lu]DOTA-asp^3-asp^4-MJ9	3.16 ± 0.67	−3.75 ± 0.10	+ +
First generation BBN-SiFA derivatives			
DOTA-GA-[dap(SiFA)^6]MJ9	238 ± 27	n.d.	− −
DOTA-GA-Asp^4-[dap(SiFA)^6]MJ9	483 ± 18	n.d.	− −
DOTA-GA-Asp^3-Asp^4-[dap(SiFA)^6]MJ9	585 ± 28	n.d.	− −
DOTA-GA-Ala^4-[dap(SiFA)^6]MJ9	1380 ± 51	n.d.	− − −
DOTA-GA-Ala^3-Ala^4-[dap(SiFA)^6]MJ9	910 ± 83	n.d.	− −
[dap(SiFA)^6]MJ9	593 ± 21	n.d.	− −
DOTA-GA-[*des*Pip^5, dap(SiFA)^6]MJ9	873 ± 72	n.d.	− −
DOTA-GA-[Ala^5, dap(SiFA)^6]MJ9	971 ± 13	n.d.	− −
DOTA-GA-dap(SiFA)^4-MJ9	27.6 ± 7.0	0.67 ± 0.06	−
Second generation BBN-SiFA derivatives			
[^{nat}Ga]DOTA-GA-dap(SiFA)^1-Gln^2-Arg^3-Leu^4-MJ9	6.27 ± 0.42	/	−
[^{nat}Lu]DOTA-GA-dap(SiFA)^1-Gln^2-Arg^3-Leu^4-MJ9	5.13 ± 0.53	0.58 ± 0.06	−
[^{nat}Ga]DOTA-GA-dap(SiFA)^1-Asn^2-Arg^3-Asn^4-MJ9	28.2 ± 9.1	/	o
[^{nat}Lu]DOTA-GA-dap(SiFA)^1-Asn^2-Arg^3-Asn^4-MJ9	30.9 ± 0.1	−1.41 ± 0.06	o
[^{nat}Lu]DOTA-GA-dap(SiFA)^1-Gln^2-Arg^3-Dap^4-MJ9	5.45 ± 0.39	−0.60 ± 0.08	o
[^{nat}Lu]DOTA-GA-dap(SiFA)^1-Gln^2-Dap^3-Orn^4-MJ9	4.23 ± 0.19	−0.94 ± 0.05	o
[^{nat}Lu]DOTA-GA-dap(SiFA)^1-Gln^2-Orn^3-Dap^4-MJ9	3.96 ± 0.29	−0.90 ± 0.05	o
Third generation BBN-SiFA derivatives			
eue-dap(SiFA)^1-dap([^{nat}Lu]DOTA-GA)^2-orn^3-dap^4-MJ9	10.0 ± 0.1	−1.71 ± 0.09	+
eue-dap(SiFA)-dap([^{nat}Lu]DOTA-GA)^1-asp^2-orn^3-dap^4-MJ9	10.4 ± 1.5	−1.71 ± 0.06	+
eue-dap(SiFA)-dap([^{nat}Lu]DOTA-GA)-asp^1-asp^2-orn^3-dap^4-MJ9	9.74 ± 1.01	−1.96 ± 0.15	+ +
eue-dap(SiFA)-dap([^{nat}Lu]DOTA-GA)^1-orn^2-asp^3-dap^4-MJ9	14.3 ± 1.5	−1.96 ± 0.15	+
eue-dap(SiFA)-dap([^{nat}Lu]DOTA-GA)^1-asp^2-Pip^3-Pip^4-MJ9	9.69 ± 2.14	−2.05 ± 0.08	+ +

The gold standard among BBN-based ligands, RM2, as well as its complexes with ^{nat}Ga-gallium or ^{nat}Lu-lutetium were used as reference compounds within the novel antagonistic competition assay in terms of GRPR affinity. Using [3-[^{125}I]*I*-tyr^6]MJ9 as radiolabeled reference, unlabeled RM2 as well as [^{nat}Ga]RM2 and [^{nat}Lu]RM2 showed a low nanomolar IC_{50} value. Furthermore, RM2 revealed a good hydrophilic character with a log$D_{7.4}$ of −2.51 ± 0.02. As a second reference, the literature-cited antagonist NeoBOMB1 was established. It revealed a comparable IC_{50} value but a distinctly higher lipophilicity than RM2.

Based on the results of the studies on the MJ9 sequence, only a few substitutions were considered as potential alternatives (**Tab. 3**): Txa^5, Hse^7, Bta^8, Cpg^{10}, Chg^{10} and [desPip^5, arg^6]. We thus attached a DOTA chelator *N*-terminally and evaluated the resulting ligands in terms of GRPR affinity and lipophilicity. Despite an equal IC_{50} value of MJ9 and [Txa^5]MJ9, addition of a chelator led to a slightly decreased affinity and distinctly higher lipophilicity for DOTA-[Txa^5]MJ9 compared to RM2. Substitution of Pip (tertiary amine) by Dap (primary amine) led to higher IC_{50} values, which was unexpected, as BBN analogs were reported to prefer positive charges at the *N*-terminus. As substitution of Pip by the neutral Txa resulted in a comparable IC_{50} value, we assumed that the molecular structure of Pip or Txa is more important for GRPR affinity at this site than a positive charge. This was further corroborated by comparison of DOTA-[*des*Pip^5, arg^6]MJ9 and [*des*Pip^5, arg^6]MJ9, neither of which comprise a Pip moiety. Without a coupled chelator, high affinity was determined (IC_{50}: 0.91 ± 0.21 nM), whereas the DOTA-conjugated analog revealed a distinctly decreased GRPR affinity (IC_{50}: 12.8 ± 0.9 nM). However, due to the substitution of phe by the more hydrophilic arg, DOTA-[*des*Pip^5, arg^6]MJ9 revealed a high hydrophilic character. Surprisingly, RM2 analogs comprising either Cpg^{10} or Chg^{10} only exhibited moderate to poor GRPR affinity. As expected, substitution by either Cpg^{10} or Chg^{10} led to increased log$D_{7.4}$ values, as both amino acids were considered more lipophilic than valine. However, none of the above described substitutions still showed promising overall data after the coupling of DOTA.

We thus focused on the Gln^7-Trp^8 dipeptide and the Hse or Bta modifications. Due to the necessity of having a stabilizing amino acid at the Gln^7-Trp^8 site, we additionally introduced two other unnatural amino acids: citrulline and α-methyl tryptophan. With the exception of AMTG and AMTG2, ^{nat}Ga-complexed compounds showed lower IC_{50} values than their ^{nat}Lu-complexed analogs. Among the $^{nat/177}$Lu-labeled Gln^7-Trp^8-modified compounds, AMTG exhibited the lowest IC_{50} value, which was comparable to [^{177}Lu]RM2. Whereas DOTA-[Bta^8]MJ9 also displayed high GRPR affinity, DOTA-[Cit^7]MJ9 and DOTA-[Hse^7]MJ9 revealed only moderate affinity. However, both compounds showed an enhanced lipophilicity compared to DOTA-[Bta^8]MJ9, with DOTA-[Cit^7]MJ9 exhibiting the lowest lipophilicity among all Gln^7-Trp^8-modified ligands. The noticeably higher lipophilicity of DOTA-[Bta^8]MJ9 compared to RM2 was unexpected, as both compounds only differ in one atom (indole nitrogen [RM2] vs. indole sulfur). Due to high GRPR affinity and good lipophilicity, AMTG and AMTG2 were considered as the most promising conjugates among these Gln^7-Trp^8-modified RM2 derivatives. Nonetheless, despite showing certain weaknesses, the other Gln^7-Trp^8-modified RM2 analogs were also

considered as potential alternatives to the metabolic unstable RM2. However, an improved metabolic stability first has to be shown in further experiments. The only exceptions of these positive assessments were DOTA-[α-Me-trp^8]MJ9 (diastereomer of AMTG) and the disubstituted DOTA-[Hse^7, Bta^8]MJ9, as both revealed IC_{50} values in the high nanomolar range.

In another set of structural studies, we aimed to improve pharmacokinetic properties of RM2 derivatives by modification of a prolonged linker section. Therefore, we inserted different amino acids (positively/negatively charged, neutral) between the chelating agent (DOTA or DOTA-GA) and its binding sequence. Coupling of L-/D-2,3-diaminopropionic acid (L-/D-Dap) was accomplished using 2,4,6-collidine (6.0 eq.) instead of DIPEA. The desired products resulted in > 95% enantiomeric excess after the coupling of the respective Dap enantiomer. Except for DOTA-Dap^4-[Txa^5]MJ9, each linker-extended RM2 derivative displayed either enhanced GRPR affinity, lipophilicity or both compared to the parent compound (IC_{50}: 3.45 ± 0.18, log$D_{7.4}$: −2.51 ± 0.02). In particular, beneficial effects on the affinity were observed for most linker-extended ligands. Positively charged primary amines of L-/D-Dap or Orn at position 4 contributed more for GRPR affinity than the positively charged tertiary amine of Pip. Nonetheless, the positive charge of Pip improved GRPR affinity to a higher extent than the neutral ser, cit, respectively, or the negatively charged asp.

Position 3 did not show distinct effects on GRPR affinity, except for L-/D-Orn, which further decreased IC_{50} values. Not surprisingly, DOTA-Orn^3-Dap^4-MJ9 and DOTA-orn^3-dap^4-MJ9 exhibited the highest affinity among the linker-extended RM2 analogs. Coupling of DOTA-GA instead of DOTA led to slightly decreased GRPR affinity but also slightly improved lipophilicity. Analogously, addition of asp generated minor GRPR affinity but also decreased lipophilicity. As RM2 already showed favorable pharmacokinetics in preclinical and clinical studies, only the linker-extended compounds with distinctly improved GRPR affinity and lipophilicity were considered as a potential upgrade. L-/D-ornithine-containing compounds such as DOTA-Orn^4-MJ9, DOTA-GA/DOTA-orn^3-dap^4-MJ9 and DOTA-orn^3-Pip^4-MJ9 exhibited (nearly) subnanomolar affinity as well as a log$D_{7.4}$ < −3. Also worth mentioning is DOTA-asp^3-asp^4-MJ9, which revealed a similar IC_{50} value to RM2 despite the introduction of two asp residues at the positive charge-preferring *N*-terminus but, due to this modification, also displayed the lowest lipophilicity among all ligands in this study (log$D_{7.4}$: −3.75 ± 0.10). Because of this favorable combination of high GRPR affinity and low lipophilicity, these ligands could be appropriate standalone compounds. However, the applied modifications (L-/D-Orn, L-/D-Dap, asp) could also be implemented if pharmacokinetics were not sufficient, for example to compensate the loss of affinity and hydrophilic character when the bulky, lipophilic SiFA group is introduced into BBN analogs.

As already mentioned, the radiohybrid (rh) concept, developed by our group for PSMA inhibitors, led to favorable pharmacokinetic properties preclinically and clinically. In order to transfer this successful strategy to GRPR-targeted compounds, a SiFA moiety along with several (hydrophilic) amino acids was introduced at the *N*-terminal end. This was accomplished by the coupling strategy described under **II. 3.3.5**. In brief, after successful coupling of Fmoc-L-/D-Dap(Dde)-OH, the Dde group was deprotected first, followed by the coupling of either a SiFA moiety or a chelator to the then free sidechain of Dap. Thereafter, the *N*-terminal Fmoc group was deprotected and another coupling was enabled. Complying with this strategy, no isomer formations were observed over the course of this study.

A first attempt for the introduction of the bulky SiFA group was made at position 6 (instead of phe) of the RM2 sequence, as the MJ9 analog [nal^6]MJ9 revealed high affinity (**Tab. 3**). We thus hypothesized that there is sufficient space for steric demanding moieties at this site, even allowing for the introduction of a SiFA building block. Therefore, several ligands were designed with a dap moiety at position 6, which acted as a trifunctional linker, thereby enabling the coupling of the SiFA group to its free amine side chain. Except for the [dap(SiFA)^6]MJ9 derivative, each ligand of this series contained a DOTA-GA chelator. In order to evaluate the effect of the introduction of the SiFA group, only IC_{50} values were determined, which was executed as described in chapter **II. 2.5.1**. Each BBN-SiFA compound of this series revealed poor GRPR affinity. As none of the modifications applied (addition of Ala or Asp in position 3 and 4, deletion/substitution of Pip^5) led to enhanced affinity, we designed a novel BBN-SiFA conjugate (DOTA-GA-dap(SiFA)^4-MJ9), which contained the dap(SiFA) moiety at position 4 instead of position 6. As this ligand displayed the highest GRPR affinity of all first generation BBN-SiFA derivatives, we suggested that the bulky SiFA building block does not fit into the binding pocket and had thus to adjust our design concept. However, as DOTA-GA-dap(SiFA)^4-MJ9 only showed moderate GRPR affinity as well as poor lipophilicity (log$D_{7.4}$: 0.67 ± 0.06), we assumed that the distance between the SiFA group and the pharmacophore has to increase and the SiFA moiety must be compensated, in terms of lipophilicity, with hydrophilic amino acids.

Therefore, we designed a series of dap(SiFA)^1-containing BBN-SiFA ligands with a prolonged linker that comprised hydrophilic building blocks (second generation BBN-SiFA compounds). First, we introduced the tripeptide Gln-Arg-Leu into positions 2-4, which is derived from the sequence of the native BBN. This did not improve the high lipophilicity but the GRPR affinity, revealing an IC_{50} value in the low nanomolar range. Substitution of Gln^2 and Leu^4 by asparagine residues led to a massive decrease in lipophilicity (log$D_{7.4}$: −1.41 ± 0.06) but also in GRPR affinity, as the IC_{50} value was only moderate. Complexation of either ^{nat}Ga-gallium or ^{nat}Lu-lutetium was not observed to have a distinct impact. As we noticed positive effects in our studies on linker-extended RM2 analogs when positively charged amino acids (Dap, Orn) were located in position 4, we synthesized three novel conjugates, which contained either a Dap or a Dap and an Orn moiety at positions 3 and 4. Indeed, each of these three compounds displayed an IC_{50} value in the low nanomolar range. However, log$D_{7.4}$ values were not considered sufficient for in vivo purposes.

The inappropriate lipophilicity was thus addressed by further hydrophilic modifications such as dap, orn, asp and Pip as well as the highly hydrophilic glu-urea-glu (eue) motif at the *N*-terminus (third generation BBN-SiFA ligands). These complex structures were synthesized as described under **II. 3.3.5.3**). As expected, the modifications applied distinctly improved lipophilicity, as each of these ligands displayed a log$D_{7.4}$ value in a range of −2.1 to −1.7, which was assessed as sufficient for *in vivo* studies. Due to the addition of the hydrophilic amino acids and the eue unit, GRPR affinity was decreased compared to the most affine second generation BBN-SiFA ligands. However, we evaluated these affinities as sufficient and assumed that *in vivo* kinetics would be favorable as a consequence of the improved lipophilicity.

2.3. Cyclic MJ9-based compounds

Besides substituting amino acids on one or more sites within linear compounds to enhance metabolic stability, cyclization of linear structures was also shown to be effective, for example for CXCR4- or SST2R-targeted peptides. As both receptors as well as the bombesin receptor family are part of the GPCR family, we assumed that such cyclization approaches could thus be feasible for GRPR-targeted ligands. Therefore, cyclization of MJ9 derivatives was carried out by two different approaches, on the one hand *via* disulfide bridge formation and on the other hand *via Click* chemistry. Both concepts and their impact on GRPR affinity are described in the following.

2.3.1. Cyclization by disulfide bridge formation

In a first set of experiments, GRPR-targeted ligands were designed on the basis of typical SST derivatives such as DOTATATE, which consists of eight amino acids and a *N*-terminal attached chelator. Within its structure, two cysteine residues are located in the penultimate positions of both termini that form a disulfide bridge. For a simplified spatial cyclization, a D-amino acid is included at the fifth position counting from the *C*-terminal end (**Fig. 12**)[186].

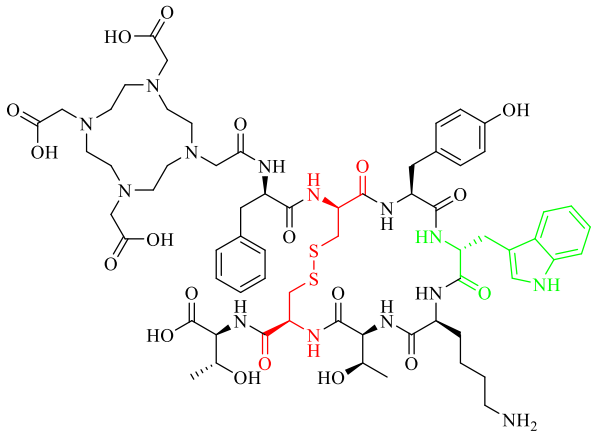

Fig. 12: Typical structure of a cyclic SST2R-targeted ligand (DOTATATE) containing two cysteine residues (red), which form a disulfide bridge within the six amino acid cycle, as well as a D-amino acid (green) which facilitates spatial cyclization.

For the cyclic BBN approach, the sequence of MJ9, comprising ten amino acids, was truncated by two amino acids to obtain a similar backbone length as for DOTATATE. The amino acid sequence was additionally modified by two cysteine residues and a D-amino acid in the above described positions. As we used different (*C*-terminal) starting points for our syntheses, we obtained three different cyclic MJ9-based compounds: *H*-Gln-Cys-cyclo[Ala-val-Gly-His]-Cys-Leu-NH_2, *H*-phe-Cys-cyclo[Trp-ala-Val-Gly]-Cys-Sta-NH_2 and *H*-Pip-Cys-cyclo[Gln-trp-Ala-Val]-Cys-His-NH_2 (**Fig. 13**).

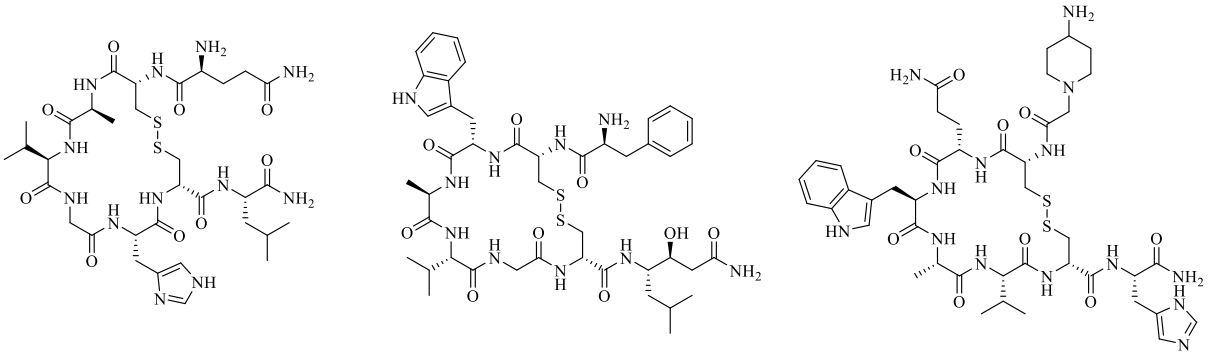

Fig. 13: Chemical structure of the three cyclic BBN derivatives *H*-Gln-Cys-cyclo[Ala-val-Gly-His]-Cys-Leu-NH_2 (left), *H*-phe-Cys-cyclo[Trp-ala-Val-Gly]-Cys-Sta-NH_2 (middle) and *H*-Pip-Cys-cyclo[Gln-trp-Ala-Val]-Cys-His-NH_2 (right).

The respective linear derivatives were synthesized *via* standard Fmoc-based SPPS, cleaved from the resin and cyclized by sulfide oxidation according to a procedure published by our group[182]. After purification by RP-HPLC, all three cyclic ligands were obtained in total yields of 14-16%. The cyclization step resulted in conversion rates of ≥ 85%. The non-cyclized peptide was removed by RP-HPLC using a linear gradient (25→35% MeCN in H_2O in 20 min). Analysis by ESI-MS revealed the abstraction of two protons compared to the respective linear educts.

IC_{50} values of the three cyclic compounds were determined as described in chapter **II. 2.5.1** on PC-3 cells (1.5×10^5 cells/well) and [3-[^{125}I]*I*-tyr^6]MJ9 (c = 0.2 nM) as radiolabeled reference (2 h, rt, HBSS + 1% BSA, *v*/*v*). None of the three ligands showed any GRPR affinity (IC_{50} values > 10 µM), suggesting that the GRPR does not tolerate the limited flexibility of the cyclic ligands. In order to verify this suggestion, we additionally evaluated their linear counterparts (*H*-Gln-Cys-Ala-val-Gly-His-Cys-Leu-NH_2, *H*-phe-Cys-Trp-ala-Val-Gly-Cys-Sta-NH_2 and *H*-Pip-Cys-Gln-trp-Ala-Val-Cys-His-NH_2). Interestingly, also none of the linear compounds showed any GRPR affinity (IC_{50} values > 10 µM). We thus assumed that the substitutions performed (two cysteine residues, one respective D-conformer) within the pharmacophoric sequence impede the interaction of the ligands within the binding pocket of GRPR. For this reason, we tried to design cyclic BBN derivatives without major substitutions within the pharmacophore and this will be described in the following chapter.

2.3.2. Cyclization by *Click* chemistry

In order to avoid substitutions of one or more amino acids within the pharmacophore, we developed a strategy to cyclize linear BBN-based compounds using backbone modifications. We therefore attached an alkyne as well as a *N*-azido alkyl group on different amidic nitrogen atoms within the peptide backbone to perform a cyclization reaction *via Click* chemistry. The synthesis of these backbone-modified compounds was performed according to a modified procedure (**II. 3.4.2**), which is depicted in general in **Scheme 3**[187].

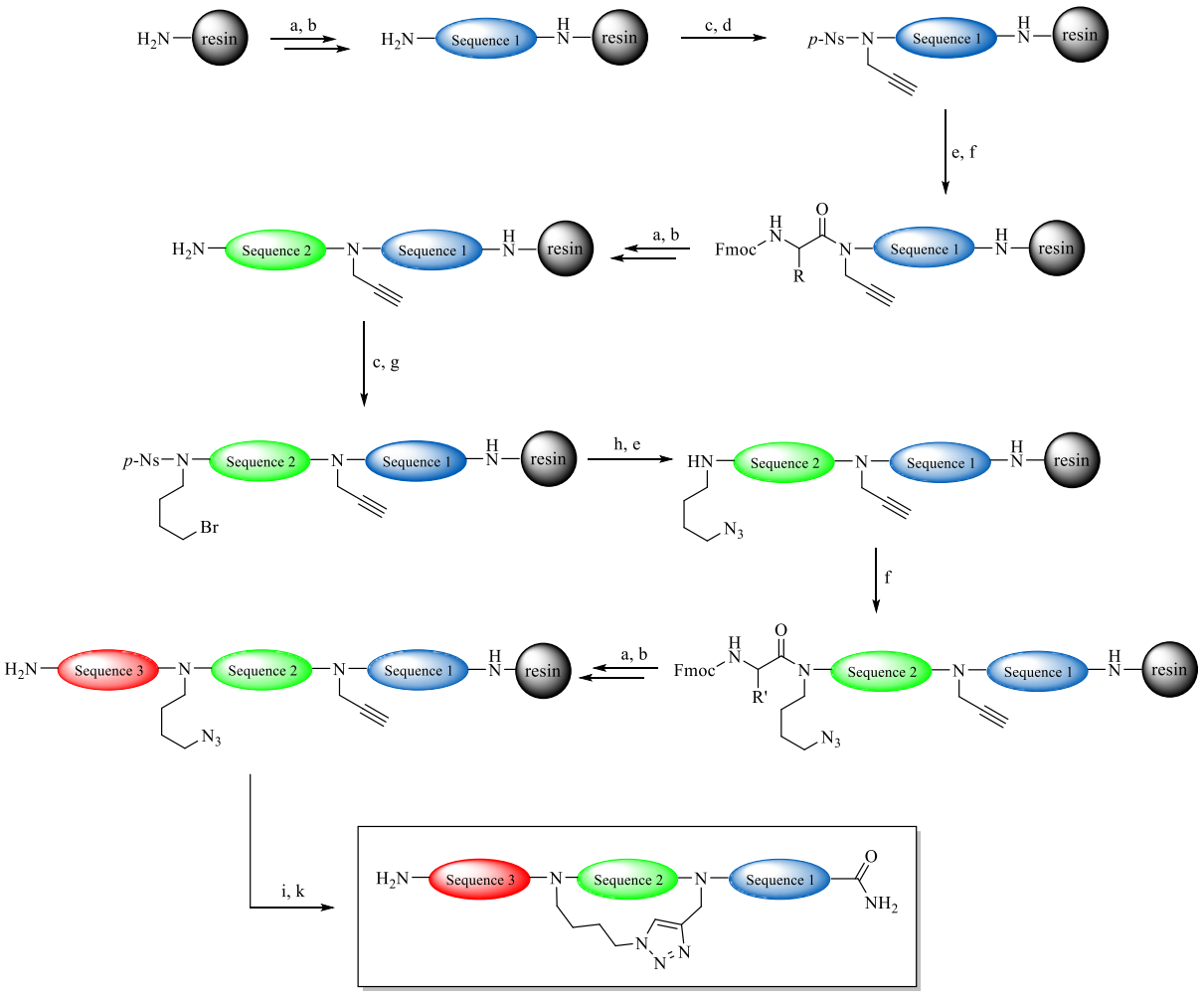

Scheme 3: Novel strategy for the general synthesis of backbone-modified cyclic BBN ligands obtained by a final *Click* reaction. a) Fmoc-X-OH (1.5 eq.), HOAt (1.5 eq.), TBTU (1.5 eq.), DIPEA (4.5 eq.), NMP, 1 h, rt; b) piperidine/NMP (*v*/*v* = 1/4), 1×5 min/1×15 min, rt; c) *p*-NsCl (5.0 eq.), 2,4,6-collidine (10.0 eq.), NMP, 30 min, rt; d) Propargyl alcohol (10.0 eq.), PPh_3 (5.0 eq.), DIAD (5.0 eq.), THF, 2×30 min, rt; e) 2-Mercaptoethanol (10.0 eq.), DBU (5.0 eq.), NMP, 2×15 min, rt; f) Fmoc-X-OH (5.0 eq.), BTC (2.0 eq.), 2,4,6-collidine (14.0 eq.), THF, 2 × 2 h, 60 °C; g) 4-Bromobutan-1-ol (10.0 eq.), PPh_3 (5.0 eq.), DIAD (5.0 eq.), THF, 2 × 2 h, rt; h) NaN_3 (5.0 eq.), DMF, 16 h, rt; i) TFA/TIPS/DCM (*v*/*v*/*v* = 95/2.5/2.5), 30 min, rt; k) $CuSO_4 \cdot 5\ H_2O$ (4.4 eq.), L-ascorbic acid (6.7 eq.), Tracepur® H_2O/^{t}BuOH (*v*/*v* = 2/1), 16 h, rt. Fmoc-X-OH = respective, Fmoc-protected amino acid.

Due to the results of the partial *N*-methyl scan (**Tab. 3**), we aimed to substitute the amide proton of the Val[10]-Gly[11] bond by an alkyne residue, as the abstraction of this proton still led to a low nanomolar

GRPR affinity. The *N*-azido alkyl group required for a *Click* reaction was inserted into the peptide backbone at several sites at the *N*-terminal side of the MJ9 sequence to generate different cycle sizes (**Fig. 14**).

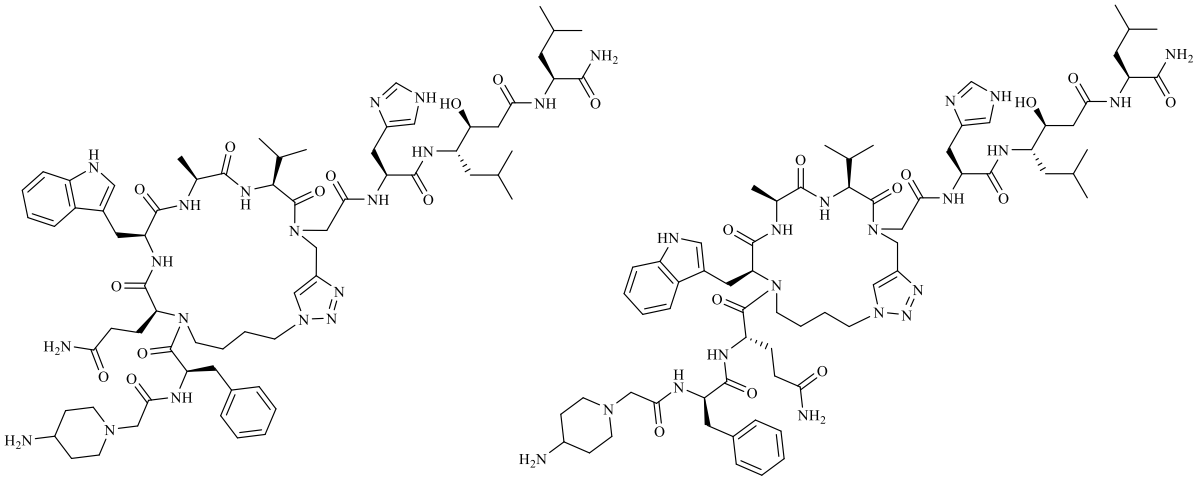

Fig. 14: Chemical structures of the cyclic GRPR-targeted ligands by *Click* chemistry: *H*-Pip-phe-cyclo[*N*(Gln-Trp-Ala-Val)]-Gly-His-Sta-Leu-NH_2 (left) and *H*-Pip-phe-Gln-cyclo[*N*(Trp-Ala-Val)]-Gly-His-Sta-Leu-NH_2 (right).

In order to achieve the desired products, the derivatives were synthesized by standard Fmoc-based SPPS up to the first alkylation step. Selective monoalkylation of the terminal amine was obtained by transient *p*-Ns protection (**Scheme 3**, c). The following alkylation with propargyl alcohol under *Fukuyama-Mitsunobu* conditions (2 × 30 min, **Scheme 3**, d) yielded conversion rates of > 85%, except for the sterically more demanding valine. In this case, another repetition of the alkylation reaction was required to generate equal conversion rates. After quantitative *p*-Ns deprotection (**Scheme 3**, e), the respective amino acid had to be activated by *bis*(trichloromethyl) carbonate (BTC) to generate highly reactive acyl chlorides (**Scheme 3**, f). This was necessary, as the activation agents (HOAt, TBTU, etc.) usually applied did not lead to successful coupling of the respective amino acids to the terminal alkyne-containing secondary amine.

Subsequently, the synthesis was continued by standard SPPS up to the second alkylation. After another *p*-Ns protection of the respective sulfonamide, the second alkylation was accomplished by coupling of 4-bromobutan-1-ol under *Mitsunobu* conditions (**Scheme 3**, g). This step was carried out with an enhanced reaction time of 2 h and was repeated once. The *N*-terminal 4-bromobutyl moiety obtained was azidated using NaN_3, which showed conversion rates of > 90% after 16 h (**Scheme 3**, h). After quantitative *p*-Ns deprotection, the following coupling step was performed using BTC as activating agent. The coupling was repeated once to obtain higher conversion rates. After finishing the sequence by SPPS, the peptide was cleaved, purified by RP-HPLC and then cyclized quantitatively by a *Click* reaction in solution (**Scheme 3**, i/k). Unlike cyclization in solution, several on-resin attempts did not yield the desired product. Successfully obtained products were determined *via* RP-HPLC using a linear gradient (25→35% MeCN in H_2O in 20 min). In general, the cyclic products exhibited retention times shorter by a magnitude of about 2 min compared to their respective linear precursors.

After purification by preparative RP-HPLC, IC_{50} values of the cyclic BBN ligands were determined as described under **II. 2.5.1**. Both compounds, *H*-Pip-phe-cyclo[*N*(Gln-Trp-Ala-Val)]-Gly-His-Sta-Leu-NH_2 as well as *H*-Pip-phe-Gln-cyclo[*N*(Trp-Ala-Val)]-Gly-His-Sta-Leu-NH_2 demonstrated IC_{50} values > 10 µM, suggesting that the cyclic structure is not capable of interacting with the receptor.

In order to eliminate potential conceptual mistakes with regard to the positions of the alkyne and *N*-azido alkyl group, these two alkylations required for *Click* chemistry were varied within the MJ9 sequence. This resulted in five additional ligands with different cycle sized, which were also evaluated in terms of GRPR affinity via IC_{50} studies (**Fig. 15**).

H-Pip-phe-cyclo[*N*(Gln-Trp-Ala-Val-Gly)]-His-Sta-Leu-NH_2

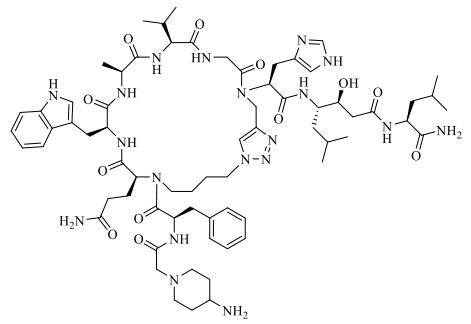

H-Pip-phe-cyclo[*N*(Gln-Trp-Ala)]-Val-Gly-His-Sta-Leu-NH_2

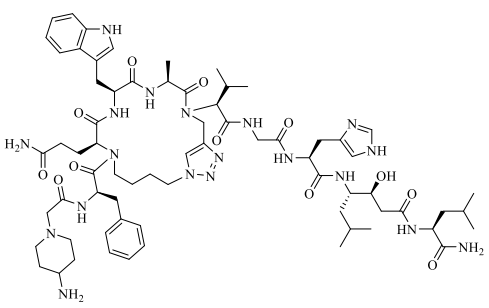

H-Pip-phe-cyclo[*N*(Gln-Trp)]-Ala-Val-Gly-His-Sta-Leu-NH_2

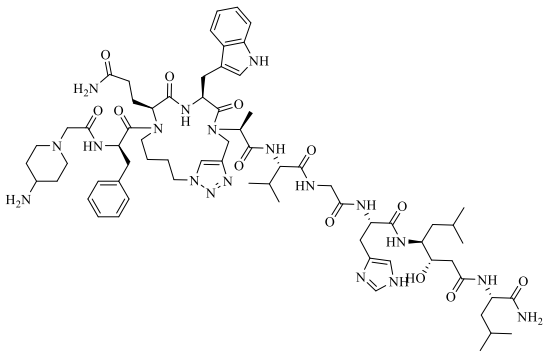

H-Pip-phe-Gln-cyclo[*N*(Trp-Ala-Val-Gly)]-His-Sta-Leu-NH_2

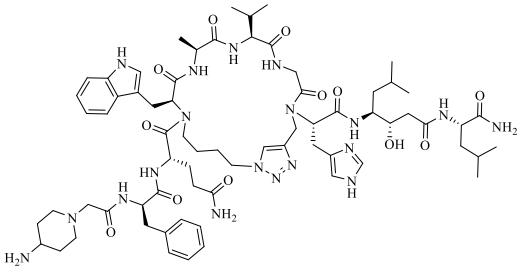

H-Pip-phe-Gln-cyclo[*N*(Trp-Ala)]-Val-Gly-His-Sta-Leu-NH_2

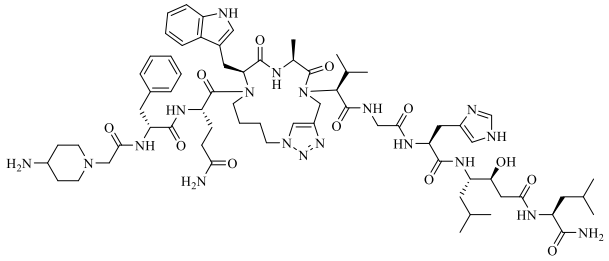

Fig. 15: Chemical structure of cyclic BBN ligands with different cycle sizes obtained by the *Click* chemistry concept.

Similar to other cyclic BBN ligand in this study, each of these five cyclic ligands revealed an IC_{50} value > 10 µM, although we did not modify the amino acid sequence but only the peptidic backbone. However, the interaction of cyclic BBN compounds within the binding pocket of the GRPR is probably impeded by its increased rigidity not allowing for high binding affinities. We thus did not continue with any cyclization approach, as high GRPR affinity is a prerequisite for successful tracer applications.

2.4. Receptor-mediated internalization studies and plasma stability *in vitro*

Within our previous studies on the MJ9 and RM2 structure, respectively (chapter **II. 2.1-II. 2.2**), we discovered only a handful of RM2 derivatives which may be superior to the established RM2 (and NeoBOMB1) due to a potential enhanced metabolic stability. Although several studies revealed that the antagonistic behavior of BBN analogs is mainly decided by the (unnatural) amino acids present at the *C*-terminus, we aimed to confirm the supposed antagonistic character of our RM2 analogs first. Therefore, we performed receptor-mediated internalization studies on PC-3 cells at 1 h as described under **II. 2.5.3**. Furthermore, comparative studies in murine and human plasma under the same conditions (37 °C, 72 ± 2 h) were executed as described in chapter **II. 2.5.4** to investigate the metabolic stability *in vitro*. For both experiments, the literature-known antagonists [^{177}Lu]RM2 and [^{177}Lu]NeoBOMB1 were used as reference compounds. All previously determined *in vitro* data of the most promising candidates DOTA-[Cit^{7}]MJ9, DOTA-[Hse^{7}]MJ9, DOTA-[Bta^{8}]MJ9, AMTG and AMTG2 as well as the reference ligands RM2 and NeoBOMB1 are given in **Tab. 5**. The radiolabeled reference used for IC_{50} studies, [3-[^{125}I]*I*-tyr^{6}]MJ9, was only analyzed in terms of receptor-mediated internalization to prove its antagonistic character, which was required for the antagonistic competition assay we developed. Neither its lipophilicity nor its metabolic stability *in vitro* was determined.

Tab. 5: *In vitro* data of the GRPR-targeted compounds. Data are expressed as mean ± SD. Affinities were determined on PC-3 cells (1.5 × 10^{5} cells/well) and [3-[^{125}I]*I*-tyr^{6}]MJ9 (c = 0.2 nM) as radiolabeled reference (2 h, rt, HBSS + 1% BSA, *v*/*v*). Receptor-mediated internalization of the ^{177}Lu-labeled compounds (0.25 pmol/well) was determined on PC-3 cells as percent [%] of the applied activity after incubation for 1 h (37 °C, DMEM/F-12 + 5% BSA (*v*/*v*), 1.5 × 10^{5} cells/well). Data is corrected for non-specific binding (10^{-3} M [^{nat}Lu]RM2). Metabolic stability *in vitro* was determined in murine and human plasma by incubation at 37 °C for 72 ± 2 h (*n* = 3). * ^{nat}Lu-labeled, ** ^{177}Lu-labeled, *** ^{125}I-labeled

GRPR ligand	IC_{50} [nM] (*n* = 3)*	log$D_{7.4}$ (*n* = 6)**	Receptor-mediated internalization [%] (*n* = 5)**	Amount of intact tracer in murine plasma (*n* = 3)**	Amount of intact tracer in human plasma (*n* = 3)**
[3-*I*-tyr^{6}]MJ9	1.3 ± 0.4	n.d.	3.57 ± 0.57***	n.d.	n.d.
RM2	3.5 ± 0.2	−2.51 ± 0.02	2.92 ± 0.20	71.2 ± 3.6%	33.5 ± 2.7%
NeoBOMB1	4.2 ± 0.1	−0.57 ± 0.03	13.91 ± 0.64	73.5 ± 3.4%	60.8 ± 1.2%
DOTA-[Cit^{7}]MJ9	11.6 ± 2.1	−3.22 ± 0.15	1.82 ± 0.16	72.9 ± 0.8%	38.3 ± 12.4%
DOTA-[Hse^{7}]MJ9	19.7 ± 1.6	−2.25 ± 0.06	1.40 ± 0.16	70.8 ± 3.5%	45.4 ± 7.6%
DOTA-[Bta^{8}]MJ9	4.6 ± 0.2	−1.81 ± 0.02	2.26 ± 0.18	58.3 ± 6.0%	16.2 ± 3.5%
DOTA-[*α*-Me-Trp^{8}]MJ9 (=AMTG)	3.0 ± 0.1	−2.28 ± 0.06	3.03 ± 0.18	75.0 ± 11.5%	77.6 ± 10.1%
DOTA-GA-[*α*-Me-Trp^{8}]MJ9 (=AMTG2)	4.7 ± 0.2	−2.51 ± 0.11	5.88 ± 0.33	80.8 ± 3.8%	64.4 ± 4.7%

Most compounds revealed comparable or lower receptor-mediated internalization values to [^{177}Lu]RM2 after incubation on PC-3 cells (1.5×10^5 cells/well) at 37 °C for 1 h, so that each of these conjugates were considered as antagonists. Not surprisingly, the radiolabeled reference for all IC_{50} studies also exhibited low receptor-mediated internalization, which further validated our developed antagonistic competition assay (**III. 1.4**). AMTG2 showed a slightly enhanced receptor-mediated internalization, which was indeed distinctly lower than the value determined for the literature-cited antagonist NeoBOMB1. For this reason, AMTG2 was also considered as an antagonist.

Metabolic stability *in vitro* for each ligand was analyzed in both, murine and human plasma *via* incubation at 37 °C for 72 ± 2 h. Subsequent to the work-up of the respective samples, radio RP-HPLC was performed to determine the remaining amount of the respective intact ^{177}Lu-labeled compound. For each conjugate, these experiments were repeated twice ($n = 3$). *In vitro* stability studies in murine plasma revealed comparable amounts of intact tracer for the ^{177}Lu-labeled compounds, with AMTG and AMTG2 showing the highest (75.0 ± 11.5% and 80.8 ± 3.8%, respectively) and DOTA-[Bta^8]MJ9 the lowest amounts (58.3 ± 6.0%).

To further evaluate whether this metabolic stability pattern is also representative of the human situation, studies on the metabolic stability *in vitro* in human plasma were also conducted under the same conditions (^{177}Lu-labeled, 37 °C, 72 ± 2 h). Interestingly, the metabolic stability pattern was noticeably different to the murine situation. High metabolic stability *in vitro* was observed for AMTG, AMTG2 and NeoBOMB1, with AMTG showing the highest intact amounts (77.6 ± 10.1%). In contrast, RM2 displayed less than half the intact amount compared to AMTG, suggesting that the Trp→*α*-Me-Trp substitution indeed has a high impact on stability, as these two compounds only differ in this one methyl group. Both, DOTA-[Cit^7]MJ9 and DOTA-[Hse^7]MJ9 exhibited slightly increased metabolic stability in human plasma compared to RM2. Similar to the murine situation, DOTA-[Bta^8]MJ9 also exhibited the lowest metabolic stability in the human plasma (16.2 ± 3.5%). This was unexpected, as we hypothesized that substitution of the Gln^7-Trp^8 dipeptide by unnatural amino acids leads to improved metabolic stability. However, as NEP is known for the cleavage at the *N*-terminal side of lipophilic amino acids, this increased metabolism was attributed to the enhanced lipophilicity of DOTA-[Bta^8]MJ9 compared to RM2 despite differing in only one atom (indole sulfur vs. nitrogen).

Exemplary RP-HPLC chromatograms of each ^{177}Lu-labeled ligand for both plasma species (murine and human) are shown in **Fig. 16-17**. Interestingly, the major metabolite present at early retention times when incubated in human plasma was not or only to a limited extent present when incubated in murine plasma. However, particularly for AMTG but also for AMTG2 and NeoBOMB1, distinctly decreased amounts of the major metabolite at early retention times were observed. We thus assume that there are significant differences in the metabolic activity of murine and human NEP, with the human NEP demonstrating accelerated metabolism rates under these conditions.

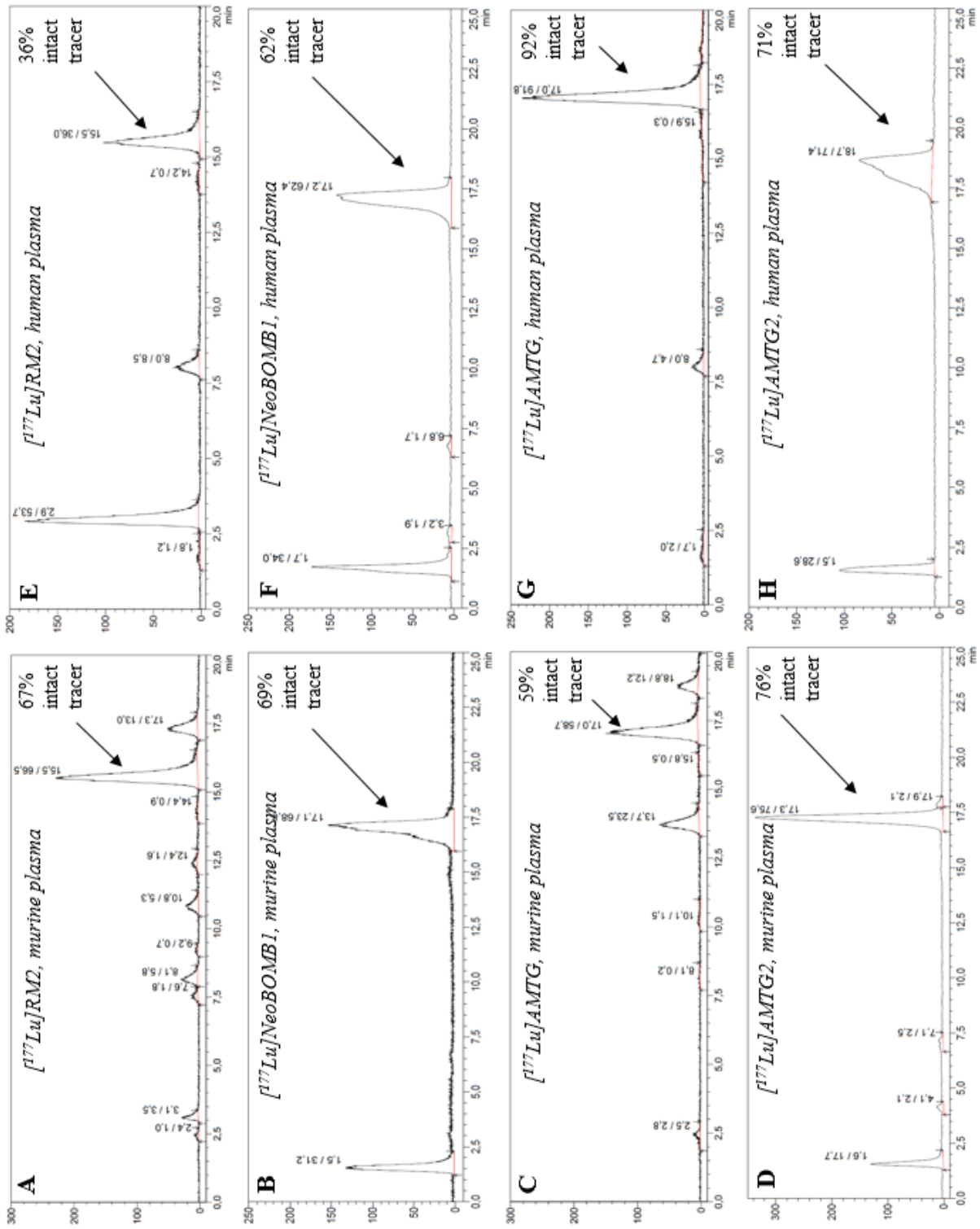

Fig. 16: Exemplary radio RP-HPLC chromatograms (20→35% MeCN in H_2O + 0.1% TFA in 20 min) of plasma samples incubated *in vitro* with [^{177}Lu]RM2, [^{177}Lu]NeoBOMB1, [^{177}Lu]AMTG and [^{177}Lu]AMTG2. Stability of **A**: [^{177}Lu]RM2 in murine plasma; **B**: [^{177}Lu]NeoBOMB1 in murine plasma; **C**: [^{177}Lu]AMTG in murine plasma; **D**: [^{177}Lu]AMTG2 in murine plasma, **A**: [^{177}Lu]RM2 in human plasma; **B**: [^{177}Lu]NeoBOMB1 in human plasma; **C**: [^{177}Lu]AMTG in human plasma; **D**: [^{177}Lu]AMTG2 in human plasma; all samples incubated at 37 °C for 72 ± 2 h. Fractions representing the intact, non-metabolized compounds are indicated by black arrows ([^{177}Lu]RM2: K' = 11.9, t_R = 15.5 min; [^{177}Lu]NeoBOMB1: K' = 10.4, t_R = 17.1 min; [^{177}Lu]AMTG: K' = 13.2, t_R = 17.0 min; [^{177}Lu]AMTG2: K' = 11.5, t_R = 18.7 min).

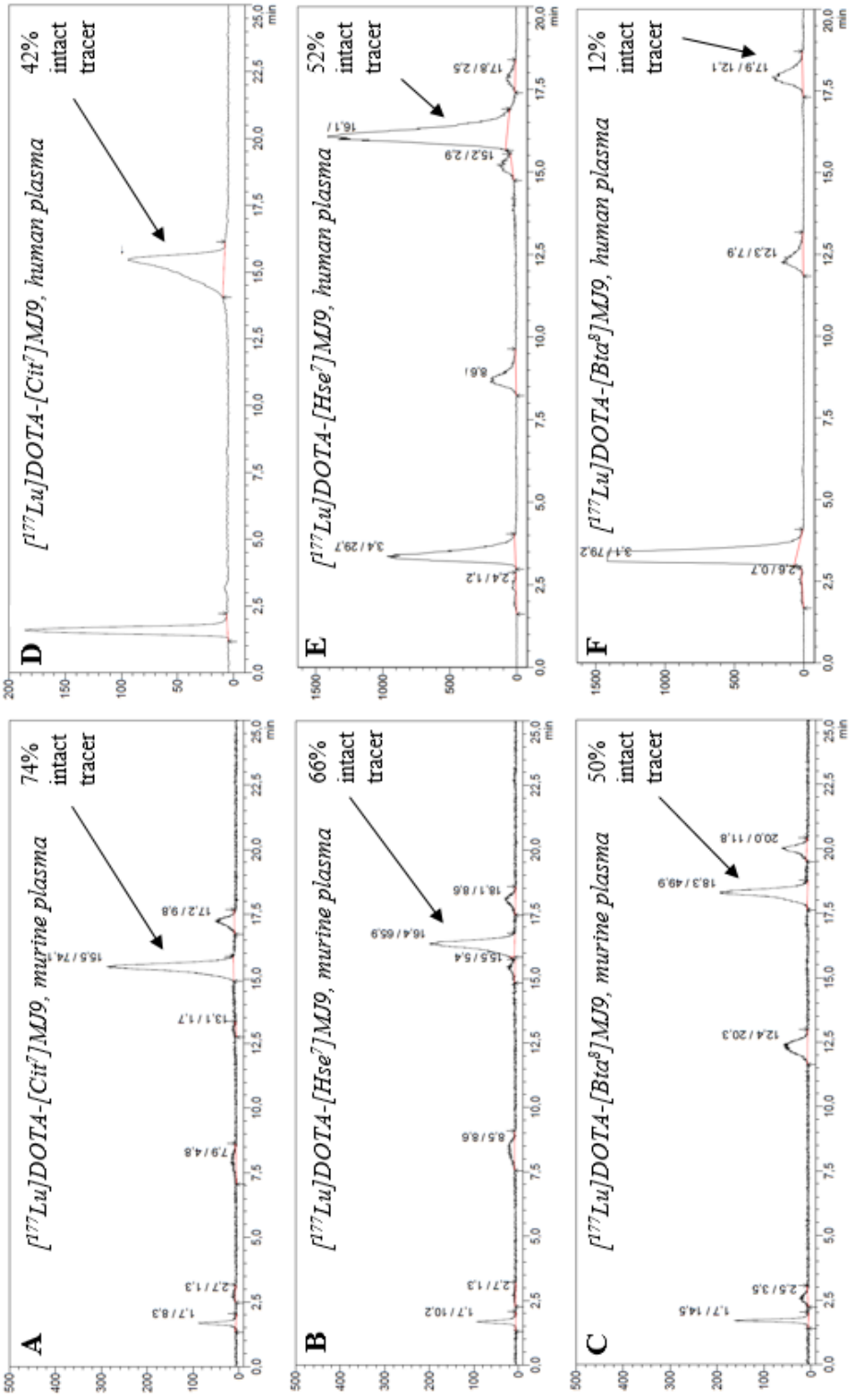

Fig. 17: Exemplary radio RP-HPLC chromatograms (20→35% MeCN in H_2O + 0.1% TFA in 20 min) of plasma samples incubated *in vitro* with [^{177}Lu]DOTA-[Cit^7]MJ9, [^{177}Lu]DOTA-[Hse^7]MJ9 or [^{177}Lu]DOTA-[Bta^8]MJ9. Stability of **A**: [^{177}Lu]DOTA-[Cit^7]MJ9 in murine plasma; **B**: [^{177}Lu]DOTA-[Hse^7]MJ9 in murine plasma; **C**: [^{177}Lu]DOTA-[Bta^8]MJ9 in murine plasma; **D**: [^{177}Lu]DOTA-[Cit^7]MJ9 in human plasma; **E**: [^{177}Lu]DOTA-[Hse^7]MJ9 in human plasma; **F**: [^{177}Lu]DOTA-[Bta^8]MJ9 in human plasma; all samples incubated at 37 °C for 72 ± 2 h. Fractions representing the intact, non-metabolized tracers are indicated by black arrows ([^{177}Lu]DOTA-[Cit^7]MJ9: K' = 9.3, t_R = 15.5 min; [^{177}Lu]DOTA-[Hse^7]MJ9: K' = 9.9, t_R = 16.4 min; [^{177}Lu]DOTA-[Bta^8]MJ9: K' = 11.2, t_R = 18.3 min).

3. Biodistribution studies

Based on the overall data determined *in vitro*, AMTG and AMTG2 seem to be promising candidates to compete with the established GRPR antagonists RM2 and NeoBOMB1, particularly due to improved metabolic stability and lipophilicity, respectively. By virtue of these encouraging overall *in vitro* data of our Gln^7-Trp^8-modified RM2 analogs, we performed biodistribution studies with each ^{177}Lu-labeled compound on PC-3 tumor-bearing mice 24 h p.i. to evaluate the effect of these modifications on the metabolic stability under *in vivo* conditions. In terms of metabolic stability *in vitro*, all modified compounds revealed enhanced stability compared to RM2 in both murine and human plasma, except for DOTA-[Bta^8]MJ9. However, this ligand was evaluated as well to examine the validity of our metabolic stability studies *in vitro*. ^{177}Lu-labeling was carried out with a precursor amount of 100 pmol of the respective ligands and 1-5 MBq of [^{177}Lu]$LuCl_3$ as described under **II. 2.4.2**. The results of the biodistribution studies are given in **Fig. 18**.

As expected, the pharmacokinetic profile of RM2 exhibited high retention in the tumor (> 8% ID/g) and low background activity 24 h p.i., especially in the GRPR-positive organs (pancreas, stomach, intestine). In contrast, NeoBOMB1 still revealed high pancreatic and slightly enhanced retention in liver, spleen, stomach, intestine, adrenals and blood. Retention of NeoBOMB1 in tumor tissue was also high but lower than that of RM2. Most of the observed background retention was expected and attributed to its increased lipophilicity compared to RM2. As expected from the comparable overall *in vitro* data, particularly the metabolic stability in murine plasma, both AMTG and AMTG2 showed similar biodistribution profiles to RM2 with high retention in the tumor and low background activity. Retention in most organs was comparable to RM2. However, AMTG revealed slightly increased hepatic retention to RM2 and AMTG2, whereas AMTG2 exhibited slightly enhanced pancreatic retention to RM2 and AMTG. On the other hand, RM2 displayed slightly increased retention in the adrenals. As the major difference of these three compounds was observed in metabolic stability in human plasma, we assume a noticeable stabilization effect in patients through the α-Me-Trp substitution, which has indeed to be evaluated in clinical studies.

The low retention of DOTA-[Bta^8]MJ9 in tumor tissue corroborated well with its metabolic stability *in vitro*, as it was the least stable compound in both murine and human plasma. Apart from that, background activity was comparable to RM2, except for a slightly increased hepatic retention. The low metabolic stability of DOTA-[Bta^8]MJ9 was anticipated due to the plasma stability data and disproved our hypothesis that substitution of either Gln^7 or Trp^8 by unnatural amino acids leads to enhanced metabolic stability as a consequence of a minor recognition by proteases. Our hypothesis was further weakened by the results of DOTA-[Cit^7]MJ9 and DOTA-[Hse^7]MJ9, respectively. Both ligands exhibited similar or increased metabolic stability in both murine and human plasma compared to RM2. However, biodistribution suggests decreased metabolic stability, showing low retention in the tumor (< 2 %ID/g 24 h p.i.), which was comparable to the retention of DOTA-[Bta^8]MJ9 in the tumor.

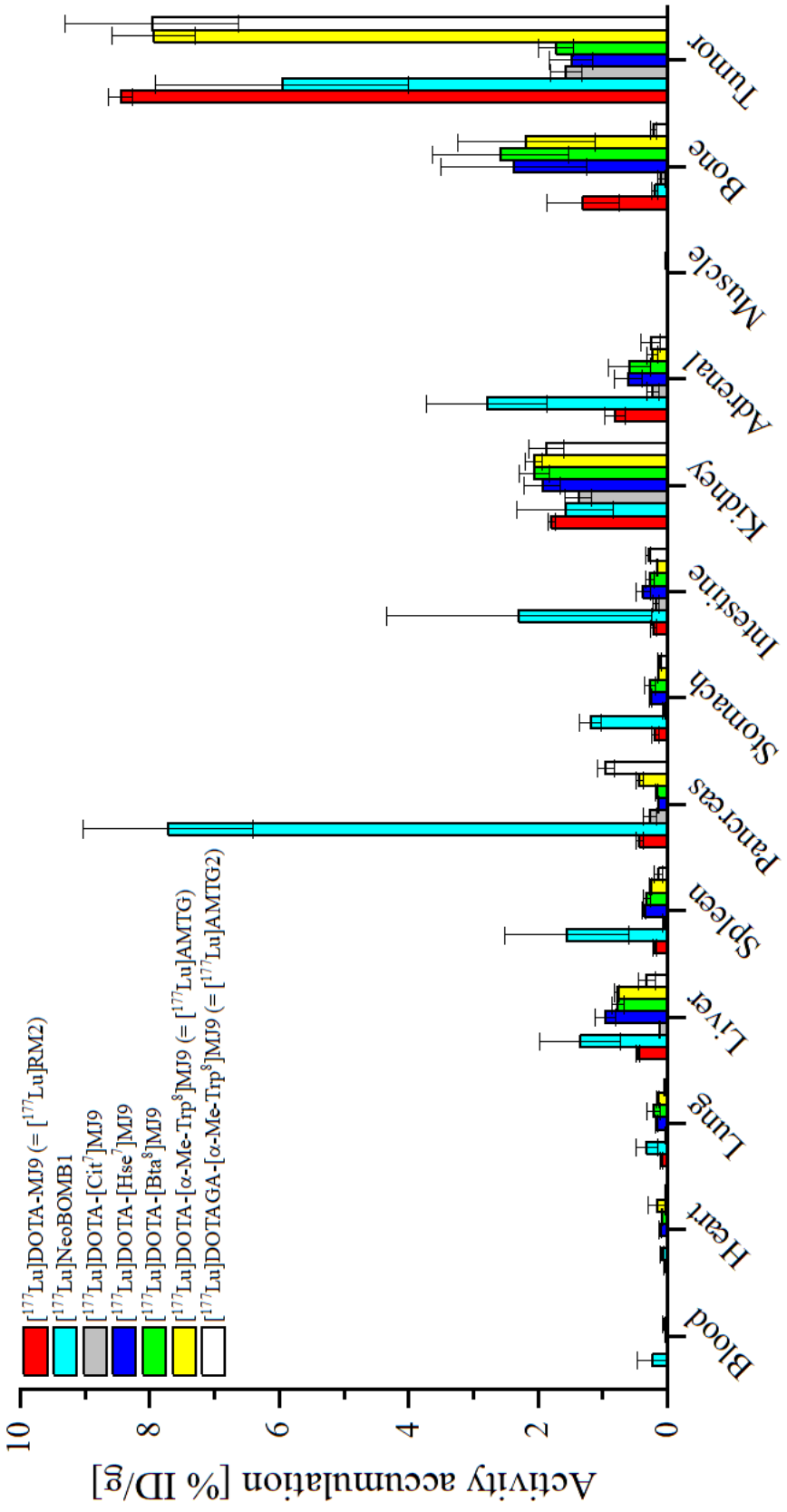

Fig. 18: Biodistribution of [^{177}Lu]RM2 (red), [^{177}Lu]NeoBOMB1 (cyan), [^{177}Lu]DOTA-[Cit^{7}]MJ9 (gray), [^{177}Lu]DOTA-[Hse^{7}]MJ9 (blue), [^{177}Lu]DOTA-[Bta^{8}]MJ9 (green), [^{177}Lu]AMTG (yellow) and [^{177}Lu]AMTG2 (white) in selected organs (in %ID/g) 24 h p.i. on PC-3 tumor-bearing CB17-SCID mice (100 pmol each). Data is expressed as mean ± SD (n = 4).

DOTA-[Hse^{7}]MJ9 exhibited comparable retention to RM2 in most organs, except for a slightly enhanced retention in liver and spleen but also slightly reduced pancreatic retention. DOTA-[Cit^{7}]MJ9 showed the lowest retention of all Gln^{7}-Trp^{8}-modified RM2 analogs in non-tumor organs, which was attributed to an enhanced clearance due to its favorable lipophilicity.

It has to be mentioned that increased bone uptake was caused by small amounts of free ^{177}Lu-lutetium within the injected solution, as ^{177}Lu-labeling for the respective compounds did not result in quantitative yields. The labeling issues were attributed to the presence of sodium ascorbate during the heating step of the ^{177}Lu-labeling, suggesting that the buffer capacity of sodium acetate (1 M, *pH* = 5.50) was not sufficient for the amount of sodium ascorbate added (0.1 M, 10 vol-%). In later labeling experiments, this issue was addressed by adding sodium ascorbate only after the heating step. Only quantitative yields for the ^{177}Lu-lutetium incorporation were determined on use of this experimental modification. As biodistribution data of NeoBOMB1, AMTG2 and DOTA-[Cit^{7}]MJ9 were collected at later times, these compounds were labeled by means of the novel concept and thus did not reveal increased bone uptake. For this reason, we are convinced that RM2, AMTG, DOTA-[Hse^{7}]MJ9 and DOTA-[Bta^{8}]MJ9 would also display low bone uptake if labeled *via* the novel concept.

Not surprisingly, tumor-to-background (T/B) ratios 24 h p.i. were generally higher for the more stable ligands such as RM2, NeoBOMB1, AMTG and AMTG2 (**Fig. 19**). Interestingly, DOTA-[Hse^{7}]MJ9 and DOTA-[Bta^{8}]MJ9 both displayed distinctly lower T/B ratios although tumor retention was only about fourfold decreased compared to RM2, AMTG and AMTG2. This also indicates a less rapid clearance from non-tumor organs. Surprisingly, DOTA-[Cit^{7}]MJ9 also revealed good T/B ratios in most organs, despite its low retention in the tumor. This was attributed to its rapid clearance kinetics and thus low background activity in non-tumor tissue. In contrast, NeoBOMB1, which displayed high retention in the tumor, exhibited noticeably lower T/B ratios to RM2, AMTG, AMTG2 and DOTA-[Cit^{7}]MJ9 for all organs, except for tumor-to-muscle ratio. We assume that the minor T/B ratios of NeoBOMB1 are caused by its high lipophilicity and thus increased accumulation and retention in non-tumor tissues.

In general, T/B ratios of both AMTG and AMTG2 were comparable or even superior to RM2. AMTG2 showed the highest T/B ratios for most organs, especially tumor-to-heart, tumor-to-lung and tumor-to-muscle ratio. However, tumor-to-blood ratio was clearly in favor of AMTG, which is a strong indicator for rapid blood clearance. This is important as enhanced blood retention was observed to lead to increased doses to the red bone marrow, which has to be taken into consideration for TRT as elevated doses to this critical organ could cause leukemia. Considering these results, overall biodistribution data and T/B ratios point to AMTG as the most promising compound of this study.

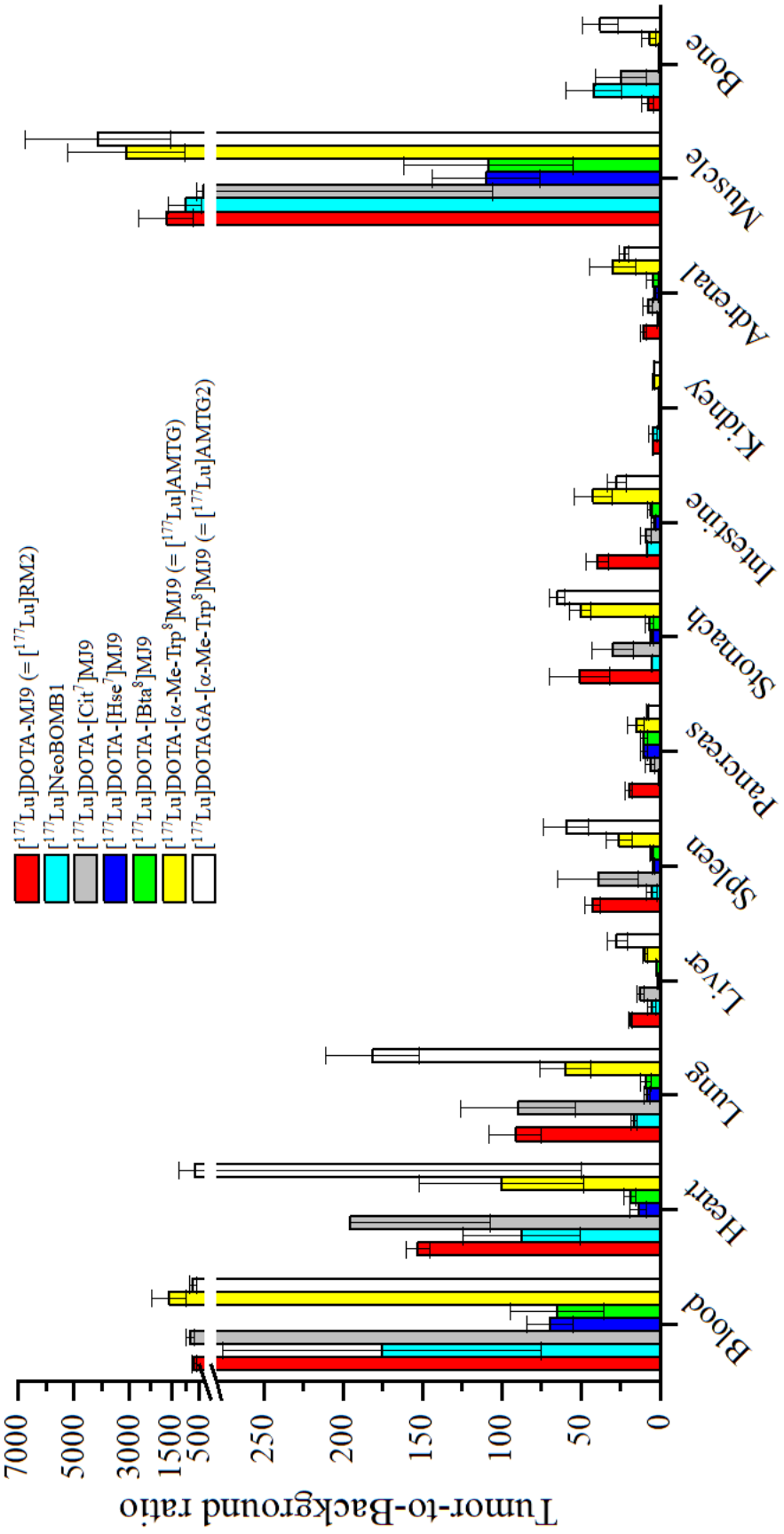

Fig. 19: Tumor-to-background ratios for the selected organs of [^{177}Lu]RM2 (red), [^{177}Lu]NeoBOMB1 (cyan), [^{177}Lu]DOTA-[Cit^{7}]MJ9 (gray), [^{177}Lu]DOTA-[Hse^{7}]MJ9 (blue), [^{177}Lu]DOTA-[Bta^{8}]MJ9 (green), [^{177}Lu]AMTG (yellow) and [^{177}Lu]AMTG2 (white) 24 h p.i. on PC-3 tumor-bearing CB17-SCID mice. Data is expressed as mean ± SD (n = 4).

By virtue of the unexpected results for the Gln^7-Trp^8-modified RM2 analogs, which did not comprise an α-Me-Trp modification in position 8 and exhibited distinctly lower tumor retention, we aimed to evaluate early pharmacokinetics of these ligands. Therefore, we additionally performed biodistribution studies 1 h p.i. with the least stable compounds (DOTA-[Hse^7]MJ9 and DOTA-[Bta^8]MJ9) as well as RM2 as a reference. All labelings were executed with a precursor amount of 100 pmol of the respective ligands and 1-5 MBq of [^{177}Lu]LuCl$_3$ and carried out as described in chapter **II. 2.4.2**. Each conjugate revealed low background activity 1 h p.i. (n = 4), except for the GRPR-positive organs such as pancreas, stomach, intestine and tumor (**Fig. 20**).

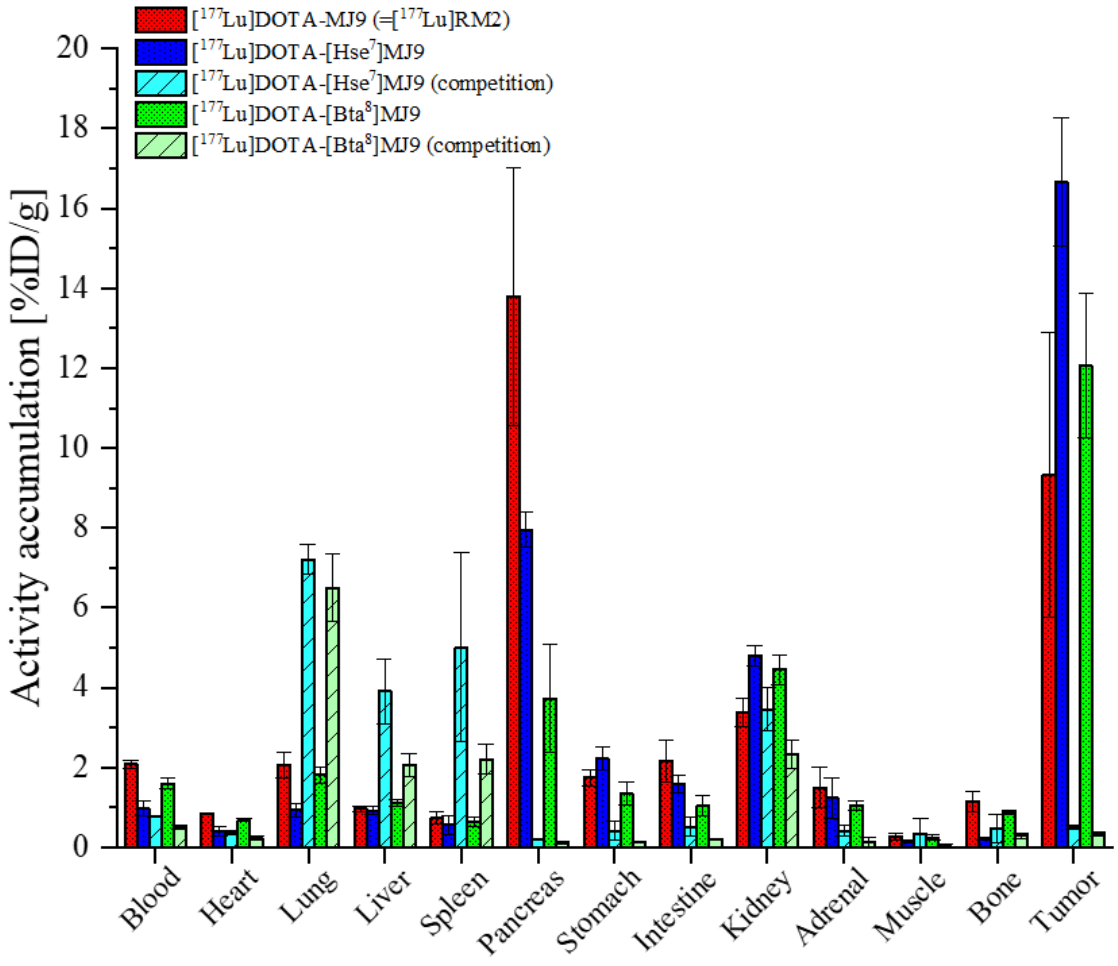

Fig. 20: Biodistribution of [^{177}Lu]RM2 (red, dotted), [^{177}Lu]DOTA-[Hse^7]MJ9 (blue, dotted) and [^{177}Lu]DOTA-[Bta^8]MJ9 (green, dotted) in selected organs (in %ID/g) 1 h p.i. on PC-3 tumor-bearing CB17-SCID mice (100 pmol each). Data is expressed as mean ± SD (n = 4). For competition studies (hatched) of [^{177}Lu]DOTA-[Hse^7]MJ9 (light blue) and [^{177}Lu]DOTA-[Bta^8]MJ9 (light green) 1 h p.i., an excess of [^{nat}Lu]RM2 (3.62 mg/kg) was co-injected. Data is expressed as mean ± SD (n = 3).

Interestingly, both modified ligands revealed higher uptake values in the tumor compared to the parent compound 1 h p.i., with DOTA-[Hse^7]MJ9 showing the highest accumulation. Both conjugates also displayed decreased accumulation in most non-tumor organs compared to RM2, especially in the pancreas. These findings point to a decreased metabolic stability but also to different metabolism rates of tumor and non-tumor organs, as tumor accumulation was not affected 1 h p.i. As a consequence of this inferior metabolic stability and the different metabolism rates, an improved biodistribution profile was

observed for the modified RM2 derivatives at early but not a later time points. This could be useful for the future design of purely diagnostic compounds.

In order to investigate whether the accumulation of both DOTA-[Hse^{7}]MJ9 and DOTA-[Bta^{8}]MJ9 (100 pmol each) observed in the GRPR-positive organs of PC-3 tumor-bearing CB17-SCID mice is specific, an excess of [^{nat}Lu]RM2 (3.62 mg/kg) was co-injected and biodistribution profiles were determined 1 h p.i. (n = 3). The competition experiments revealed that it is possible to successfully block the uptake in the GRPR-positive organs (pancreas, stomach, intestine and tumor). Surprisingly, enhanced uptake was observed in lung, liver and spleen for both modified RM2 analogs, but this was not examined further.

T/B ratios for each organ further illustrated the improved pharmacokinetics of DOTA-[Hse^{7}]MJ9 and DOTA-[Bta^{8}]MJ9 compared to RM2 1 h p.i. (**Fig. 21**). DOTA-[Hse^{7}]MJ9 showed the highest T/B ratios for most organs. However, DOTA-[Bta^{8}]MJ9 revealed slightly increased tumor-to-pancreas, tumor-to stomach and tumor-to-intestine ratios. Based on these results, both RM2 analogs can be considered as potential diagnostic tracers, which indeed has first to be evaluated with diagnostic isotopes such as ^{68}Ga-gallium.

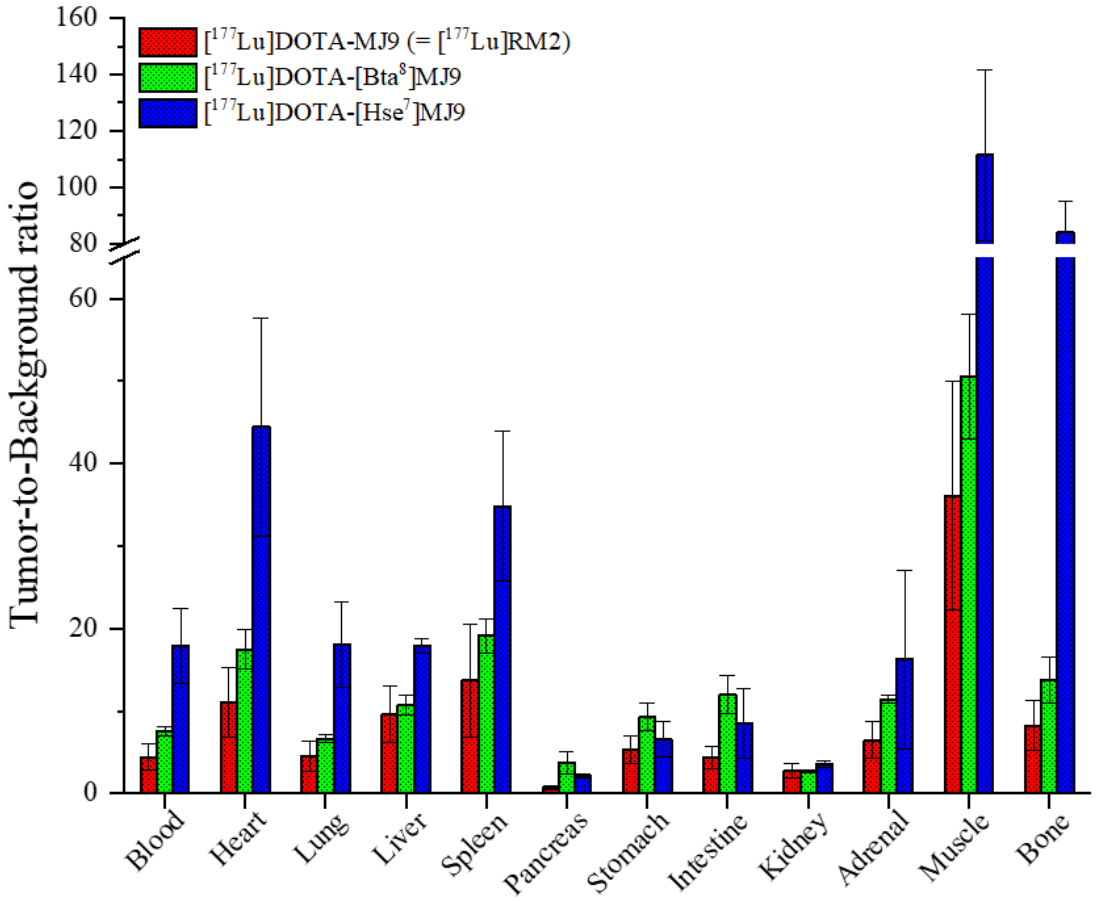

Fig. 21: Tumor-to-background ratios for the selected organs of [^{177}Lu]RM2 (red), [^{177}Lu]DOTA-[Bta^{8}]MJ9 (green) and [^{177}Lu]DOTA-[Hse^{7}]MJ9 (blue) 1 h p.i. (dotted) on PC-3 tumor-bearing CB17-SCID mice (n = 4).

In another biodistribution study the effect of *N*-terminal modifications, especially the introduction of positively charged amino acids that led to improved GRPR affinity and lipophilicity, was investigated under *in vivo* conditions. Therefore, promising RM2 analogs containing a prolonged linker unit (DOTA-Orn^3-Dap^4-MJ9, DOTA-GA-orn^3-dap^4-MJ9, DOTA-Pip^3-Pip^4-MJ9 and DOTA-orn^3-Pip^4-MJ9) as well as three third generation BBN-SiFA ligands were ^{177}Lu-labeled (1-5 MBq and 100 pmol each) and evaluated on PC-3 tumor-bearing CB17-SCID mice 24 h p.i. (n = 4) and compared to the data of RM2 (**Fig. 22**).

Similar to the parent conjugate, each RM2 analog displayed low background activity 24 h p.i. in most organs. Not surprisingly, enhanced hepatic retention was observed for the more lipophilic BBN-SiFA compounds. However, the non-SiFA-containing DOTA-Orn^3-Dap^4-MJ9 also showed increased retention in the liver, which could be due to a minor metabolic stability within the linker, as two L-amino acids (Dap, Orn) were introduced into this *N*-terminal section. This was assumed since the other three non-SiFA-containing compounds, which comprised D-amino acids instead of L-amino acids within the linker, did not show enhanced hepatic retention. DOTA-Orn^3-Dap^4-MJ9, DOTA-GA-orn^3-dap^4-MJ9 and two BBN-SiFA ligands also revealed slightly increased retention in the spleen. Bone uptake was enhanced for RM2 and DOTA-Orn^3-Dap^4-MJ9, as these two compounds were ^{177}Lu-labeled by the old concept (sodium ascorbate was present during the heating step), which did not result in quantitative yields due to the issues described above.

Major differences within this series were observed for the retention in the kidneys. Whereas RM2 and DOTA-Pip^3-Pip^4-MJ9 revealed comparably low renal retention, DOTA-Orn^3-Dap^4-MJ9, DOTA-GA-orn^3-dap^4-MJ9 and DOTA-orn^3-Pip^4-MJ9 exhibited distinctly increased retention in the kidneys (15-25 %ID/g). Astonishingly, the three BBN-SiFA ligands displayed massively elevated renal retention (> 100 %ID/g), which was not expected. Because of its stereoinversion, the attached eue (glu-urea-glu) unit should not show the typical accumulation characteristics of the well-known PSMA inhibitor motif EuE (Glu-urea-Glu), which is indeed observed to exhibit high renal accumulation and retention. For this reason, we suspect the dap(SiFA) moiety in combination with the (negatively) charged amino acids within the *N*-terminal section to be responsible for these massively increased kidney values.

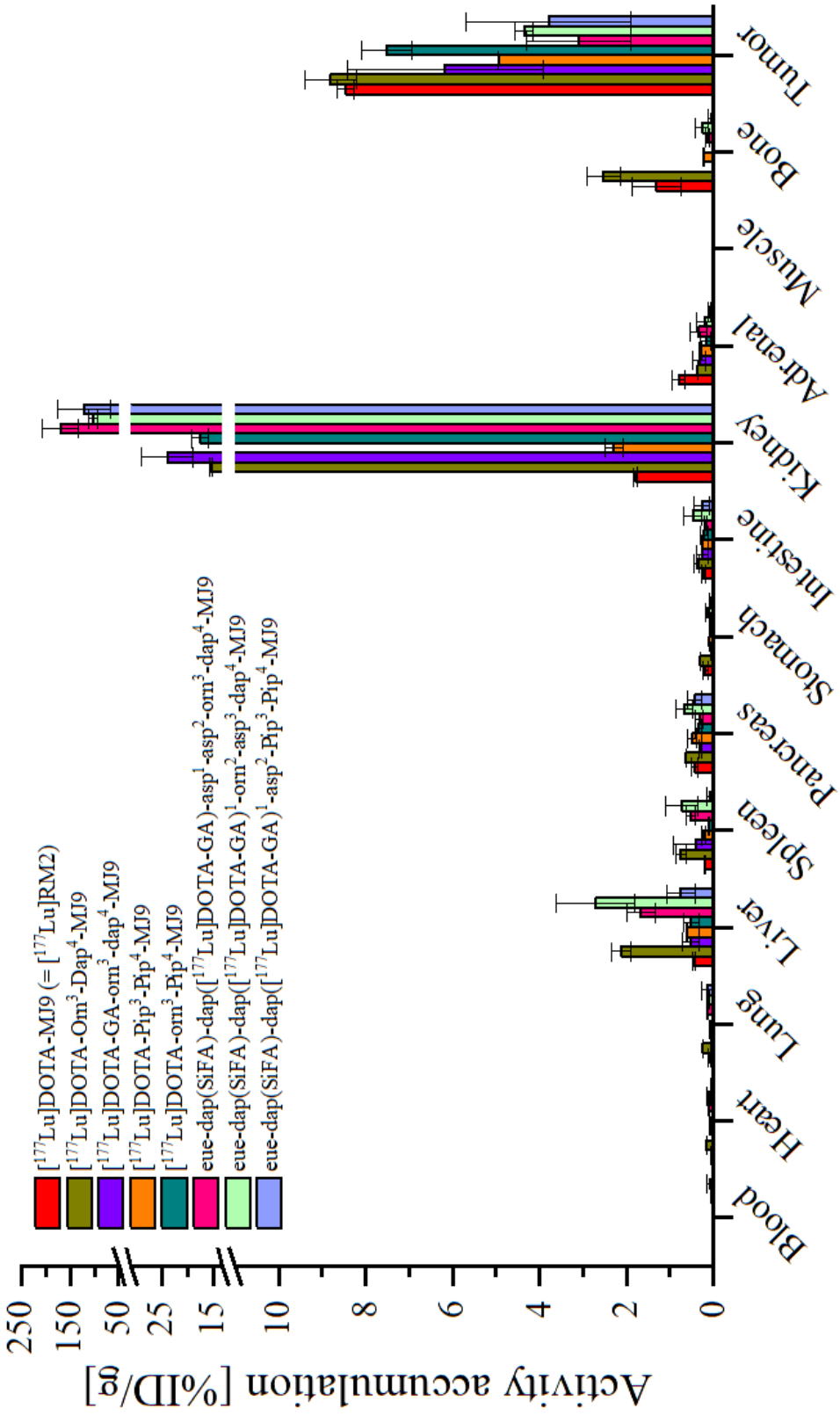

Fig. 22: Biodistribution of [^{177}Lu]RM2 (red), [^{177}Lu]DOTA-Orn^3-Dap^4-MJ9 (ocher), [^{177}Lu]DOTA-GA-orn^3-dap^4-MJ9 (purple), [^{177}Lu]DOTA-Pip^3-Pip^4-MJ9 (orange), [^{177}Lu]DOTA-orn^3-Pip^4-MJ9 (cyan green), eue-dap(SiFA)-dap([^{177}Lu]DOTA-GA)-asp^1-asp^2-orn^3-dap^4-MJ9 (magenta), eue-dap(SiFA)-dap([^{177}Lu]DOTA-GA)^1-orn^2-asp^3-dap^4-MJ9 (light green) as well as eue-dap(SiFA)-dap([^{177}Lu]DOTA-GA)^1-asp^2-Pip^3-Pip^4-MJ9 (steel blue) in selected organs (in %ID/g) 24 h p.i. on PC-3 tumor-bearing CB17-SCID mice (100 pmol each). Data is expressed as mean ± SD (n = 4).

Apart from that, noticeable differences were also discovered for the retention of the *N*-terminally modified ligands in the tumor. DOTA-Orn^3-Dap^4-MJ9 and DOTA-orn^3-Pip^4-MJ9 displayed a comparable retention in the tumor to RM2 (> 7.5 %ID/g). Both ligands suffered from elevated kidney retention, which was why none was considered a satisfactory alternative. Despite its enhanced GRPR affinity, DOTA-GA-orn^3-dap^4-MJ9 revealed slightly decreased retention in the tumor compared to these three conjugates. This was attributed to the increased renal retention, as these tracer molecules could not further participate in the blood circulation and were thus not available for potential tumor uptake. Interestingly, DOTA-Pip^3-Pip^4-MJ9, which exhibited a biodistribution pattern similar to RM2, showed distinctly decreased retention in the tumor and was thus also not considered a satisfactory alternative to the parent conjugate.

In addition to massively elevated renal retention, the three BBN-SiFA ligands also revealed the lowest retention in the tumor. Interestingly, the least affine of these three third generation compounds, eue-dap(SiFA)-dap([DOTA-GA)^1-orn^2-asp^3-dap^4-MJ9 (IC_{50} of 14.3 ± 1.5 nM, log$D_{7.4}$ of −1.96 ± 0.15), exhibited the highest retention in the tumor. For this reason, these retention patterns cannot be explained by the lack of high GRPR affinity. However, they could be also attributed to the high renal retention, which trapped most of these tracer molecules and prevented further circulation in the blood and thus tumor accumulation. We assume that a solution of the renal retention issue would also improve the retention pattern in the tumor. Based on the results of this biodistribution study, none of the BBN-SiFA compounds can be considered sufficient for clinical translation despite their improved *in vitro* data compared to first and second generation BBN-SiFA ligands, respectively.

4. *μ*SPECT/CT imaging studies

Due to the most favorable *in vitro* and *in vivo* characteristics among all RM2 analogs, [^{177}Lu]AMTG was selected for additional imaging studies *via* *μ*SPECT/CT to visualize the biodistribution pattern over time. Furthermore, [^{177}Lu]RM2 was investigated as a reference. Therefore, both compounds were ^{177}Lu-labeled as described under **II. 2.6.3** (2-4 MBq, 100 pmol each) and injected *via* the tail vein of PC-3 tumor-bearing mice (n = 1). Imaging was performed 1, 4, 8, 24 and 28 h p.i. (**Fig. 23**).

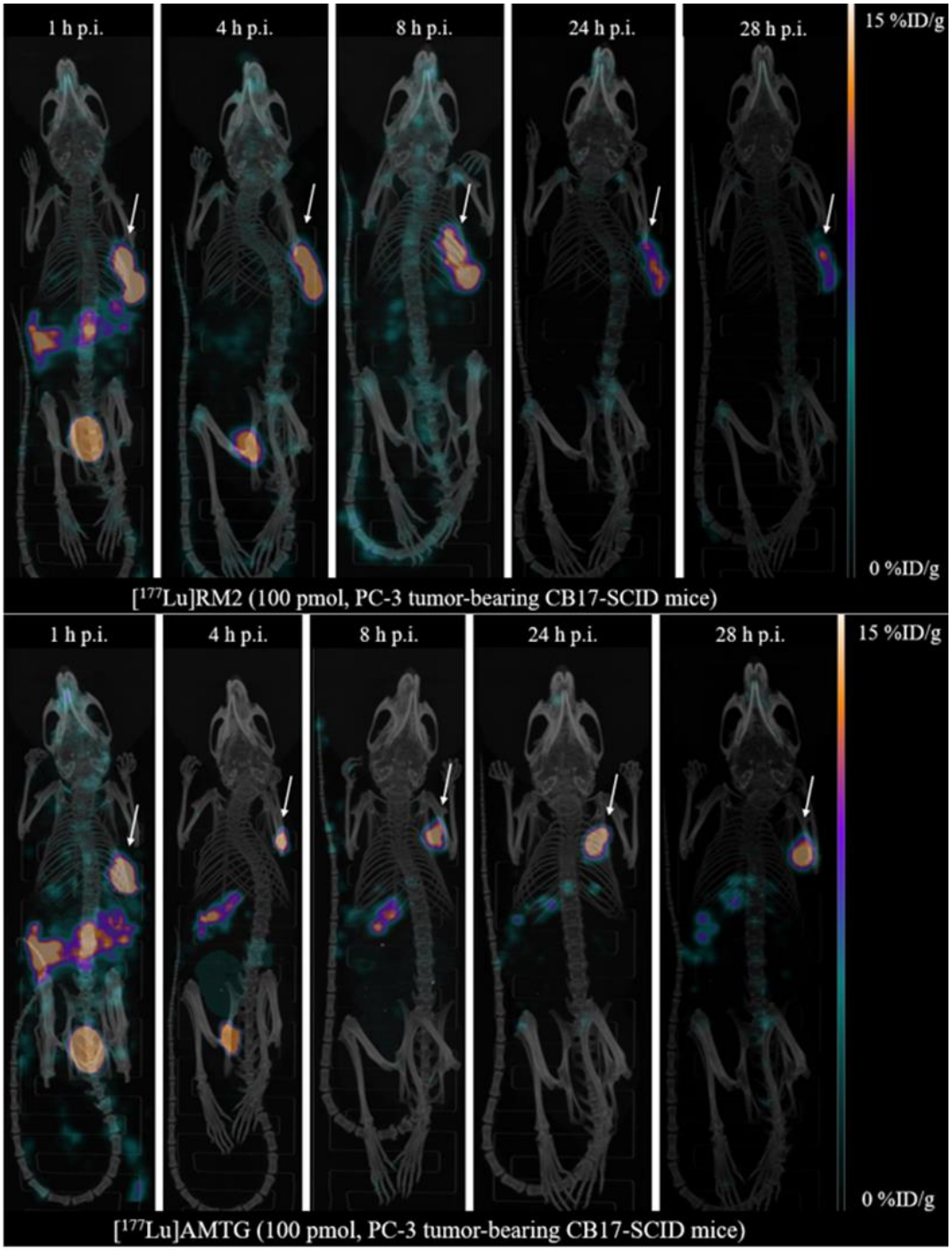

Fig. 23: Maximum intensity projection of PC-3 tumor-bearing CB17-SCID mice injected with each 100 pmol of [^{177}Lu]RM2 (top) and [^{177}Lu]AMTG (bottom). Images were acquired 1, 4, 8, 24 and 28 h p.i. PC-3 tumors are depicted by white arrows.

Both compounds revealed favorable biodistribution profiles, especially at later time points, which had already been observed in the biodistribution studies (**Fig. 18**). Uptake in GRPR-positive organs (pancreas, intestine, stomach and tumor) was high for both ligands 1 h p.i. However, RM2 did not show noticeable retention in the pancreas, stomach or intestine 4 h p.i., whereas retention in the tumor was still high. This is attributed to the metabolic instability of RM2 as well as to the different metabolism rates of tumor and non-tumor tissue. In contrast, AMTG displayed high retention in the tumor and the pancreas, most likely due to its enhanced metabolic stability. Nevertheless, clearance of pancreatic activity was mostly completed 24 h p.i., as only slight pancreatic retention was observed.

The less rapid pancreatic clearance of AMTG compared to RM2 might be a disadvantage on first glance; however, the enhanced metabolic stability was also reflected in the retention in the tumor, as AMTG showed higher retention 24 and 28 h p.i. than RM2. Interestingly, this was not observed in the biodistribution studies (**Fig. 18**), as both compounds revealed similar retention in the tumor 24 h p.i. As these imaging studies were only performed with one PC-3 tumor-bearing mouse in each, there could be differences in metabolic activity between these two mice. Apart from these potential differences, both imaging studies clearly visualized the favorable biodistribution profiles and the clearance kinetics of RM2 and AMTG over time. As AMTG revealed enhanced metabolic stability *in vitro* in human but comparable stability in murine plasma, we assume that the beneficial effects of the α-Me-Trp substitution will be more pronounced in humans. However, this has first to be evaluated in clinical studies.

In order to confirm receptor-specific accumulation, both AMTG and AMTG2 were further analyzed *via* competition experiments by co-injection of an excess of [^{nat}Lu]RM2 (3.62 mg/kg). As expected, tumor accumulation for both α-Me-Trp-modified RM2 derivatives was found to be specific, as GRPR-positive organs (pancreas, stomach, intestine and tumor) were successfully blocked (**Fig. 24**). As already observed for the competition studies with DOTA-[Hse^{7}]MJ9 and DOTA-[Bta^{8}]MJ9 1 h p.i. (**Fig. 20**), both AMTG and AMTG2 revealed slightly increased retention in lung, liver and spleen, which was not observed for the biodistribution of both compounds without added competitor.

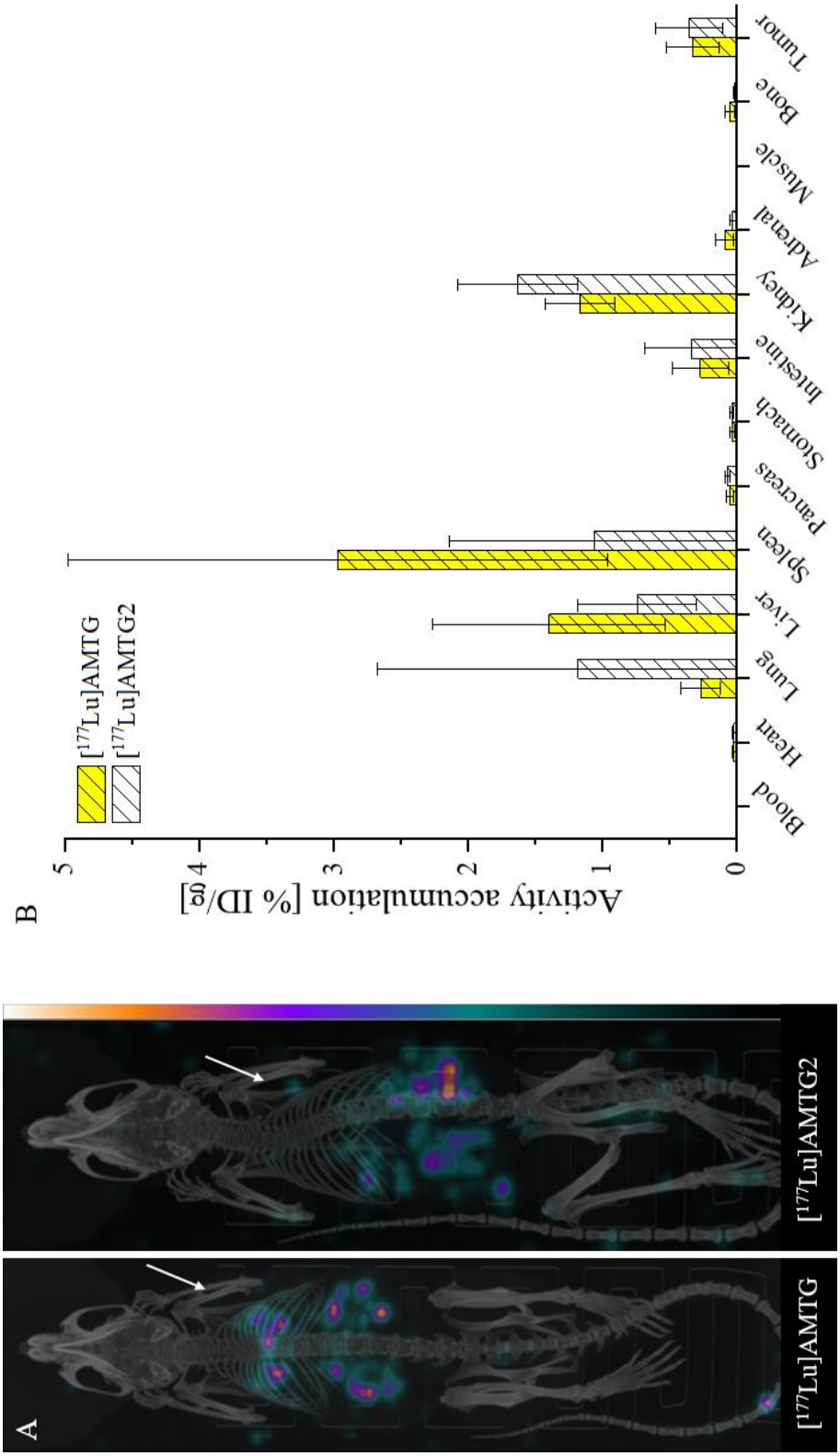

Fig. 24: **A**: Maximum intensity projection of PC-3 tumor-bearing CB17-SCID mice injected with each 100 pmol of [^{177}Lu]AMTG (left) as well as [^{177}Lu]AMTG2 (right) and co-injected with an excess of [^{nat}Lu]RM2 (3.62 mg/kg). Images were acquired 24 h p.i. PC-3 tumors are depicted by white arrows; **B**: Biodistribution of [^{177}Lu]AMTG (yellow) and [^{177}Lu]AMTG2 (white) co-injected with an excess of [^{nat}Lu]RM2 (3.62 mg/kg) in selected organs (in %ID/g) 24 h p.i. on PC-3 tumor-bearing CB17-SCID mice (100 pmol each). Data is expressed as mean ± SD (n = 3).

5. Patient studies

By virtue of its overall promising preclinical pharmacokinetic profile *in vitro* and *in vivo*, the modified RM2 analog [^{177}Lu]AMTG was selected for a PoC study in a patient suffering from metastatic castration resistant prostate cancer (mCRPC).

In preliminary labeling experiments, the amount of precursor used was studied at the *Klinikum rechts der Isar* (TU Munich, Germany). For a typical labeling approach, 25 µg AMTG (TFA salt) and 80 µg AMTG (TFA salt) were each mixed with approximately 1 GBq [^{177}Lu]$LuCl_3$ (0.04 M in HCl) and heated to 95 °C for 15 min, yielding a radiochemical purity (RCP) of 7% and 99%, respectively. Labeling with approximately 1 GBq [^{177}Lu]$LuCl_3$ (0.04 M in HCl) as well as 10 µg AMTG (AcOH salt) and 20 µg AMTG (AcOH salt) at 95 °C for 15 min resulted in a RCP of 8% and 99.9%, respectively.

In a PoC study, the distribution pattern of [^{177}Lu]AMTG was determined 1 h and 4 h p.i. in a mCRPC patient. Therefore, 1.11 GBq of [^{177}Lu]AMTG were administered and the activity uptake was visualized *via* SPECT (**Fig. 25**). Furthermore, the images obtained were compared to former SPECT (24 h p.i., 8.2 GBq of [^{177}Lu]PSMA I&T, **Fig. 26**) and PET (1 h p.i., 312 MBq of [^{18}F][^{nat}Ga]rhPSMA-7.3, **Fig. 27**) images of the same patient.

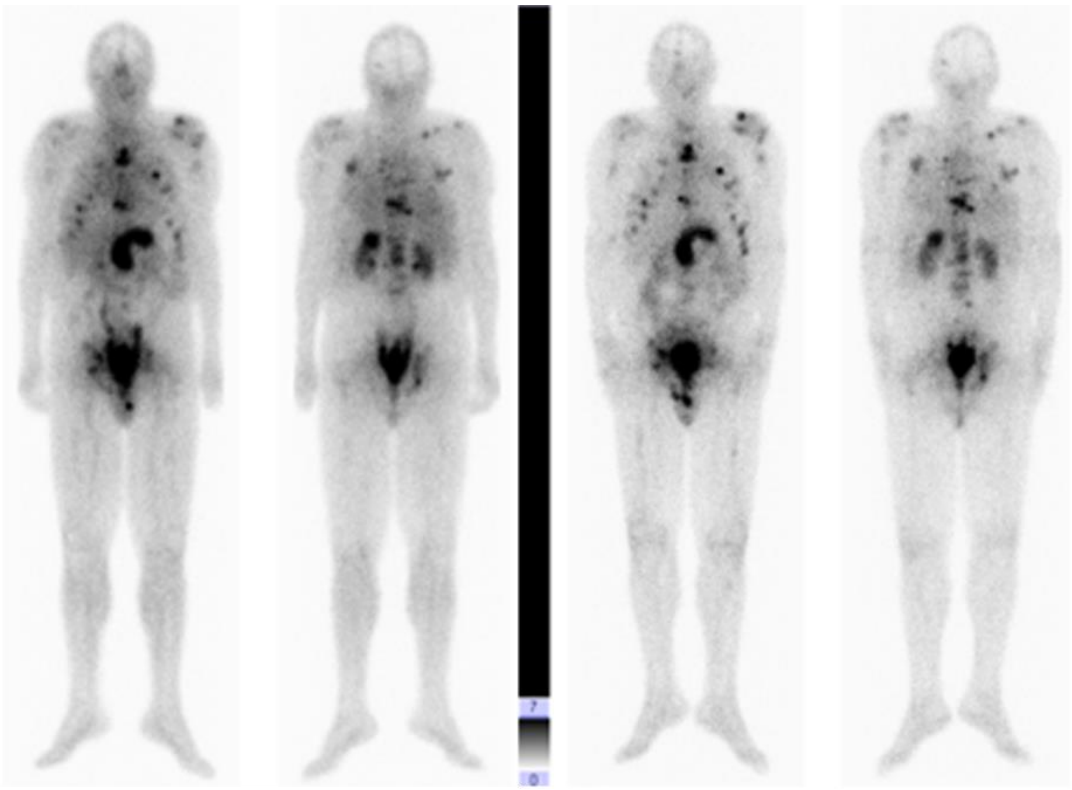

Fig. 25: Whole body scan (SPECT) of a patient suffering from mCRPC visualizing several detectable tumor lesions (1.11 GBq of [^{177}Lu]AMTG) 1 (left) and 4 h p.i. (right).

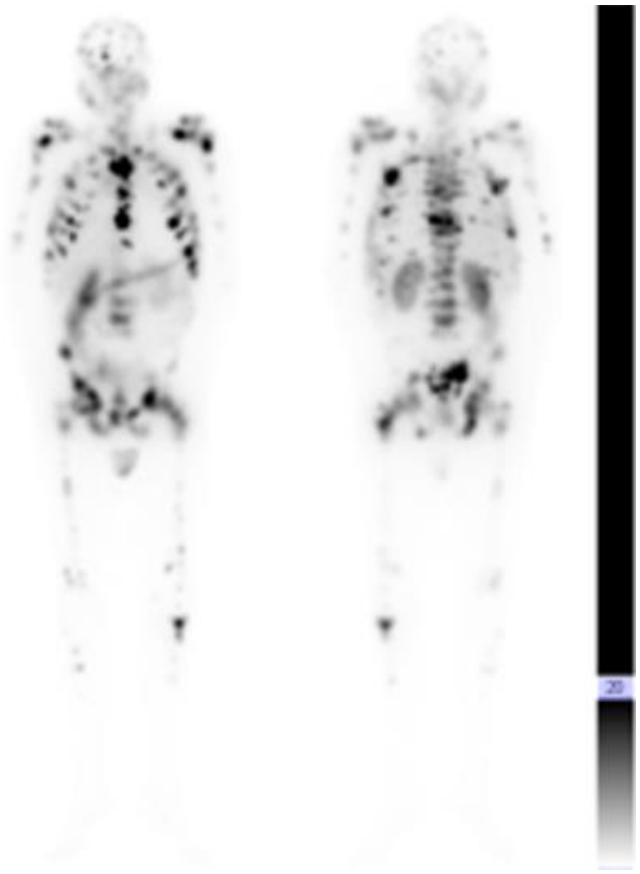

Fig. 26: Former whole body scan (SPECT) of the same subject (as depicted in **Fig. 25**) 24 h p.i. after administration of 8.2 GBq of [^{177}Lu]PSMA I&T for targeted radiotherapy (TRT).

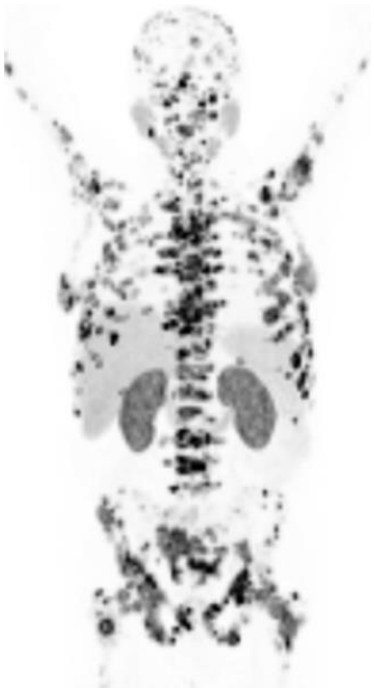

Fig. 27: Former whole body scan (PET) of the same subject (as depicted in **Fig. 25** and **Fig. 26**) demonstrating several detectable tumor lesions (312 MBq of [^{18}F][^{nat}Ga]rhPSMA-7.3) 1 h p.i.

The SPECT scan of the mCRPC patient injected with diagnostic amounts of [^{177}Lu]AMTG revealed clearly visible uptake in several tumor lesions 1 and 4 h p.i. (**Fig. 25**). Except for the GRPR-positive pancreas and the bladder, none of the background organs displayed high accumulation. Bladder uptake indicated rapid renal clearance of the tracer, which confirmed the favorable pharmacokinetics observed in preclinical studies. However, further clinical studies have to be performed to determine a potential advantage over established GRPR-targeted compounds such as RM2 or NeoBOMB1.

A comparison of the images obtained with former SPECT and PET scans of the same patient using PSMA-based tracers ([^{177}Lu]PSMA I&T 24 h p.i. [**Fig. 26**] and [^{18}F][^{nat}Ga]rhPSMA-7.3 [**Fig. 27**] 1 h p.i.) highlighted noticeably enhanced uptake in all tumor lesions as well as an increased number of lesions in contrast to our GRPR-targeted ligand. This was attributed to the advanced disease stage of this patient, as high PSMA expression on PCa cells was found especially in metastatic disease. As expected, enhanced retention of [^{177}Lu]PSMA I&T 24 h p.i. in normal organs was found for PSMA-positive tissues such as spleen, kidneys and duodenum. Accumulation of the diagnostic compound [^{18}F][^{nat}Ga]rhPSMA-7.3 was visualized in the salivary glands, liver, spleen, kidneys and several tumor lesions 1 h p.i.

Despite its inferior performance in an mCRPC patient compared to established PSMA inhibitors, AMTG showed promising PoC data. A comparison of PSMA inhibitors and GRPR-targeted compounds is strongly dependent on the disease stage of the patient. It was shown that GRPR expression is high on primary tumors but decreased in metastatic disease, whereas PSMA expression generally reveals the opposite behavior. Therefore, further studies with AMTG have to be carried out in more appropriate patients (primary PCa, PSMA-negative PCa) in order to define its value for nuclear medicine. Moreover, a direct comparison to other GRPR-addressing ligands such as RM2 and NeoBOMB1 would be desirable.

IV. Discussion

In the search for improved treatments for PCa and BCa, GRPR-targeted compounds have emerged as an attractive option in recent years, as GRPR is overexpressed on both PCa cells and BCa cells in high density, especially in early disease stages (primary PCa/BCa). Numerous BBN-based ligands revealed promising preclinical as well as clinical results (RM2, NeoBOMB1). Whereas NeoBOMB1 exhibited unfavorable blood clearance due to its increased lipophilicity, RM2 suffers from low metabolic stability *in vivo*, as BBN analogs are reportedly degraded enzymatically, particularly at the Gln^7-Trp^8 site within the pharmacophore. Hence, we aimed to address this issue by several approaches (cyclization, substitution by hydrophilic or unnatural amino acids) as we hypothesized that an enhanced metabolic stability would increase tumor retention and thus lead to improved treatment outcomes *via* TRT. We therefore investigated the effect of certain modifications on GRPR affinity, as we suggest that high affinity is a prerequisite for molecular imaging or TRT. In order to do so, we first had to establish a valid competition assay.

Development of a cell-based assay for GRPR-targeted compounds

All uptake and competition studies in this work were carried out on PC-3 cells, which overexpress GRPR in high density. As most groups use [3-[^{125}I]*I*-Tyr^4]BBN as radiolabeled reference, we wanted to use this compound as well. Radioiodination in *ortho* position to the hydroxyl group of tyrosyl residues was accomplished by means of the Iodo-Gen® method. Due to the excess of the respective precursor used, 3,5-disubstitutions were not observed. However, ^{125}I-iodination of [Tyr^4]BBN did not yield the desired product. We suggest that the oxidative conditions of the Iodo-Gen® method were not compatible with the easily oxidized methionine residue within the precursor sequence. We thus decided to implement another literature-cited BBN agonist as a radiolabeled reference, [3-[^{125}I]*I*-tyr^6, β-Ala^{11}, Phe^{13}, Nle^{14}]BBN_{6-14}, also called *Universal Ligand* (UL) due to its ability to effectively bind to all four receptors of the BBN family[188]. Due to its enhanced stability towards oxidation, ^{125}I-iodination by means of the Iodo-Gen® method could be carried out with good RCYs (22-32%).

First cellular uptake studies with an increased cell number (2.0×10^5 cells/well) revealed distinct differences in cellular uptake of [3-[^{125}I]*I*-tyr^6, β-Ala^{11}, Phe^{13}, Nle^{14}]BBN_{6-14} when incubated for 2.5 h. Whereas uptake was only about 2-3% on ice, it was up to 10% at rt. This was attributed to the slower accumulation kinetics of the tracer at the receptor at lower temperatures. Indeed, *Reile et al.* showed that specific binding of the agonistic [3-[^{125}I]*I*-Tyr^4]BBN towards GRPR was saturable as well as time- and temperature-dependent, as maximal cellular binding was reached at 6 h, 60-90 min and 30-40 min at 4 °C, rt and 37 °C, respectively[189]. As we observed a decline in cellular uptake of [3-[^{125}I]*I*-tyr^6, β-Ala^{11}, Phe^{13}, Nle^{14}]BBN_{6-14} depending on the day of the experiment, we attributed this radiolytic degradation issues. Indeed, *de Blois et al.* and *Salako et al.* determined the importance of stabilization of the radiolabeled reference towards radiolysis[185, 190]. As expected, the addition of ascorbic acid (0.1 M, 10 vol-%)

noticeably increased radiolytic stability, as > 95% of the compound was still intact four weeks after radiosynthesis. This concomitantly led to an increased cellular uptake of 20-25%, which confirmed the necessity of radiolytic stabilization. We suggest that prior to this stabilization, vast amounts of the radiolabeled reference were not intact and thus resulted in only ~10% overall uptake.

First IC_{50} studies (**Tab. 1**) exhibited moderate GRPR affinity for BBN and [phe^{6}, β-Ala^{11}, Phe^{13}, Nle^{14}]BBN$_{6-14}$, which is less affine than reported by other groups[103, 104]. Evaluation of the antagonistic MJ9 within this assay did not yield a definite IC_{50} value (0.002 ± 0.000 nM and 33.2 ± 1.6 nM, respectively, depending on the day of the experiment). This was attributed to undefined fractions of [3-[^{125}I]*I*-tyr^{6}, β-Ala^{11}, Phe^{13}, Nle^{14}]BBN$_{6-14}$ that internalized over the course of 2 h (incubation time) at rt and were thus not available for the competition against MJ9. As agonists are able to internalize at increased temperatures[189]. *Reile et al.* demonstrated increasing internalization rates for [3-[^{125}I]*I*-Tyr^{4}]BBN with enhanced temperature, which is why why competition studies with agonists are usually performed on ice[189]. However, as we already observed slow uptake kinetics on ice, we wanted to maintain the temperature at rt.

As only antagonists were to be be investigated in this study, [3-[^{125}I]*I*-tyr^{6}]MJ9, which revealed high GRPR affinity (IC_{50} of [3-*I*-tyr^{6}]MJ9: 1.3 ± 0.4 nM) and antagonistic properties (receptor-mediated internalization: 3.57 ± 0.57%), was introduced as a radiolabeled reference. Ascorbic acid had to be added immediately after labeling to increase the stability of [3-[^{125}I]*I*-tyr^{6}]MJ9 to over 6 weeks (instead of 2-3 days without any quencher). As shown in various uptake studies, maximum cellular uptake of the agonistic radiolabeled reference did not exceed 25%. However, the novel antagonistic radiolabeled reference usually showed > 50% cellular uptake without added competitor. Similar observations were reported by *Cescato et al.*[112]. Antagonists are reported to bind to a higher number of receptor binding sites compared to agonists, as they are also able to bind to inactive receptors (non-G protein-coupled state)[34, 111].

As expected, indefinite IC_{50} values were not observed over the course of this study when evaluating antagonists within the antagonistic competition assay developed. However, IC_{50} values of agonists such as [Tyr^{4}]BBN were indeed distinctly different depending on the day of the experiment (0.61 ± 0.05 nM and 42.9 ± 2.3 nM, respectively). We thus suggest that antagonists will not compete against agonists when the assay is carried out at rt to avoid such IC_{50} issues. Both MJ9 and the modified precursor ([tyr^{6}]MJ9) displayed IC_{50} values in the high picomolar and low nanomolar range, which is in accordance with similar GRPR antagonists reported by other groups[112, 179]. As the cold standard ([3-*I*-tyr^{6}]MJ9) displayed high affinity towards GRPR (1.33 ± 0.36 nM), the radiolabeled reference could be considered as very potent itself. IC_{50} values determined by this assay were thus considered as valid, as novel GRPR-targeted ligands had to compete against this highly affine radiolabeled reference.

Linear MJ9 derivatives

Metabolic stabilization by substitution of amino acids within the pharmacophore of BBN-based compounds (Gln^{7}-Trp^{8}-Ala^{9}-Val^{10}-Gly^{11}-His^{12}) is often avoided as many modifications were shown to negatively affect overall pharmacokinetics, particularly GRPR affinity. Indeed, successful substitutions within the pharmacophore of BBN-based ligands are not described frequently[105, 106]. For this reason, many groups prefer to address these issues indirectly by co-injection of NEP inhibitors such as Phosphoramidon (PA)[94, 129, 180]. Although a few NEP inhibitors are approved, (long-term) effects of such inhibitors on cancer patients still need to be investigated. Moreover, as metabolism and thus the effect of the inhibitor on the metabolic stability of the respective compound is different from men to men, we assume that consistent TRT would be difficult. In order to circumvent this uncertainty for potential clinical use, we concentrated on increasing metabolic stability chemically by various substitutions, particularly at the Gln^{7}-Trp^{8} site. In order to get some insight into the tolerability of GRPR towards modifications within the MJ9 sequence, an alanine substitution scan was performed first. This technique was implemented for several different compounds throughout multiple fields of pharmacology[191-194]. As the small side-chain methyl group of alanine has been shown not to participate noticeably in ligand-receptor interactions, substitution by alanine may prevent the side-chain interaction of the respective substituted amino acid.

Substitution by alanine at the *N*-terminus (Pip, phe) was tolerated well by GRPR (**Tab. 3**). This was expected, as several BBN analogs that contain a different *N*-terminal design exhibited high GRPR affinity[112, 123, 138, 173, 195]. Introduction of Pip^{5} and phe^{6} was reported to increase GRPR affinity due to its positive charge and metabolic stability, respectively[39, 196]. Nevertheless, both modifications are not necessary for high GRPR affinity, as shown by various GRPR-addressing ligands[121, 197, 198]. Substitution of amino acids within the pharmacophore (Gln-Trp-Ala-Val-Gly-His) had a drastic effect on GRPR affinity, with substitution of either Trp^{8} or Gly^{11} resulting in the highest IC_{50} values. Stabilization of the helical arrangement of BBN-based compounds inside GRPR *via* π-π stacking interactions between Trp^{8} and His^{12} was reported[37]. Substitution of Trp was thus expected to decrease GRPR affinity.

Substitution of Gly by Ala/ala led to a distinct decrease in GRPR affinity, which was unexpected, as there are BBN derivatives containing ala instead of the Gly that still display high GRPR affinity (**Tab. 3**)[101, 129]. Several groups described BBN analogs that were substituted at the Gly site by β-Ala, which was not considered an appropriate option within our group, as β-amino acids at this position decrease selectivity towards BRS-3[90, 104, 108, 199, 200]. To the best of our knowledge there are no high-affinity Sta^{13}-based BBN analogs reported, which comprise an amino acid with stereoinformation in position 11[40]. We thus suggest that the design of the *C*-terminus of BBN-based compounds has a distinct effect on the Gly site, which has to be considered for future studies.

C-terminal substitution also reduced GRPR affinity noticeably, which was expected as the unnatural amino acid Sta is important for antagonistic behavior in statine-based BBN analogs (**Tab. 3**). Interestingly, substitution of Leu^{14} by more hydrophilic amino acids (Orn, Ser, Thr, His, Hse) also resulted in noticeably decreased GRPR affinity. We thus assume that more lipophilic or spatial demanding side chains such as leucine are favored at this site, why *C*-terminal modifications were not further considered. It is worth mentioning that alternative designs to Sta-based BBN analogs at the *C*-terminus are reported that display high GRPR affinity[41, 94, 138]. However, these were not considered in this work as we aimed to improve Sta-based GRPR antagonists.

A partial *N*-methyl scan performed to analyze the effect of the deletion of proton donor atoms for hydrogen bonding interactions due to backbone methylations within the tripeptidic Val^{10}-Gly^{11}-His^{12} section revealed that only the methylation of the amidic nitrogen atom of the Gly-Val dipeptide maintains high GRPR affinity (**Tab. 3**). This was also observed by other groups for various BBN analogs[191, 197]. Hence, this amidic proton does not seem to be involved in the stabilization of the secondary structure *via* hydrogen bonding. A similar scan experiment by *Coy et al.*, in which peptide bonds were reduced to the corresponding amines, exhibited a distinct loss of GRPR affinity for most of the BBN derivatives examined. The authors also suggested that this is caused by destabilization of the secondary structure of the respective ligands due to the absence of hydrogen bonding[43]. We thus assume that potential backbone modifications are only tolerated at the amidic nitrogen atom of the Gly-Val bond.

Further substitutions by other amino acids within the MJ9 sequence confirmed the highly conserved nature of the pharmacophore of BBN analogs. Except for substitution of Pip^5 by the structurally similar tranexamic acid (Txa), each modified MJ9 derivative exhibited decreased GRPR affinity (**Tab. 3**). Substitution of phe by other aromatic residues (tyr, nal, (4-NH_2)Phe), a positively charged D/-L-arginine or a neutral D/-L-citrulline resulted in slightly decreased, but still high GRPR affinity. However, as phe was reported to increase metabolic stability and we only aimed to substitute it to improve lipophilicity without loss of GRPR affinity, none of the substitutions performed were considered beneficial.

As expected, substitution of amino acids within the pharmacophore (Gln-Trp-Ala-Val-Gly-His) resulted mostly in noticeably decreased GRPR affinity, which is why most of the substitutions performed were not considered appropriate alternatives for the respective sites (**Tab. 3**). In case of the critical Gln^7-Trp^8 site, introduction of the neutral Hse at position 7 as well as substitution of Trp by the structurally very similar *β*-(3-benzothienyl)alanine (Bta) only exhibited slightly decreased GRPR affinity for either modification. Due to the great importance of metabolic stabilization at this site, Hse and Bta were thus considered to be effective alternatives to Gln and Trp, respectively. *Nock et al.* reported ^{99m}Tc-labeled ligands containing either gln^7 or Gln^7, both exhibiting similar GRPR affinity[40]. In addition, there are reports of BBN analogs comprising His instead of Gln^7, which is derived from the mammalian GRP[107, 121]. However, these options were not considered in this study.

Substitution of Ala by the small, neutral Ser revealed only slightly decreased GRPR affinity, whereas substitution by the positively charged Dap or prolonged Hse led to decreased affinity (**Tab. 3**). Stereoinversion of this site introducing ala or ser resulted in a massively decreased GRPR affinity. As the pharmacophore is reported to form a helix-like arrangement inside GRPR, this loss of affinity was expected[37]. Similarly, *Prasad et al.* reported three derivatives containing an α-amino-isobutyric acid (Aib) moiety at the alanine position, which did not show GRPR affinity[201]. Substitution of Val[10] while maintaining high affinity could only be accomplished when the structurally restrained amino acids cyclohexyl (Chg) and cyclopentyl glycine (Cpg) were introduced. However, as both amino acids were unnatural, we assumed there would be a positive effect on metabolic stability, which is why both Chg and Cpg were considered potential alternatives to Val. As π-π stacking interactions were reported for Trp[8] and His[12], His was substituted by aromatic (β-(1,2,3-triazolyl) alanine = Tza, (4-NH_2)Phe) amino acids, which resulted in a distinct decrease of GRPR affinity. We thus suggest that an exact histidine mimic is necessary to maintain high GRPR affinity.

In terms of the applied multisubstitutions, an overall trend could be observed, as modifications at the *N*-terminus were tolerated best. Nevertheless, most multisubstituted MJ9 analogs displayed distinctly decreased GRPR affinity and were thus not considered sufficient for further studies (**Tab. 3**). Those showing a low nanomolar IC_{50} value were also not assessed positively as the *N*-terminal amino acids were not shown to be critical for metabolic degradation. However, the truncated [*des*Pip[5], arg[6]]MJ9, which revealed a ninefold lower IC_{50} value than its Pip-containing analog ([arg[6]]MJ9) and a similar IC_{50} value to MJ9, was selected for further optimizations.

As already observed for various monosubstitutions, multisubstitutions within the pharmacophore had a noticeably negative impact on GRPR affinity (**Tab. 3**). We suggest that these modifications impeded the helix-like arrangement, which is preferred inside GRPR. As a metabolic instability was reported for the Val[10]-Gly[11] site and the amidic proton of this bond was shown to not participate in hydrogen bonding, we aimed to substitute this dipeptide by comparable structural motifs (**Fig. 28**).

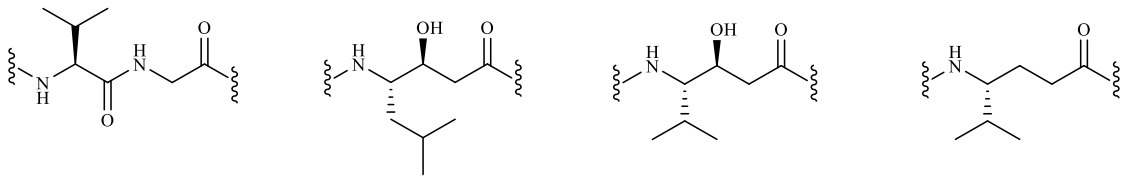

Fig. 28: Molecular structure of the dipeptidic Val-Gly unit (left) of natural BBN-based ligands as well as the examined modifications Sta (second from the left), Valyl-Sta (second from the right) and γ-Val (right).

However, each approach resulted in a distinct loss of GRPR affinity (**Tab. 3**). Despite containing a similar structure as the Val-Gly dipeptide, none of the three unnatural amino acids comprised an exact backbone length, as more suitable unnatural amino acids were not commercially available. Hence, we suggest that the isopropyl or isobutyl residue of the respective unnatural amino acids thus point in the wrong direction, which is why receptor-ligand interactions are impeded. Interestingly, substitution by

γ-Val led to a complete loss of GRPR affinity. As substitution by Valyl-Sta ((3*S*,4*S*)-4-amino-3-hydroxy-5-methyl-hexanoic acid) led to poor but distinctly higher GRPR affinity than the γ-Val modification, we assume that an oxygen as proton acceptor moiety is important at this site. Furthermore, it was surprising that the isopropyl residue of the Valyl-Sta motif, which is more similar to the side chain of Val, led to a decreased GRPR affinity compared to the isobutyl residue of the Sta motif. In conclusion, we suggest that the slightly shorter backbone length is mainly responsible for the decreased GRPR affinity. Therefore, moieties containing the exact backbone length as the Val-Gly dipeptide could be considered in future experiments. However, the deletion of the nitrogen atom as well as the presence of a hydroxyl instead of a carbonyl group in this section could also negatively impact GRPR affinity.

Linear RM2 derivatives

As we aimed to develop RM2 analogs with improved pharmacokinetics compared to the parent compound and NeoBOMB1, we introduced the most promising substitutions from previous studies on the MJ9 sequence. Both [^{nat}Ga]RM2 and [^{nat}Lu]RM2 exhibited even higher GRPR affinity than the reported uncomplexed RM2 and [^{nat}In]RM2, respectively (IC_{50}: 7.7 ± 3.3 nM and 9.3 ± 3.3 nM)[39]. [^{nat}Lu]NeoBOMB1 also displayed high GRPR affinity, which was in accordance with the results described by *Kaloudi et al*.[41]. Most established compounds in nuclear medicine display a log$D_{7.4}$ value < −2.0, which typically results in desired renal clearance *in vivo*[39, 170, 202]. However, many compounds exhibiting extremely low lipophilicity (log$D_{7.4}$ < −4.0) showed undesired rapid clearance from the blood, which hampered further accumulation in the tumor[171, 203-205]. [^{177}Lu]RM2, which revealed favorable biodistribution profiles in animals and men, displayed a log$D_{7.4}$ value of −2.51 ± 0.02 (**Tab. 4**)[87, 206]. Despite its elevated lipophilicity (log$D_{7.4}$: −0.88 ± 0.02), [^{68}Ga]NeoBOMB1 also showed favorable pharmacokinetics *in vivo*[138]. However, [^{177}Lu]NeoBOMB1 revealed enhanced hepatic and intestinal retention 24 h p.i.[41, 137, 139].

Structural studies on the MJ9 sequence revealed only a few substitutions, which were considered to be potential alternatives and thus introduced into the RM2 sequence (**Tab. 3**): Txa^5, Hse^7, Bta^8, Cpg^{10}, Chg^{10} and [desPip^5, arg^6]. As the Gln^7-Trp^8 dipeptide was suspected to be the major cleavable site of RM2 analogs *in vivo*, we additionally introduced two novel unnatural amino acids: Cit at position 7 and α-Me-Trp at position 8. In general, RM2 derivatives showed higher IC_{50} values compared to their MJ9 analogs (**Tab. 4**). This was expected, since BBN ligands were shown to prefer positive charges at the *N*-terminus and the positive charge that is contributed by the free *N*-terminal amine group in MJ9 derivatives is removed by the coupling of a chelator[40, 128, 135, 136]. However, substitution of Pip by Dap led to higher IC_{50} values, indicating that positive charges at this site are not the only requirement for high GRPR affinity. This was confirmed by substitution by the neutral Txa, which is structurally similar to Pip and did not cause a decrease in GRPR affinity. However, DOTA-[Txa^5]MJ9 displayed noticeably enhanced lipophilicity compared to RM2, which is attributed to the absent positive charge within the Txa compared to the Pip moiety. Interestingly, coupling of DOTA to the highly affine [*des*Pip^5,

arg[6]]MJ9 resulted in a distinct decrease in GRPR affinity (IC_{50}: 0.91 ± 0.21 nM vs. 12.8 ± 0.9 nM) compared to coupling of DOTA to the Pip-containing MJ9 (IC_{50} of MJ9 vs. DOTA-MJ9 [=RM2]: 0.74 ± 0.09 nM vs. 4.45 ± 0.11 nM). These observations further highlight the superiority of the Pip moiety at this site.

Both DOTA-[Chg[10]]MJ9 and DOTA-[Cpg[10]]MJ9 exhibited only moderate GRPR affinity, which was expected for the former, as [Chg[10]]MJ9 already revealed moderate GRPR affinity and the coupling of DOTA was shown to further decrease GRPR affinity (**Tab. 3**-**4**). However, the high IC_{50} value of the latter was surprising, as [Cpg[10]]MJ9 showed a 20-fold lower IC_{50} value. Further substitution of Chg- or Cpg-containing RM2 analogs by Bta in the Trp position led to a distinct decrease in GRPR affinity and increase in lipophilicity, which was expected, as the sole substitution of Trp by Bta also led to a higher IC_{50} and log$D_{7.4}$ value. As each of the four compounds displayed unfavorable GRPR affinity and lipophilicity, we did not further pursue substitution at the Val[10] site.

Substitution of the critical Gln[7]-Trp[8] site in RM2 by either Cit[7], Hse[7], Bta[8] or α-Me-Trp[8] each led to a favorable combination of GRPR affinity and lipophilicity (**Tab. 4**). Whereas substitution of Gln by Cit and Hse resulted in decreased, but sufficient GRPR affinity as well as improved and comparable lipophilicity to RM2, respectively, substitution of Trp by Bta and α-Me-Trp maintained high affinity, but slightly increased and comparable lipophilicity, respectively. It is worth mentioning that the introduction of Cit led to a remarkable decrease in lipophilicity. This was unexpected, as Cit was not supposed to be that more hydrophilic than Gln[138, 207]. In addition, the lipophilic shift by the introduction of Bta was also surprising as it differs from the Trp residue in only one atom (sulfur atom instead of a nitrogen atom within the indole ring). Despite displaying sufficient GRPR affinity and lipophilicity when either Hse or Bta was substituted, a combination of both unnatural amino acids within the same RM2 analog drastically impaired both GRPR affinity and lipophilicity. As most of the RM2 derivatives multisubstituted within the pharmacophore revealed unfavorable data, we did not further pursue this approach in this study.

In general, all ^{nat}Ga-complexed ligands yielded higher GRPR affinities than their ^{nat}Lu-lutetium counterparts, except for DOTA-[α-Me-Trp[8]]MJ9 (= AMTG). This was unexpected, as we assumed that the additional negative charge of DOTA, which is present when gallium is complexed instead of lutetium, would be detrimental for GRPR affinity. *Gourni et al.* observed that a NODAGA-containing MJ9 derivative enabled a more facile labeling compared to its NOTA analog, indicating a positive influence of the additional negative charge of the chelator[135]. Additionally, beneficial effects for tumor retention using a DOTA-GA moiety was also reported for other targets[78, 208]. Hence, the DOTA-GA analog of AMTG (= AMTG2) was synthesized and evaluated as well, revealing slightly decreased GRPR affinity but improved lipophilicity (**Tab. 4**).

In another approach, the D-enantiomeric α-Me-trp was introduced in the Trp position, which led to poor GRPR affinity. We suggest that this was caused by the lack of π-π stacking interaction between α-Me-

trp[8] and His[12] due to an elevated distance because of the stereoinversion. As the interaction of Trp[8] and His[12] was described as crucial for the stabilization of the secondary helix-like structure of the ligand within GRPR, the loss of affinity was expected[37]. In summary, only RM2 analogs generated by substitution of either Gln[7] or Trp[8] revealed favorable GRPR affinity and lipophilicity. As we hypothesized that substitution of this site by unnatural amino acids would lead to enhanced metabolic stability, these five compounds (DOTA-[Cit[7]]MJ9, DOTA-[Hse[7]]MJ9, DOTA-[Bta[8]]MJ9, AMTG and AMTG2) were investigated in further *in vitro* and *in vivo* studies.

So far, ^{18}F-labeled BBN analogs have not been reported frequently. The non-SiFA-containing ligands $AmBF_3$-MJ9 and 3-cyano-4-trimethylammonium-benzoyl-Ala(SO_3H)-Ala(SO_3H)-Ava-Gln-Trp-Ala-Val-*N*-Me-Gly-His-Sta-Leu-NH_2 both revealed IC_{50} values in the low nanomolar range (0.6 ± 0.1 and 0.94 ± 0.19 nM, respectively)[23, 151]. However, both precursors suffered from increased reaction times, which resulted in moderate to poor RCYs (~23% [n.d.c.] and ~15% [d.c.], respectively). As shown for radiohybrid (rh)-based PSMA inhibitors within our group, the silicon fluoride acceptor (SiFA) methodology enables fast labeling [~15 min] under very mild conditions that allows for high molar activities (A_M), RCYs (50 ± 10% [d.c.]) and radiochemical purities (RCPs)[166, 209]. However, the introduction of the bulky SiFA moiety is associated with a drastic impairment in affinity and lipophilicity, which is attributed to the two ^{t}Bu residues at the silicon atom that are required to prevent hydrolysis of the Si-F bond[162, 178, 183, 210]. First BBN-SiFA ligands reported displayed good to moderate GRPR affinity[148]. *Lindner et al.* described several agonistic SiFA-PESIN derivatives, which revealed sufficient GRPR affinity[164]. In contrast, *Höhne et al.* described BBN-SiFA compounds, which showed moderate to poor GRPR affinity[178].

We thus assume that the design of rh-based BBN derivatives that compensates the negative effects of the SiFA moiety on GRPR affinity and lipophilicity, could improve molecular imaging (and potentially TRT) of GRPR-expressing malignancies noticeably. In order to improve GRPR affinity, several positively charged amino acids were thus introduced at the *N*-terminal linker, as this was shown to be beneficial for BBN analogs[39, 40, 121, 127, 128, 136, 173]. Prior to the introduction of the SiFA moiety, we evaluated these linker-extended RM2 derivatives in order to obtain some insight into positive effects on GRPR affinity and lipophilicity. As the coupling of L-/D-2,3-diaminopropionic acid (L-/D-Dap) or L-/D-ornithine with the commonly used DIPEA (4.5 eq.) led to undesired racemization during the pre-activation step, this was addressed *via* a switch to 2,4,6-collidine (6.0 eq.). This sterically more demanding and weaker base was shown to prevent racemization of the structurally related amino acid cysteine[211, 212]. Adapting this strategy resulted in > 95% enantiomeric excess of the desired products.

Within this series of linker-extended RM2 derivatives, most compounds displayed improved GRPR affinity and lipophilicity compared to the reference RM2, indicating a broad tolerance towards potential modifications of the linker section regarding length and charge distribution (**Tab. 4**). This was expected, as a variety of BBN analogs that comprise linkers with different charge distribution and length, revealed

good overall pharmacokinetics[39, 40, 106, 128, 138, 154, 179, 195, 197, 213]. Interestingly, enhanced GRPR affinity was particularly observed for BBN analogs that contain positively charged primary amine residues (L/D-Dap, L/D-Orn) within the linker, whereas positively charged tertiary amines (Pip) within the linker only had a slight effect. The low log$D_{7.4}$ value of DOTA-Orn^4-MJ9 was surprising, as other ligands within this series possessed an enhanced number of charges, which resulted in higher lipophilicity. As expected, DOTA-Orn^3-Dap^4-MJ9 displayed a similar GRPR affinity to its diastereomer DOTA-orn^3-dap^4-MJ9. However, both differed noticeably in lipophilicity (log$D_{7.4}$: −2.78 ± 0.08 and −3.46 ± 0.14, respectively). This was not expected, as the difference in sterical information did not suggest to that this would result in a distinct impact on lipophilicity. In general, insertion of a negatively charged asparagine residue yielded slightly reduced GRPR affinities, but decreased log$D_{7.4}$ values as well. The increase in hydrophilic character was expected, as several reports described similar benefits by addition of negatively charged moieties, irrespective of the target vector[121, 126, 128, 135, 154, 165]. It is worth mentioning that a few derivatives revealed a remarkable combination of low lipophilicity and GRPR affinity. which could be valuable in compensation of the introduction of the bulky and highly lipophilic SiFA moiety.

Throughout this study, the SiFA group was attached by coupling to the side chain of L-/D-Dap. Although 2,4,6-collidine was used during the pre-activation step, the formation of two isomers was observed after occurred coupling of Fmoc-L-/D-Dap(Dde)-OH, whenever the Fmoc protection group was removed prior to the Dde protection group, which was also described by other groups. The authors suggested a chemical rearrangement of the side chain-bound Dde group to the free *N*-terminal amine because of the spatial proximity in the case of 2,3-diaminopropionic acid[211, 212]. Therefore, it was of utmost importance to couple the SiFA moiety (or a chelating agent) after removal of the Dde protection group to the then available free side chain amine. Only thereafter could cleavage of the Fmoc group be achieved without the formation of undesired isomers. Employing these strategies, all desired BBN-SiFA were obtained in > 95% enantiomeric excess.

Most of the first generation BBN-SiFA compounds displayed poor GRPR affinity, which is attributed to the small distance of the SiFA moiety to the pharmacophore, as the dap(SiFA) unit was introduced at position 6 instead of phe. Hence, we introduced the dap(SiFA) moiety into a prolonged sequence at position 4, which resulted in distinctly improved GRPR affinity (IC_{50} of DOTA-GA-dap(SiFA)^4-MJ9: 27.6 ± 7.0 nM), indicating an enhanced spatial flexibility at this site within GRPR. Indeed, *Sharma et al.* revealed an α-helical structure for the Gln^6→Met^{14} sequence of BBN and a type I β-turn for its Gln^2→Gly^5 section inside GRPR[37]. This β-sheet arrangement exhibits more flexibility than the helix-like conformation inside the receptor. We thus suggest that bulky residues should be introduced *N*-terminally of position 6. Despite its improved GRPR affinity, DOTA-GA-dap(SiFA)^4-MJ9 displayed an unfavorably high lipophilicity (log$D_{7.4}$: 0.67 ± 0.06). These values are in accordance with a first BBN-SiFA compound (log$D_{7.4}$: 1.3 ± 0.1) reported by *Höhne et al.*[178]. Another BBN-SiFA ligand reported by *Dialer et al.* exhibited a log$D_{7.4}$ value of 0.3 ± 0.1, which resulted in enhanced accumulation in liver and intestines in animal studies[148].

Both GRPR affinity and lipophilicity issues were addressed within a series of second generation BBN-SiFA compounds, which comprised an extended linker unit between the MJ9 sequence and the *N*-terminal DOTA-GA-dap(SiFA)[1] building block. Introduction of the tripeptide Gln-Arg-Leu at positions 2-4, which is derived from the natural BBN, led to high GRPR affinity (IC_{50}: 7.73 ± 0.68 nM), but still revealed high lipophilicity (log$D_{7.4}$: 0.58 ± 0.06). Substitution of both Gln^2 and Leu^4 by Asn residues resulted in 3-4-fold decreased GRPR affinity, but also in distinctly improved lipophilicity (log$D_{7.4}$: −1.41 ± 0.06). Introduction of positively charged Orn or Dap residues at positions 3 and 4 resulted in the highest GRPR affinity among BBN-SiFA compounds in this work, which was in accordance with our previous studies on RM2 analogs comprising a prolonged linker. However, the effect of the introduction of Dap and Orn on the decrease of lipophilicity was minor. In general, introduction of hydrophilic moieties into spatial proximity of the SiFA group led to improved lipophilicity, which was also described for a PESIN-SiFA derivative[164].

In order to further compensate the high lipophilicity of the dap(SiFA) unit, it was sandwiched by a dap(DOTA-GA) moiety *C*-terminally and the glu-urea-glu (eue) motif *N*-terminally. Based on its D-enantiomeric character, the highly hydrophilic eue motif was not supposed to comprise any PSMA-related drawbacks, such as high accumulation in kidney, spleen and the salivary glands and should thus be perfectly suited for decreasing lipophilicity[75, 82, 170]. Additionally, one or more negatively charged asp residues were inserted into the linker unit to further increase the hydrophilic character[207]. Finally, positively charged residues (dap, orn or Pip) were introduced at position 3 and 4 to compensate the projected loss of GRPR affinity due to the addition of negative charges (**II. 3.3.5.3**). Due to these severe modifications within the prolonged linker section, the third generation BBN-SiFA analogs thus displayed decreased GRPR affinity (IC_{50}: 9.7-14.3 nM). However, the enhanced lipophilicity through the introduction of the SiFA moiety was successfully compensated (log$D_{7.4}$: −2.05 to −1.71). It is worth mentioning that the established PSMA inhibitors PSMA-617 and PSMA-1007 showed a similar lipophilicity (log$D_{7.4}$: −2.0 and −1.6), which is why we suggest that these third generation BBN-SiFA compounds could be feasible for translation into animal studies[170, 214].

Cyclic MJ9-based compounds

In addition to the chemical modification of linear BBN-based structures, we also aimed to design cyclic MJ9-based compounds. The enhanced metabolic stability of cyclic compounds generally supposed had already been observed for other target molecules[215-217]. Cyclization of linear structures limits the possibilities of peptidic structures to arrange within the active site of enzymes and thus prevents degradation[93-95, 98, 180, 215, 218, 219]. As SST2R, CCK2R, CXCR4 as well as GRPR belongs to the family of GPCRs, we suspected structural similarities among these receptors[139, 220]. Due to encouraging results with respect to the metabolic stabilization of SST2R-, CCK2R- and CXCR4-targeted ligands by cyclization, we assumed that this concept could be also transferred to BBN-based conjugates[215-217].

However, both cyclization concepts applied to MJ9-derived compounds did not result in sufficient GRPR affinity. The poor GRPR affinity observed for the cycles obtained by disulfide bridge formation was attributed to the necessary modifications within the pharmacophore (eight amino acids, two cysteine residues, one D-enantiomeric amino acid). This was confirmed, as the respective linear compounds prior to the disulfide bridge formation also exhibited poor GRPR affinity. Hence, cyclization was intended without substitution of amino acids within the sequence, but only on its backbone. Although modifications required for *Click* chemistry (alkyne and azide residue) were only introduced at the peptidic backbone, formation of the respective cycles also led to poor GRPR affinity. Other reported cyclic GRPR-targeted compounds also suffered from poor GRPR affinity, indicating a general issue of the arrangement of cyclic structures inside GRPR[102, 221]. We assumed that the cycles obtained could not mimic the helix-like conformation of linear BBN analogs inside the receptor and thus could not maintain high GRPR affinity. Due to the low amount of substance administered in nuclear medicine, high affinity to the respective target is indeed a prerequisite. For this reason, metabolic stabilization by cyclization approaches was no longer pursued.

Although cyclic BBN derivatives did not accomplish the desired aim, the modified on-resin cyclization concept *via* Click chemistry (**Scheme 3**) was carried out successfully and could be thus valuable for other target structures[187]. Moreover, after quantitative *p*-Ns deprotection, different approaches for the coupling of the subsequent amino acid onto the alkylated amine using typical coupling reagents (HOAt/TBTU or HOAt/HATU in combination with DIPEA or DIC) did not show any conversion. Nor did an increase in equivalents (from 1.5 eq. to 20 eq.) or reaction time (from 1.5 h to 5.5 h) solve this issue. Similar observations were reported, in which the authors supposed that steric hindrance of the *N*-methylated amines in combination with the sterically demanding HOBt/HOAt esters impedes a successful conversion[222]. Sufficient coupling was then achieved *via* conversion of the respective amino acids into highly reactive acyl chlorides using *bis*(trichloromethyl) carbonate (BTC)[223]. Furthermore, it has to be mentioned that on-resin cyclization attempts by *Click* reactions were reported to be difficult and often unsuccessful. Hence, we cleaved the modified linear peptides from the resin, which were subsequently purified by RP-HPLC and cyclized by a *Click* reaction in solution, resulting in quantitative yields[224-226].

Receptor-mediated internalization studies and plasma stability *in vitro*

As several reports describe massive side effects (nausea, diarrhea, hot flush and abdominal cramps) whenever agonistic GRPR-targeted ligands were administered in men, GRPR-addressing antagonists are desired in today's clinical application[58, 108, 110, 112, 179]. In order to investigate antagonistic behavior, promising RM2 analogs were evaluated in terms of receptor-mediated internalization, as antagonists usually do not internalize into cells. As expected for antagonists, each ^{177}Lu-labeled RM2 analog (DOTA-[Cit^{7}]MJ9, DOTA-[Hse^{7}]MJ9, DOTA-[Bta^{8}]MJ9, AMTG, AMTG2) as well as the reference RM2 revealed low internalization rates (1.4-5.9%) after incubation at 37 °C for 1 h[109, 112, 114, 227]. After 1 h, the receptor-mediated internalization of [^{177}Lu]RM2 (2.92 ± 0.20%) showed good correlation with

the results of other published studies[39, 109, 179]. In contrast, [^{177}Lu]NeoBOMB1 displayed a distinctly enhanced receptor-mediated internalization (13.91 ± 0.64%). However, typical agonistic BBN derivatives (PESIN, AMBA or BBN) showed an amount of receptor-mediated internalization of more than 25% after 1 h[109, 228, 229]. Nevertheless, as its pharmacokinetic profile exhibited a prolonged retention in the GRPR-positive pancreas and intestine, we suspect that this antagonist also comprises a slightly agonistic character[137].

In order to get some insight into the effects of our modifications on metabolic stability within the pharmacophore, we adapted a methodology described by *Linder et al.*, who evaluated the GRPR-targeted agonist [^{177}Lu]AMBA (DO3A-CH_2CO-Gly-(4-aminobenzoyl)-Gln-Trp-Ala-Val-Gly-His-Leu-Met-NH_2) in human, rat and murine plasma. This study revealed several cleavage sites (Gln-Trp, Trp-Ala, His-Leu, Leu-Met) within the AMBA sequence[177]. Based on this concept, we aimed to compare the metabolic stability of our BBN analogs to the reference compounds in both murine and human plasma. It has to be mentioned that in comparison to the studies conducted by *Linder et al.*, the procedure was slightly modified by our group. For their experiments, 990 µL of human plasma and 10 µL of [^{177}Lu]AMBA (~37 MBq, 6 nmol) were incubated at 37 °C for 3 d[177]. In contrast, we incubated 200 µL of human plasma with 100 µL of the respective ^{177}Lu-labeled tracers (~5 MBq, 1 nmol) at 37 °C for 72 ± 2 h. Although *Linder et al.* observed a more rapid degradation of [^{177}Lu]AMBA in murine plasma, *Pourghiasian et al.* observed no metabolites for ^{18}F-AmBF_3-MJ9 when incubated under similar conditions for 2 h. Hence, we assumed that a prolonged incubation time is required for a valid determination of metabolic stability[23].

Unlike the four observed cleavage sites for AMBA, two were not expected for RM2 and its derivatives. This was due to the Sta[13] and Leu[14] moieties inserted, which should impede the cleavage of both unstable *C*-terminal peptide bonds (His-Leu, Leu-Met) by NEP and aminopeptidase 3.4.11.1[177, 178]. We thus focused on the Gln-Trp as well as the Trp-Ala bond as the possible major unstable sites within the RM2-based sequence. In general, only one major and one minor metabolite was observed for the RM2 analogs compared to the four reported for AMBA in human plasma (**Fig. 16-17**), which affirmed our assumption in terms of the modified *C*-terminus[114, 129, 151, 230]. Interestingly, overall degradation in our studies seemed to be enhanced in human plasma (**Tab. 5**), which is in contrast to the observations by *Linder et al.*, as metabolism in murine plasma was distinctly accelerated (**Fig. 29**)[231]. However, the fact that we used 200 µL of human and only 100 µL of murine plasma for our experiments due to a scarcity of the latter must be taken into account.

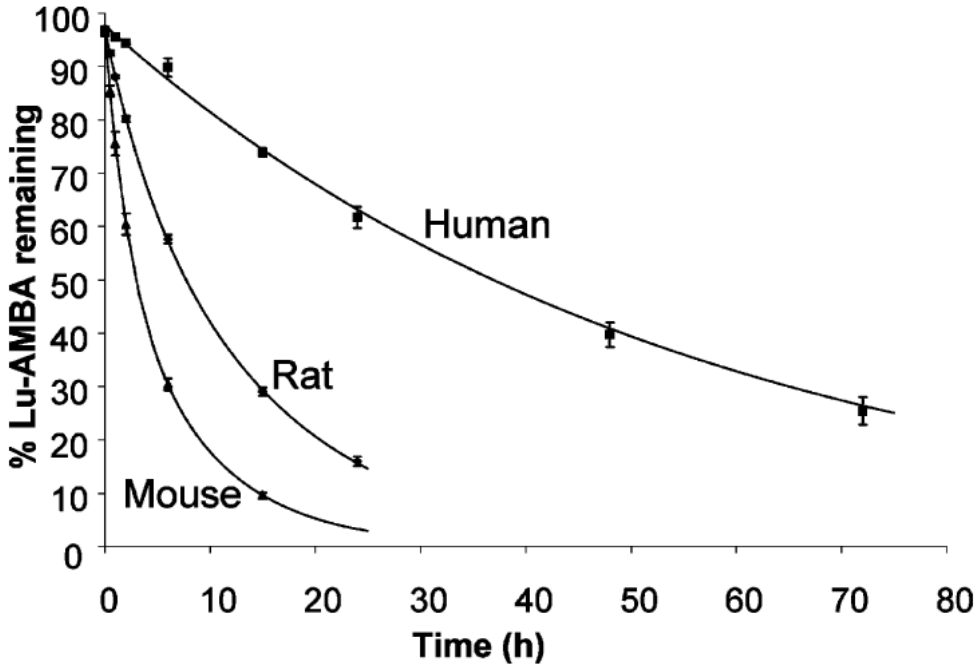

Fig. 29: Metabolic degradation of [177Lu]AMBA in murine, rat and human plasma over time[231].

Despite an increased incubation time in murine plasma, most RM2 derivatives exhibited comparable intact tracer amounts (70-81%), which was unexpected, as most of the substitutions by unnatural amino acids did not seem to influence overall metabolic stability. However, when incubated in human plasma under the same conditions, the intact tracer amounts differed noticeably. Whereas DOTA-[Bta^{8}]MJ9 revealed the lowest metabolic stability, each of the other derivatives evaluated displayed increased amounts of intact tracer compared to RM2. We thus assumed that there are major differences in metabolic activity between the human and the murine NEP, which is mainly responsible for the cleavage of BBN-based peptides at the Gln^{7}-Trp^{8} site.

The low metabolic stability of DOTA-[Bta^{8}]MJ9 in both murine and human plasma was unexpected, as we hypothesized decreased enzymatic degradation when either Gln^{7} or Trp^{8} is substituted. Moreover, we did not expect a distinct difference between DOTA-[Bta^{8}]MJ9 and RM2, as both differ in only one atom (Bta: indole sulfur vs. Trp: indole nitrogen atom). However, log$D_{7.4}$ values already revealed noticeable differences in lipophilicity despite their high structural similarity (**Tab. 5**). We thus suppose that the enhanced lipophilicity at this specific position led to an increased recognition and degradation by NEP[93-95, 178].

Among the RM2 derivatives, AMTG and AMTG2 exhibited the highest amounts of intact tracer when incubated in human plasma. This corroborated well with the suggestion that the Gln^{7}-Trp^{8} bond is indeed the weakest site within the RM2 structure. The methyl group at the same carbon atom that also contains the indole residue of Trp probably impedes the arrangement of the peptide into the active site of NEP, resulting in decreased enzymatic degradation[93-95, 98, 178]. Positive effects on the *in vivo* stability by inser-

tion of α-methyl groups were already assumed by *Eden et al.* for peptoidic NMBR-selective antagonists[232, 233]. Moreover, AMTG also displayed an increased metabolic stability *in vitro* compared to NeoBOMB1, which is reported to be one of the most stable BBN analogs *in vivo*[41]. A comparison of typical chromatograms of RM2 and AMTG after incubation in human plasma (**Fig. 16**) revealed a major metabolite of RM2 at early retention times, which was almost absent for AMTG. We thus suppose that this major metabolite, which was also observed for all other RM2 analogs, is generated by enzymatic degradation of the Gln^7-Trp^8 site. This corroborates our suggestion that the more lipophilic Bta at the Trp site leads to increased metabolism, as DOTA-[Bta^8]MJ9 also showed only one major metabolite at an early retention time (**Fig. 17**). Furthermore, we assume that both the Cit^7 and Hse^7 substitution positively affect metabolic stability, as both compounds revealed increased amounts of intact tracer compared to RM2 in human plasma when incubated under the same conditions.

Most groups describe the metabolic stability of BBN derivatives as absolute values, which were generated in mice *in vivo*. However, a standardized procedure for the determination of these values has not yet been described, as different circulation times *in vivo* were found throughout the literature. For example, the [^{68}Ga]RM2 was reported to exhibit an intact tracer amount of 55% 15 min p.i. in mice[179]. In contrast, 90% of [^{67}Ga]NeoBOMB1 was intact 30 min p.i., whereas 96% and 86% of [^{68}Ga]ProBOMB1 and [^{177}Lu]ProBOMB1, respectively, remained intact 5 min p.i. *in vivo*[41, 138, 139]. [^{111}In]SB3 only displayed an intact tracer amount of 37% 5 min p.i. *in vivo*, which was increased to an amount of 87% by co-injection of the NEP inhibitor Phosphoramidon (PA)[94]. Therefore, a comparison of our results *in vitro* with other reported GRPR-targeted antagonists in terms of metabolic stability is difficult, as most of these ligands were only evaluated *in vivo*. Overestimation of metabolic stability of radiopeptides *in vitro* was reported due to differences in metabolic activity *in vitro* and *in vivo*. On the other hand, disregarding differences between the human and murine species, even though only observed *in vitro*, could also falsify expectations for clinical translation and should therefore be considered as well[93, 116, 177]. We thus suggest that a relative comparison of our compounds with established derivatives (RM2, NeoBOMB1) under the same conditions is most valid. However, the discrepancy between the murine and human plasma has to be further analyzed in future studies. We currently suggest that validity of our results when incubated in human plasma is higher than when incubated in murine plasma.

Biodistribution and μSPECT/CT imaging studies

Based on the promising overall data *in vitro*, several ^{177}Lu-labeled RM2 analogs were further evaluated in female CB17-SCID mice to investigate their pharmacokinetic profile *in vivo* 24 h p.i. (**Fig. 18**). RM2 revealed a favorable biodistribution pattern with high tumor retention and low retention in non-tumor organs, which was also observed by *Dumont et al.* 4 and 24 h p.i. (**Tab. 6**)[234]. Tumor retention and most tumor-background ratios were distinctly higher in our experiments for RM2 24 h p.i., which was attributed to the higher molar activity (30 MBq/nmol vs. 17.2 MBq/nmol) due to the smaller amount of substance (100 vs. 250 pmol) applied.

Tab. 6: Biodistribution and tumor-to-background ratios of [^{177}Lu]RM2 in selected organs (in %IA/g) 4 and 24 h p.i. on PC-3 tumor-bearing CB17-SCID mice (250 pmol, 4.3 MBq each). Data is expressed as mean ± SD (n = 5)[234].

Organs	Time (h)	
	4	24
Blood	0.07 ± 0.02	0.01 ± 0.00
Heart	0.05 ± 0.02	0.02 ± 0.00
Liver	0.31 ± 0.01	0.16 ± 0.01
Spleen	0.11 ± 0.01	0.06 ± 0.01
Lung	0.10 ± 0.01	0.04 ± 0.01
Kidney	2.09 ± 0.19	0.88 ± 0.09
Stomach	0.51 ± 0.19	0.05 ± 0.02
Intestine	0.14 ± 0.03	0.04 ± 0.00
Adrenal	0.59 ± 0.11	0.49 ± 0.07
Pancreas	0.70 ± 0.12	0.11 ± 0.02
Muscle	0.03 ± 0.00	0.01 ± 0.01
Bone	0.12 ± 0.02	0.10 ± 0.03
Tumor	10.97 ± 0.99	4.66 ± 0.44
Tumor-to-nontumor ratios		
Tumor to blood	156.7	466
Tumor to liver	35.4	29.1
Tumor to kidney	5.3	5.3
Tumor to pancreas	15.7	42.4
Tumor to muscle	365.7	466

Data are %IA/g ± SD; n = 5.

The RM2 analogs DOTA-[Cit^7]MJ9, DOTA-[Hse^7]MJ9 and DOTA-[Bta^8]MJ9 revealed noticeably decreased tumor retention 24 h p.i. compared to RM2. This was expected for DOTA-[Bta^8]MJ9, resulting from its low metabolic stability already observed *in vitro* as a consequence of its increased lipophilicity at the critical positions 7 and 8. However, it was not expected for DOTA-[Cit^7]MJ9 and DOTA-[Hse^7]MJ9, as both ligands showed similar metabolic stability to the parent conjugate *in vitro* in the murine plasma. This corroborates the reported assumption of overestimation of metabolic stability of peptides based on their results *in vitro*[41, 93]. It is worth noting that DOTA-[Cit^7]MJ9 displayed comparable tumor-to-background ratios to RM2 (except for tumor-to-muscle ratio) despite its low tumor retention, which was attributed to its low lipophilicity and thus rapid clearance from non-tumor tissue.

The α-Me-Trp-containing RM2 derivatives, AMTG and AMTG2 exhibited comparable tumor retention to RM2 24 h p.i. (**Fig. 18**). This corroborated well with the metabolic stability determined in murine plasma. However, as already mentioned, the validity of this experiment in murine plasma has to be further investigated. Nonetheless, overall retention in non-tumor organs was also low for both, indicating rapid renal clearance. Overall T/B ratios of AMTG and AMTG2 were thus superior or comparable to the parent ligand in most organs 24 h p.i. (**Fig. 19**). Moreover, AMTG revealed an approximately threefold increased tumor-to-blood ratio to its DOTA-GA counterpart and the parent compound. As the probability of developing leukemia was determined to be approximately 2% when the absorbed dose to the red bone marrow exceeds 2 Gy, this organ is considered the critical organ for most TRTs[87, 235].

Hence, tumor-to-blood ratio is a critical factor for the assessment of the biosafety of TRTs in men with regard to the dose administered to the bone marrow[236].

A comparison of AMTG and its DOTA-GA counterpart AMTG2 exhibited a comparable biodistribution pattern as well as T/B ratios in most organs. Both displayed GRPR-specific accumulation in the tumor, as no tumor retention was observed 24 h p.i. in competition experiments when excess of [^{nat}Lu]RM2 (3.62 mg/kg) was co-injected (**Fig. 24**). Interestingly, both compounds showed slightly enhanced retention in lung, liver and spleen in these competition experiments, but this was not investigated further. Due to the structural similarity of these two compounds, comparable biodistribution profiles were expected, although distinct effects of the additional negative charge of DOTA-GA compared to DOTA were reported. Indeed, slightly enhanced tumor retention using a DOTA-GA instead of a DOTA moiety was described by *Rinne et al.* for anti-HER3 affibodies[208]. *Banerjee et al.* also reported noticeably higher tumor retention for a PSMA inhibitor that contained a DOTA-GA chelator compared to other chelators they had used. However, the inhibitors comprising a DOTA-GA moiety also displayed a threefold increased kidney retention[78]. In contrast, *Gourni et al.* reported a slightly decreased tumor retention for [^{64}Cu]NODA-GA-MJ9 compared to its NOTA analog 24 h p.i.[135]. Each of these observations are in contrast to our results, as AMTG2 revealed similar tumor and kidney retention to AMTG.

Based on overall data and particularly due to the highest tumor-to-blood ratio, we decided to select AMTG for further imaging studies alongside RM2 to compare pharmacokinetics over time. Therefore, imaging studies with [^{177}Lu]RM2 and [^{177}Lu]AMTG 1, 4, 8, 24 and 28 h p.i. on PC-3 tumor-bearing mice (100 pmol each, $n = 1$) were performed (**Fig. 23**). Clearance from tumor and non-tumor organs was less rapid for the latter, especially from the pancreas. This was anticipated as a consequence of the projected increased metabolic stability by the α-Me-Trp substitution (instead of Trp). As mentioned earlier, we hypothesized that the methyl group at the carbon atom, which also contains the indole residue of Trp, impedes an arrangement of the respective ligand within the active site of peptidases such as NEP. As this additional methyl group did not negatively affect GRPR affinity, lipophilicity or receptor-mediated internalization, we considered it a valuable tool for metabolic stabilization. This was confirmed by metabolic stabilization studies in human plasma. However, biodistribution studies 24 h p.i. in mice (n = 4) revealed only comparable but not enhanced tumor retention, which was however favorable. Interestingly, in those two mice that were used for imaging studies, a difference between RM2 and AMTG was clearly observable. Due to the enhanced metabolic stability determined in human plasma, we expected improved tumor retention and thus therapeutic outcomes in men as well. For this reason, AMTG was then selected for a first PoC study in an mCPRC patient.

In contrast, the non-statin-comprising GRPR antagonist NeoBOMB1 exhibited an increased overall retention in non-tumor organs, especially in the pancreas (**Fig. 18**), which had also been observed by other groups[41, 137]. Moreover, tumor retention was high, but slightly decreased compared to RM2, AMTG and AMTG2, which resulted in minor T/B ratios in all organs in our studies (100 pmol, 24 h p.i.). However,

an enhanced metabolic stability compared to RM2 in mice was reported for this compound, although it is only modified at both termini, but not within the pharmacophoric section[41, 130]. In our plasma stability studies, NeoBOMB1 revealed a comparable metabolic stability to RM2 in murine, but an approximately twofold stability in human plasma. Interestingly, *Dalm et al.* reported an increased tumor and noticeably decreased pancreatic retention when a lower molar activity (5 MBq/nmol vs. 100 MBq/nmol) was administered (**Fig. 30**)[137].

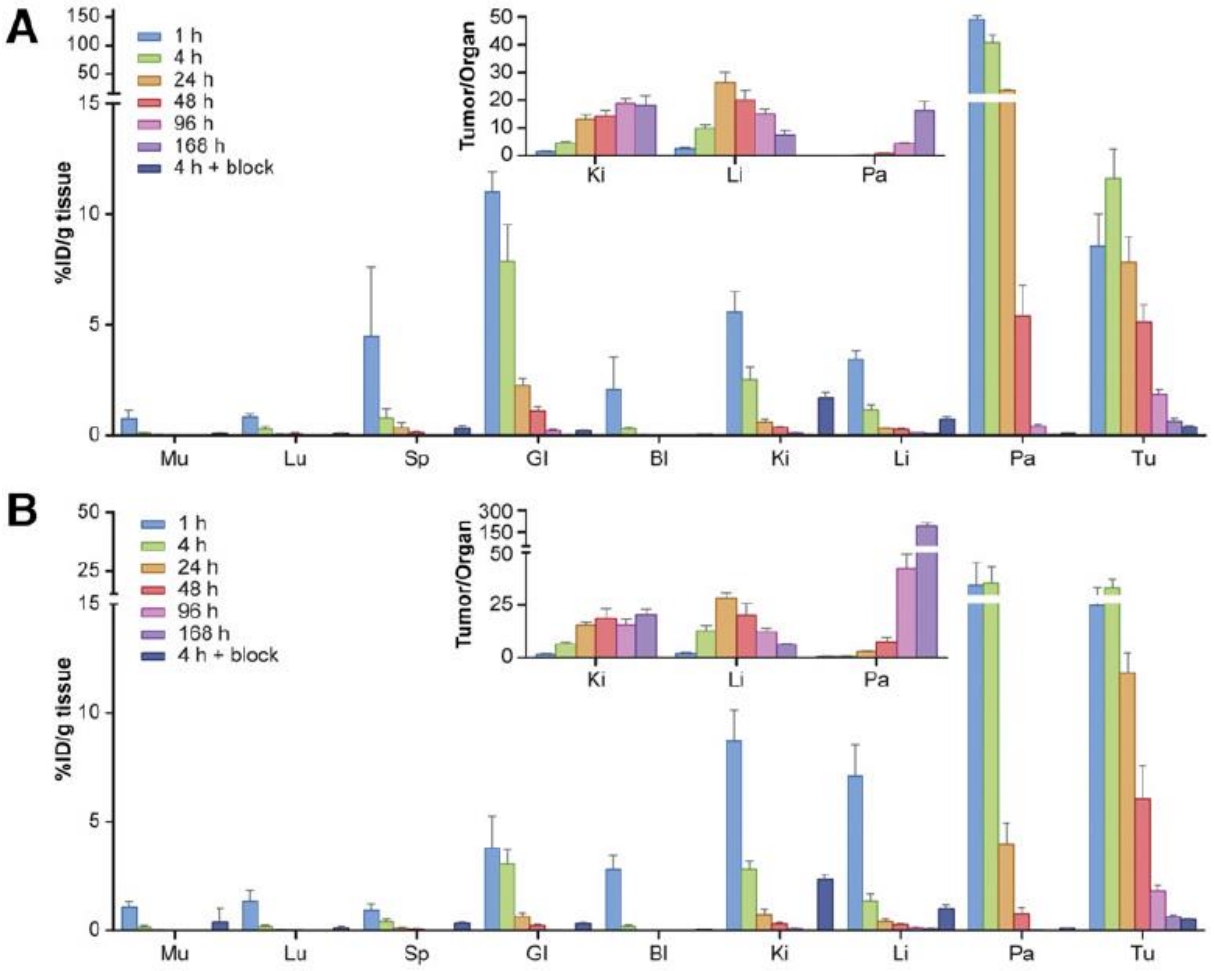

Fig. 30: Biodistribution of 10 (**A**) and 200 pmol (**B**) of [^{177}Lu]NeoBOMB1 (1 MBq each) in selected organs (in %ID/g) on PC-3 tumor-bearing mice. Tumor-to-background ratios are displayed in upper bar graphs. Bl = blood; GI = gastrointestinal tract; Ki = kidney; Li = liver; Lu = lungs; Mu = muscle; Pa = pancreas; Sp = spleen; Tu = PC-3 tumor[137].

Compounds with a decreased molar activity contain higher amounts of still highly-affine unlabeled precursors, which compete against the labeled amounts for target sites. The higher the amount of unlabeled compound, the lower the retention in organs is expected to be. Decreased retention was thus expected in non-tumor organs but a concomitant increased tumor retention was surprising. Based on its increased metabolic stability, NeoBOMB1 displayed good pharmacokinetic profiles at later time points (≥ 24 h p.i.) when a precursor amount of 200 pmol was applied[41, 137]. [^{177}Lu]NeoBOMB1 was thus selected for a phase 1 study[144]. However, initial dosimetric extrapolation revealed unfavorable characteristics due to the slow clearance from background organs, especially from the blood, which is probably a consequence

of its enhanced lipophilicity and thus decreased clearance[137]. As AMTG displayed a slightly and distinctly enhanced metabolic stability to NeoBOMB1 and RM2 in human plasma, respectively, as well as improved overall pharmacokinetics to NeoBOMB1, we predict a superior performance in men regarding biosafety and therapeutic efficiency. However, this has to be investigated in men in order to rule out an overestimation of the metabolic stability of AMTG based on preclinical data.

In another experiment, ^{177}Lu-labeled DOTA-[Bta^{8}]MJ9 and DOTA-[Hse^{7}]MJ9, which revealed low tumor retention 24 h p.i., were further examined at 1 h p.i. to study initial tumor (and non-tumor) uptake, as both compounds displayed distinctly decreased GRPR affinity compared to RM2 and we thus suspected decreased accumulation in GRPR-positive organs. However, both compounds outperformed the parent compound 1 h p.i., exhibiting higher tumor and lower overall non-tumor uptake (**Fig. 20**), which led to superior T/B ratios 1 h p.i. (**Fig. 21**). *Mansi et al.* reported a tumor and pancreatic uptake of 15.2 %ID/g and 22.6 %ID/g for [^{111}In]RM2 (10 pmol) 1 h p.i., which was slightly enhanced due to the higher molar activity administered, but generally in accordance with our results for RM2 (100 pmol)[39]. Surprisingly, DOTA-[Hse^{7}]MJ9 exhibited the highest tumor uptake of this series despite showing the lowest GRPR affinity (**Tab. 4**). Despite only having been observed for DOTA-[Bta^{8}]MJ9 and the results of the stability studies in murine plasma having to be considered carefully, we assumed that the superior clearance rate to RM2 was caused by a decreased metabolic stability of these two RM2 derivatives. In general, metabolism in non-tumor tissue was shown to be more rapid than in tumor tissue (**Fig. 31**)[195, 230]. Further destabilization as a consequence of the lipophilic Bta^{8} substitution within the pharmacophoric section of BBN analogs thus led to an accelerated clearance from non-tumor organs, whereas clearance from the tumor was not affected at early time points. However, we currently have no explanation for the enhanced tumor accumulation 1 h p.i. despite showing a distinctly lower GRPR affinity than RM2. Moreover, the reason for a metabolic destabilization *via* substitution of Gln by Hse is also unclear, as we actually hypothesized that introduction of unnatural amino acids at either the Gln or the Trp site would increase metabolic stability.

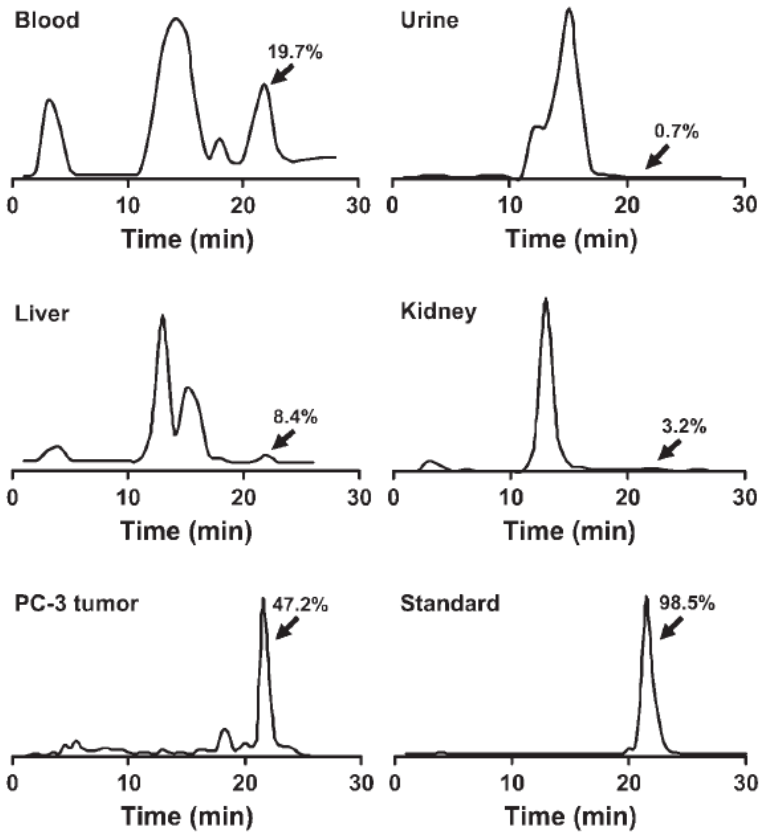

Fig. 31: HPLC profiles of blood, urine, liver, kidney, and PC-3 tumor homogenates collected 1 h p.i. of a BBN analog on a PC-3 tumor-bearing mouse as well as QC of said compound prior to injection[230]. Clearance rates for the PC-3 tumor were noticeably lower than for the other organs depicted.

A recently reported compound, [^{68}Ga]ProBOMB1 (20 pmol), displayed similar data as [^{177}Lu]DOTA-[Bta^{8}]MJ9 1 h p.i., as both exhibited low overall background and reduced pancreatic accumulation (4.7 %ID/g and 3.7 %ID/g, respectively). However, tumor uptake was in favor of [^{177}Lu]DOTA-[Bta^{8}]MJ9 (12.1 %ID/g vs. 8.3 %ID/g). Moreover, competition experiments of [^{68}Ga]ProBOMB1 exhibited enhanced unspecific uptake in GRPR-positive organs[138]. This could be excluded for our ^{177}Lu-labeled compounds as both DOTA-[Hse^{7}]MJ9 and DOTA-[Bta^{8}]MJ9 (100 pmol each) did not show considerable uptake in GRPR-positive organs 1 h p.i. when co-injected with [^{nat}Lu]RM2 (3.62 mg/kg, **Fig. 20**). As already observed in competition studies for AMTG and AMTG2 24 h p.i., enhanced uptake was found in lung, liver and spleen for both DOTA-[Hse^{7}]MJ9 and DOTA-[Bta^{8}]MJ9. This phenomenon has generally not been observed in the literature, as only kidney uptake was increased compared to the background in competition studies with GRPR-targeted ligands[39, 179]. However, *Zhang et al.* also reported enhanced accumulation in lung, liver and spleen when blocking ^{18}F-labeled BBN derivatives, which was not further investigated[230]. Therefore, future studies have to be performed to investigate these findings.

Based on our data, we suggest that BBN analogs with decreased metabolic stability result in improved biodistribution profiles at early time points. This could be valuable for molecular imaging in clinics, as a favorable contrast is obtained more rapidly than with other GRPR-targeted ligands. However, the

transferability of this concept from animals to humans has yet to be investigated in men. If such modified compounds indeed exhibit a comparable contrast to other BBN derivatives at distinctly earlier times, it would enable short waiting times for both the patients and the clinic personnel and facilitate daily routine. To our knowledge, the concept of decreasing metabolic stability has not yet been applied to GRPR-targeted ligands, as most groups focus on increasing metabolic stability, particularly at both termini.

A second objective of this study was the transfer of our radiohybrid (rh) concept to BBN-based compounds, which led to outstanding results when applied to PSMA inhibitors[166, 237-239]. As there are currently no ^{18}F-labeled BBN-based tracers in clinical practice, we aimed to design SiFA-comprising RM2 analogs. Hence, several *N*-terminal linker modifications were examined to determine their effects on GRPR affinity and lipophilicity prior to the introduction of the SiFA moiety (**Tab. 4**). In order to get some insight into the effects of these linker modifications, a couple of promising ^{177}Lu-labeled ligands (DOTA-Orn^3-Dap^4-MJ9, DOTA-GA-orn^3-dap^4-MJ9, DOTA-Pip^3-Pip^4-MJ9, DOTA-orn^3-Pip^4-MJ9) was investigated further *in vivo*. Despite improved GRPR affinity and lipophilicity, tumor retention was only comparable to or even lower than for RM2 24 h p.i. (**Fig. 22**). Moreover, elevated kidney retention was observed for three ligands of this series. Similar observations were reported by *Lindner et al.* for multimeric PESIN conjugates due to an increased tubular reabsorption as a result of an increased number of positive charges[240]. Moreover, *García Garayoa et al.* reported that a BBN-based compound that contained a positive charge at the *N*-terminus displayed unfavorably high retention in kidneys and liver in mice, which was in accordance with our findings[126]. We suggest that this enhanced kidney retention was caused by small metabolites, which comprise the *N*-terminal linker with its several (positive) charges. As a consequence, these short fragments containing several charges are absorbed by the kidneys to a greater extent.

Interestingly, DOTA-Pip^3-Pip^4-MJ9, which comprises three consecutive positively charged Pip moieties within the linker, did not show an elevated kidney retention 24 h p.i. However, tumor retention was lower than that of the other compounds of this series. We thus assume that the enhanced kidney retention was particularly caused by positively charged primary amine residues (L/D-Dap, L/D-Orn) within the linker, but not by positively charged tertiary amines (Pip). Indeed, several reported GRPR-targeted conjugates that comprise positive charges at the *N*-terminus do not exhibit increased kidney retention[39, 40, 128]. It is woth noting that most of these conjugates contain a positively charged chelator, but no free amines within the *N*-terminal linker.

Based on these observations, a variety of BBN-SiFA ligands was designed. However, sufficiently reducing the high lipophilicity obtained by the introduction of the SiFA group while maintaining high GRPR affinity was difficult. Most of the first and second generation BBN-SiFA compounds suffered from insufficient GRPR affinity or lipophilicity. As we considered the necessity of compensating lipophilicity more important than maintaining high GRPR affinity, we introduced several negatively charged moieties (asp, eue motif) into the *N*-terminal linker section, although it was shown that BBN analogs

prefer positive charges at the *N*-terminus. This resulted in five third-generation BBN-SiFA compounds, which displayed reasonable GRPR affinity (IC_{50} of 10-14 nM) and lipophilicity (log$D_{7.4}$ of −2.1 to −1.8). The three compounds showing the lowest lipophilicity were investigated further *in vivo*.

Biodistribution studies revealed low retention in non-tumor organs (except for the liver and the kidneys) as well as moderate tumor retention 24 h p.i. (**Fig. 22**). The massively increased kidney retention (> 100 %ID/g) was attributed to the combination of the SiFA moiety along with the negative charges in its spatial vicinity, which leads to elevated human serum albumin (HSA) binding. Similar results were also observed for PSMA-SiFA inhibitors within our group. A comparison to other BBN-SiFA ligands is difficult, as other groups evaluated their compounds ^{18}F-labeled 1 h p.i. However, a first BBN-SiFA ligand reported by *Höhne et al.* did not show significant tumor uptake but distinctly increased accumulation in liver, gallbladder and intestines as a consequence of moderate GRPR affinity and high lipophilicity (IC_{50}: 22.9 ± 5.8 nM, log$D_{7.4}$:1.3 ± 0.1)[178]. *Dialer et al.* also reported unfavorably high accumulation of a PESIN-based SiFA-containing GRPR agonist in the liver despite improved lipophilicity (log$D_{7.4}$: −1.22)[148]. In contrast, we were able to compensate the high lipophilicity of the SiFA moiety by various hydrophilic modifications within the linker section, as hepatic and intestinal retention 24 h p.i. was low. However, these modifications had a drastic effect on renal retention, which has to be addressed.

Although exhibiting promising results compared to BBN-SiFA compounds reported, our current ligands are not considered suitable for clinical translation. Hence, further studies on the *N*-terminal linker sequence containing a SiFA moiety are required to optimize overall pharmacokinetics of BBN-SiFA ligands. As it is intended to use these ligands for diagnostic purposes, biodistribution and imaging studies with ^{18}F-labeled BBN-SiFA compounds 1 h p.i. have to be peformed in future studies.

Patient studies

GRPR-targeted diagnosis and therapy is currently not employed broadly in clinical practice. This was attributed to the inferior standardized uptake values (SUVs) of BBN analogs in most prostate tumors and metastases compared to PSMA inhibitors as a consequence of decreased GRPR expression and receptor density at later stages of PCa[66, 75, 76, 82, 85, 86]. However, a recently published first-in-human dosimetric study on [^{177}Lu]RM2 revealed favorable pharmacokinetics for this compound, such as low uptake in all non-tumor organs except for the pancreas and high uptake in tumor lesions[87]. This study included 35 mCRPC patients, who did not respond to PSMA-targeted diagnosis and/or therapy and who were thus further examined *via* [^{68}Ga]RM2-PET/CT. Out of these, four patients showed appropriate accumulation in tumor lesions and were thus treated with [^{177}Lu]RM2 (160 µg, 4.5 ± 0.9 GBq). Mean absorbed doses for pancreas, kidneys and bone marrow were 1.08 ± 0.44 Gy/GBq, 0.35 ± 0.14 Gy/GBq and 15.9 ± 5.5 mGy/GBq, respectively. For tumor lesions, a mean absorbed dose of 6.20 ± 3.00 Gy/GBq was determined.

The authors suggest that a maximum activity of about 56 GBq by multiple treatment cycles would be imaginable applying [^{177}Lu]RM2. This maximum applicable dose would be higher than that of the recommended dose for the current gold standard among PSMA-addressing therapeutic compounds, [^{177}Lu]PSMA-617 (36 GBq)[169]. Moreover, *Kratochwil et al.* observed enhanced xerostomia for several patients after three therapy cycles with [^{177}Lu]PSMA-617 (~6 GBq per cycle), which is derived from the high salivary gland uptake. However, the authors considered this side effect harmless. Interestingly, the absorbed dose per administered activity for the kidneys was more than twofold higher for [^{177}Lu]PSMA-617 (0.75 ± 0.19 Gy/GBq) compared to [^{177}Lu]RM2 (0.35 ± 0.14 Gy/GBq)[87, 169, 241]. However, it has to be mentioned that tumor dose rates for [^{177}Lu]RM2 are less than half of those generally achieved *via* PSMA-targeted therapies, which is attributed to the reduced receptor density on prostate tumors[87, 120].

Furthermore, *Dalm et al.* reported an extrapolated dosimetric study based on the preclinical results of [^{177}Lu]NeoBOMB1. An absorbed dose per administered activity of 0.11 Gy/GBq, 0.03 Gy/GBq and 0.11 Gy/GBq for pancreas, kidneys and red bone marrow was estimated, respectively[137]. Based on the maximal absorbed dose permitted for the red bone marrow (< 2 Gy), a maximal activity of only 18 GBq of [^{177}Lu]NeoBOMB1 could be thus administered, which would be less than a third of the potential activity applicable using [^{177}Lu]RM2. However, extrapolated doses cannot be considered reliable, which is why further dosimetric studies in humans are required for a more detailed assessment.

Despite promising pre-clinical and first clinical studies, metabolically stable BBN analogs are still not available, as even RM2 and NeoBOMB1 are metabolized rapidly *in vivo*, which hampers overall bioavailability[130, 132, 137]. *Haubner et al.* reported a distinctly elevated tumor uptake and thus retention for a glycosylated (compared to a non-glycosylated) RGD-comprising peptide. The authors concluded that the metabolism of this compound in the liver was decreased as a result of the improved lipophilicity, which increased overall bioavailability[242]. We thus assume that improved detection rates and treatment of GRPR-expressing malignancies for metabolically stabilized or more hydrophilic BBN ligands are due to the increased bioavailability thus obtained.

Based on its improved metabolic stability in human plasma and its projected increased bioavailability, [^{177}Lu]AMTG was selected for a PoC study in an mCPRC patient. Interestingly, labeling studies with both the TFA and the AcOH salt of AMTG revealed that a fourfold amount of the former (80 µg vs. 20 µg) was necessary to obtain a RCY > 99% when labeled with 1 GBq [^{177}Lu]$LuCl_3$. The AcOH salt was obtained adapting a RP-HPLC concept reported by *McCalley et al.*[243]. Therefore, both MeCN and H_2O were supplemented with 0.1% AcOH (instead of 0.1% TFA) and adjusted to a *pH* = 5 (using NH_4OH) to improve the elution from the RP-HPLC column. Originally, this concept was only developed to generate alternative salts to the widely used TFA salts. However, in our case the AcOH salt delivered distinctly improved results, which is why the AcOH salt will be used exclusively in future studies. We assume that preparation of TRT could be performed using 200 µg AMTG (AcOH salt) and up to 10 GBq

of [^{177}Lu]$LuCl_3$. However, we currently have no explanation for this difference in RCY between the TFA and AcOH salt.

Similar to [^{177}Lu]RM2 reported by *Kurth et al.*, [^{177}Lu]AMTG (1.11 GBq) exhibited low uptake in all non-tumor organs 1 and 4 h p.i. in the acquired SPECT/CT scans, except for the GRPR-positive pancreas (**Fig. 25**)[87]. Moreover, tumor accumulation and retention was clearly visible at both time points. The favorable biodistribution profile was in accordance with several reports on BBN-based compounds revealing relatively low background activity (except for the pancreas) and good uptake in tumor lesions as well[20, 58, 60, 66, 82, 85, 87, 113, 130]. However, an improved metabolic stability in men compared to [^{177}Lu]RM2 was not observed, as only early time points (1 and 4 h p.i.) were examined. Additional SPECT/CT scans and dosimetric studies with [^{177}Lu]AMTG at later time points (≥ 24 h p.i) have thus to be carried out to demonstrate its projected increased metabolic stability in men.

It has to be mentioned that the same patient was treated with [^{177}Lu]PSMA I&T (8.2 GBq) at a similar time, showing significantly increased numbers of metastases and low background accumulation in most organs (**Fig. 26**). Nonetheless, this SPECT scan was acquired 24 h p.i., which apparently results in a lower background activity due to the longer excretion time. In addition, a PET scan of this patient was also acquired a few weeks before the start of TRT using [^{18}F][^{nat}Ga]rhPSMA-7.3. Similarly, an enhanced number of metastases was detected compared to [^{177}Lu]AMTG 1 h p.i. (**Fig. 27**). The superior performance of the PSMA-targeted compounds was anticipated because of the advanced stage of the patient's PCa, as GRPR expression is reported to decrease in later stages of PCa[52, 75, 87]. Moreover, the unique characteristics of ^{18}F-fluorine enabled an improved rate of detection of metastases when using [^{18}F][^{nat}Ga]rhPSMA-7.3 compared to [^{177}Lu]AMTG. However, as shown by *Kurth et al.*, AMTG could be valuable in the treatment of primary PCa or PSMA-negative PCa, as the role of GRPR-targeted and PSMA-targeted compounds is generally assumed to be complementary[84, 87].

Although currently only evaluated with ^{177}Lu-lutetium, AMTG could also be used as a diagnostic tool if labeled with ^{68}Ga-gallium or ^{111}In-indium, as a comparable biodistribution is expected. Such conjugates could be favorable for primary staging of (PSMA-negative or -absent) patients with high-risk prostate cancer[169-171]. Several reports suggest that GRPR expression is high in early, Androgen-dependent disease stages, which could be beneficial because early detection of recurrent PCa was reported to be crucial[51, 52, 57, 58, 60, 85]. Indeed, an approximately 80% chance for progression-free survival at five years was observed for patients when initiating TRT below a PSA level of 0.5 ng/mL[58, 244, 245].

We thus suggest that the novel GRPR-targeted antagonist AMTG could be a beneficial tool for both diagnosis and therapy of GRPR-expressing malignancies, such as PCa, (ER-rich) BCa and neuroendocrine tumors[30, 59-61, 246].

V. Conclusion

Throughout this work, novel GRPR antagonists based on the structure of RM2 were designed with the aim of increasing metabolic stability and evaluated by state-of-the-art experiments (IC_{50}, log$D_{7.4}$, receptor-mediated internalization, plasma stability, biodistribution and imaging studies). We hypothesized that either cyclic ligands or compounds containing unnatural amino acids at metabolically less stable sites (especially the Gln^7-Trp^8 dipeptide) within the pharmacophore impede enzymatic recognition and thus degradation. Cyclization of MJ9-based compounds *via* both disulfide bridge formation and *Click* chemistry resulted in poor GRPR affinity due to suspected drastic changes in the structural arrangement within GRPR, which prevents ligand-receptor interactions. We suspect that a wide variety of design approaches (phage display) would be necessary to identify a sufficient lead structure for cyclic BBN derivatives. However, at this point it is not assessable whether GRPR tolerates cyclic ligands to the same degree as other GPCRs such as SST2R or CXCR4.

Among all linear RM2 derivatives, particularly $^{nat/177}$Lu-labeled Gln^7-Trp^8-modified conjugates revealed promising preclinical results (favorable or sufficient GRPR affinity and lipophilicity, antagonistic character). Except for DOTA-[Bta^8]MJ9, all Gln^7-Trp^8-modified RM2 analogs displayed similar metabolic stability to RM2 in murine plasma. However, metabolic stability in human plasma differed distinctly, as only DOTA-[Bta^8]MJ9 revealed a minor stability to RM2. The low stability of DOTA-[Bta^8]MJ9 was in contrast to our hypothesis but was attributed to its increased lipophilicity at the critical site (Gln^7-Bta^8 distinctly more lipophilic than Gln^7-Trp^8), which leads to enhanced degradation by NEP. Whereas DOTA-[Cit^7]MJ9 and DOTA-[Hse^7]MJ9 showed a slightly enhanced metabolic stability to RM2, both DOTA-[α-Me-Trp^8]MJ9 (= AMTG) and DOTA-GA-[α-Me-Trp^8]MJ9 (= AMTG2) exhibited noticeably increased metabolic stability, even surpassing NeoBOMB1. Except for the Bta substitution, these *in vitro* results confirmed our hypothesis that substitution of the metabolically unstable Gln^7-Trp^8 site by unnatural amino acids leads to enhanced metabolic stability.

In vivo studies further confirmed our hypothesis, as both AMTG and AMTG2 displayed the highest T/B ratios. Whereas NeoBOMB1 suffers from its high lipophilicity, which led to low T/B ratios except for the tumor-to-muscle ratio, both α-Me-Trp-modified RM2 derivatives benefit from the favorable biodistribution pattern of RM2 and additionally from an increased metabolic stability. As RM2 and AMTG structurally differ in only one methyl group (α-Me-Trp instead of Trp), we suggest that indeed enzymatic degradation of RM2 and its analogs occurs at the Gln^7-Trp^8 site. Exhibiting the highest tumor-to-blood ratio, AMTG was selected for a proof of concept study in an mCRPC patient. AMTG showed a favorable biodistribution profile with rapid renal clearance as well as high accumulation and retention in several tumor lesions and the GRPR-positive pancreas 1 and 4 h p.i. Due to its excellent overall data *in vitro* and *in vivo*, we consider AMTG a promising GRPR antagonist for TRT of GRPR-expressing malignancies in men, which might outperform currently established compounds (RM2, NeoBOMB1). However,

further clinical and dosimetric studies with enlarged patient cohorts at later time points (≥ 24 h p.i.) are required to verify these conclusions.

In contrast to the positive *in vivo* results of both AMTG and AMTG2, DOTA-[Cit^{7}]MJ9, DOTA-[Hse^{7}]MJ9 and DOTA-[Bta^{8}]MJ9 exhibited low retention in the tumor 24 h p.i. Due to its decreased plasma stability, this was expected for the latter compound. However, the low retention of the Gln^{7}-modified RM2 analogs was surprising in the context of their increased metabolic stability *in vitro*. As both ligands displayed decreased GRPR affinity, we considered this as a potential explanation. However, biodistribution studies 1 h p.i. revealed enhanced tumor uptake for both DOTA-[Hse^{7}]MJ9 and DOTA-[Bta^{8}]MJ9 compared to RM2 despite a decreased GRPR affinity and metabolic stability, respectively. Interestingly, background activity was concomitantly lower in all non-tumor organs compared to RM2, which led to increased tumor-to-background (T/B) ratios 1 h p.i. We suggest that this was indeed due to an enhanced metabolic instability, which resulted in a more rapid clearance from non-tumor organs but not from the tumor in the early window, as metabolism in tumor was reported to be less rapid. Nevertheless, the decreased metabolic stability *in vivo* compared to the *in vitro* situation in the case of DOTA-[Cit^{7}]MJ9 and DOTA-[Hse^{7}]MJ9 has to be further analyzed.

Furthermore, as all experiments were executed with ^{177}Lu-labeled RM2 analogs, additional *in vivo* studies with diagnostic isotopes ($^{67/68}$Ga-gallium or ^{111}In-indium) have to be performed to verify the pharmacokinetic profile for the diagnostic situation. Moreover, promising diagnostic compounds still have to be evaluated in men to confirm the beneficial effect of the decreased metabolic stability not only in animals but also in men. Nevertheless, we are convinced that substitution by either Bta or Hse in order to increase metabolism and thus accelerate clearance from non-tumor organs could be valuable for the future design of GRPR-addressing ligands for diagnosis, for example improved ^{99m}Tc-labeled ligands as well.

In another branch of this work, the radiohybrid concept developed within our group and successfully applied to PSMA inhibitors was transferred to GRPR-addressing compounds. However, the only BBN-SiFA ligands that displayed appropriate lipophilicity (log$D_{7.4}$ < −1.8) suffered from distinctly elevated renal retention 24 h p.i. (> 100 %ID/g). We suggest that the combination of the SiFA moiety and the increased number of (negative) charges required for the compensation of the highly lipophilic SiFA unit is responsible for this issue. Currently available BBN-SiFA ligands are thus not considered sufficient for clinical translation and have to be further optimized in terms of linker length and charge distribution. Nevertheless, we are convinced that suitable BBN-SiFA compounds could be attractive for clinical application similar to PSMA-SiFA inhibitors, due to the advantage of a facilitated ^{18}F-labeling *via* the SiFA methodology as well as favorable ^{18}F-fluorine PET images. Moreover, as delayed excretion into the bladder was observed for PSMA-SiFA inhibitors, which is beneficial for the diagnosis of PCa, this may also be possible with BBN-SiFA compounds.

VI. References

1. Global Burden of Disease Cancer, C.; Fitzmaurice, C.; Allen, C.; Barber, R. M.; Barregard, L.; Bhutta, Z. A.; Brenner, H.; Dicker, D. J.; Chimed-Orchir, O.; Dandona, R.; Dandona, L.; Fleming, T.; Forouzanfar, M. H.; Hancock, J.; Hay, R. J.; Hunter-Merrill, R.; Huynh, C.; Hosgood, H. D.; Johnson, C. O.; Jonas, J. B.; Khubchandani, J.; Kumar, G. A.; Kutz, M.; Lan, Q.; Larson, H. J.; Liang, X.; Lim, S. S.; Lopez, A. D.; MacIntyre, M. F.; Marczak, L.; Marquez, N.; Mokdad, A. H.; Pinho, C.; Pourmalek, F.; Salomon, J. A.; Sanabria, J. R.; Sandar, L.; Sartorius, B.; Schwartz, S. M.; Shackelford, K. A.; Shibuya, K.; Stanaway, J.; Steiner, C.; Sun, J.; Takahashi, K.; Vollset, S. E.; Vos, T.; Wagner, J. A.; Wang, H.; Westerman, R.; Zeeb, H.; Zoeckler, L.; Abd-Allah, F.; Ahmed, M. B.; Alabed, S.; Alam, N. K.; Aldhahri, S. F.; Alem, G.; Alemayohu, M. A.; Ali, R.; Al-Raddadi, R.; Amare, A.; Amoako, Y.; Artaman, A.; Asayesh, H.; Atnafu, N.; Awasthi, A.; Saleem, H. B.; Barac, A.; Bedi, N.; Bensenor, I.; Berhane, A.; Bernabe, E.; Betsu, B.; Binagwaho, A.; Boneya, D.; Campos-Nonato, I.; Castaneda-Orjuela, C.; Catala-Lopez, F.; Chiang, P.; Chibueze, C.; Chitheer, A.; Choi, J. Y.; Cowie, B.; Damtew, S.; das Neves, J.; Dey, S.; Dharmaratne, S.; Dhillon, P.; Ding, E.; Driscoll, T.; Ekwueme, D.; Endries, A. Y.; Farvid, M.; Farzadfar, F.; Fernandes, J.; Fischer, F.; TT, G. H.; Gebru, A.; Gopalani, S.; Hailu, A.; Horino, M.; Horita, N.; Husseini, A.; Huybrechts, I.; Inoue, M.; Islami, F.; Jakovljevic, M.; James, S.; Javanbakht, M.; Jee, S. H.; Kasaeian, A.; Kedir, M. S.; Khader, Y. S.; Khang, Y. H.; Kim, D.; Leigh, J.; Linn, S.; Lunevicius, R.; El Razek, H. M. A.; Malekzadeh, R.; Malta, D. C.; Marcenes, W.; Markos, D.; Melaku, Y. A.; Meles, K. G.; Mendoza, W.; Mengiste, D. T.; Meretoja, T. J.; Miller, T. R.; Mohammad, K. A.; Mohammadi, A.; Mohammed, S.; Moradi-Lakeh, M.; Nagel, G.; Nand, D.; Le Nguyen, Q.; Nolte, S.; Ogbo, F. A.; Oladimeji, K. E.; Oren, E.; Pa, M.; Park, E. K.; Pereira, D. M.; Plass, D.; Qorbani, M.; Radfar, A.; Rafay, A.; Rahman, M.; Rana, S. M.; Soreide, K.; Satpathy, M.; Sawhney, M.; Sepanlou, S. G.; Shaikh, M. A.; She, J.; Shiue, I.; Shore, H. R.; Shrime, M. G.; So, S.; Soneji, S.; Stathopoulou, V.; Stroumpoulis, K.; Sufiyan, M. B.; Sykes, B. L.; Tabares-Seisdedos, R.; Tadese, F.; Tedla, B. A.; Tessema, G. A.; Thakur, J. S.; Tran, B. X.; Ukwaja, K. N.; Uzochukwu, B. S. C.; Vlassov, V. V.; Weiderpass, E.; Wubshet Terefe, M.; Yebyo, H. G.; Yimam, H. H.; Yonemoto, N.; Younis, M. Z.; Yu, C.; Zaidi, Z.; Zaki, M. E. S.; Zenebe, Z. M.; Murray, C. J. L.; Naghavi, M., Global, Regional, and National Cancer Incidence, Mortality, Years of Life Lost, Years Lived With Disability, and Disability-Adjusted Life-years for 32 Cancer Groups, 1990 to 2015: A Systematic Analysis for the Global Burden of Disease Study. *JAMA Oncol* **2017,** *3* (4), 524-548.

2. James, N. D.; Spears, M. R.; Clarke, N. W.; Dearnaley, D. P.; De Bono, J. S.; Gale, J.; Hetherington, J.; Hoskin, P. J.; Jones, R. J.; Laing, R.; Lester, J. F.; McLaren, D.; Parker, C. C.; Parmar, M. K. B.; Ritchie, A. W. S.; Russell, J. M.; Strebel, R. T.; Thalmann, G. N.; Mason, M. D.; Sydes, M. R., Survival with Newly Diagnosed Metastatic Prostate Cancer in the "Docetaxel Era": Data from 917 Patients in the Control Arm of the STAMPEDE Trial (MRC PR08, CRUK/06/019). *Eur Urol* **2015,** *67* (6), 1028-1038.

3. Maajani, K.; Jalali, A.; Alipour, S.; Khodadost, M.; Tohidinik, H. R.; Yazdani, K., The Global and Regional Survival Rate of Women With Breast Cancer: A Systematic Review and Meta-analysis. *Clin Breast Cancer* **2019,** *19* (3), 165-177.

4. Cornford, P.; Bellmunt, J.; Bolla, M.; Briers, E.; De Santis, M.; Gross, T.; Henry, A. M.; Joniau, S.; Lam, T. B.; Mason, M. D.; van der Poel, H. G.; van der Kwast, T. H.; Rouviere, O.; Wiegel, T.; Mottet, N., EAU-ESTRO-SIOG Guidelines on Prostate Cancer. Part II: Treatment of Relapsing, Metastatic, and Castration-Resistant Prostate Cancer. *Eur Urol* **2017,** *71* (4), 630-642.

5. Mottet, N.; Bellmunt, J.; Bolla, M.; Briers, E.; Cumberbatch, M. G.; De Santis, M.; Fossati, N.; Gross, T.; Henry, A. M.; Joniau, S.; Lam, T. B.; Mason, M. D.; Matveev, V. B.; Moldovan, P. C.; van den Bergh, R. C. N.; Van den Broeck, T.; van der Poel, H. G.; van der Kwast, T. H.; Rouviere, O.; Schoots, I. G.; Wiegel, T.; Cornford, P., EAU-ESTRO-SIOG Guidelines on Prostate Cancer. Part 1: Screening, Diagnosis, and Local Treatment with Curative Intent. *Eur Urol* **2017,** *71* (4), 618-629.

6. Fenton, J. J.; Weyrich, M. S.; Durbin, S.; Liu, Y.; Bang, H.; Melnikow, J., Prostate-Specific Antigen-Based Screening for Prostate Cancer: Evidence Report and Systematic Review for the US Preventive Services Task Force. *JAMA* **2018,** *319* (18), 1914-1931.

7. Thompson, I. M.; Pauler, D. K.; Goodman, P. J.; Tangen, C. M.; Lucia, M. S.; Parnes, H. L.; Minasian, L. M.; Ford, L. G.; Lippman, S. M.; Crawford, E. D.; Crowley, J. J.; Coltman, C. A. J.,

Prevalence of prostate cancer among men with a prostate-specific antigen level or =4.0 ng per milliliter. *N Engl J Med* **2004,** *350* (22), 2239-46.
8. Sindhwani, P.; Wilson, C. M., Prostatitis and serum prostate-specific antigen. *Current Prostate Reports* **2005,** *3* (2), 81-86.
9. Benson, M. C.; Seong Whang, I.; Pantuck, A.; Ring, K.; Kaplan, S. A.; Olsson, C. A.; Cooner, W. H., Prostate Specific Antigen Density: A Means of Distinguishing Benign Prostatic Hypertrophy and Prostate Cancer. *Journal of Urology* **1992,** *147* (3 Part 2), 815-816.
10. Gøtzsche, P. C.; Nielsen, M., Screening for breast cancer with mammography. *Cochrane Database Syst Rev* **2011,** *1*.
11. Cardoso, F.; Kyriakides, S.; Ohno, S.; Penault-Llorca, F.; Poortmans, P.; Rubio, I. T.; Zackrisson, S.; Senkus, E.; Committee, E. G., Early breast cancer: ESMO Clinical Practice Guidelines for diagnosis, treatment and follow-updagger. *Ann Oncol* **2019,** *30* (8), 1194-1220.
12. Marmot, M. G.; Altman, D. G.; Cameron, D. A.; Dewar, J. A.; Thompson, S. G.; Wilcox, M., The benefits and harms of breast cancer screening: an independent review. *Br J Cancer* **2013,** *108* (11), 2205-40.
13. Houssami, N., Overdiagnosis of breast cancer in population screening: does it make breast screening worthless? *Cancer Biol Med* **2017,** *14* (1), 1-8.
14. Nelson, H. D.; O'Meara, E. S.; Kerlikowske, K.; Balch, S.; Miglioretti, D., Factors Associated With Rates of False-Positive and False-Negative Results From Digital Mammography Screening: An Analysis of Registry Data. *Ann Intern Med* **2016,** *164* (4), 226-35.
15. Gleason, D. F.; Mellinger, G. T., Prediction of Prognosis for Prostatic Adenocarcinoma by Combined Histological Grading and Clinical Staging. *Journal of Urology* **1974,** *111* (1), 58-64.
16. Epstein, J. I.; Allsbrook, W. C. J.; Amin, M. B.; Egevad, L. L.; Committee, I. G., The 2005 International Society of Urological Pathology (ISUP) Consensus Conference on Gleason Grading of Prostatic Carcinoma. *Am J Surg Pathol* **2005,** *29* (9), 1228-42.
17. Bertero, L.; Massa, F.; Metovic, J.; Zanetti, R.; Castellano, I.; Ricardi, U.; Papotti, M.; Cassoni, P., Eighth Edition of the UICC Classification of Malignant Tumours: an overview of the changes in the pathological TNM classification criteria-What has changed and why? *Virchows Arch* **2018,** *472* (4), 519-531.
18. Israel, O.; Pellet, O.; Biassoni, L.; De Palma, D.; Estrada-Lobato, E.; Gnanasegaran, G.; Kuwert, T.; la Fougere, C.; Mariani, G.; Massalha, S.; Paez, D.; Giammarile, F., Two decades of SPECT/CT - the coming of age of a technology: An updated review of literature evidence. *Eur J Nucl Med Mol Imaging* **2019,** *46* (10), 1990-2012.
19. Fani, M.; Maecke, H. R.; Okarvi, S. M., Radiolabeled peptides: valuable tools for the detection and treatment of cancer. *Theranostics* **2012,** *2* (5), 481-501.
20. Minamimoto, R.; Sonni, I.; Hancock, S.; Vasanawala, S.; Loening, A.; Gambhir, S. S.; Iagaru, A., Prospective Evaluation of (68)Ga-RM2 PET/MRI in Patients with Biochemical Recurrence of Prostate Cancer and Negative Findings on Conventional Imaging. *J Nucl Med* **2018,** *59* (5), 803-808.
21. Bouchelouche, K.; Choyke, P. L., Advances in prostate-specific membrane antigen PET of prostate cancer. *Curr Opin Oncol* **2018,** *30* (3), 189-196.
22. von Eyben, F. E.; Baumann, G. S.; Baum, R. P., PSMA diagnostics and treatments of prostate cancer become mature. *Clin Transl Imaging* **2018,** *6* (2), 145-148.
23. Pourghiasian, M.; Liu, Z.; Pan, J.; Zhang, Z.; Colpo, N.; Lin, K. S.; Perrin, D. M.; Benard, F., (18)F-AmBF3-MJ9: a novel radiofluorinated bombesin derivative for prostate cancer imaging. *Bioorg Med Chem* **2015,** *23* (7), 1500-6.
24. Abouzayed, A.; Yim, C. B.; Mitran, B.; Rinne, S. S.; Tolmachev, V.; Larhed, M.; Rosenstrom, U.; Orlova, A., Synthesis and Preclinical Evaluation of Radio-Iodinated GRPR/PSMA Bispecific Heterodimers for the Theranostics Application in Prostate Cancer. *Pharmaceutics* **2019,** *11* (7).
25. Reubi, J. C.; Wenger, S.; Schmuckli-Maurer, J.; Schaer, J. C.; Gugger, M., Bombesin receptor subtypes in human cancers: detection with the universal radioligand (125)I-[D-TYR(6), beta-ALA(11), PHE(13), NLE(14)] bombesin(6-14). *Clin Cancer Res* **2002,** *8* (4), 1139-46.
26. Reubi, C.; Gugger, M.; Waser, B., Co-expressed peptide receptors in breast cancer as a molecular basis for in vivo multireceptor tumour targeting. *Eur J Nucl Med Mol Imaging* **2002,** *29* (7), 855-62.

27. Eder, M.; Schafer, M.; Bauder-Wust, U.; Haberkorn, U.; Eisenhut, M.; Kopka, K., Preclinical evaluation of a bispecific low-molecular heterodimer targeting both PSMA and GRPR for improved PET imaging and therapy of prostate cancer. *Prostate* **2014,** *74* (6), 659-68.
28. Wright, G. L. J.; Grob, B. M.; Haley, C.; Grossman, K.; Newhall, K.; Petrylak, D.; Troyer, J.; Konchuba, A.; Schellhammer, P. F.; Moriarty, R., Upregulation of prostate-specific membrane antigen after androgen-deprivation therapy. *Urology* **1996,** *48* (2), 326-34.
29. Dalm, S. U.; Sieuwerts, A. M.; Look, M. P.; Melis, M.; van Deurzen, C. H.; Foekens, J. A.; de Jong, M.; Martens, J. W., Clinical Relevance of Targeting the Gastrin-Releasing Peptide Receptor, Somatostatin Receptor 2, or Chemokine C-X-C Motif Receptor 4 in Breast Cancer for Imaging and Therapy. *J Nucl Med* **2015,** *56* (10), 1487-93.
30. Morgat, C.; MacGrogan, G.; Brouste, V.; Velasco, V.; Sevenet, N.; Bonnefoi, H.; Fernandez, P.; Debled, M.; Hindie, E., Expression of Gastrin-Releasing Peptide Receptor in Breast Cancer and Its Association with Pathologic, Biologic, and Clinical Parameters: A Study of 1,432 Primary Tumors. *J Nucl Med* **2017,** *58* (9), 1401-1407.
31. Jensen, R. T.; Battey, J. F.; Spindel, E. R.; Benya, R. V., International Union of Pharmacology. LXVIII. Mammalian bombesin receptors: nomenclature, distribution, pharmacology, signaling, and functions in normal and disease states. *Pharmacol Rev* **2008,** *60* (1), 1-42.
32. Corjay, M. H.; Dobrzanski, D. J.; Way, J. M.; Viallet, J.; Shapira, H.; Worland, P.; Sausville, E. A.; Battey, J. F., Two distinct bombesin receptor subtypes are expressed and functional in human lung carcinoma cells. *J Biol Chem* **1991,** *266* (28), 18771-9.
33. Fathi, Z.; Corjay, M. H.; Shapira, H.; Wada, E.; Benya, R.; Jensen, R. T.; Viallet, J.; Sausville, E. A.; Battey, J. F., BRS-3 a novel bombesin receptor subtype selectively expressed in testis and lung carcinoma cells. *J Biol Chem* **1993,** *268* (8), 5979-84.
34. Dufresne, M.; Seva, C.; Fourmy, D., Cholecystokinin and gastrin receptors. *Physiol Rev* **2006,** *86* (3), 805-47.
35. Nakagawa, T.; Hocart, S. J.; Schumann, M.; Tapia, J. A.; Mantey, S. A.; Coy, D. H.; Tokita, K.; Katsuno, T.; Jensen, R. T., Identification of key amino acids in the gastrin-releasing peptide receptor (GRPR) responsible for high affinity binding of gastrin-releasing peptide (GRP). *Biochem Pharmacol* **2005,** *69* (4), 579-93.
36. Benya, R. V.; Kusui, T.; Katsuno, T.; Tsuda, T.; Mantey, S. A.; Battey, J. F.; Jensen, R. T., Glycosylation of the gastrin-releasing peptide receptor and its effect on expression, G protein coupling, and receptor modulatory processes. *Mol Pharm* **2000,** *58* (6), 1490-501.
37. Sharma, P.; Singh, P.; Bisetty, K.; Corcho, F. J.; Perez, J. J., Conformational profile of bombesin assessed using different computational protocols. *J Mol Graph Model* **2010,** *29* (4), 581-90.
38. Tokita, K.; Katsuno, T.; Hocart, S. J.; Coy, D. H.; Llinares, M.; Martinez, J.; Jensen, R. T., Molecular basis for selectivity of high affinity peptide antagonists for the gastrin-releasing peptide receptor. *J Biol Chem* **2001,** *276* (39), 36652-63.
39. Mansi, R.; Wang, X.; Forrer, F.; Waser, B.; Cescato, R.; Graham, K.; Borkowski, S.; Reubi, J. C.; Maecke, H. R., Development of a potent DOTA-conjugated bombesin antagonist for targeting GRPr-positive tumours. *Eur J Nucl Med Mol Imaging* **2011,** *38* (1), 97-107.
40. Nock, B. A.; Charalambidis, D.; Sallegger, W.; Waser, B.; Mansi, R.; Nicolas, G. P.; Ketani, E.; Nikolopoulou, A.; Fani, M.; Reubi, J. C.; Maina, T., New Gastrin Releasing Peptide Receptor-Directed [(99m)Tc]Demobesin 1 Mimics: Synthesis and Comparative Evaluation. *J Med Chem* **2018,** *61* (7), 3138-3150.
41. Kaloudi, A.; Lymperis, E.; Giarika, A.; Dalm, S.; Orlandi, F.; Barbato, D.; Tedesco, M.; Maina, T.; de Jong, M.; Nock, B. A., NeoBOMB1, a GRPR-Antagonist for Breast Cancer Theragnostics: First Results of a Preclinical Study with [(67)Ga]NeoBOMB1 in T-47D Cells and Tumor-Bearing Mice. *Molecules* **2017,** *22* (11).
42. Mitran, B.; Thisgaard, H.; Rosenstrom, U.; Dam, J. H.; Larhed, M.; Tolmachev, V.; Orlova, A., High Contrast PET Imaging of GRPR Expression in Prostate Cancer Using Cobalt-Labeled Bombesin Antagonist RM26. *Contrast Media Mol Imaging* **2017,** *2017*, 6873684.
43. Coy, D. H.; Heinz-Erian, P.; Jiang, N. Y.; Sasaki, Y.; Taylor, J.; Moreau, J. P.; Wolfrey, W. T.; Gardner, J. D.; Jensen, R. T., Probing peptide backbone function in bombesin. A reduced peptide bond analogue with potent and specific receptor antagonist activity. *J Biol Chem* **1988,** *263* (11), 5056-60.

44. Xiao, D.; Wang, J.; Hampton, L. L.; Weber, H. C., The human gastrin-releasing peptide receptor gene structure, its tissue expression and promoter. *Gene* **2001,** *264* (1), 95-103.
45. Roesler, R.; Schwartsmann, G., Gastrin-releasing peptide receptors in the central nervous system: role in brain function and as a drug target. *Front Endocrinol (Lausanne)* **2012,** *3*, 159.
46. Ghatei, M. A.; Jung, R. T.; Stevenson, J. C.; Hillyard, C. J.; Adrian, T. E.; Lee, Y. C.; Christofides, N. D.; Sarson, D. L.; Mashiter, K.; MacIntyre, I.; Bloom, S. R., Bombesin: action on gut hormones and calcium in man. *J Clin Endocrinol Metab* **1982,** *54* (5), 980-5.
47. Modlin, I. M.; Lamers, C. B.; Walsh, J. H., Stimulation of canine pancreatic polypeptide, gastrin, and gastric acid secretion by ranatensin, litorin, bombesin nonapeptide and substance P. *Regul Pept* **1981,** *1* (4), 279-88.
48. Gonzalez, N.; Moody, T. W.; Igarashi, H.; Ito, T.; Jensen, R. T., Bombesin-related peptides and their receptors: recent advances in their role in physiology and disease states. *Curr Opin Endocrinol Diabetes Obes* **2008,** *15* (1), 58-64.
49. Del Rio, M.; Hernanz, A.; de la Fuente, M., Bombesin, gastrin-releasing peptide, and neuromedin C modulate murine lymphocyte proliferation through adherent accessory cells and activate protein kinase C. *Peptides* **1994,** *15* (1), 15-22.
50. Subramaniam, M.; Sugiyama, K.; Coy, D. H.; Kong, Y.; Miller, Y. E.; Weller, P. F.; Wada, K.; Wada, E.; Sunday, M. E., Bombesin-like peptides and mast cell responses: relevance to bronchopulmonary dysplasia? *Am J Respir Crit Care Med* **2003,** *168* (5), 601-11.
51. Schroeder, R. P.; de Visser, M.; van Weerden, W. M.; de Ridder, C. M.; Reneman, S.; Melis, M.; Breeman, W. A.; Krenning, E. P.; de Jong, M., Androgen-regulated gastrin-releasing peptide receptor expression in androgen-dependent human prostate tumor xenografts. *Int J Cancer* **2010,** *126* (12), 2826-34.
52. de Visser, M.; van Weerden, W. M.; de Ridder, C. M.; Reneman, S.; Melis, M.; Krenning, E. P.; de Jong, M., Androgen-dependent expression of the gastrin-releasing peptide receptor in human prostate tumor xenografts. *J Nucl Med* **2007,** *48* (1), 88-93.
53. Mattei, J.; Achcar, R. D.; Cano, C. H.; Macedo, B. R.; Meurer, L.; Batlle, B. S.; Groshong, S. D.; Kulczynski, J. M.; Roesler, R.; Dal Lago, L.; Brunetto, A. T.; Schwartsmann, G., Gastrin-releasing peptide receptor expression in lung cancer. *Arch Pathol Lab Med* **2014,** *138* (1), 98-104.
54. Markwalder, R.; Reubi, J. C., Gastrin-releasing peptide receptors in the human prostate relation to neoplastic transformation. *Cancer Res* **1999,** *59* (5), 1152-9.
55. Stott Reynolds, T. J.; Smith, C. J.; Lewis, M. R., Peptide-Based Radiopharmaceuticals for Molecular Imaging of Prostate Cancer. *Adv Exp Med Biol* **2018,** *1096*, 135-158.
56. Sah, B. R.; Burger, I. A.; Schibli, R.; Friebe, M.; Dinkelborg, L.; Graham, K.; Borkowski, S.; Bacher-Stier, C.; Valencia, R.; Srinivasan, A.; Hany, T. F.; Mu, L.; Wild, P. J.; Schaefer, N. G., Dosimetry and first clinical evaluation of the new 18F-radiolabeled bombesin analogue BAY 864367 in patients with prostate cancer. *J Nucl Med* **2015,** *56* (3), 372-8.
57. Beer, M.; Montani, M.; Gerhardt, J.; Wild, P. J.; Hany, T. F.; Hermanns, T.; Muntener, M.; Kristiansen, G., Profiling gastrin-releasing peptide receptor in prostate tissues: clinical implications and molecular correlates. *Prostate* **2012,** *72* (3), 318-25.
58. Mather, S. J.; Nock, B. A.; Maina, T.; Gibson, V.; Ellison, D.; Murray, I.; Sobnack, R.; Colebrook, S.; Wan, S.; Halberrt, G.; Szysko, T.; Powles, T.; Avril, N., GRP Receptor Imaging of Prostate Cancer Using [99mTc]Demobesin 4: a First-in-Man Study. *Molecular Imaging and Biology* **2014,** *16* (6), 888-895.
59. Morgat, C.; Schollhammer, R.; Macgrogan, G.; Barthe, N.; Velasco, V.; Vimont, D.; Cazeau, A. L.; Fernandez, P.; Hindie, E., Comparison of the binding of the gastrin-releasing peptide receptor (GRP-R) antagonist 68Ga-RM2 and 18F-FDG in breast cancer samples. *PLoS One* **2019,** *14* (1), e0210905.
60. Maina, T.; Bergsma, H.; Kulkarni, H. R.; Mueller, D.; Charalambidis, D.; Krenning, E. P.; Nock, B. A.; de Jong, M.; Baum, R. P., Preclinical and first clinical experience with the gastrin-releasing peptide receptor-antagonist [(6)(8)Ga]SB3 and PET/CT. *Eur J Nucl Med Mol Imaging* **2016,** *43* (5), 964-973.
61. Stoykow, C.; Erbes, T.; Maecke, H. R.; Bulla, S.; Bartholoma, M.; Mayer, S.; Drendel, V.; Bronsert, P.; Werner, M.; Gitsch, G.; Weber, W. A.; Stickeler, E.; Meyer, P. T., Gastrin-releasing Peptide Receptor Imaging in Breast Cancer Using the Receptor Antagonist (68)Ga-RM2 And PET. *Theranostics* **2016,** *6* (10), 1641-50.

62. Zang, J.; Mao, F.; Wang, H.; Zhang, J.; Liu, Q.; Peng, L.; Li, F.; Lang, L.; Chen, X.; Zhu, Z., 68Ga-NOTA-RM26 PET/CT in the Evaluation of Breast Cancer: A Pilot Prospective Study. *Clin Nucl Med* **2018,** *43* (9), 663-669.
63. Frucht, H.; Gazdar, A. F.; Park, J. A.; Oie, H.; Jensen, R. T., Characterization of functional receptors for gastrointestinal hormones on human colon cancer cells. **1992,** *52* (5), 1114-22.
64. Carroll, R. E.; Matkowskyj, K. A.; Chakrabarti, S.; McDonald, T. J.; Benya, R. V., Aberrant expression of gastrin-releasing peptide and its receptor by well-differentiated colon cancers in humans. *Am J Physiol* **1999,** *276* (3), G655-65.
65. Ghosh, A.; Heston, W. D., Tumor target prostate specific membrane antigen (PSMA) and its regulation in prostate cancer. *J Cell Biochem* **2004,** *91* (3), 528-39.
66. Wieser, G.; Mansi, R.; Grosu, A. L.; Schultze-Seemann, W.; Dumont-Walter, R. A.; Meyer, P. T.; Maecke, H. R.; Reubi, J. C.; Weber, W. A., Positron emission tomography (PET) imaging of prostate cancer with a gastrin releasing peptide receptor antagonist--from mice to men. *Theranostics* **2014,** *4* (4), 412-9.
67. Mesters, J. R.; Barinka, C.; Li, W.; Tsukamoto, T.; Majer, P.; Slusher, B. S.; Konvalinka, J.; Hilgenfeld, R., Structure of glutamate carboxypeptidase II, a drug target in neuronal damage and prostate cancer. *EMBO J* **2006,** *25* (6), 1375-84.
68. Silver, D. A.; Pellicer, I.; Fair, W. R.; Heston, W. D.; Cordon-Cardo, C., Prostate-specific membrane antigen expression in normal and malignant human tissues. *Clin Cancer Res* **1997,** *3* (1), 81-5.
69. Udovicich, C.; Perera, M.; Hofman, M. S.; Siva, S.; Del Rio, A.; Murphy, D. G.; Lawrentschuk, N., (68)Ga-prostate-specific membrane antigen-positron emission tomography/computed tomography in advanced prostate cancer: Current state and future trends. *Prostate Int* **2017,** *5* (4), 125-129.
70. Sweat, S. D.; Pacelli, A.; Murphy, G. P.; Bostwick, D. G., Prostate-specific membrane antigen expression is greatest in prostate adenocarcinoma and lymph node metastases. *Urology* **1998,** *52* (4), 637-40.
71. Bostwick, D. G.; Pacelli, A.; Blute, M.; Roche, P.; Murphy, G. P., Prostate specific membrane antigen expression in prostatic intraepithelial neoplasia and adenocarcinoma a study of 184 cases. *Cancer* **1998,** *82* (11), 2256-61.
72. Afshar-Oromieh, A.; Haberkorn, U.; Schlemmer, H. P.; Fenchel, M.; Eder, M.; Eisenhut, M.; Hadaschik, B. A.; Kopp-Schneider, A.; Rothke, M., Comparison of PET/CT and PET/MRI hybrid systems using a 68Ga-labelled PSMA ligand for the diagnosis of recurrent prostate cancer: initial experience. *Eur J Nucl Med Mol Imaging* **2014,** *41* (5), 887-97.
73. Gourni, E.; Canovas, C.; Goncalves, V.; Denat, F.; Meyer, P. T.; Maecke, H. R., (R)-NODAGA-PSMA: A Versatile Precursor for Radiometal Labeling and Nuclear Imaging of PSMA-Positive Tumors. *PLoS One* **2015,** *10* (12), e0145755.
74. Weineisen, M.; Schottelius, M.; Simecek, J.; Baum, R. P.; Yildiz, A.; Beykan, S.; Kulkarni, H. R.; Lassmann, M.; Klette, I.; Eiber, M.; Schwaiger, M.; Wester, H. J., 68Ga- and 177Lu-Labeled PSMA I&T: Optimization of a PSMA-Targeted Theranostic Concept and First Proof-of-Concept Human Studies. *J Nucl Med* **2015,** *56* (8), 1169-76.
75. Hoberuck, S.; Michler, E.; Wunderlich, G.; Lock, S.; Holscher, T.; Froehner, M.; Braune, A.; Ivan, P.; Seppelt, D.; Zophel, K.; Kotzerke, J., 68Ga-RM2 PET in PSMA- positive and -negative prostate cancer patients. *Nuklearmedizin* **2019,** *58* (5), 352-362.
76. Emmett, L.; Crumbaker, M.; Ho, B.; Willowson, K.; Eu, P.; Ratnayake, L.; Epstein, R.; Blanksby, A.; Horvath, L.; Guminski, A.; Mahon, K.; Gedye, C.; Yin, C.; Stricker, P.; Joshua, A. M., Results of a Prospective Phase 2 Pilot Trial of (177)Lu-PSMA-617 Therapy for Metastatic Castration-Resistant Prostate Cancer Including Imaging Predictors of Treatment Response and Patterns of Progression. *Clin Genitourin Cancer* **2019,** *17* (1), 15-22.
77. Afshar-Oromieh, A.; Malcher, A.; Eder, M.; Eisenhut, M.; Linhart, H. G.; Hadaschik, B. A.; Holland-Letz, T.; Giesel, F. L.; Kratochwil, C.; Haufe, S.; Haberkorn, U.; Zechmann, C. M., PET imaging with a [68Ga]gallium-labelled PSMA ligand for the diagnosis of prostate cancer: biodistribution in humans and first evaluation of tumour lesions. *Eur J Nucl Med Mol Imaging* **2013,** *40* (4), 486-95.
78. Banerjee, S. R.; Kumar, V.; Lisok, A.; Chen, J.; Minn, I.; Brummet, M.; Boinapally, S.; Cole, M.; Ngen, E.; Wharram, B.; Brayton, C.; Hobbs, R. F.; Pomper, M. G., (177)Lu-labeled low-

molecular-weight agents for PSMA-targeted radiopharmaceutical therapy. *Eur J Nucl Med Mol Imaging* **2019,** *46* (12), 2545-2557.
79. Rauscher, I.; Maurer, T.; Beer, A. J.; Graner, F. P.; Haller, B.; Weirich, G.; Doherty, A.; Gschwend, J. E.; Schwaiger, M.; Eiber, M., Value of 68Ga-PSMA HBED-CC PET for the Assessment of Lymph Node Metastases in Prostate Cancer Patients with Biochemical Recurrence: Comparison with Histopathology After Salvage Lymphadenectomy. *J Nucl Med* **2016,** *57* (11), 1713-1719.
80. Rupp, N. J.; Umbricht, C. A.; Pizzuto, D. A.; Lenggenhager, D.; Topfer, A.; Muller, J.; Muhlematter, U. J.; Ferraro, D. A.; Messerli, M.; Morand, G. B.; Huber, G. F.; Eberli, D.; Schibli, R.; Muller, C.; Burger, I. A., First clinico-pathological evidence of a non PSMA-related uptake mechanism for (68)Ga-PSMA-11 in salivary glands. *J Nucl Med* **2019**.
81. Perera, M.; Papa, N.; Christidis, D.; Wetherell, D.; Hofman, M. S.; Murphy, D. G.; Bolton, D.; Lawrentschuk, N., Sensitivity, Specificity, and Predictors of Positive (68)Ga-Prostate-specific Membrane Antigen Positron Emission Tomography in Advanced Prostate Cancer: A Systematic Review and Meta-analysis. *Eur Urol* **2016,** *70* (6), 926-937.
82. Minamimoto, R.; Hancock, S.; Schneider, B.; Chin, F. T.; Jamali, M.; Loening, A.; Vasanawala, S.; Gambhir, S. S.; Iagaru, A., Pilot Comparison of (6)(8)Ga-RM2 PET and (6)(8)Ga-PSMA-11 PET in Patients with Biochemically Recurrent Prostate Cancer. *J Nucl Med* **2016,** *57* (4), 557-62.
83. Schollhammer, R.; De Clermont Gallerande, H.; Yacoub, M.; Quintyn Ranty, M. L.; Barthe, N.; Vimont, D.; Hindie, E.; Fernandez, P.; Morgat, C., Comparison of the radiolabeled PSMA-inhibitor (111)In-PSMA-617 and the radiolabeled GRP-R antagonist (111)In-RM2 in primary prostate cancer samples. *EJNMMI Res* **2019,** *9* (1), 52.
84. Baratto, L.; Duan, H.; Maecke, H. R.; Iagaru, A., Imaging the Distribution of Gastrin Releasing Peptide Receptors in Cancer. *J Nucl Med* **2020**.
85. Kahkonen, E.; Jambor, I.; Kemppainen, J.; Lehtio, K.; Gronroos, T. J.; Kuisma, A.; Luoto, P.; Sipila, H. J.; Tolvanen, T.; Alanen, K.; Silen, J.; Kallajoki, M.; Roivainen, A.; Schafer, N.; Schibli, R.; Dragic, M.; Johayem, A.; Valencia, R.; Borkowski, S.; Minn, H., In vivo imaging of prostate cancer using [68Ga]-labeled bombesin analog BAY86-7548. *Clin Cancer Res* **2013,** *19* (19), 5434-43.
86. Iagaru, A., Will GRPR Compete with PSMA as a Target in Prostate Cancer? *J Nucl Med* **2017,** *58* (12), 1883-1884.
87. Kurth, J.; Krause, B. J.; Schwarzenböck, S. M.; Bergner, C.; Hakenberg, O. W.; Heuschkel, M., First-in-human dosimetry of gastrin-releasing peptide receptor antagonist [177Lu]Lu-RM2: a radiopharmaceutical for the treatment of metastatic castration-resistant prostate cancer. *European Journal of Nuclear Medicine and Molecular Imaging* **2019**.
88. Erspamer, V.; Erspamer, G. F.; Inselvini, M.; Negri, L., Occurrence of bombesin and alytesin in extracts of the skin of three European discoglossid frogs and pharmacological actions of bombesin on extravascular smooth muscle. *Br J Pharmacol* **1972,** *45* (2), 333-48.
89. McDonald, T. J.; Jörnvall, H.; Nilsson, G.; Vagne, M.; Ghatei, M.; Bloom, S. R.; Mutt, V., Characterization of a gastrin releasing peptide from porcine non-antral gastric tissue. *Biochem Biophys Res Commun* **1979,** *90* (1), 227-33.
90. Maina, T.; Nock, B.; Mather, S., Targeting prostate cancer with radiolabelled bombesins. *Cancer Imaging* **2006,** *6*, 153-7.
91. Wang, L. H.; Mantey, S. A.; Lin, J. T.; Frucht, H.; Jensen, R. T., Ligand binding, internalization, degradation and regulation by guanine nucleotides of bombesin receptor subtypes: A comparative study. *Biochim Biophys Acta* **1993,** *1175* (2), 232-42.
92. Swope, S. L.; Schonbrunn, A., Characterization of ligand binding and processing by bombesin receptors in an insulin-secreting cell line. *Biochem J* **1987,** *247* (3), 731-38.
93. Nock, B. A.; Maina, T.; Krenning, E. P.; de Jong, M., "To serve and protect": enzyme inhibitors as radiopeptide escorts promote tumor targeting. *J Nucl Med* **2014,** *55* (1), 121-7.
94. Bakker, I. L.; van Tiel, S. T.; Haeck, J.; Doeswijk, G. N.; de Blois, E.; Segbers, M.; Maina, T.; Nock, B. A.; de Jong, M.; Dalm, S. U., In Vivo Stabilized SB3, an Attractive GRPR Antagonist, for Pre- and Intra-Operative Imaging for Prostate Cancer. *Mol Imaging Biol* **2018,** *20* (6), 973-983.
95. Shipp, M. A.; Tarr, G. E.; Chen, C. Y.; Switzer, S. N.; Hersh, L. B.; Stein, H.; Sunday, M. E.; Reinherz, E. L., CD10neutral endopeptidase 24.11 hydrolyzes bombesin-like peptides and regulates the growth of small cell carcinomas of the lung. *Proc Natl Acad Sci U S A* **1991,** *88* (23), 10662-6.

96. Bruno, B. J.; Miller, G. D.; Lim, C. S., Basics and recent advances in peptide and protein drug delivery. *Ther Deliv* **2013,** *4* (11), 1443-67.
97. Yu, Z.; Ananias, H. J.; Carlucci, G.; Hoving, H. D.; Helfrich, W.; Dierckx, R. A.; Wang, F.; de Jong, I. J.; Elsinga, P. H., An Update of Radiolabeled Bombesin Analogs for Gastrin-Releasing Peptide Receptor Targeting. *Curr Pharm Des* **2013,** *19* (18), 3329-41.
98. Gentilucci, L.; De Marco, R.; Cerisoli, L., Chemical modifications designed to improve peptide stability: incorporation of non-natural amino acids, pseudo-peptide bonds, and cyclization. *Curr Pharm Des* **2010,** *16* (28), 3185-203.
99. Dijkgraaf, I.; Franssen, G. M.; McBride, W. J.; D'Souza, C. A.; Laverman, P.; Smith, C. J.; Goldenberg, D. M.; Oyen, W. J.; Boerman, O. C., PET of tumors expressing gastrin-releasing peptide receptor with an 18F-labeled bombesin analog. *J Nucl Med* **2012,** *53* (6), 947-52.
100. Coy, D.; Wang, L.-H.; Jiang, N.-Y.; Jensen, R. T., Short chain bombesin pseudopeptides with potent bombesin receptor antagonist activity in rat and guinea pig pancreatic acinar cells. *Eur J Pharmacol* **1990,** *190* (1-2), 31-38.
101. Coy, D. H.; Mungan, Z.; Rossowski, W. J.; Cheng, B. L.; Lin, J.-T.; Mrozinski Jr., J. E.; Jensen, R. T., Development of a potent bombesin receptor antagonist with prolonged in vivo inhibitory activity on bombesin-stimulated amylase. *Peptides* **1992,** *13* (4), 775-81.
102. Lin, J. T.; Coy, D. H.; Mantey, S. A.; Jensen, R. T., Comparison of the peptide structural requirements for high affinity interaction with bombesin receptors. *Eur J Pharmacol* **1995,** *294* (1), 55-69.
103. Pradhan, T. K.; Katsuno, T.; Taylor, J. E.; Kim, S. H.; Ryan, R. R.; Mantey, S. A.; Donohue, P. J.; Weber, H. C.; Sainz, E.; Battey, J. F.; Coy, D. H.; Jensen, R. T., Identification of a unique ligand which has high affinity for all four bombesin receptor subtypes. *Eur J Pharmacol* **1998,** *343* (2-3), 275-87.
104. Zhang, H.; Chen, J.; Waldherr, C.; Hinni, K.; Waser, B.; Reubi, J. C.; Maecke, H. R., Synthesis and evaluation of bombesin derivatives on the basis of pan-bombesin peptides labeled with indium-111, lutetium-177, and yttrium-90 for targeting bombesin receptor-expressing tumor. *Cancer Res* **2004,** *64* (18), 6707-15.
105. Vlieghe, P.; Lisowski, V.; Martinez, J.; Khrestchatisky, M., Synthetic therapeutic peptides: science and market. *Drug Discov Today* **2010,** *15* (1-2), 40-56.
106. Sancho, V.; Di Florio, A.; Moody, T. W.; Jensen, R. T., Bombesin receptor-mediated imaging and cytotoxicity: review and current status. *Curr Drug Deliv* **2011,** *8* (1), 79-134.
107. Knight, M.; Takahashi, K.; Chandrasekhar, B.; Geblaoui, A. Z.; Jensen, R. T.; Strader, D.; Moody, T. W., Inhibitory cyclic analogues and chlorambucil derivatives of bombesin-like peptides. *Peptides* **1995,** *16* (6), 1109-15.
108. Schroeder, R. P.; Muller, C.; Reneman, S.; Melis, M. L.; Breeman, W. A.; de Blois, E.; Bangma, C. H.; Krenning, E. P.; van Weerden, W. M.; de Jong, M., A standardised study to compare prostate cancer targeting efficacy of five radiolabelled bombesin analogues. *Eur J Nucl Med Mol Imaging* **2010,** *37* (7), 1386-96.
109. Mansi, R.; Wang, X.; Forrer, F.; Kneifel, S.; Tamma, M. L.; Waser, B.; Cescato, R.; Reubi, J. C.; Maecke, H. R., Evaluation of a 1,4,7,10-tetraazacyclododecane-1,4,7,10-tetraacetic acid-conjugated bombesin-based radioantagonist for the labeling with single-photon emission computed tomography, positron emission tomography, and therapeutic radionuclides. *Clin Cancer Res* **2009,** *15* (16), 5240-9.
110. Basso, N.; Lezoche, E.; Speranza, V., Studies with bombesin in man. *World Journal of Surgery* **1979,** *3* (5), 579-85.
111. Ginj, M.; Zhang, H.; Waser, B.; Cescato, R.; Wild, D.; Wang, X.; Erchegyi, J.; Rivier, J.; Maecke, H. R.; Reubi, J. C., Radiolabeled somatostatin receptor antagonists are preferable to agonists for in vivo peptide receptor targeting of tumors. *Proc Natl Acad Sci U S A* **2006,** *103* (44), 16436-41.
112. Cescato, R.; Maina, T.; Nock, B.; Nikolopoulou, A.; Charalambidis, D.; Piccand, V.; Reubi, J. C., Bombesin receptor antagonists may be preferable to agonists for tumor targeting. *J Nucl Med* **2008,** *49* (2), 318-26.
113. Wieser, G.; Popp, I.; Christian Rischke, H.; Drendel, V.; Grosu, A. L.; Bartholoma, M.; Weber, W. A.; Mansi, R.; Wetterauer, U.; Schultze-Seemann, W.; Meyer, P. T.; Jilg, C. A., Diagnosis of recurrent prostate cancer with PET/CT imaging using the gastrin-releasing peptide receptor

antagonist (68)Ga-RM2: Preliminary results in patients with negative or inconclusive [(18)F]Fluoroethylcholine-PET/CT. *Eur J Nucl Med Mol Imaging* **2017,** *44* (9), 1463-1472.
114. Lymperis, E.; Kaloudi, A.; Kanellopoulos, P.; Krenning, E. P.; de Jong, M.; Maina, T.; Nock, B. A., Comparative evaluation of the new GRPR-antagonist (111) In-SB9 and (111) In-AMBA in prostate cancer models: Implications of in vivo stability. *J Labelled Comp Radiopharm* **2019**.
115. Wild, D.; Frischknecht, M.; Zhang, H.; Morgenstern, A.; Bruchertseifer, F.; Boisclair, J.; Provencher-Bolliger, A.; Reubi, J. C.; Maecke, H. R., Alpha- versus beta-particle radiopeptide therapy in a human prostate cancer model (213Bi-DOTA-PESIN and 213Bi-AMBA versus 177Lu-DOTA-PESIN). *Cancer Res* **2011,** *71* (3), 1009-18.
116. Maina, T.; Kaloudi, A.; Valverde, I. E.; Mindt, T. L.; Nock, B. A., Amide-to-triazole switch vs. in vivo NEP-inhibition approaches to promote radiopeptide targeting of GRPR-positive tumors. *Nucl Med Biol* **2017,** *52*, 57-62.
117. Valverde, I. E.; Vomstein, S.; Mindt, T. L., Toward the Optimization of Bombesin-Based Radiotracers for Tumor Targeting. *J Med Chem* **2016,** *59* (8), 3867-77.
118. Schottelius, M.; Wester, H. J., Molecular imaging targeting peptide receptors. *Methods* **2009,** *48* (2), 161-77.
119. Maina, T.; Konijnenberg, M. W.; KolencPeitl, P.; Garnuszek, P.; Nock, B. A.; Kaloudi, A.; Kroselj, M.; Zaletel, K.; Maecke, H.; Mansi, R.; Erba, P.; von Guggenberg, E.; Hubalewska-Dydejczyk, A.; Mikolajczak, R.; Decristoforo, C., Preclinical pharmacokinetics, biodistribution, radiation dosimetry and toxicity studies required for regulatory approval of a phase I clinical trial with (111)In-CP04 in medullary thyroid carcinoma patients. *Eur J Pharm Sci* **2016,** *91*, 236-42.
120. Ananias, H. J.; Yu, Z.; Hoving, H. D.; Rosati, S.; Dierckx, R. A.; Wang, F.; Yan, Y.; Chen, X.; Pruim, J.; Lub-de Hooge, M. N.; Helfrich, W.; Elsinga, P. H.; de Jong, I. J., Application of (99m)Technetium-HYNIC(tricine/TPPTS)-Aca-Bombesin(7-14) SPECT/CT in prostate cancer patients: a first-in-man study. *Nucl Med Biol* **2013,** *40* (7), 933-8.
121. Kaloudi, A.; Lymperis, E.; Kanellopoulos, P.; Waser, B.; de Jong, M.; Krenning, E. P.; Reubi, J. C.; Nock, B. A.; Maina, T., Localization of (99m)Tc-GRP Analogs in GRPR-Expressing Tumors: Effects of Peptide Length and Neprilysin Inhibition on Biological Responses. *Pharmaceuticals (Basel)* **2019,** *12* (1).
122. Ferreira, C. A.; Fuscaldi, L. L.; Townsend, D. M.; Rubello, D.; Barros, A. L. B., Radiolabeled bombesin derivatives for preclinical oncological imaging. *Biomed Pharmacother* **2017,** *87*, 58-72.
123. Nock, B. A.; Nikolopoulou, A.; Galanis, A.; Cordopatis, P.; Waser, B.; Reubi, J. C.; Maina, T., Potent bombesin-like peptides for GRP-receptor targeting of tumors with 99mTc: a preclinical study. *J Med Chem* **2005,** *48* (1), 100-10.
124. Ananias, H. J. K.; Yu, Z.; Dierckx, R. A.; van der Wiele, C.; Helfrich, W.; Wang, F.; Yan, Y.; Chen, X.; de Jong, I. J.; Elsinga, P. H., 99mTechnetium-HYNIC(tricine/TPPTS)-Aca-Bombesin(7–14) as a Targeted Imaging Agent with MicroSPECT in a PC-3 Prostate Cancer Xenograft Model. *Molecular Pharmaceutics* **2011,** *8* (4), 1165-1173.
125. Dapp, S.; Garcia Garayoa, E.; Maes, V.; Brans, L.; Tourwe, D. A.; Muller, C.; Schibli, R., PEGylation of (99m)Tc-labeled bombesin analogues improves their pharmacokinetic properties. *Nucl Med Biol* **2011,** *38* (7), 997-1009.
126. Garcia Garayoa, E.; Schweinsberg, C.; Maes, V.; Brans, L.; Bläuenstein, P.; Tourwe, D. A.; Schibli, R.; Schubiger, P. A., Influence of the molecular charge on the biodistribution of bombesin analogues labeled with the [99mTc(CO)3]-core. *Bioconjug Chem* **2008,** *19* (12), 2409-16.
127. Marsouvanidis, P. J.; Maina, T.; Sallegger, W.; Krenning, E. P.; de Jong, M.; Nock, B. A., Tumor diagnosis with new 111In-radioligands based on truncated human gastrin releasing peptide sequences: synthesis and preclinical comparison. *J Med Chem* **2013,** *56* (21), 8579-87.
128. Mitran, B.; Varasteh, Z.; Selvaraju, R. K.; Lindeberg, G.; Sorensen, J.; Larhed, M.; Tolmachev, V.; Rosenstrom, U.; Orlova, A., Selection of optimal chelator improves the contrast of GRPR imaging using bombesin analogue RM26. *Int J Oncol* **2016,** *48* (5), 2124-34.
129. Lymperis, E.; Kaloudi, A.; Kanellopoulos, P.; de Jong, M.; Krenning, E. P.; Nock, B. A.; Maina, T., Comparing Gly(11)/dAla(11)-Replacement vs. the in-Situ Neprilysin-Inhibition Approach on the Tumor-targeting Efficacy of the (111)In-SB3/(111)In-SB4 Radiotracer Pair. *Molecules* **2019,** *24* (6).
130. Nock, B. A.; Kaloudi, A.; Lymperis, E.; Giarika, A.; Kulkarni, H. R.; Klette, I.; Singh, A.; Krenning, E. P.; de Jong, M.; Maina, T.; Baum, R. P., Theranostic Perspectives in Prostate Cancer with

the Gastrin-Releasing Peptide Receptor Antagonist NeoBOMB1: Preclinical and First Clinical Results. *J Nucl Med* **2017,** *58* (1), 75-80.
131. Banerjee, S. R.; Kumar, V.; Lisok, A.; Plyku, D.; Novakova, Z.; Brummet, M.; Wharram, B.; Barinka, C.; Hobbs, R.; Pomper, M. G., Evaluation of (111)In-DOTA-5D3, a Surrogate SPECT Imaging Agent for Radioimmunotherapy of Prostate-Specific Membrane Antigen. *J Nucl Med* **2019,** *60* (3), 400-406.
132. Roivainen, A.; Kahkonen, E.; Luoto, P.; Borkowski, S.; Hofmann, B.; Jambor, I.; Lehtio, K.; Rantala, T.; Rottmann, A.; Sipila, H.; Sparks, R.; Suilamo, S.; Tolvanen, T.; Valencia, R.; Minn, H., Plasma pharmacokinetics, whole-body distribution, metabolism, and radiation dosimetry of 68Ga bombesin antagonist BAY 86-7548 in healthy men. *J Nucl Med* **2013,** *54* (6), 867-72.
133. Mansour, N.; Dumulon-Perreault, V.; Ait-Mohand, S.; Paquette, M.; Lecomte, R.; Guerin, B., Impact of dianionic and dicationic linkers on tumor uptake and biodistribution of [(64) Cu]Cu/NOTA peptide-based gastrin-releasing peptide receptors antagonists. *J Labelled Comp Radiopharm* **2017,** *60* (4), 200-212.
134. Mansour, N.; Paquette, M.; Ait-Mohand, S.; Dumulon-Perreault, V.; Guerin, B., Evaluation of a novel GRPR antagonist for prostate cancer PET imaging: [(64)Cu]-DOTHA2-PEG-RM26. *Nucl Med Biol* **2018,** *56*, 31-38.
135. Gourni, E.; Mansi, R.; Jamous, M.; Waser, B.; Smerling, C.; Burian, A.; Buchegger, F.; Reubi, J. C.; Maecke, H. R., N-terminal modifications improve the receptor affinity and pharmacokinetics of radiolabeled peptidic gastrin-releasing peptide receptor antagonists: examples of 68Ga- and 64Cu-labeled peptides for PET imaging. *J Nucl Med* **2014,** *55* (10), 1719-25.
136. Varasteh, Z.; Mitran, B.; Rosenstrom, U.; Velikyan, I.; Rosestedt, M.; Lindeberg, G.; Sorensen, J.; Larhed, M.; Tolmachev, V.; Orlova, A., The effect of macrocyclic chelators on the targeting properties of the 68Ga-labeled gastrin releasing peptide receptor antagonist PEG2-RM26. *Nucl Med Biol* **2015,** *42* (5), 446-454.
137. Dalm, S. U.; Bakker, I. L.; de Blois, E.; Doeswijk, G. N.; Konijnenberg, M. W.; Orlandi, F.; Barbato, D.; Tedesco, M.; Maina, T.; Nock, B. A.; de Jong, M., 68Ga/177Lu-NeoBOMB1, a Novel Radiolabeled GRPR Antagonist for Theranostic Use in Oncology. *J Nucl Med* **2017,** *58* (2), 293-299.
138. Lau, J.; Rousseau, E.; Zhang, Z.; Uribe, C. F.; Kuo, H. T.; Zeisler, J.; Zhang, C.; Kwon, D.; Lin, K. S.; Benard, F., Positron Emission Tomography Imaging of the Gastrin-Releasing Peptide Receptor with a Novel Bombesin Analogue. *ACS Omega* **2019,** *4* (1), 1470-1478.
139. Rousseau, E.; Lau, J.; Zhang, Z.; Zhang, C.; Kwon, D.; Uribe, C. F.; Kuo, H. T.; Zeisler, J.; Bratanovic, I.; Lin, K. S.; Benard, F., Comparison of biological properties of [(177) Lu]Lu-ProBOMB1 and [(177) Lu]Lu-NeoBOMB1 for GRPR-targeting. *J Labelled Comp Radiopharm* **2019**.
140. 68-Ga-RM2 PET/MRI in Imaging Patients With Estrogen Receptor-Positive Breast Cancer. https://ClinicalTrials.gov/show/NCT03831711.
141. 68Ga-RM2 Compared to 68Ga-PSMA-617 PET/CT for Prostate Cancer Imaging According to Various Metastatic Risks. https://ClinicalTrials.gov/show/NCT03604757.
142. 68Ga-RM2 PET/CT in Detecting Regional Nodal and Distant Metastases in Patients With Intermediate or High-Risk Prostate Cancer. https://ClinicalTrials.gov/show/NCT03113617.
143. 68Ga-RM2 PET/MRI in Biochemically Recurrent Prostate Cancer. https://ClinicalTrials.gov/show/NCT02624518.
144. 177Lu -NeoB in Patients With Advanced Solid Tumors and With 68Ga -NeoB Lesion Uptake. https://ClinicalTrials.gov/show/NCT03872778.
145. 68Ga -NeoBOMB1 Imaging in Patients With Malignancies Known to Overexpress Gastrin Releasing Peptide Receptor (GRPR). https://ClinicalTrials.gov/show/NCT03724253.
146. Jacobson, O.; Kiesewetter, D. O.; Chen, X., Fluorine-18 radiochemistry, labeling strategies and synthetic routes. *Bioconjug Chem* **2015,** *26* (1), 1-18.
147. Cai, L.; Lu, S.; Pike, V. W., Chemistry with [18F]Fluoride Ion. *European Journal of Organic Chemistry* **2008,** *2008* (17), 2853-2873.
148. Dialer, L. O.; Selivanova, S. V.; Muller, C. J.; Muller, A.; Stellfeld, T.; Graham, K.; Dinkelborg, L. M.; Kramer, S. D.; Schibli, R.; Reiher, M.; Ametamey, S. M., Studies toward the development of new silicon-containing building blocks for the direct (18)F-labeling of peptides. *J Med Chem* **2013,** *56* (19), 7552-63.
149. Schirrmacher, R.; Bradtmoller, G.; Schirrmacher, E.; Thews, O.; Tillmanns, J.; Siessmeier, T.; Buchholz, H. G.; Bartenstein, P.; Wangler, B.; Niemeyer, C. M.; Jurkschat, K., 18F-labeling of

peptides by means of an organosilicon-based fluoride acceptor. *Angew Chem Int Ed Engl* **2006,** *45* (36), 6047-50.
150. Chatalic, K. L.; Franssen, G. M.; van Weerden, W. M.; McBride, W. J.; Laverman, P.; de Blois, E.; Hajjaj, B.; Brunel, L.; Goldenberg, D. M.; Fehrentz, J. A.; Martinez, J.; Boerman, O. C.; de Jong, M., Preclinical comparison of Al18F- and 68Ga-labeled gastrin-releasing peptide receptor antagonists for PET imaging of prostate cancer. *J Nucl Med* **2014,** *55* (12), 2050-6.
151. Honer, M.; Mu, L.; Stellfeld, T.; Graham, K.; Martic, M.; Fischer, C. R.; Lehmann, L.; Schubiger, P. A.; Ametamey, S. M.; Dinkelborg, L.; Srinivasan, A.; Borkowski, S., 18F-labeled bombesin analog for specific and effective targeting of prostate tumors expressing gastrin-releasing peptide receptors. *J Nucl Med* **2011,** *52* (2), 270-8.
152. Varasteh, Z.; Aberg, O.; Velikyan, I.; Lindeberg, G.; Sorensen, J.; Larhed, M.; Antoni, G.; Sandstrom, M.; Tolmachev, V.; Orlova, A., In vitro and in vivo evaluation of a (18)F-labeled high affinity NOTA conjugated bombesin antagonist as a PET ligand for GRPR-targeted tumor imaging. *PLoS One* **2013,** *8* (12), e81932.
153. Carlucci, G.; Kuipers, A.; Ananias, H. J.; de Paula Faria, D.; Dierckx, R. A.; Helfrich, W.; Rink, R.; Moll, G. N.; de Jong, I. J.; Elsinga, P. H., GRPR-selective PET imaging of prostate cancer using [(18)F]-lanthionine-bombesin analogs. *Peptides* **2015,** *67*, 45-54.
154. Yang, M.; Gao, H.; Zhou, Y.; Ma, Y.; Quan, Q.; Lang, L.; Chen, K.; Niu, G.; Yan, Y.; Chen, X., 18F-Labeled GRPR Agonists and Antagonists A Comparative Study in Prostate Cancer Imaging. *Theranostics* **2011,** *1*, 220-229.
155. Iovkova-Berends, L.; Wangler, C.; Zoller, T.; Hofner, G.; Wanner, K. T.; Rensch, C.; Bartenstein, P.; Kostikov, A.; Schirrmacher, R.; Jurkschat, K.; Wangler, B., t-Bu2SiF-derivatized D2-receptor ligands: the first SiFA-containing small molecule radiotracers for target-specific PET-imaging. *Molecules* **2011,** *16* (9), 7458-79.
156. Bernard-Gauthier, V.; Bailey, J. J.; Liu, Z.; Wangler, B.; Wangler, C.; Jurkschat, K.; Perrin, D. M.; Schirrmacher, R., From Unorthodox to Established: The Current Status of (18)F-Trifluoroborate- and (18)F-SiFA-Based Radiopharmaceuticals in PET Nuclear Imaging. *Bioconjug Chem* **2016,** *27* (2), 267-79.
157. Rosenthal, M. S.; Bosch, A. L.; Nickles, R. J.; Gatley, S. J., Synthesis and some characteristics of no-carrier added [18F]fluorotrimethylsilane. *Int J Appl Radiat Isot* **1985,** *36* (4), 318-9.
158. Niedermoser, S.; Chin, J.; Wangler, C.; Kostikov, A.; Bernard-Gauthier, V.; Vogler, N.; Soucy, J. P.; McEwan, A. J.; Schirrmacher, R.; Wangler, B., In Vivo Evaluation of (1)(8)F-SiFAlin-Modified TATE: A Potential Challenge for (6)(8)Ga-DOTATATE, the Clinical Gold Standard for Somatostatin Receptor Imaging with PET. *J Nucl Med* **2015,** *56* (7), 1100-5.
159. Wangler, C.; Niedermoser, S.; Chin, J.; Orchowski, K.; Schirrmacher, E.; Jurkschat, K.; Iovkova-Berends, L.; Kostikov, A. P.; Schirrmacher, R.; Wangler, B., One-step (18)F-labeling of peptides for positron emission tomography imaging using the SiFA methodology. *Nat Protoc* **2012,** *7* (11), 1946-55.
160. Wessmann, S. H.; Henriksen, G.; Wester, H. J., Cryptate mediated nucleophilic 18F-fluorination without azeotropic drying. *Nuklearmedizin* **2012,** *51* (1), 1-8.
161. Wängler, C.; Waser, B.; Alke, A.; Iovkova, L.; Buchholz, H. G.; Niedermoser, S.; Jurkschat, K.; Fottner, C.; Bartenstein, P.; Schirrmacher, R.; Reubi, J. C.; Wester, H. J.; Wängler, B., One-step ^{18}F-labeling of carbohydrate-conjugated octreotate-derivatives containing a silicon-fluoride-acceptor (SiFA): in vitro and in vivo evaluation as tumor imaging agents for positron emission tomography (PET). *Bioconjug Chem* **2010,** *21* (12), 2289-96.
162. Bernard-Gauthier, V.; Wangler, C.; Schirrmacher, E.; Kostikov, A.; Jurkschat, K.; Wangler, B.; Schirrmacher, R., (1)(8)F-labeled silicon-based fluoride acceptors: potential opportunities for novel positron emitting radiopharmaceuticals. *Biomed Res Int* **2014,** *2014*, 454503.
163. Kostikov, A. P.; Iovkova, L.; Chin, J.; Schirrmacher, E.; Wängler, B.; Wängler, C.; Jurkschat, K.; Cosa, G.; Schirrmacher, R., N-(4-(di-tert-butyl[18F]fluorosilyl)benzyl)-2-hydroxy-N,N-dimethylethylammonium bromide ([18F]SiFAN+Br−): A novel lead compound for the development of hydrophilic SiFA-based prosthetic groups for 18F-labeling. *Journal of Fluorine Chemistry* **2011,** *132* (1), 27-34.
164. Lindner, S.; Michler, C.; Leidner, S.; Rensch, C.; Wangler, C.; Schirrmacher, R.; Bartenstein, P.; Wangler, B., Synthesis and in vitro and in vivo evaluation of SiFA-tagged bombesin and RGD

peptides as tumor imaging probes for positron emission tomography. *Bioconjug Chem* **2014,** *25* (4), 738-49.
165. Litau, S.; Niedermoser, S.; Vogler, N.; Roscher, M.; Schirrmacher, R.; Fricker, G.; Wangler, B.; Wangler, C., Next Generation of SiFAlin-Based TATE Derivatives for PET Imaging of SSTR-Positive Tumors: Influence of Molecular Design on In Vitro SSTR Binding and In Vivo Pharmacokinetics. *Bioconjug Chem* **2015,** *26* (12), 2350-9.
166. Wurzer, A.; DiCarlo, D.; Schmidt, A.; Beck, R.; Eiber, M.; Schwaiger, M.; Wester, H. J., Radiohybrid ligands: a novel tracer concept exemplified by (18)F- or (68)Ga-labeled rhPSMA-inhibitors. *J Nucl Med* **2019**.
167. Kirby, M.; Hirst, C.; Crawford, E. D., Characterising the castration-resistant prostate cancer population: a systematic review. *Int J Clin Pract* **2011,** *65* (11), 1180-92.
168. Jadvar, H., Targeted Radionuclide Therapy: An Evolution Toward Precision Cancer Treatment. *AJR Am J Roentgenol* **2017,** *209* (2), 277-288.
169. Kratochwil, C.; Giesel, F. L.; Stefanova, M.; Benesova, M.; Bronzel, M.; Afshar-Oromieh, A.; Mier, W.; Eder, M.; Kopka, K.; Haberkorn, U., PSMA-Targeted Radionuclide Therapy of Metastatic Castration-Resistant Prostate Cancer with 177Lu-Labeled PSMA-617. *J Nucl Med* **2016,** *57* (8), 1170-6.
170. Robu, S.; Schmidt, A.; Eiber, M.; Schottelius, M.; Gunther, T.; Hooshyar Yousefi, B.; Schwaiger, M.; Wester, H. J., Synthesis and preclinical evaluation of novel (18)F-labeled Glu-urea-Glu-based PSMA inhibitors for prostate cancer imaging: a comparison with (18)F-DCFPyl and (18)F-PSMA-1007. *EJNMMI Res* **2018,** *8* (1), 30.
171. Schmidt, A.; Wirtz, M.; Farber, S. F.; Osl, T.; Beck, R.; Schottelius, M.; Schwaiger, M.; Wester, H. J., Effect of Carbohydration on the Theranostic Tracer PSMA I&T. *ACS Omega* **2018,** *3* (7), 8278-8287.
172. Rahbar, K.; Ahmadzadehfar, H.; Kratochwil, C.; Haberkorn, U.; Schafers, M.; Essler, M.; Baum, R. P.; Kulkarni, H. R.; Schmidt, M.; Drzezga, A.; Bartenstein, P.; Pfestroff, A.; Luster, M.; Lutzen, U.; Marx, M.; Prasad, V.; Brenner, W.; Heinzel, A.; Mottaghy, F. M.; Ruf, J.; Meyer, P. T.; Heuschkel, M.; Eveslage, M.; Bogemann, M.; Fendler, W. P.; Krause, B. J., German Multicenter Study Investigating 177Lu-PSMA-617 Radioligand Therapy in Advanced Prostate Cancer Patients. *J Nucl Med* **2017,** *58* (1), 85-90.
173. Abiraj, K.; Mansi, R.; Tamma, M. L.; Fani, M.; Forrer, F.; Nicolas, G.; Cescato, R.; Reubi, J. C.; Maecke, H. R., Bombesin antagonist-based radioligands for translational nuclear imaging of gastrin-releasing peptide receptor-positive tumors. *J Nucl Med* **2011,** *52* (12), 1970-8.
174. Günther, T.; Beck, R.; Felber, V.; Deiser, S.; Wester, H. J., OP-758: Development and preclinical evaluation of 177Lu-AMTG, a novel pharmacophore-modified GRPR-targeted antagonist with improved metabolic stability. European Association of Nuclear Medicine October 22 – 30, 2020 Virtual. *European Journal of Nuclear Medicine and Molecular Imaging* **2020,** *47* (1), 374.
175. Guenther, T.; Fischer, S.; Beck, R.; Wester, H., Preclinical results of novel GRPR-targeted antagonists with modified binding sequences. *Journal of Nuclear Medicine* **2020,** *61* (supplement 1), 1054.
176. Varasteh, Z.; Rosenstrom, U.; Velikyan, I.; Mitran, B.; Altai, M.; Honarvar, H.; Rosestedt, M.; Lindeberg, G.; Sorensen, J.; Larhed, M.; Tolmachev, V.; Orlova, A., The effect of mini-PEG-based spacer length on binding and pharmacokinetic properties of a 68Ga-labeled NOTA-conjugated antagonistic analog of bombesin. *Molecules* **2014,** *19* (7), 10455-72.
177. Linder, K. E.; Metcalfe, E.; Arunachalam, T.; Chen, J.; Eaton, S. M.; Feng, W.; Fan, H.; Raju, N.; Cagnolini, A.; Lantry, L. E.; Nunn, A. D.; Swenson, R. E., In vitro and in vivo metabolism of Lu-AMBA, a GRP-receptor binding compound, and the synthesis and characterization of its metabolites. *Bioconjugate Chem.* **2009,** *20* (6), 1171-78.
178. Höhne, A.; Mu, L.; Honer, M.; Schubiger, P. A.; Ametamey, S. M.; Graham, K.; Stellfeld, T.; Borkowski, S.; Berndorff, D.; Klar, U.; Voigtmann, U.; Cyr, J. E.; Friebe, M.; Dinkelborg, L.; Srinivasan, A., Synthesis, 18F-labeling, and in vitro and in vivo studies of bombesin peptides modified with silicon-based building blocks. *Bioconjug Chem* **2008,** *19* (9), 1871-9.
179. Popp, I.; Del Pozzo, L.; Waser, B.; Reubi, J. C.; Meyer, P. T.; Maecke, H. R.; Gourni, E., Approaches to improve metabolic stability of a statine-based GRP receptor antagonist. *Nucl Med Biol* **2017,** *45*, 22-29.

180. Chatalic, K. L.; Konijnenberg, M.; Nonnekens, J.; de Blois, E.; Hoeben, S.; de Ridder, C.; Brunel, L.; Fehrentz, J. A.; Martinez, J.; van Gent, D. C.; Nock, B. A.; Maina, T.; van Weerden, W. M.; de Jong, M., In Vivo Stabilization of a Gastrin-Releasing Peptide Receptor Antagonist Enhances PET Imaging and Radionuclide Therapy of Prostate Cancer in Preclinical Studies. *Theranostics* **2016,** *6* (1), 104-17.
181. Accardo, A.; Galli, F.; Mansi, R.; Del Pozzo, L.; Aurilio, M.; Morisco, A.; Ringhieri, P.; Signore, A.; Morelli, G.; Aloj, L., Pre-clinical evaluation of eight DOTA coupled gastrin-releasing peptide receptor (GRP-R) ligands for in vivo targeting of receptor-expressing tumors. *EJNMMI Res* **2016,** *6* (1), 17.
182. Schottelius, M.; Wester, H. J.; Reubi, J. C.; Senekowitsch-Schmidtke, R.; Schwaiger, M., Improvement of Pharmacokinetics of Radioiodinated Tyr3-Octreotide by Conjugation with Carbohydrates. *Bioconjug Chem* **2002,** *13* (5), 1021-30.
183. Iovkova, L.; Wangler, B.; Schirrmacher, E.; Schirrmacher, R.; Quandt, G.; Boening, G.; Schurmann, M.; Jurkschat, K., para-Functionalized aryl-di-tert-butylfluorosilanes as potential labeling synthons for (18)F radiopharmaceuticals. *Chemistry* **2009,** *15* (9), 2140-7.
184. Weineisen, M.; Simecek, J.; Schottelius, M.; Schwaiger, M.; Wester, H. J., Synthesis and preclinical evaluation of DOTAGA-conjugated PSMA ligands for functional imaging and endoradiotherapy of prostate cancer. *EJNMMI Res* **2014,** *4* (1), 63.
185. de Blois, E.; Chan, H. S.; Konijnenberg, M. W.; de Zanger, R.; Breeman, W. A., Effectiveness of quenchers to reduce radiolysis of (111)In- or (177)Lu-labelled methionine-containing regulatory peptides. Maintaining radiochemical purity as measured by HPLC. *Curr Top Med Chem.* **2012,** *12* (23), 2677-85.
186. Biron, E.; Chatterjee, J.; Ovadia, O.; Langenegger, D.; Brueggen, J.; Hoyer, D.; Schmid, H. A.; Jelinek, R.; Gilon, C.; Hoffman, A.; Kessler, H., Improving oral bioavailability of peptides by multiple N-methylation: somatostatin analogues. *Angew Chem Int Ed Engl* **2008,** *47* (14), 2595-9.
187. Demmer, O.; Dijkgraaf, I.; Schottelius, M.; Wester, H. J.; Kessler, H., Introduction of Functional Groups into Peptides via N-Alkylation. *Org Lett* **2008,** *10* (10), 2015-2018.
188. Uehara, H.; Hocart, S. J.; Gonzalez, N.; Mantey, S. A.; Nakagawa, T.; Katsuno, T.; Coy, D. H.; Jensen, R. T., The molecular basis for high affinity of a universal ligand for human bombesin receptor (BnR) family members. *Biochem Pharmacol* **2012,** *84* (7), 936-48.
189. Reile, H.; Armatis, P. E.; Schally, A. V., Characterization of high-affinity receptors for bombesin/gastrin releasing peptide on the human prostate cancer cell lines PC-3 and DU-145: Internalization of receptor bound 125I-(Tyr4) bombesin by tumor cells. *Prostate* **1994,** *25* (1), 29-38.
190. Salako, Q. A.; O'Donnell, R. T.; DeNardo, S. J., Effects of radiolysis on yttrium-90-labeled Lym-1 antibody preparations. *J Nucl Med* **1998,** *39* (4), 667-70.
191. Horwell, D. C.; Howson, W.; Naylor, D.; Osborne, S.; Pinnock, R. D.; Ratcliffe, G. S.; Suman-Chauhan, N., Alanine scan and N-methyl amide derivatives of Ac-bombesin[7-14]. Development of a proposed binding conformation at the neuromedin B (NMB) and gastrin releasing peptide (GRP) receptors. *Int J Pept Protein Res* **1996,** *48* (6), 522-31.
192. Silvente-Poirot, S.; Escrieut, C.; Wank, S. A., Role of the extracellular domains of the cholecystokinin receptor in agonist binding. *Mol Pharmacol* **1998,** *54* (2), 364-71.
193. Raguine, L.; Ali, M.; Bender, V.; Diefenbach, E.; Doddareddy, M. R.; Hibbs, D.; Manolios, N., Alanine scan of an immunosuppressive peptide (CP): analysis of structure-function relationships. *Chem Biol Drug Des* **2013,** *81* (2), 167-74.
194. Migon, D.; Jaskiewicz, M.; Neubauer, D.; Bauer, M.; Sikorska, E.; Kamysz, E.; Kamysz, W., Alanine Scanning Studies of the Antimicrobial Peptide Aurein 1.2. *Probiotics Antimicrob Proteins* **2019,** *11* (3), 1042-1054.
195. Nanda, P. K.; Pandey, U.; Bottenus, B. N.; Rold, T. L.; Sieckman, G. L.; Szczodroski, A. F.; Hoffman, T. J.; Smith, C. J., Bombesin analogues for gastrin-releasing peptide receptor imaging. *Nucl Med Biol* **2012,** *39* (4), 461-71.
196. Accardo, A.; Mansi, R.; Salzano, G.; Morisco, A.; Aurilio, M.; Parisi, A.; Maione, F.; Cicala, C.; Ziaco, B.; Tesauro, D.; Aloj, L.; De Rosa, G.; Morelli, G., Bombesin peptide antagonist for target-selective delivery of liposomal doxorubicin on cancer cells. *J Drug Target* **2013,** *21* (3), 240-249.
197. Lim, J. C.; Cho, E. H.; Kim, J. J.; Choi, S. M.; Lee, S.; Nam, S. S.; Park, U. J.; Park, S. H., Biological evaluation of (177)Lu-labeled DOTA-Ala(SO3H)-Aminooctanoyl-Gln-Trp-Ala-Val-N

methyl Gly-His-Statine-Leu-NH2 for gastrin-releasing peptide receptor-positive prostate tumor targeting. *Nucl Med Biol* **2015,** *42* (2), 131-6.
198. Maina, T.; Nock, B. A., From Bench to Bed: New Gastrin-Releasing Peptide Receptor-Directed Radioligands and Their Use in Prostate Cancer. *PET Clin* **2017,** *12* (2), 205-217.
199. de Visser, M.; Bernard, H. F.; Erion, J. L.; Schmidt, M. A.; Srinivasan, A.; Waser, B.; Reubi, J. C.; Krenning, E. P.; de Jong, M., Novel 111In-labelled bombesin analogues for molecular imaging of prostate tumours. *Eur J Nucl Med Mol Imaging* **2007,** *34* (8), 1228-38.
200. Mantey, S. A.; Coy, D. H.; Pradhan, T. K.; Igarashi, H.; Rizo, I. M.; Shen, L.; Hou, W.; Hocart, S. J.; Jensen, R. T., Rational design of a peptide agonist that interacts selectively with the orphan receptor, bombesin receptor subtype 3. *J Biol Chem* **2001,** *276* (12), 9219-29.
201. Prasad, S.; Mathur, A.; Gupta, N.; Jaggi, M.; Singh, A. T.; Rajendran, P.; Sanna, V. K.; Datta, K.; Mukherjee, R., Bombesin analogs containing alpha-amino-isobutyric acid with potent anticancer activity. *J Pept Sci* **2007,** *13* (1), 54-62.
202. von Guggenberg, E.; Rangger, C.; Sosabowski, J.; Laverman, P.; Reubi, J. C.; Virgolini, I. J.; Decristoforo, C., Preclinical evaluation of radiolabeled DOTA-derivatized cyclic minigastrin analogs for targeting cholecystokinin receptor expressing malignancies. *Mol Imaging Biol* **2012,** *14* (3), 366-75.
203. Nedrow, J. R.; Latoche, J. D.; Day, K. E.; Modi, J.; Ganguly, T.; Zeng, D.; Kurland, B. F.; Berkman, C. E.; Anderson, C. J., Targeting PSMA with a Cu-64 Labeled Phosphoramidate Inhibitor for PET/CT Imaging of Variant PSMA-Expressing Xenografts in Mouse Models of Prostate Cancer. *Mol Imaging Biol* **2016,** *18* (3), 402-10.
204. Lepage, M. L.; Kuo, H. T.; Roxin, A.; Huh, S.; Zhang, Z.; Kandasamy, R. L.; Merkens, H.; Kumlin, J.; Limoges, A.; Zeisler, S. K.; Benard, F.; Lin, K. S.; Perrin, D., Toward 18F-Labeled Theranostics: A Single Agent that can be Labeled with 18F, 64Cu, or 177Lu. *Chembiochem* **2019**.
205. Rottenburger, C.; Nicolas, G. P.; McDougall, L.; Kaul, F.; Cachovan, M.; Vija, A. H.; Schibli, R.; Geistlich, S.; Schumann, A.; Rau, T.; Glatz, K.; Behe, M.; Christ, E. R.; Wild, D., Cholecystokinin 2 Receptor Agonist (177)Lu-PP-F11N for Radionuclide Therapy of Medullary Thyroid Carcinoma: Results of the Lumed Phase 0a Study. *J Nucl Med* **2020,** *61* (4), 520-526.
206. Breier, R. D.; Rold, T. L.; Szczodroski, A. F.; Hoffman, T. J., Evaluation of Lu-177 RM2 as a targeted radiopharmaceutical in a PC-3 xenograft model of androgen-independent prostate cancer. *Journal of Clinical Oncology* **2011,** *29* (15_suppl), e13522-e13522.
207. Pliška, V.; Schmidt, M.; Fauchère, J. L., Partition coefficients of amino acids and hydrophobic parameters π of their side-chains as measured by thin-layer chromatography. *Journal of Chromatography* **1981,** *216* (30), 79-92.
208. Rinne, S. S.; Leitao, C. D.; Mitran, B.; Bass, T. Z.; Andersson, K. G.; Tolmachev, V.; Stahl, S.; Lofblom, J.; Orlova, A., Optimization of HER3 expression imaging using affibody molecules: Influence of chelator for labeling with indium-111. *Sci Rep* **2019,** *9* (1), 655.
209. Wurzer, A.; Di Carlo, D.; Schmidt, A.; Beck, R.; Eiber, M.; Schwaiger, M.; Wester, H.-J., Radiohybrid Ligands: A Novel Tracer Concept Exemplified by 18F- or 68Ga-Labeled rhPSMA Inhibitors. *Journal of Nuclear Medicine* **2020,** *61* (5), 735-742.
210. Iovkova, L.; Könning, D.; Wängler, B.; Schirrmacher, R.; Schoof, S.; Arndt, H.-D.; Jurkschat, K., SiFA-Modified Phenylalanine: A Key Compound for the Efficient Synthesis of 18F-Labelled Peptides. *European Journal of Inorganic Chemistry* **2011,** *2011* (14), 2238-2246.
211. Han, Y.; Albericio, F.; Barany, G., Occurrence and Minimization of Cysteine Racemization during Stepwise Solid-Phase Peptide Synthesis(1)(,)(2). *J Org Chem* **1997,** *62* (13), 4307-4312.
212. Carpino, L. A.; El-Faham, A., Effect of Tertiary Bases on O-Benzotriazolyluronium Salt-Induced Peptide Segment Coupling. *J Org Chem* **1994,** *59* (4), 695-698.
213. Jamous, M.; Tamma, M. L.; Gourni, E.; Waser, B.; Reubi, J. C.; Maecke, H. R.; Mansi, R., PEG spacers of different length influence the biological profile of bombesin-based radiolabeled antagonists. *Nucl Med Biol* **2014,** *41* (6), 464-70.
214. Benesova, M.; Schafer, M.; Bauder-Wust, U.; Afshar-Oromieh, A.; Kratochwil, C.; Mier, W.; Haberkorn, U.; Kopka, K.; Eder, M., Preclinical Evaluation of a Tailor-Made DOTA-Conjugated PSMA Inhibitor with Optimized Linker Moiety for Imaging and Endoradiotherapy of Prostate Cancer. *J Nucl Med* **2015,** *56* (6), 914-20.
215. Tornesello, A. L.; Buonaguro, L.; Tornesello, M. L.; Buonaguro, F. M., New Insights in the Design of Bioactive Peptides and Chelating Agents for Imaging and Therapy in Oncology. *Molecules* **2017,** *22* (8).

216. Aboye, T. L.; Ha, H.; Majumder, S.; Christ, F.; Debyser, Z.; Shekhtman, A.; Neamati, N.; Camarero, J. A., Design of a novel cyclotide-based CXCR4 antagonist with anti-human immunodeficiency virus (HIV)-1 activity. *J Med Chem* **2012,** *55* (23), 10729-34.
217. von Guggenberg, E.; Sallegger, W.; Helbok, A.; Ocak, M.; King, R.; Mather, S. J.; Decristoforo, C., Cyclic minigastrin analogues for gastrin receptor scintigraphy with technetium-99m: preclinical evaluation. *J Med Chem* **2009,** *52* (15), 4786-93.
218. Kessler, H., Conformation and Biological Activity of Cyclic Peptides. *Angew Chem Int Ed Engl* **1982,** *21*, 512-23.
219. Samanen, J.; Ali, F.; Romoff, T.; Calvo, R.; Sorenson, E.; Vasko, J.; Storer, B.; Berry, D.; Bennett, D.; Strohsacker, M., Development of a small RGD peptide fibrinogen receptor antagonist with potent antiaggregatory activity in vitro. *J Med Chem* **1991,** *34* (10), 3114-25.
220. Fani, M.; Peitl, P. K.; Velikyan, I., Current Status of Radiopharmaceuticals for the Theranostics of Neuroendocrine Neoplasms. *Pharmaceuticals (Basel)* **2017,** *10* (1).
221. Ashwood, V.; Brownhill, V.; Higginbottom, M.; Horwell, D. C.; Hughes, J.; Lewthwaite, R. A.; McKnight, A. T.; Pinnock, R. D.; Pritchard, M. C.; Suman-Chauhan, N.; Webb, C.; Williams, S. C., PD 176252 - the first high affinity non-peptide gastrin-releasing peptide (BB2) receptor antagonist. *Bioorg. Med. Chem. Lett.* **1998,** *8* (18), 2589-94.
222. Fernández-Llamazares, A. I.; García, J.; Adan, J.; Meunier, D.; Mitjans, F.; Spengler, J.; Albericio, F., The backbone N-(4-azidobutyl) linker for the preparation of peptide chimera. *Org Lett* **2013,** *15* (17), 4572-5.
223. Falb, E.; Yechezkel, T.; Salitra, Y.; Gilon, C., In situ generation of Fmoc-amino acid chlorides using bis-(trichloromethyl)carbonate and its utilization for difficult couplings in solid-phase peptide synthesis. *J Peptide Res* **1999,** *53* (5), 507-17.
224. Holub, J. M.; Jang, H.; Kirshenbaum, K., Fit to be tied conformation-directed macrocyclization of peptoid foldamers. *Org Lett* **2007,** *9* (17), 3275-8.
225. Castro, V.; Rodriguez, H.; Albericio, F., CuAAC: An Efficient Click Chemistry Reaction on Solid Phase. *ACS Comb Sci* **2016,** *18* (1), 1-14.
226. Cantel, S.; Isaad Ale, C.; Scrima, M.; Levy, J. J.; DiMarchi, R. D.; Rovero, P.; Halperin, J. A.; D'Ursi, A. M.; Papini, A. M.; Chorev, M., Synthesis and conformational analysis of a cyclic peptide obtained via i to i+4 intramolecular side-chain to side-chain azide-alkyne 1,3-dipolar cycloaddition. *J Org Chem* **2008,** *73* (15), 5663-74.
227. Marsouvanidis, P. J.; Nock, B. A.; Hajjaj, B.; Fehrentz, J. A.; Brunel, L.; M'Kadmi, C.; van der Graaf, L.; Krenning, E. P.; Maina, T.; Martinez, J.; de Jong, M., Gastrin releasing peptide receptor-directed radioligands based on a bombesin antagonist: synthesis, (111)in-labeling, and preclinical profile. *J Med Chem* **2013,** *56* (6), 2374-84.
228. Zhang, H.; Schuhmacher, J.; Waser, B.; Wild, D.; Eisenhut, M.; Reubi, J. C.; Maecke, H. R., DOTA-PESIN, a DOTA-conjugated bombesin derivative designed for the imaging and targeted radionuclide treatment of bombesin receptor-positive tumours. *Eur J Nucl Med Mol Imaging* **2007,** *34* (8), 1198-208.
229. Lantry, L. E.; Cappelletti, E.; Maddalena, M. E.; Fox, J. S.; Feng, W.; Chen, J.; Thomas, R.; Eaton, S. M.; Bogdan, N. J.; Arunachalam, T.; Reubi, J. C.; Raju, N.; Metcalfe, E. C.; Lattuada, L.; Linder, K. E.; Swenson, R. E.; Tweedle, M. F.; Nunn, A. D., 177Lu-AMBA: Synthesis and characterization of a selective 177Lu-labeled GRP-R agonist for systemic radiotherapy of prostate cancer. *J Nucl Med* **2006,** *47* (7), 1144-52.
230. Zhang, X.; Cai, W.; Cao, F.; Schreibmann, E.; Wu, Y.; Wu, J. C.; Xing, L.; Chen, X., ^{18}F-Labeled Bombesin Analogs for Targeting GRP Receptor-Expressing Prostate Cancer. *J Nucl Med* **2006,** *47*, 492-501.
231. Linder, K. E.; Metcalfe, E.; Arunachalam, T.; Chen, J.; Eaton, S. M.; Feng, W.; Fan, H.; Raju, N.; Cagnolini, A.; Lantry, L. E.; Nunn, A. D.; Swenson, R. E., In vitro and in vivo metabolism of Lu-AMBA, a GRP-receptor binding compound, and the synthesis and characterization of its metabolites. *Bioconjug Chem* **2009,** *20* (6), 1171-8.
232. Eden, J. M.; Hall, M. D.; Higginbottom, M.; Horwell, D. C.; Howson, W.; Hughes, J.; Jordan, R. E.; Lewthwaite, R. A.; Martin, K.; McKnight, A. T.; O'Toole, J. C.; Pinnock, R. D.; Pritchard, M. C.; Suman-Chauhan, N.; Williams, S. C., PD 165929 — the first high affinity non-peptide neuromedin-B (NMB) receptor selective antagonist. *Bioorg Med Chem Lett* **1996,** *6* (21), 2617-22.

233. Horwell, D. C.; Ratcliffe, G.; Roberts, E., Stabilities of tryptophanylpnenethylamides to acid and alkaline conditions. *Bioorg Med Chem Lett* **1991,** *1* (3), 169-72.
234. Dumont, R. A.; Tamma, M.; Braun, F.; Borkowski, S.; Reubi, J. C.; Maecke, H.; Weber, W. A.; Mansi, R., Targeted radiotherapy of prostate cancer with a gastrin-releasing peptide receptor antagonist is effective as monotherapy and in combination with rapamycin. *J Nucl Med* **2013,** *54* (5), 762-9.
235. Forrer, F.; Krenning, E. P.; Kooij, P. P.; Bernard, B. F.; Konijnenberg, M.; Bakker, W. H.; Teunissen, J. J.; de Jong, M.; van Lom, K.; de Herder, W. W.; Kwekkeboom, D. J., Bone marrow dosimetry in peptide receptor radionuclide therapy with [177Lu-DOTA(0),Tyr(3)]octreotate. *Eur J Nucl Med Mol Imaging* **2009,** *36* (7), 1138-46.
236. Coleman, C. N.; Blakely, W. F.; Fike, J. R.; MacVittie, T. J.; Metting, N. F.; Mitchell, J. B.; Moulder, J. E.; Preston, R. J.; Seed, T. M.; Stone, H. B.; Tofilon, P. J.; Wong, R. S., Molecular and cellular biology of moderate-dose (1-10 Gy) radiation and potential mechanisms of radiation protection: report of a workshop at Bethesda, Maryland, December 17-18, 2001. *Radiat Res* **2003,** *159* (6), 812-34.
237. Eiber, M.; Kronke, M.; Wurzer, A.; Ulbrich, L.; Jooss, L.; Maurer, T.; Horn, T.; Schiller, K.; Langbein, T.; Buschner, G.; Wester, H. J.; Weber, W. A., (18)F-rhPSMA-7 positron emission tomography for the detection of biochemical recurrence of prostate cancer following radical prostatectomy. *J Nucl Med* **2019**.
238. Kronke, M.; Wurzer, A.; Schwamborn, K.; Ulbrich, L.; Jooss, L.; Maurer, T.; Horn, T.; Rauscher, I.; Haller, B.; Herz, M.; Wester, H. J.; Weber, W. A.; Eiber, M., Histologically-confirmed diagnostic efficacy of (18)F-rhPSMA-7 positron emission tomography for N-staging of patients with primary high risk prostate cancer. *J Nucl Med* **2019**.
239. Oh, S. W.; Wurzer, A.; Teoh, E. J.; Oh, S.; Langbein, T.; Kronke, M.; Herz, M.; Kropf, S.; Wester, H. J.; Weber, W. A.; Eiber, M., Quantitative and Qualitative Analyses of Biodistribution and PET Image Quality of Novel Radiohybrid PSMA, (18)F- rhPSMA-7, in Patients with Prostate Cancer. *J Nucl Med* **2019**.
240. Lindner, S.; Michler, C.; Wangler, B.; Bartenstein, P.; Fischer, G.; Schirrmacher, R.; Wangler, C., PESIN multimerization improves receptor avidities and in vivo tumor targeting properties to GRPR-overexpressing tumors. *Bioconjug Chem* **2014,** *25* (3), 489-500.
241. Dawson, L. A.; Kavanagh, B. D.; Paulino, A. C.; Das, S. K.; Miften, M.; Li, X. A.; Pan, C.; Ten Haken, R. K.; Schultheiss, T. E., Radiation-associated kidney injury. *Int J Radiat Oncol Biol Phys* **2010,** *76* (3 Suppl), S108-15.
242. Haubner, R.; Wester, H. J.; Burkhart, F.; Senekowitsch-Schmidtke, R.; Weber, W. A.; Goodman, S. L.; Kessler, H.; Schwaiger, M., Glycosylated RGD-containing peptides: tracer for tumor targeting and angiogenesis imaging with improved biokinetics. *J Nucl Med* **2001,** *42* (2), 326-36.
243. McCalley, D. V., Rationalization of retention and overloading behavior of basic compounds in reversed-phase HPLC using low ionic strength buffers suitable for mass spectrometric detection. *Anal Chem* **2003,** *75* (14), 3404-10.
244. Pfister, D.; Bolla, M.; Briganti, A.; Carroll, P.; Cozzarini, C.; Joniau, S.; van Poppel, H.; Roach, M.; Stephenson, A.; Wiegel, T.; Zelefsky, M. J., Early salvage radiotherapy following radical prostatectomy. *Eur Urol* **2014,** *65* (6), 1034-43.
245. Stish, B. J.; Pisansky, T. M.; Harmsen, W. S.; Davis, B. J.; Tzou, K. S.; Choo, R.; Buskirk, S. J., Improved Metastasis-Free and Survival Outcomes With Early Salvage Radiotherapy in Men With Detectable Prostate-Specific Antigen After Prostatectomy for Prostate Cancer. *J Clin Oncol* **2016,** *34* (32), 3864-3871.
246. Cheng, C.; Pan, L.; Dimitrakopoulou-Strauss, A.; Schäfer, M.; Wängler, C.; Wängler, B.; Haberkorn, U.; Strauss, L. G., Comparison between 68Ga-bombesin (68Ga-BZH3) and the cRGD tetramer 68Ga-RGD4 studies in an experimental nude rat model with a neuroendocrine pancreatic tumor cell line. *EJNMMI Res* **2011,** *1* (34).

VII. Appendix

List of schemes

Illustration directory

List of tables

Abbreviations

L-amino acid	**first letter of the three letter code capitalized**
D-amino acid	**three letter code completely uncapitalized**
AcOH	acetic acid
Aib	α-amino-isobutyric acid
AMBA	DOTA-4-aminobenzoyl-BBN_{7-14} (GRPR agonist)
$AmBF_3$	ammoniomethyltrifluoroborate
AMTG	DOTA-Pip^5-phe^6-Gln^7-α-Me-Trp^8-Ala^9-Val^{10}-Gly^{11}-His^{12}-Sta^{13}-Leu^{14}
AMTG2	DOTA-GA-Pip^5-phe^6-Gln^7-α-Me-Trp^8-Ala^9-Val^{10}-Gly^{11}-His^{12}-Sta^{13}-Leu^{14}
Ava	5-aminopentanoic acid
BBN	bombesin
BCa	breast cancer
BCR	biochemical recurrent
B_{max}	maximal number of receptors in a particular tissue
Bn	benzyl
Boc	tert-butyloxycarbonyl
BPH	benign prostatic hyperplasia
BRS-3	bombesin receptor subtype 3 (bombesin receptor 3, BB_3)
BSA	bovines serum albumin
Bta	β-(3-benzothienyl)alanine
BTC	*bis*(trichloromethyl) carbonate
CCK	cholecystokinin
CCK2R	cholecystokinin B receptor, cholecystokinin type-2 receptor
Chg	cyclohexyl glycine
Cit	citrulline
CNS	central nervous system
Cpg	cyclopentyl glycine
CT	computed tomography
CXCR4	C-X-C chemokine receptor type 4
δ	chemical shift
Dap	2,3-diaminopropionic acid
DBU	1,8-diazabicyclo(5.4.0)undec-7-ene

d.c.	decay corrected
DCE	dichloroethane
DCM	dichloromethane
Dde	*N*-(1-(4,4-dimethyl-2,6-dioxocyclohexylidene)ethyl)
DIAD	diisopropyl azodicarboxylate
DIC	*N*,*N'*-diisopropylcarbodiimide
DIPEA	*N*,*N*-diisopropylethylamine
DMAP	4-dimethylaminopyridine
DMEM	Dulbecco´s modified eagle medium
DMF	*N*,*N*-dimethyl formamide
DOTA	1,4,7,10-tetraazacyclododecane-1,4,7,10-tetraacetic acid
DOTA-GA	5-(*tert*-butoxy)-5-oxo-4-(4,7,10-tris(2-(*tert*-butoxy)-2-oxoethyl)-1,4,7,10-tetraazacyclododecan-1-yl)pentanoic acid
DRE	digital rectal examination
DRY	Asp-Arg-Tyr
EC	extracellular domain
EDTA	ethylenediaminetetraacetic acid
eq	equivalent
ER	estrogen receptor
ESI	electron spray ionization
Et_2O	diethyl ether
EtOAc	ethyl acetate
EtOH	ethanol
eue	D-glutamate-urea-D-glutamate
Fmoc	9-fluorenylmethoxycarbonyl
GI	gastrointestinal
GP	general procedure
GPCR	G protein-coupled receptor
GRP	gastrin-releasing peptide
GRPR	gastrin-releasing peptide receptor (bombesin 2 receptor, BB_2)
GS	Gleason score
HATU	1-[Bis(dimethylamino)methylene]-1H-1,2,3-triazolo[4,5-b]pyridinium 3-oxide hexafluorophosphate
HBSS	Hank’s balanced salt solution
HEPES	4-(2-hydroxyethyl)-1-piperazineethanesulfonic acid

HOAt	1-hydroxy-7-azabenzotriazole
HOBt	1-hydroxybenzotriazole
HPLC	high performance liquid chromatography
HSA	human serum albumin
Hse	homoserine
IC_{50}	half maximal inhibitory concentration
Iodo-Gen®	1,3,4,6-tetrachloro-3*R*,6*R*-diphenylglycoluril
K'	capacity factor
kDa	kilo Dalton (unit for the molecular weight)
$KMnO_4$	potassium permanganate
KOH	potassium hydroxide
λ	wavelength
log$D_{7.4}$	distribution coefficient at *pH* = 7.4
M	molar (moles per liter)
mCRPC	metastatic castration resistant prostate cancer
MeCN	acetonitrile
MeOH	methanol
MJ9	*H*-Pip-phe-Gln-Trp-Ala-Val-Gly-His-Sta-Leu-OH
MRI	magnetic resonance imaging
MS	mass spectrometry
Nal	naphthyl alanine
NaOH	sodium hydroxide
n.d.c.	non decay corrected
NEP	neutral endopeptidase, EC 3.4.24.11
Nle	norleucine
nm	nanometer
NMB	Neuromedin-B
NMBR	Neuromedin-B receptor (bombesin 1 receptor, BB_1)
NMP	*N*-methyl-2-pyrrolidone
NMR	nuclear magnetic resonance
NOTA	1,4,7-triazacyclononane-triacetic acid
NSCLC	non-small cell lung cancer
Orn	ornithine
PA	Phosphoramidon

PBS	phosphate buffered salt solution
PCa	prostate cancer
PET	positron emission tomography
Pip	4-amino-1-carboxymethyl-piperidine
PKC	protein kinase C
p-Ns	*p*-Nosyl, 4-nitrobenzenesulfonyl
PoC	proof of concept
PPh_3	triphenylphosphine
PSA	prostate-specific antigen
PSMA	prostate-specific membrane antigen
QC	quality control
RCP	radiochemical purity
RCY	radiochemical yield
RGD	arginine-glycine-aspartate
rh	radiohybrid
RM1	DOTA-CH_2CO-Gly-4-aminobenzoyl-phe-Gln-Trp-Ala-Val-Gly-His-Sta-Leu-NH_2
RM2	DOTA-Pip-phe-Gln-Trp-Ala-Val-Gly-His-Sta-Leu-NH_2
RP	reversed phase
rt	room temperature
A_M	molar activity
SAR	structure-activity relationship
SCLC	small cell lung cancer
SD	standard deviation
SiFA	silicon fluoride acceptor
SPECT	single-photon emission computed tomography
SPPS	solid-phase peptide synthesis
SST	somatostatin
SST2R	somatostatin type-2 receptor
Sta	(3*S*,4*S*)-4-amino-3-hydroxy-6-methylheptanoic acid
SUV	standardized uptake value
T/B ratio	tumor-to-background ratio
TBDMS-Cl	*tert*-butyldimethylsilyl chloride
TBTU	2-(1*H*-benzotriazole-1-yl)-1,1,3,3-tetramethylaminium tetrafluoroborate

^{t}Bu	*tert*-butyl
^{t}BuLi	*tert*-butyllithium
TEA	triethylamine
TFA	trifluoroacetic acid
THF	tetrahydrofurane
TIPS	triisopropylsilane
TLC	thin layer chromatography
TNM classification	tumor, node, metastasis classification
t_R	retention time
Tris	tris(hydroxymethyl)aminomethane
TRT	targeted radiotherapy
Trt	trityl
Txa	tranexamic acid
Tza	β-(1,2,3-triazolyl) alanine
UL	universal ligand, phe-Gln-Trp-Ala-Val-β-Ala-His-Phe-Nle-NH_2
UV	ultraviolet
Valyl-Sta	(3*S*,4*S*)-4-amino-3-hydroxy-5-methyl-hexanoic acid
v/*v*	volume ratio
vol-%	percentage of the volume